The Impact of Rapamycin and Metformin on Genome Organization and Function in Normal Human Fibroblasts

A Thesis Submitted to the College of

Graduate Studies and Research

in Partial Fulfilment of the Requirements

For the Degree of Master of Science

In the Department of Food and Bioproduct Sciences

University of Saskatchewan

Saskatoon

By

Zoe Elizabeth Gillespie

Permission to Use

In presenting this thesis/dissertation in partial fulfillment of the requirements for a Postgraduate degree from the University of Saskatchewan, I agree that the Libraries of this University may make it freely available for inspection. I further agree that permission for copying of this thesis/dissertation in any manner, in whole or in part, for scholarly purposes may be granted by the professor or professors who supervised my thesis/dissertation work or, in their absence, by the Head of the Department or the Dean of the College in which my thesis work was done. It is understood that any copying or publication or use of this thesis/dissertation or parts thereof for financial gain shall not be allowed without my written permission. It is also understood that due recognition shall be given to me and to the University of Saskatchewan in any scholarly use which may be made of any material in my thesis/dissertation.

Requests for permission to copy or to make other uses of materials in this thesis/dissertation in whole or part should be addressed to:

Head of the Department of Food and Bioproduct Sciences
Agriculture Building
51 Campus Drive
University of Saskatchewan
Saskatoon
Saskatchewan, S7N 5A8
Canada

Abstract

For decades, dietary restriction (DR) has been documented to extend health and lifespan across numerous model organisms. Two compounds, rapamycin (an immuno-suppressant) and metformin (a drug used to treat type II diabetes) have been proposed to mimic these health and lifespan benefits. Interestingly, DR, rapamycin and metformin result in the inhibition of the mammalian target of rapamycin (mTOR), a major nutrient sensing and signalling hub in the cell. The unexpected side-effect of this inhibition is the proposed extension in both health and lifespan in cell cultures and organisms. Despite the impact of inhibiting mTOR being well established at the biochemical level, the impact of mTOR inhibition on genome function (gene expression) and organization (organization of the genome in three-dimensional space) is poorly understood. Normal human fibroblasts were grown in culture and treated with either rapamycin or metformin for 120 h. It was established that with both treatments applied individually, population doubling times increased with no evidence of cell death; however, cellular morphology was divergent, with rapamycin-treated fibroblasts reminiscent of quiescence, whilst metformin-treated fibroblasts still exhibited the morphology of proliferating cells. Analysis of chromosome territory positioning revealed similar re-location of chromosomes 18 and 10 whilst RNA sequencing analyses demonstrated divergent transcript profiles. In particular, transcripts changing significantly in response to rapamycin treatment were enriched for the cytokine-cytokine receptor interaction pathway, whilst genes changing significantly in response to metformin were enriched in the AP-1 transcription factor pathway. Chromatin immuno-precipitation analyses revealed STAT5A/B as a potential mediator of rapamycin-mediated changes in gene expression. Together, these data demonstrated that although rapamycin and metformin are potential mimetics of DR, they elicit differential changes in gene expression and function through divergent mechanisms. Finally, these findings indicate that there are multiple targets for treatments which could result in increased health and lifespan in humans.

Acknowledgements

I would first like to thank Dr. Christopher Eskiw, not only for giving me the opportunity to move to Canada to complete this thesis in his laboratory, but also for the support, time and guidance put into my training as a scientist. I would also like to thank all members of the Eskiw Lab; Joshua Pickering, Kira Wang, Dr. Zachery Belak and especially Michelle Sander for her technical guidance and expertise. I would additionally like to thank members of Dr. Anthony Kusaliks group, specifically Kimberly MacKay, for their bioinformatics assistance and expertise.

I would like to thank my family, especially my mother, Elizabeth Gillespie and brother, Andrew Gillespie, for supporting my move to Canada and for their continued support during the preparation of this thesis. I would also like to thank all the friends who have supported me during this time, both at home and in Canada, although there are too many to list. Finally, I would like to thank Jeffrey Elder for his continuous friendship, support and encouragement.

Table of Contents

List of Tables

List of Figures

List of Abbreviations

2DD – Primary Foreskin Fibroblasts

AMP – Adenosine Monophosphate

AMPK – Adenosine Monophosphate Kinase

ATP – Adenosine Triphosphate

BSA – Bovine Serum Albumin

Cat - Catalogue

ChIP – Chromatin Immuno-Precipitation

CT – Chromosome Territory

CLOVER – *Cis*-element over-representation

DNA – Deoxyribonucleic Acid

DR – dietary restriction

EdU - 5-ethynyl-2-deoxyuridine

EtOH – Ethanol

g - Gravity

FA – Formaldehyde

FBS – Fetal Bovine Serum

GO – Gene Ontology

H33342 - Hoechst 33342

H – Histone

h - Hour

HGPS – Hutchinson Gilford Progeria Syndrome

HRP – Horse Raddish Peroxidase

ICD – Interchromatin Domain

kB - Kilobase

KCl – Potassium Chloride

KEGG – Kyoto Encyclopedia of Genes and Genomes

kDa – kildo Dalton

LADS – Lamin Associated Domains

LC3 – Light Chain 3

LCR – Locus Control Region

LKB1 – Liver Kinase B1

min – Minutes

mM – Millimolar

mTOR – Mammalian target of rapamycin

mTORC1/2 – Mammalian target of rapamycin Complex 1/2

PBS – Phosphate Buffered Saline Solution

NaCl – Sodium Chloride

NAD – Nicotinamide Adenine Dinucleotide

nm – Nanometre

nM – Nanomolar

RNA – Ribonucleic Acid

RNAPII – RNA Polymerase II

ROS – Reactive Oxygen Species

RT – Room Temperature

SASP – Senescence Associated Secretory Phenotype

SCC - Saline Sodium Citrate

SDS – Sodium Dodecyl Sulphate

S.E.M. – Standard Error of the Mean

SIRT1 – Sirtuin 1

T2D – Type II Diabetes

TADs – Topologically Associating Domains

TSC1/2 Tuberous Sclerosis Complex 1/2

STAT5A/B – Signal Transduction and Activator of Transcription A/B

1.0 Review of the Literature

1.1 Introduction

Physical organisation of the genome is essential for the proper maintenance of cellular function. Genome disruption has been implicated in a number of diseases, including Hutchinson-Gilford Progeria Syndrome (HGPS), a premature ageing disease in which patients usually die from age-related complications (Cao *et al.* 2011). Within the last decade, the importance of genome function (transcription) and organisation (folding in three-dimensional space) as an area of active research has become apparent, and although focus is now shifting towards this field, many questions remain on how genome function links with genome organization.

Dietary restriction (DR) can be defined as the reduction of nutrient intake without inducing malnutrition. In both primate and non-primate model organisms, DR has been demonstrated to extend lifespan, delaying the onset of age-related diseases such as cancer, diabetes and cardiovascular disease (McCay *et al.* 1935; Bordone and Guarente 2005; Colman *et al.* 2009; Cruzen and Colman 2009). One major impact of DR is the inhibition of the mammalian target of rapamycin (mTOR) pathway, a major nutrient-sensing pathway within the cell responding to cellular nutrients such as glucose and amino acids. This inhibition induces downstream effects such as up-regulating autophagy (*self-eating*) and inhibiting protein synthesis (Stanfel *et al.* 2009). The commonly-used compounds, rapamycin and metformin (an immunosuppressant and treatment for type II diabetes, respectively), both disrupt mTOR signalling with the unexpected side effect of extending longevity in several species including model organisms (Harrison *et al.* 2009; Onken and Driscoll 2010; Anisimov *et al.* 2011; Martin-Montalvo *et al.* 2013; Miller *et al.* 2014), non-human primates (Colman *et al.* 2009; Cruzen and Colman 2009; Mattison *et al.* 2012; Colman *et al.* 2014) and human cells growing in tissue culture (Dowling *et al.* 2007; Chen *et al.* 2009; Dowling *et al.* 2011). Although the mTOR cascade has been extensively studied, it is unclear what impact decreased mTOR function, either through decreased nutrient levels or disrupted nutrient sensing, has on genome function and organisation in normal human cells. Understanding changes in genome function and organisation will be essential in understanding how rapamycin and metformin act to promote extended health and lifespan.

1.2 Genome Organization

1.2.1 Basic Genome Organization: From Helix to Chromatin

A genome contains all of the information necessary for an organism to grow, develop, and exhibit certain behavioural characteristics. The basic building blocks of life that make up the genome are nucleotides (adenine (A), guanine (G), cytosine (C), thymine (T)) that will base-pair with complementary partners (A with T; C with G) in a sequence that combine with a deoxyribose-phosphate backbone to form the DNA double helix. Two copies of the human genome exist in the majority of cells (with the exception of, for example, red blood cells and the germline), comprising ~3.2 billion base pairs (bp). Such a large volume of genetic information presents a packaging problem for the cell. From end-to-end the human genome measures ~2 metres in length and must be condensed into a nuclear volume measuring ~10 μm in diameter (Schneider and Grosschedl 2007). Furthermore, this DNA is negatively charged and must remain readily and quickly accessible for processes such as transcription, DNA repair and replication. In order to address these requirements, several levels of genome organization exist [reviewed in (Schneider and Grosschedl 2007)].

1.2.2 Topology of Chromatin Folding

One method by which the problem of genome packaging within the nucleus is addressed is via the wrapping of DNA into nucleosomes. This wrapping is the first of many levels of organization within human cells. Oudet *et al.*, provided the first evidence of these structures within the eukaryotic genome (Oudet *et al.* 1975). Nucleosomes consist of ~147 base pairs of DNA wrapped ~1.65 times around a histone octamer (Kornberg 1974; Noll 1974; Oudet *et al.* 1975; Finch *et al.* 1977; Luger *et al.* 1997). Histones are groups of basic proteins found in chromatin that, in the case of DNA packaging, favour binding to negatively charged DNA polymers, neutralizing charges and allowing for the folding of DNA. An octamer consists of two copies of the histones (H) H2A, H2B, H3 and H4; known as the canonical histones. The genes encoding for the histone proteins are normally only expressed during DNA synthesis (S-Phase) (Kornberg 1974; Kamakaka and Biggins 2005). Core histones all contain a conserved C-terminal histone fold domain and an N-terminal tail. The N-terminal tail, when modified, gains various different biophysical properties and can act as binding sites for other proteins, allowing for additional interactions between proteins and nucleosomes. Each 11 nm nucleosome is linked to the next in a "beads-on-a-string" type structure, with stretches of linker DNA, bound by linker histone 1 (H1) (Olins and Olins 1974; Oudet *et al.* 1975; Holde 1995). The resultant protein-DNA complex arising from the wrapping of DNA around histones is

known as chromatin and may have higher-order folding structures, the first of which is a proposed 30 nm fibre partially mediated by nucleosome-nucleosome interactions (Kornberg 1974). There are several models that exist for the wrapping of the genome into higher order structures, the first of which is the One Start model. In this model, nucleosomes are organized along the same helical path, with sequential interactions between the histone cores. The second model, the Two Start model proposes that two opposite nucleosomes are connected by linker DNA creating a structure of alternate histone cores which interact. The resulting linked structure is further folded onto itself, with other structures in between, forming a 300 nm structure with sub-chromosomal domains (Figure 1-1) (reviewed in (Cremer and Cremer 2001; Belmont 2014)). Controversy exists over whether or not the 30 nm chromatin structure is present *in vivo*. Multiple studies claim that original observations were artefacts and that the basic structure of a chromosome is a compact aggregation of 11 nm nucleosome fibres (Dubochet *et al.* 1988; Maeshima and Eltsov 2008; Maeshima *et al.* 2014). Yet some argue that methods used to form this conclusion involved a technique called "defocusing" which may in fact hide the presence of the structures. Further study by Conway and Steven attempted to elucidate the existence of a 30 nm fibre, and again, the fibre was not detected; however, controversy still exists (Conway and Steven 1999). For a more in-depth review of the existence of the 30 nm chromatin fibre, see publications by (Fussner *et al.* 2011; Maeshima *et al.* 2014).

The primary purpose of canonical histones is to form the core of nucleosomes; however, other classes of histones exist with specialised functions, known as histone variants. Histone variants differ from canonical histones in that the gene coding for the protein is normally expressed throughout the cell cycle, not just during S-Phase. Some variants have unique biophysical characteristics which act to facilitate various cellular processes by modulating chromatin via altering nucleosome properties, whilst others localise to specific regions of the genome to achieve similar affects (reviewed in (Kamakaka and Biggins 2005; Weber and Henikoff 2014)). A unique H2A histone variant, macroH2A, has a 30 kDa non-histone domain at its C-terminal, making it three times larger than its canonical counterpart (Pehrson and Fried 1992). MacroH2A is generally associated with heterochromatin and has been linked to X chromosome inactivation in eutherian female mammals, with further evidence suggesting that macroH2A is involved in regulation of gene expression programs during cellular differentiation with some studies proposing the variant as an epigenetic regulator of cancer (Buschbeck *et al.* 2009; Buschbeck and Di Croce 2010).

EviIn 1928, Emil Heitz characterised two forms of chromatin; euchromatin and heterochromatin [Reviewed in (Straub 2003)]. These two forms can be observed in distinct structures; highly-compact heterochromatin and less-compact euchromatin. Evidence suggests that these regions are important for gene expression, with data linking regions of heterochromatin to silencing gene expression and euchromatic regions to activating gene expression. This argues that occupancy in three-dimensional space is important for gene regulation (Cavalli and Misteli 2013).

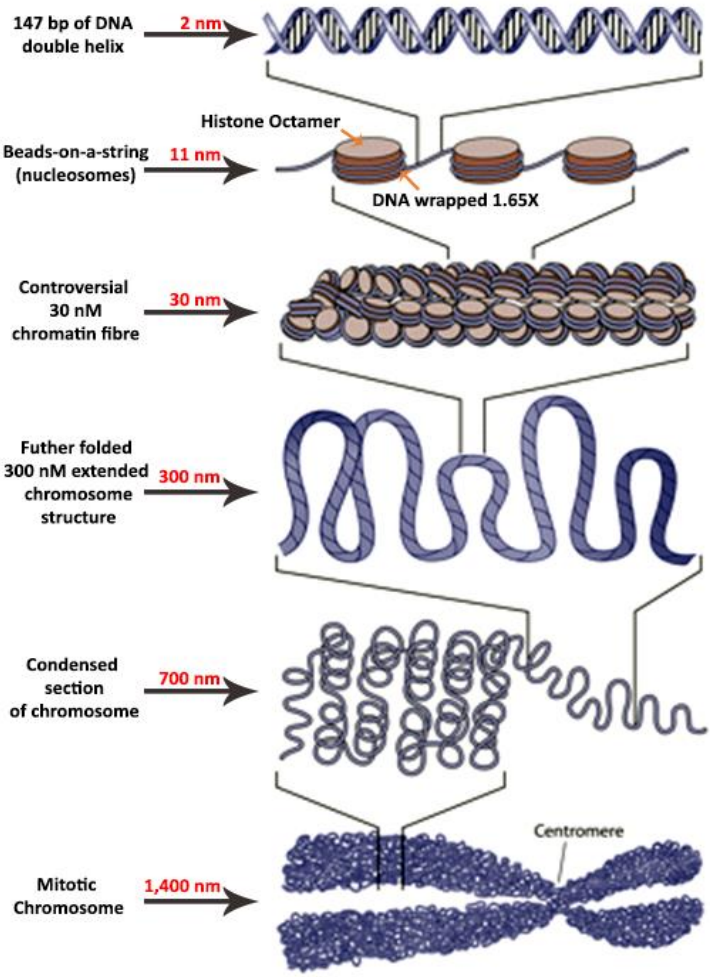

Figure 1-1: The Proposed Levels of Genome Organization Within the Mammalian Genome. Double stranded DNA (2 nm) wraps around nucleosomes (11 nm) which then undergo further folding to form the controversial 30 nm chromatin fibre. Further folding to form mitotic chromosomes (1,400 nm) occurs in a somewhat undefined manner. Reproduced with permission and adapted from (Felsenfeld and Groudine 2003).

1.2.3 Epigenetics and Chromatin

Multicellular organisms, including humans, have large genomes that have evolved to produce cell-type specific phenotypes. Although nearly all cells share the same genome, various phenotypes are observed, allowing cells to carry out diverse functions. This specificity is normally determined during development, whereby DNA is packaged with both histone and non-histone proteins, giving rise to distinct gene expression patterns, although it is important to note that other features, such as transcription factors (discussed later) are also very important in determining the gene expression of a cell. The packaging of chromatin is regulated by multiple mechanisms, including DNA modifications (e.g. methylation), and post-translational modifications of histones (phosphorylation, acetylation, etc.) [reviewed in (Chen and Maklakov 2014)]. Changes in these DNA modifications, or post-translational modifications, have been linked to diseases such as cancer (Rodriguez-Paredes and Esteller 2011). These covalent modifications to DNA and its associated histones are often referred to as epigenetics [reviewed in (Siggens and Ekwall 2014)]. The majority of epigenetic modifications are reversible, meaning it is possible to change the behaviour of genomes. The reversible nature of these epigenetic modifications could provide a potential route for developing disease treatments.

Combinatorial patterns of DNA and histone modifications, alongside histone variants, mark areas of distinct genome function. These areas of function are reflected in their influence on chromatin-associated processes (transcription, DNA replication, DNA repair, etc.) and can define which regions of the genome are active or inactive [reviewed in (Siggens and Ekwall 2014)]. Epigenetically, heritable domains of heterochromatin exist, and these control the structure and expression of large chromosome domains. Heterochromatin is assembled by many enzymes and proteins that work in unison in a stepwise manner that involves rounds of histone modification (Eissenberg and Elgin 2014).

Post-translational modification of histones and DNA can occur throughout a lifetime. These post-translational modifications directly alter genome function, with work in twins demonstrating that the ageing process is influenced predominantly by epigenetic modification of histones and chromatin as a result of lifestyle (Fraga *et al.* 2005). It has previously been described that the difference in epigenetic patterns between identical twins is likely the result of internal factors (such as ageing and defects in the transmission of epigenetic information through cell divisions) and external factors (such as smoking, physical activity and diet) (Fraga *et al.* 2005). Specifically, evidence suggests DNA methylation and histone modifications linked

to chromatin structure are involved in a global response to DR, regulating the expression of key genes (reviewed in (Li *et al.* 2011)).

1.2.4 Genome Organization on the Linear Chromosome

All human cells, with the exception of the gametes, contain 46 chromosomes. Chromosomes are the result of DNA packaging, with the entire genome tightly-coiled around histones to carry genetic material. Organization of genes along the linear chromosome is important for genome function, with disruption of this organization often resulting in disease. One level of this organization is via the formation of gene clusters, regions of genes along the chromosome that interact with one another as a result of genome folding. These clusters can range from a few to hundreds of genes (Hurst *et al.* 2004). These gene clusters are non-random and are essential in understanding both evolution (with gene clusters conserved across eukaryotic species (Lee and Sonnhammer 2003)) and disease (Joos *et al.* 1992; Zhou *et al.* 2003; Hurst *et al.* 2004; Kleinjan and van Heyningen 2005). Examples of gene clusters include the *Hox* and *globin* gene cluster, initially thought to have occurred by chance but now recognized as having a function, and mammalian imprinted genes (Reik and Walter 2001). Additional examples include the immunoglobulin heavy-chain variable-region (*Ig* V_H) gene cluster, reported in both mice and humans (Hughes and Yeager 1997). Interestingly, genes physically clustering on the chromosome often share functionality, indicating that the genome is organized to facilitate the expression of like-regulated genes, with functionally-linked genes able to span over 1000 kb in more complex organisms (Cho *et al.* 1998; Cohen *et al.* 2000; Spellman and Rubin 2002; Lercher *et al.* 2003). In addition to these findings, it has been proposed that gene clusters are cell-type specific.

1.2.5 Spatial Genome Organization

Gene clusters exist along the linear chromosome. Interactions between these genes have created further levels of genome organization, which when folded, are defined as linear units of chromatin that fold in discrete three-dimensional structures favouring internal interactions (Ciabrelli and Cavalli 2015). These structures are referred to as topologically associated domains (TADs). TADs have only been detected in animal cell types, spanning on average every 1 mega base (Mb) in humans (Caron *et al.* 2001). TADs usually have distinct boundaries and are proposed to be involved in genome regulation and function, contain housekeeping genes (genes required for basic cellular function and are constitutively active) and insulator sites (a boundary that prevents interaction between enhancers and promoters) (Figure 1-2) (Phillips-

Cremins and Corces 2013). This results in highly interacting genes within TADs, but less frequent interactions between the genes in the TADs and genes of other TADs.

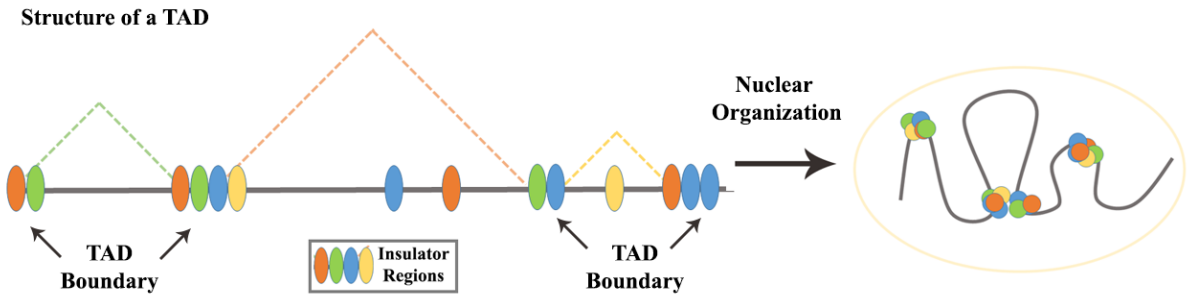

Figure 1-2: The Structure of Topologically Associated Domains and Nuclear Organization. Visualization of the structuring of a topologically associating domain (TADs). TADs can span variable regions of the genome and at their edges contain high concentrations of insulators, preventing interaction between genes with the TAD and others in other TADs. Reproduced with permission and adapted from (Matharu and Ahanger 2015).

1.2.6 Chromosome Territories

Chromosomes are organized within the nuclear volume and are known to occupy specific regions, referred to as chromosome territories (Figure 1-3) (Cremer *et al.* 2006; Meaburn *et al.* 2009). The existence of chromosome territories was first proposed in 1885 by Carl Rabl in *Salamandra maculate*; however, direct visual evidence remained unavailable until the development of fluorescence *in-situ* hybridization (FISH) with chromosome paints [reviewed in (Cavalli and Misteli 2013)]. In order to further understand chromosome territories and their positioning, experiments were conducted identifying chromosome 19 (a gene-rich chromosome) as existing predominantly in the nuclear interior whilst the gene-poor chromosome 18 exists primarily at the periphery. This work highlighted a correlation between gene density and chromosome positioning, and proposed that similar findings would be found for all human chromosomes (Boyle *et al.* 2001; Cremer and Cremer 2001). Since this work HiC, a derivative of chromatin conformation capture (3C), as providing concordant data demonstrating other gene rich chromosomes (1, 16, 17, 19 and 22) as localised at the nuclear interior (reviewed in (Bickmore 2013)). A further level of organization has been proposed within the chromosome territory, with gene-poor regions of the chromosome preferentially orientated towards the nuclear periphery (Boyle *et al.* 2001; Kupper *et al.* 2007). Additionally, it has been documented that parts of the genome preferentially associated with components of the nuclear periphery, with >1000 domains documented as coming into contact with the nuclear

periphery. These domains were called lamin-associated domains (LADS) and are gene-poor (Guelen *et al.* 2008). Furthermore, tethering of loci to the nuclear periphery induced the down-regulation of a number of relocated genes (Finlan *et al.* 2008). Other research, such as that by Bolzer *et al.*, has demonstrated that small chromosomes move towards the nuclear interior, whilst larger chromosomes preferentially locate towards the periphery (Bolzer *et al.* 2005). Although this may be a partial factor in chromosome territory positioning, it has previously been demonstrated that chromosome 18, a relatively small chromosome, exists preferentially at the periphery; therefore, other factors should also be considered [161]. Although it is often argued that chromosome territories are based on the presence of greater regions of heterochromatin at the nuclear periphery and greater regions of euchromatin at the nuclear interior, it is far more likely that chromosome territory positioning is more complex.

Chromosome territories do not remain stationary within the nucleus. In primary human fibroblasts, chromosome territory positioning is altered during quiescence and senescence (Bridger *et al.* 2000; Meaburn *et al.* 2007; Mehta *et al.* 2010; Mehta *et al.* 2011). When exiting the cell cycle, gene-poor human chromosome 18 relocates to the nuclear interior before returning to the periphery upon re-entering the cell cycle. Further to this, chromosome territory repositioning has been observed in serum-starved fibroblasts; perhaps not surprising as this induces quiescence. This change in nuclear location occurred within 15 minutes of serum starvation. This process requires energy, with evidence suggesting the involvement of nuclear actins and myosins (Mehta *et al.* 2010). Actin (which forms filaments) and myosin (a molecular motor) may potentially be involved in chromosome territory re-location (Bridger *et al.* 2000; Mehta *et al.* 2010). Interestingly, pathogens have also been implicated in altering host genome organisation in order to induce favourable conditions for the pathogen; however, this has only been observed once in *Biomphalaria glabrata* (snails) (Arican-Goktas *et al.* 2014). Viruses have also been documented to reorganize the nucleus to meet their transcriptional demands (Lieberman 2008). These studies have provided further evidence of the plasticity of the human genome in somatic cells, demonstrating that the removal of growth factors impacts chromosome territory positioning.

Genome organization and chromosome territory positioning has been associated with human health and disease. Mutations of genes encoding proteins known as lamins at the nuclear periphery cause diseases known as laminopathies, with alteration in radial chromosome organization reported in patients suffering laminopathies (Meaburn *et al.* 2007). In the premature ageing disease Hutchinson-Gilford Progeria Syndrome (HGPS), mutation in *lamin*

A results in the accumulation of the mutation protein progerin (Cao *et al.* 2007; Dechat *et al.* 2007) with altered genome interactions reported when comparing lamin A and progerin, specifically that lamin A-associated genes are often transcriptionally-silent and that loss of this silencing results in relocation of chromosomes from the periphery (Kubben *et al.* 2012). Furthermore, in HGPS cells, loss of heterochromatin has been documented. Cao *et al.* reported restoration of heterochromatin domains in response to rapamycin treatment, improving DNA repair kinetics and inducing autophagy mediated degradation of progerin (Cao *et al.* 2011). Contributing to the statement of the plasticity of the human genome, when treated with farnesyltransferase inhibitors (Mehta *et al.* 2011) chromosome territories returned to a position similar to those in normal human fibroblasts, indicating the importance of genome organization in health and disease.

There is some debate over whether or not chromosome territories are truly discrete. Genes have been reported to loop distances out of the chromosome territory in regions of constitutively high gene expression or when gene expression is induced (reviewed by (Fraser and Bickmore 2007)). Some models have suggested that active genes are found in direct contact with an inter-chromatin domain (ICD) which separates chromosome territories (Kosak and Groudine 2004; Scheuermann *et al.* 2004). However, this does not allow for the existence of significant chromosome territory intermingling proposed by simulations (Holley *et al.* 2002). Intermingling of chromosome territories has been detected for all chromosome pairs analysed by Branco & Pombo across multiple cell types, with data indicating chromosome intermingling is influenced by transcription dependent interactions (Branco and Pombo 2006). Using the *Hoxb* gene cluster, which is activated as it relocates away from the chromosome territory, it has been suggested that looping allows the locus to interact with a greater number of chromosomes. This raises a number of questions, including, where are the genes going and why and how are the genes leaving the territory (Chambeyron *et al.* 2005; Branco and Pombo 2006)?

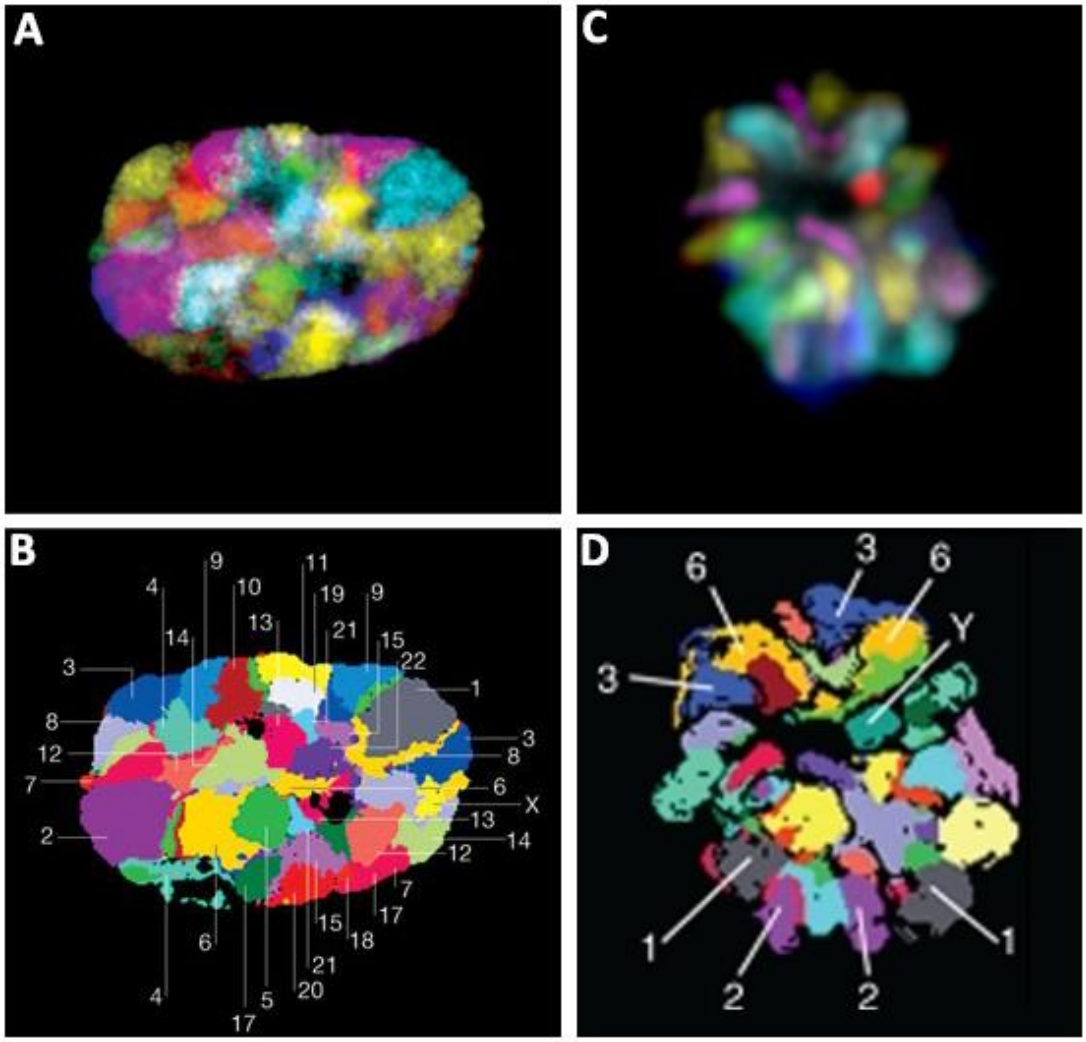

Figure 1-3: Chromosomes Organized in Chromosome Territories. (A) A deconvoluted mid-plane section of the nuclear volume with chromosome territories labelled by spectral karyotype (SKY) FISH. Every individual colour represents a chromosome territory. (B) RGB colors of the 23 differentially labelled chromosome territories within the nucleus. (C) Deconvoluted mid-plane section of a prometaphase rosette from a male fibroblast. Chromosome territories labelled by 24-colour SKY FISH. (D) RGB colours of labelled chromosome territories. Reproduced with permission and adapted from (Bolzer *et al.* 2005).

1.2.7 Organization of Transcription within the Nuclear Volume – The Transcription Factory Model

Contrary to the traditionally taught model of transcription, evidence now indicates that transcription machinery exists at discrete sites throughout the nucleus. Transcription factories are protein-rich nuclear sub-compartments containing high concentrations of hyper-phosphorylated RNA Polymerase II (RNAPII) (Iborra *et al.* 1996; Eskiw *et al.* 2008). The low numbers of transcription factories to active genes and transcription suggests that factories are

shared among active genes, further supported by evidence of co-localization at RNAPII foci between genes involved in the same processes (e.g. globin synthesis), indicating the existence of large scale transcription networks (Osborne *et al.* 2004; Schoenfelder *et al.* 2010). Genes transcribed by RNAPII (the majority of protein coding genes), engage in long-range, transcription-dependent associations (Osborne *et al.* 2004; Mitchell and Fraser 2008). The existence of specialised transcription factories, or transcription networks, could act to influence genome organisation. These specialised transcription factories may arise either via the deterministic model in which key players in transcription become concentrated at a subset of factories, where genes requiring the factory will move towards it, or via the self-organisation model in which genes and their bound regulatory factors engage factories in their local environments (reviewed in (Cope *et al.* 2010)).

1.2.8 Transcription and Genome Folding

A long range chromatin interaction is an interface that exists between two or more regions of the chromosome. Long-range chromatin interactions can occur either between regions of the same chromosome (*cis*) or between regions of different chromosomes (*trans*) (Figure 1-4). These long-range interactions between genes and enhancers (regulatory DNA sequences that enhance transcription of associated genes when bound by transcription factors) have been directly associated with gene regulation. The disruption of looping as a result of these interactions causes changes in expression (Drissen *et al.* 2004; Vakoc *et al.* 2005). For example, the *cis* interaction between the erythroid-specific β-globin gene and its distal enhancer locus control region (LCR) acts to regulate β-globin gene transcription during erythroid development through the exclusion of a 50 kB loop of DNA (Carter *et al.* 2002; Tolhuis *et al.* 2002). Deletion of transcription factor binding sites and cofactors required for the aforementioned interaction leads to decreased levels of β-globin gene transcription, highlighting necessity for the LCR-β-globin interaction and the importance of the 50 kB loop (reviewed in (Cope *et al.* 2010)). Similarly, *trans* interactions, such as that between T-helper cell 2 LCR on chromosome 11 and interferon γ promoter on chromosome 10 in naïve murine T-cells have also been identified (Spilianakis *et al.* 2005). Combined, these studies further implicate that *cis*- and *trans*-interactions frequently occur throughout a genome organised in three dimensional networks of genes and regulatory elements and support the concept of genome structure affecting genome function.

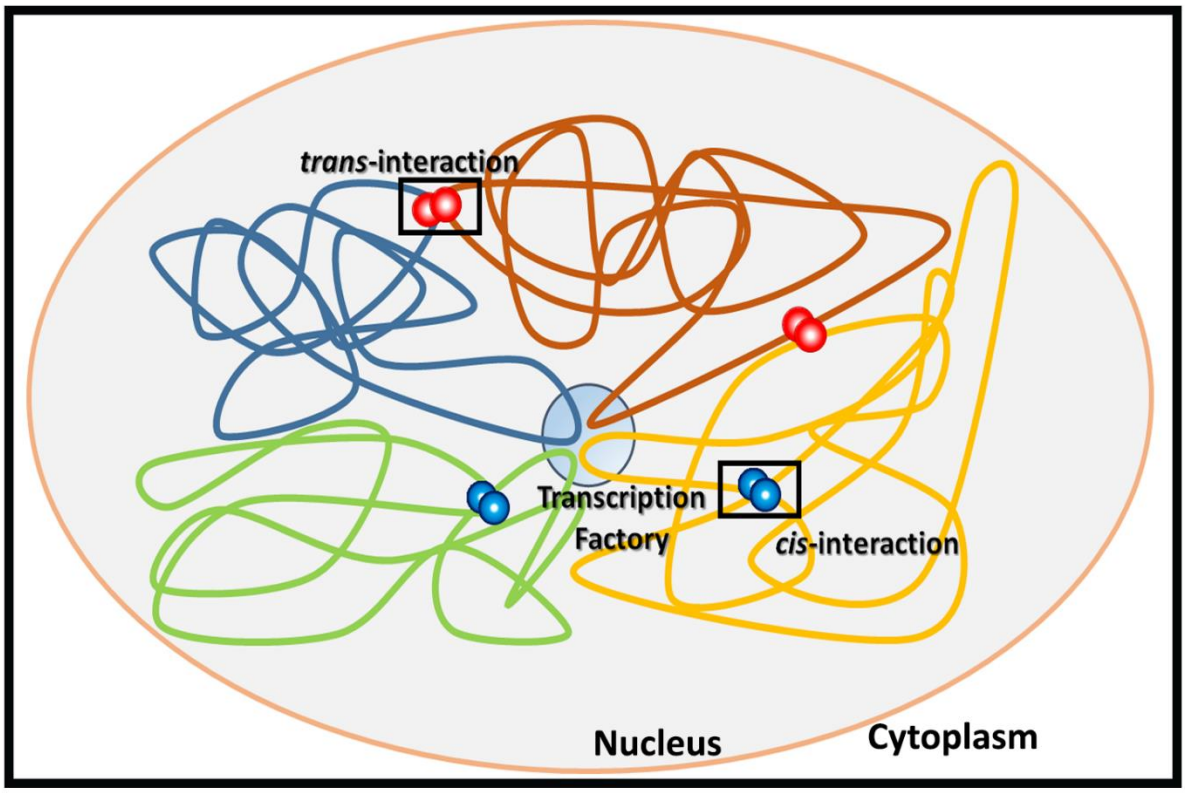

Figure 1-4: Genome Organization: *Cis/Trans* interactions. Active genes exist on chromatin loops that extend outside of chromosome territories. Both *cis* (blue) and *trans* (red) interactions are shown here. Interactions can occur at sites with local concentrations of polymerase II, called transcription factories (blue).

1.3 Nutrient Sensing and Caloric Restriction

1.3.1 How do cells sense nutrients?

Although we know that the body utilizes nutrients from our diets to perform daily functions and maintenance, such as breaking food down into basic building blocks required for use by cells, how do cells actually sense the availability of these building blocks? One major route is through the mammalian target of rapamycin (mTOR) pathway, a major nutrient-sensing pathway within cells that detects input from insulin signalling, amino acid availability, and cellular energy status (i.e. ATP:AMP ratio). The downstream effects of this pathway can result in promotion of cellular growth, repair and autophagy.

1.3.1.1 Mammalian Target of Rapamycin Pathway

The target of rapamycin (TOR) pathway is highly-conserved across species and is a major signalling hub within cells. The TOR, or mammalian (m)TOR signalling cascade, detects and responds to levels of nutrients within the cellular environment and responds accordingly, either directing growth and proliferation or promoting maintenance, repair and autophagy

[reviewed in (Laplante and Sabatini 2012; Laplante and Sabatini 2013)]. Central to the mTOR pathway is the 289 kDa mTOR serine/threonine protein kinase belonging to the phosphoinositide 3-kinase (PI3K) related kinase family which acts as a key catalytic kinase subunit within both the well-characterized mTOR complex 1 (mTORC1) and the less-characterized mTORC2, each with distinct downstream targets. An essential pathway, mTOR deregulation has been associated with numerous human diseases including cancer, cardiovascular disease, type II diabetes and neurodegeneration (Sarbassov *et al.* 2005; Zoncu *et al.* 2011). Furthermore, inhibition of the mTOR pathway has been linked to beneficial impacts in human health in addition to potentially extending lifespan (Bjedov and Partridge 2011; Evans *et al.* 2011; Wilkinson *et al.* 2012; Johnson *et al.* 2013).

1.3.1.2 The Mammalian Target of Rapamycin Complexes 1 and 2

mTOR exists as two structurally-distinct complexes, mTORC1 and mTORC2. mTORC1 is composed of 6 proteins in addition to mTOR: DEP domain containing mTOR-interacting protein (DEPTOR) (Peterson *et al.* 2009), regulatory-associated protein of mTOR (Raptor), mammalian lethal with sec-13 (mLST8), tti1/tel2, and proline-rich AKT substrate 40kDa (PRAS40) (Takahara *et al.* 2006; Wang *et al.* 2007). Within the mTORC1 complex, DEPTOR is an mTOR inhibitor (Peterson *et al.* 2009), whilst Raptor regulates the assembly, localization and substrate binding of mTORC1, tti1/tel2 is responsible for assembling and the stability of mTORC1 (Kaizuka *et al.* 2010). PRAS40 binds and inhibits mTOR under serum or nutrient deprivation (Vander Haar *et al.* 2007; Laplante and Sabatini 2012). The function of mLST8 remains unknown (Kim *et al.* 2003; Jacinto *et al.* 2004).

mTORC2 is poorly characterized in comparison to mTORC1; however, it is proposed to be involved in cytoskeletal organization, with recent work documenting that mTORC2 is insensitive to nutrients in the local environment; however, responds to growth factor signalling. As with mTORC1, mTORC2 also contains DEPTOR, mLST8 and tti1/tel2, which exhibit the same functions in both complexes. Further to these protein components, mTORC2 also consists of: rapamycin-insensitive companion of mTOR (RICTOR), protein observed with rictor 1 and 2 (Protor 1/2) and mammalian stress-activated kinase-interacting protein 1 (mSin1). RICTOR functions to regulate assembly and substrate binding of mTORC2 (Jacinto *et al.* 2004; Sarbassov *et al.* 2004), whilst protor 1/2 increases activation of SGK1 mediated by mTORC2. mSin1 complements protor 1/2, regulating mTORC2 assembly and interaction with SGK1 (Jacinto *et al.* 2004; Frias *et al.* 2006).

1.3.1.3 Activation and Inactivation of the Mammalian Target of Rapamycin Pathway

mTORC1 is activated by a number of upstream signals such as growth factors (insulin), nutrients (amino acids) (Blommaart *et al.* 1995; Hara *et al.* 1998) and cellular energy status (ATP:AMP ratio) (Inoki *et al.* 2003). mTORC1 responds to these inputs in order to control and direct downstream processes (Figure 1-5). Although all these signals are sensed via the major mTORC1 complex, the upstream pathways to mTORC1 activation are slightly varied.

Growth factors (such as insulin-like growth factor 1 (IGF1)) activate mTORC1 through the PI3K-phosphoinositide-dependent kinase 1 (PDK1)-AKT pathway (reviewed by (Laplante and Sabatini 2013)). Activated AKT phosphorylates the tuberous sclerosis complex 2 (TSC2) causing inhibition of TSC1 (Inoki *et al.* 2002; Manning *et al.* 2002; Roux *et al.* 2004; Ma *et al.* 2005). The resulting complex has GTPase activating protein (GAP) activity for the Rheb GTPase. GTP-loaded RHEB binds to the mtor catalytic domain, activating mTORC1, although the precise mechanisms behind this binding are unclear. Alternatively, nutrient signalling (amino acids) activates mTORC2 via RAS-realated GTP-binding protein (RAG) family of small GTPases, with a RAG heterodimer mediating translocation of mTORC1 to the surface of a lysosome from the cytoplasm (Bar-Peled and Sabatini 2014). On the lysosome membrane, mTORC1 is activated by RHEB (Saucedo *et al.* 2003). Alternatively, in response to a high ATP:AMP ratio, mTORC1 is activated by AMPK inhibition. Conversely, mTORC2 regulation (activation and inhibition) is poorly understood. Growth factors are proposed to stimulate mTORC2 through PI3K-dependent association of mTORC2 with the ribosome; however, more research is needed to form a complete picture of mTORC2 regulation and function.

A number of non-nutrient based inputs also exist for the mTOR pathway. These pathways are essential during development and include; Notch (involved in controlling cell proliferation (Bray 2006)), Hippo (which determines organ size via controlling cell number (Zhao *et al.* 2011)) and WNT (which promotes expression of genes involved in cell proliferation, differentiation, polarity and migration (Niehrs 2012)) signalling pathways. When hyper-activated, Notch signalling increases expression of RAPTOR, promoting mTOR-RAPTOR interactions and therefore promoting mTORC1 signalling (Pajvani *et al.* 2013). The major downstream effector of the Hippo signalling pathway is the yes-associated protein (YAP), which is phosphorylated and inhibited by the Hippo pathway kinase large tumor suppressor homologue (LATS). The hypo-phosphorylated YAP translocates into the nucleus, inducing and inhibiting transcription of genes encoding proteins that promote proliferation and

apoptosis. Therefore, inhibition of YAP by Hippo inhibits proliferation and activates apoptosis. YAP further promotes transcription of the micro-RNA mir-29 which inhibits translation of phosphatase and tensin homologue (PTEN), activating PI3K signalling and therefore both mTORC1 and mTORC2 (Tumaneng *et al.* 2012; Shimobayashi and Hall 2014).

WNT signalling activates mTORC1 via inhibition of the TSC1/2 complex. WNT is activated via binding of the WNT ligand to the cell surface receptor Frizzled and the co-receptors low-density lipoprotein receptor-related protein 5 (LRP5) or LRP6 (MacDonald and He 2012). Activation of the receptor results in release of GSK3b, inhibiting phosphorylation of β-catenin which translocates to the nucleus and enhances expression of genes involved in cell proliferation, differentiation, polarity and migration (Niehrs 2012). In the absence of WNT signalling, AMPK dependent phosphorylation of TSC2 by glycogen synthase kinase 3 beta (GSK3B) activates the TSC1/2 complex and inhibits mTORC1 (Valvezan *et al.* 2013).

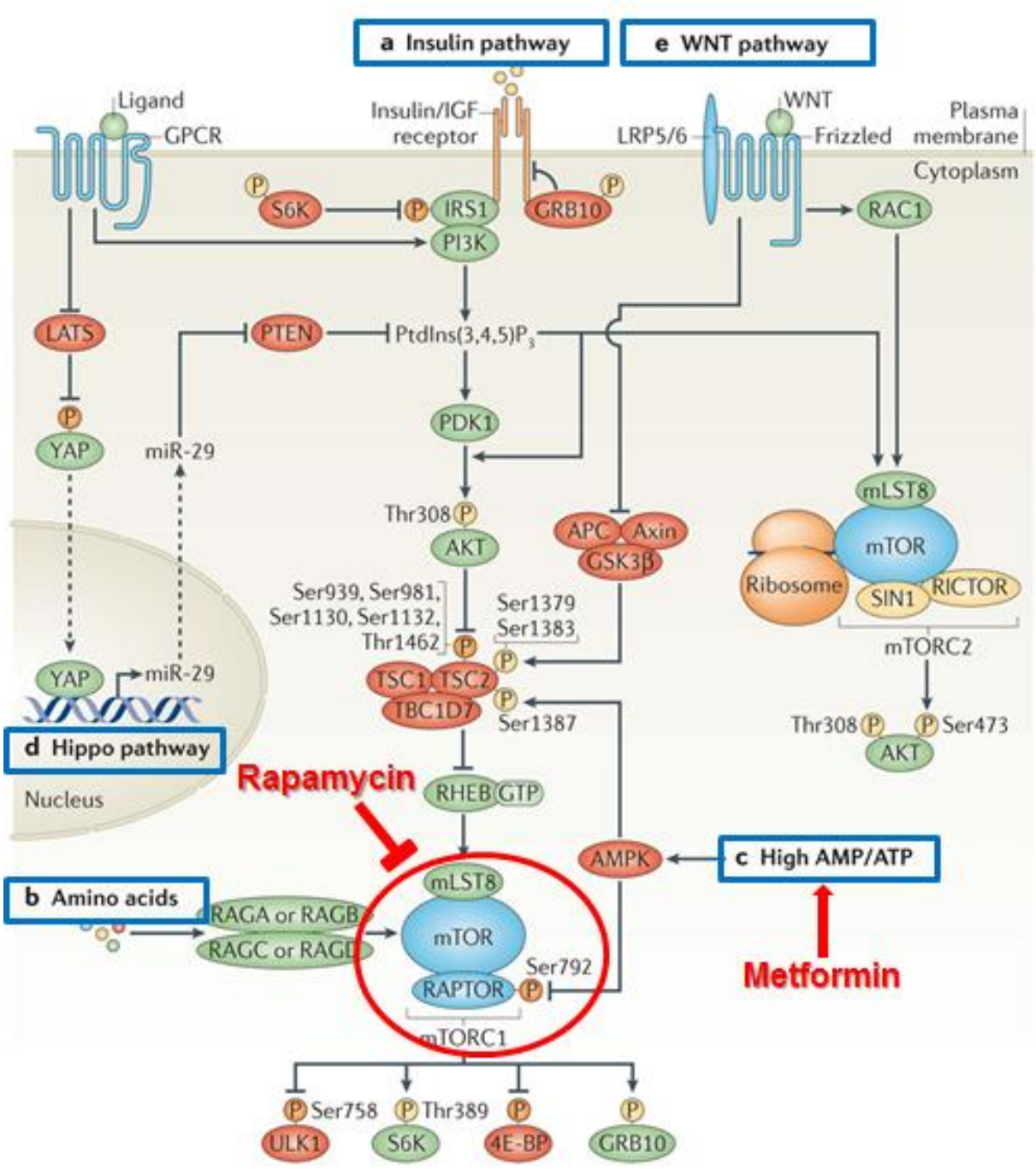

Figure 1-5: Upstream Inputs and Downstream Effects of the Mammalian Target of Rapamycin (mTOR) Pathway. A summary of the upstream and downstream pathways of mammalian target of rapamycin (mTOR) signalling. Upstream inputs and their respective signalling cascades are shown for (A) insulin pathway, (B) amino acids, (C) high AMP/ATP ratio, (D) Hippo pathway and (E) the WNT pathway, highlighted by blue boxes. Downstream effects of these pathways have been documented to include protein and lipid synthesis, autophagy, energy metabolism and cell survival (via mTORC1) and cytoskeletal organization (via mTORC2). The points in this pathway affected by rapamycin and metformin are labelled in red. Reproduced with permission and adapted from (Shimobayashi and Hall 2014).

1.3.1.4 Downstream of the Mammalian Target of Rapamycin Pathway

The mTOR pathway (specifically via mTORC1) has a number of downstream effects to complement its numerous inputs. These downstream processes include protein synthesis, regulating the synthesis of lipids required for cells to generate membranes, positively regulating cellular metabolism and ATP production and negatively regulating autophagy and the biogenesis of lysosomes.

Protein synthesis is perhaps one of the best characterized downstream processes mediated by the mTOR pathway, via the induction of ribosome biogenesis and mRNA translation (Hands *et al.* 2009). Under conditions favourable for growth, protein synthesis is promoted by mTORC1 via phosphorylation of eukaryotic translation initiation factor 4E (eIF4E)-binding protein 1 (4E-BP1) and S6K1. As a result of this phosphorylation, binding of 4E-BP1 to eIF4E is prevented, enabling eIF4E to promote cap-dependent translation (Richter and Sonenberg 2005; Ruvinsky and Meyuhas 2006). S6K also phosphorylates ribosome protein S6 (S6). In the presence of nutrients, protein synthesis machinery is upregulated by mTORC1. This is achieved via activation of the regulatory element tripartite motif-containing protein-24 (TIF1A) and via phosphorylation and inhibition of the Pol II repression Maf1, therefore inducing 5S rRNA (Mayer and Grummt 2006)and tRNA transcription (Kantidakis *et al.* 2010; Shor *et al.* 2010). In this way, mTORC1 acts via mRNA translation initiation and progression to influence the rate of protein synthesis within cells (Ma and Blenis 2009; Johnson *et al.* 2013). In *Saccharomyces cervisiae*, *Caenorhabditis elegans*, *Drosophila melanogaster* and *Mus musculus*, regulation of mRNA translation has been associated with increased longevity (Kaeberlein and Kennedy 2011), with global reduction of mRNA translation attenuating ageing, inducing a shift towards maintenance of protein homeostasis in response to protein aggregation and oxidative damage (Kaeberlein and Kennedy 2007). It could be argued that the observed changes in longevity result from the attenuation of age-associated pathologies in response to a decline in mRNA translation; however, evidence in *Saccharomyces cerevisiae*, *Caenorhabditis elegans* and *Drosophila melanogaster* indicates that the differential translation of specific mRNAs may be of greater influence on lifespan, with enhanced translation efficiency of metabolic and stress genes (Johnson *et al.* 2013).

A second highly-regulated process downstream of mTORC1 is autophagy; a multi-step catabolic process in which proteins and cellular components are degraded and recycled (Codogno *et al.* 2012). Inhibition of mTORC1 under conditions of low nutrients results in an increase in autophagy. mTORC1 mediates autophagy through unc-51-like kinase 1 (ULK1),

autophagy-related gene 13 (ATG13) and focal adhesion kinase family interacting protein of 200 kDa (FIP200) (Ganley *et al.* 2009; Hosokawa *et al.* 2009; Jung *et al.* 2009). As a result of mTORC1 inhibition, autophagosomes form and engulf cytoplasmic proteins and organelles, fusing with lysosomes to degrade cellular components and recycle building blocks. In the presence of nutrients, mTORC1 phosphorylates ULK1, preventing interaction with AMPK, inhibiting autophagy. mTORC1 impacts autophagy mechanisms such as the regulation of death-associated protein 1 (DAP1, a suppressor of autophagy) (Koren *et al.* 2010) or through a mammalian orthologue of Atg18 in yeast (Hsu *et al.* 2011). Autophagy is becoming a key player in contributing towards improved health and lifespan. Autophagy declines with age; this declination could result in the accumulation of cellular damage (Cuervo 2008; Johnson *et al.* 2013). Inhibition of TORC1, therefore activating autophagy, has been reported to maintain cellular function during ageing by degrading aged cellular components (Hansen *et al.* 2007; Alvers *et al.* 2009), with age-associated diseases such as cancer and diabetes being linked to dysregulation of autophagy (Mizushima *et al.* 2008; Johnson *et al.* 2013).

1.3.2 The Impact of Dietary Restriction on the Mammalian Target of Rapamycin, Genome Function, Organization and Longevity

1.3.2.1 Dietary Restriction

Dietary restriction (DR), the reduction of nutrient intake without inducing malnutrition, has been demonstrated to increase health and lifespan in numerous model organisms. In 1935, the first published DR studies were conducted and demonstrated increased lifespan of *Rattus norvegicus* (brown rat) (McCay *et al.* 1935), with similar results observed in yeast, worms (Walker *et al.* 2005), flies (Metaxakis and Partridge 2013), fish (Inness and Metcalfe 2008), dogs (Kealy *et al.* 2002), non-human primates (Bodkin *et al.* 2003; Mattison *et al.* 2012; Colman *et al.* 2014) and humans (McCay *et al.* 1935; Bordone and Guarente 2005). Not only was lifespan extended in these model organisms, but evidence indicated that DR delayed the onset of age-related disease and improved patient outcomes when used alongside cancer therapies (Champ *et al.* 2013). Furthermore, DR is nearly as effective when initiated in adult rodents as in those treated early in life (Weindruch and Walford 1982). However, in *Mus musculus* (mice) with varied genetic backgrounds, it was demonstrated that lifespan extension by DR may not be universal, with the majority of mice exhibiting a shortened lifespan (Liao *et al.* 2010). Advanced maternal age has often been associated with deleterious effects on offspring. In the microscopic metazoan *Brachionus manjavaos*, maternal DR partially rescued these deleterious effects in female but not male progeny (Gribble *et al.* 2014). Combined, these

data provided justification for studies in both non-primate and non-human primate model organisms.

Findings in *Macaca mulatta* (rhesus macaques), a model organism that exhibits ageing phenotypes and pathologies similar to that of humans (Ramsey *et al.* 2000; Raman *et al.* 2005; Fischer and Austad 2011), were contradictory. Bodkin, *et al.*, (Bodkin *et al.* 2003) demonstrated an increase in the average age of death in DR macaques; however, the sample size was small. This delayed death in the macaques was associated with prevention of age-related diseases and hyperinsulinemia (Bodkin *et al.* 2003). A further study in which 76 rhesus monkeys underwent DR also demonstrated increased longevity and later onset of disease when compared to non-DR animals (Colman *et al.* 2009; Colman *et al.* 2014). Contradicting these results, a parallel study demonstrated no significant difference in lifespan between DR and non-DR animals (Mattison *et al.* 2012). Re-analysis of these data by Colman *et al.* (Colman *et al.* 2014), concluded that animals in both DR and non-DR groups of the parallel study were underweight at the start of the trial, perhaps already having undergone a form of DR (Mattison *et al.* 2012; Colman *et al.* 2014). Further study attempted to elucidate the above findings and indicated that at any time point, the non-DR macaques had 2.9 times the rate of death from age related pathologies (such as cardiovascular disease) compared to animals under DR (Colman *et al.* 2014). Long term studies in rhesus monkeys have demonstrated that DR decreases the metabolic cost of movement and does not lead to a decrease in physical activity during ageing, contrary to short term DR (Yamada *et al.* 2013). DR in both non-human primates and humans has been demonstrated to have a positive effect on the risk factors of cardiovascular disease – a disease often associated with ageing (Cruzen and Colman 2009). For all studies it is important to consider where the rhesus macaques originated, their genetic background and how they were raised. These factors may influence the outcome of the animal trials, especially given that DR has been documented to have beneficial effects even if started late in life, or in early life influencing later life (Weindruch and Walford 1982). The studies provide data to support DR as a method of lifespan extension across multiple species, delaying the onset of age-related pathologies, with some evidence linking the beneficial effects of DR to changes in DNA damage accumulation and chromatin structure. The positive impact of DR in non-human primates further supports the proposal of an increase in health and lifespan as a result of depleted nutrient availability in tissue culture.

1.3.2.2 Dietary Restriction and Mechanisms of Promoting Longevity

A number of potential hypotheses exist as to how humans age, and therefore specifically how DR can promote longevity. One hypothesis states that reduced levels of reactive oxygen species (ROS) and increased DNA repair are responsible for promoting increased lifespan (Ray *et al.* 2012). Reactive oxygen species (ROS) can cause DNA damage, with reduction in ROS reducing DNA damage, and therefore decreasing the chance of mutations that could lead to cancer, often considered an age-associated disease. Evidence of DR reducing ROS has been reported in rat tissues (Cabelof *et al.* 2002; Um *et al.* 2003), although this is controversial with some data indicating that ROS are not reduced enough to have a significant impact on DNA damage (Kabil *et al.* 2007). Other hypotheses suggest that human ageing is impacted by circulating glucose and insulin, with DR decreasing levels of both. Decreased levels of both glucose and insulin have concomitantly been observed with an increased in lifespan in numerous model organisms (Kannan and Fridell 2013; Murphy and Hu 2013; Zhang and Liu 2014). The third hypothesis links ageing with circulating growth hormone and IGF1 levels (Fontana *et al.* 2008; Fontana *et al.* 2015), whilst the fourth suggests that cells move from proliferation and growth to maintenance and repair (Calabrese *et al.* 2011). Again, DR has been documented to potentially work via these hypotheses. These hypotheses are based on the mTOR pathway, specifically the upstream sensing of nutrients that dictates the outputs of this pathway.

Inhibition of the mTOR pathway has similarly been associated with promoting health and lifespan. DR is one manner in which mTOR may become inhibited, most likely through decreased levels of amino acids, growth factors and glucose/insulin. Specifically, as a result of DR, AMPK phosphorylates TSC1/2 as previously described, inhibiting TORC1 and the downstream signalling cascade (Laplante and Sabatini 2009). The sirtuin deacetylase family member SIRT1 is also stimulated in response to decreased energy levels, increasing cellular levels of nicotinamide adenine dinucleotide (NAD) (Lau *et al.* 2014). SIRT1 is a deacetylase and targets LKB1. Deacetylation of this protein further drives activation of AMPK and inhibits mTOR (Lan *et al.* 2008). AMPK and SIRT1 share common targets, such as p53, suggesting these proteins could be essential in controlling DR mediated changes in gene expression that promote health and lifespan. A number of potential mimetics of DR have been identified, including the compounds rapamycin and metformin, which have also been identified to promote health and lifespan in model organisms, potentially via modulation of the mTOR pathway.

1.4 Rapamycin

1.4.1 Overview

Rapamycin, a macrocyclic lactone-based compound, was first isolated from the bacterium *Streptomyces hygroscopicus* found in the soil of Easter Island (Sehgal *et al.* 1975). Structural similarities identified between rapamycin and the antibiotic FK506 prompted follow-up studies demonstrating the functionality of rapamycin as an antibacterial and antifungal agent and immunosuppressant (Abraham and Widerrecht 1996). As a result, rapamycin is now commonly-used in human patients following organ transplantation (Camardo 2003). Rapamycin is a well-known inhibitor of the mTOR pathway (Dumont and Su 1996), resulting in the downstream decrease in cap-mediated protein translation (Richter and Sonenberg 2005) and an increase in autophagy (Jung *et al.* 2010); both associated with promoting health and lifespan. Furthermore, rapamycin has been reported to ameliorate age-associated phenotypes, decrease cellular proliferation and increase autophagy in numerous cell-based models, including: cancer (Shapira *et al.* 2006; Fang *et al.* 2011; Suzuki *et al.* 2011), cardiovascular disease (Das *et al.* 2014), the premature ageing disease HGPS (Cao *et al.* 2011) and neurodegenerative diseases (Santos *et al.* 2011). Rapamycin has also been documented to extend the health and lifespan of a variety of model organisms, including *S. cerevisiae* (Powers *et al.* 2006), *D. melanogaster* (Bjedov *et al.* 2010) and *M. musculus* (Miller *et al.* 2014).

1.4.2 Mechanism

Rapamycin, and many derivatives known as ‘rapalogs’, have been extensively demonstrated to inhibit the mTORC1 complex, thus preventing protein and lipid synthesis and energy metabolism, whilst up-regulating autophagy (Dumont and Su 1996). Chronic rapamycin treatment has similarly been documented to inhibit mTORC2 (Jacinto *et al.* 2004; Sarbassov *et al.* 2004; Sarbassov *et al.* 2006), although the downstream impact of this inhibition is poorly understood and an open area of research. Rapamycin, and its rapalogs, achieve inhibition of mTOR by forming a complex with FK506 binding protein -12 (FKBP12), a 12 kDa cytosolic protein found in all eukaryotes (Dumont and Su 1996; Shimobayashi and Hall 2014). The rapamycin-FKBP12 complex then directly binds mTORC1, inhibiting its kinase activity (Figure 1-6). This mechanism is poorly characterized; however, crystallography of an mTOR-mLST8 complex revealed that the catalytic cleft of the mTOR kinase domain is highly restricted (reviewed in (Shimobayashi and Hall 2014)). *In vitro*, binding of rapamycin by FKBP12 inhibits mTOR. Auto-phosphorylation and phosphorylation of 4EBP1, are also indicative of changes in the FKBP-rapamycin-binding (FRB) domain supporting this theory on the influence

on the catalytic domain (Marz *et al.* 2013). Rapamycin has also been demonstrated as binding with a lower affinity to the FRB domain in the absence of FKBP12 [76].

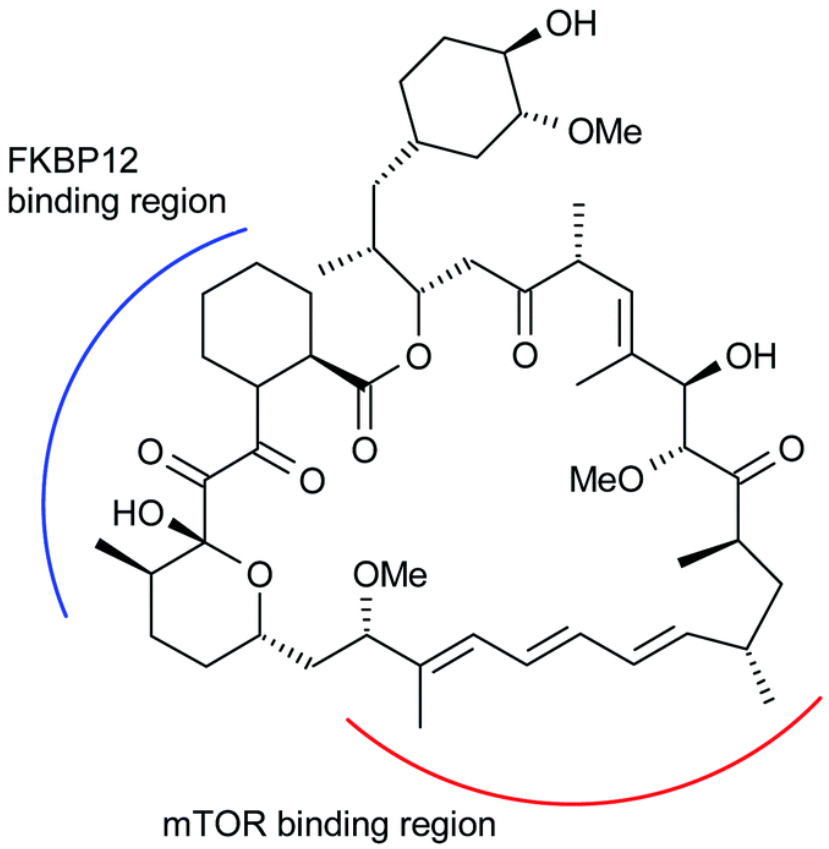

Figure 1-6: Rapamycin Chemical Structure. The chemical structure of the rapamycin with the FKBP12 binding site shown (blue). Components of the TOR protein (bottom) are also shown, with the site at which rapamycin binds (FRB, red) to inhibit mTOR activity highlighted. Reproduced with permission and adapted from (Bauer and Bronstrup 2014) .

1.4.3 Rapamycin, Genome Function and Longevity

Rapamycin functions as an immunosuppressant; however, an unusual side effect of this compound is the extensively-documented increase in both health and lifespan of model organisms treated with the drug. This extension is likely the result of downstream changes in genome function as a result of mTOR inhibition; however, these downstream changes in gene expression are poorly understood.

The accumulation of cells in senescence (no longer able to divide and grow) has been extensively linked to disease, ageing and the ageing phenotype (Kong *et al.* 2011). The clearance of senescent cells has been documented to improve symptoms of age-associated

diseases, such as decline in skeletal muscle and formation of cataracts, in mice (Baker *et al.* 2011). Mesangial cells (MC) entered senescence as a response to high glucose, increasing mTOR expression (likely as a result of excess nutrient availability) and decreased SIRT1 expression (Zhang *et al.* 2012). rapamycin treatment of MC interfered with senescence, concomitant with an increase in SIRT1 expression (Zhang *et al.* 2012). The senescence associated secretory phenotype (SASP) is a process in which pro-inflammatory cytokines are secreted from senescent cells into the local tissues, inducing further deleterious effects in the surrounding environment and is extensively linked to the ageing phenotype (Coppe *et al.* 2010). In macrophages, inhibiting SIRT1 results in the overexpression of inflammation associated genes (*tumour necrosis factor (TNF)-α, interleukin (IL)-6*) through nuclear factor (NF)-κB signalling, with rapamycin-treatment ameliorating SIRT1 inhibition and reducing NF-κB mediated inflammation (Takeda-Watanabe *et al.* 2012). rapamycin has further been linked to cytokine expression and regulation in numerous cell-types, although reports are conflicting. In orbital fibroblasts, rapamycin suppressed *programmed cell death 4* (*PDCD4)* degradation, therefore increasing TNFα induced IL-6 and IL-8 secretion (Lee *et al.* 2013). Experiments conducted in human macrophages were in agreement with these findings, with rapamycin increasing TNF, IL-6 secretion and decreasing IL-10 levels (Su *et al.* 2015). However, in human oral keratinocytes, suppression of toll-like receptor 3 (TLR3) and resultant nuclear factor-kB (NF-κB) signalling by rapamycin inhibits the production of interleukin-1 beta (*IL-1β),* *TNFα* and *IFNβ,* but increased IL-12p70 production (Zhao *et al.* 2010). Similarly, in senescent fibroblasts treated with rapamycin a decrease in cytokine production was observed (Laberge *et al.* 2015). With SIRT1 noted as inhibiting NF-kB activity, it is likely that it is essential in regulating ageing during the ageing process, reducing inflammation-linked signalling and promoting health and longevity in response to rapamycin. Furthermore, although it is clear that inflammation and SASP are core to the ageing process, there is conflicting evidence in response across various cell lines. Therefore, it is likely that this response is influenced by species, cell type and cell cycle state in addition to dose and length of rapamycin treatment. In the epididymal white adipose tissue of mice treated with rapamycin for 6 months, just 6 down-regulated genes were identified (Fok *et al.* 2014). This finding further solidifies that argument that response to rapamycin is tissue/dose/time-dependent. It is possible that cells acclimatise to long-term exposure of rapamycin. This is further supported through studies that document chronic rapamycin exposure as inducing inhibition of TORC2 under the same concentrations that only activate TORC1 under short-term exposure (Sarbassov *et al.* 2006).

1.5 Metformin

1.5.1 Overview

Metformin, (N,N- dimethylimidodicarbonimidic diamide), derived from the French Lilac (*Galega officinalis*), is a common guanidine-based hypoglycaemic agent used in the treatment of patients with type II diabetes (TIID) (Figure 1-7) (Witters 2001). Metformin functions to inhibit hepatic gluconeogenesis and increases muscle sensitivity to insulin (Hundal *et al.* 2000; Zhou *et al.* 2001). Although the mechanism by which metformin functions is poorly understood, it is proposed that the compound mimics DR, acting indirectly through AMPK to inhibit mTOR (Zhou *et al.* 2001). Previously, inhibition of mTOR has been associated with health and lifespan extension across numerous model organisms; treatment with metformin has demonstrated similar effects, decreasing cancer incidence in TIID patients treated (Evans *et al.* 2005) and extending health and lifespan in some model organisms (Onken and Driscoll 2010; Anisimov *et al.* 2011; Martin-Montalvo *et al.* 2013), although in others no significant impact is observed (Smith *et al.* 2010; Slack *et al.* 2012). Though these findings are somewhat well-documented, the impact of metformin on genome function (changes in gene expression) and genome organization are poorly understood.

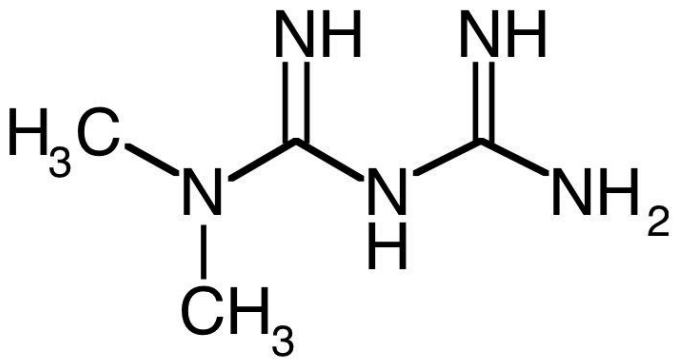

Figure 1-7: The Chemical Structure of Metformin (N,N- dimethylimidodicarbonimidic diamide). The chemical structure of metformin. In the commonly used biguanide, metformin is associated with hydrochloride.

1.5.2 Mechanism

Metformin has been widely used in T2D treatment for over 50 years (Rena *et al.* 2013). Despite this, the mechanisms behind metformin function at the cellular/molecular level are poorly documented, remaining a great question for diabetes research. In recent years, canonical and non-canonical pathways for the action of metformin have been proposed.

Metformin is thought to activate the major cellular energy sensor and regulator of homeostasis, AMPK (Zhou *et al.* 2001; Hardie *et al.* 2012). AMPK is highly-conserved and in most species, including humans, exists as a heterotrimer, containing an alpha (α) catalytic subunit and two regulatory sub units, beta (β) and gamma (γ) (reviewed in (Hardie 2011)). It is important to note that each subunit has multiple isoforms encoding it; α (α1 and α2), β (β1 and β2) and γ (γ1, γ2 and γ3) (Hardie 2007). AMPK is activated in response to energy stresses that increase either cellular ADP:ATP or AMP:ATP ratios (Hardie *et al.* 2012). Ratios are altered by decreasing catabolic production of ATP (e.g. by nutrient deprivation) or by promoting ATP usage (e.g. exercise). Specifically, as a result of lowered ATP levels, AMP or ADP directly binds to the γ subunit of AMPK, causing conformational changes that normally protect against phosphorylation and activation of AMPK (Oakhill *et al.* 2011; Xiao *et al.* 2011). Metformin has been documented to cause mild inhibition of the mitochondrial respiratory-chain complex I. Therefore, it is possible that upstream of AMPK, metformin alters production of ATP in mitochondria, thus inducing changes in ADP:ATP/AMP:ATP ratios (El-Mir *et al.* 2000; Owen *et al.* 2000; Zhou *et al.* 2001). In addition to the conformation changes of AMPK, it has been documented that phosphorylation by the serine/threonine kinase liver kinase B1 (LKB1) may be directly involved in mediating and activating AMPK at Thr172 (Hawley *et al.* 2003; Woods *et al.* 2003; Shaw *et al.* 2004). Activation of AMPK results in the inhibition of mTOR signalling and results in similar downstream influences, including promotion of autophagy (either directly through ULK1 or indirectly) and inhibition of protein synthesis, cell growth and proliferation. Although well reported as involved in cellular response to metformin, it is unlikely that the compound directly binds to AMPK, or the activator LKB1, as metformin did not affect phosphorylation of AMPK by LKB1 in cell-free assays (Hardie 2006).

Metformin has also been associated with a number of pathways acting independently of AMPK (Ben Sahra *et al.* 2011). In a mouse study in which AMPK was knocked down, it was documented that AMPK was not required for the anti-hyperglycaemic effects of metformin (Foretz *et al.* 2010), with similar results documented in prostate cancer cells (Ben Sahra *et al.* 2008). One group suggests that the inhibitory effects of metformin on the mitochondria may

result in direct change in gluconeogenesis, bypassing AMPK activation (Owen *et al.* 2000). Other mechanisms, such as the up-regulation of DNA damage inducible transcript 4 (DDIT4) expression in a p53 dependent manner have been identified (Ben Sahra *et al.* 2008). DDIT4 is up-regulated in response to DNA damage, nutrient depletion, glucocorticoid and insulin and is a target gene of hypoxia-inducible factor 1α (HIF1α) (Ellisen *et al.* 2002; Shoshani *et al.* 2002). DDIT4 has further been documented to regulate mTOR (Brugarolas *et al.* 2004), linking AMPK-independent signalling back to mTOR regulation of the cell.

1.5.3 The Impact of Metformin on Genome Function and Longevity

An unexpected, yet beneficial, side effect of metformin is its association with extending both health and lifespan *in-vitro* and *in-vivo*. Numerous studies report increased apoptosis and decreased proliferation of various cancer cell lines (e.g. lung (Kato *et al.* 2012), retinoblastoma (Leclerc *et al.* 2013) and oesophageal squamous cell carcinoma (Li *et al.* 2014)) in response to metformin treatment. Patients with TIID treated with metformin have been reported to have a lower incidence of cancer than control TIID patients (Evans *et al.* 2005). Furthermore, model organisms (*C. elegans* (Cabreiro *et al.* 2013), *M. musculus* (Martin-Montalvo *et al.* 2013)) treated with metformin have documented health and lifespan extension, although these benefits are not without controversy, with no health or lifespan extension reported in *D. melanogaster* (Slack *et al.* 2012; Na *et al.* 2015) and *R. norvegicus* (Smith *et al.* 2010). Furthermore, metformin has proven useful in treating patients with metabolic syndrome; a condition which often exhibits age-associated conditions, such as cardiovascular disease, cancer and inflammatory disorders (Orchard *et al.* 2005; Ashinuma *et al.* 2012; Song *et al.* 2012; Alimova *et al.* 2014; Brodowska *et al.* 2014; Feng *et al.* 2014; Xu *et al.* 2015). Under conditions of excess nutrients, AMPK and SIRT1 (a deacetylase), are functionally down-regulated. Metformin induces the activation of both of these proteins (Nelson *et al.* 2012; Arunachalam *et al.* 2014). A target of SIRT1, and involved in the AMPK pathway, is the LKB1 kinase that when deacetylated, further phosphorylates AMPK, driving its activation. Both AMPK and SIRT1 share common targets, such as the p53 tumor suppressor gene.

In human hepatic carcinoma (HepG2) cells, activation of AMPK and SIRT1 results in deacetylation of p53 and reduction of oxidative stress (potentially decreasing DNA damage), impeding p53 activation (Nelson *et al.* 2012). Mouse microvascular endothelial cells (MMEC) exposed to high glucose concentrations and treated with metformin were prevented from entering premature senescence as a result of up-regulated SIRT1 expression, modulating downstream *FOXO1* and p53 (Arunachalam *et al.* 2014). In blood mononuclear cells (MNC)

of patients with carotid artery atherosclerosis, metformin ameliorated the pro-inflammatory response, decreasing *Il-6*, *TNF-α*, and attenuating NF-κB binding activity (Xu *et al.* 2015), with reported lower levels of acetylation likely the result of SIRT1 function. Amelioration of inflammatory genes has also been reported in the muscle and liver of metformin-treated mice, documenting down-regulation of inflammatory-associated *Saa1* and *Saa2* genes and a decrease in inflammatory markers NF-κB and c-Jun N-terminal kinase (JNK) (Martin-Montalvo *et al.* 2013). Concordantly, *cytokine-inducible SH2-containing protein* (CISH), a negative regulator of cytokine signaling, was up-regulated (Martin-Montalvo *et al.* 2013). Martin-Montalvo's group also reported induction of stress-response and antioxidant-linked proteins in mouse livers treated with metformin, including *SOD2*, *TrxR1*, *NQ01* and *NQ02* (Martin-Montalvo *et al.* 2013). Furthermore, in macrophages treatment with metformin decreased production of IL-1β, and increased induction of anti-inflammatory IL-10 (Algire *et al.* 2012; Kelly *et al.* 2015). In contradiction, with other DR and DR mimetics, metformin resulted in increased levels of ROS which up-regulated expression of the *uncoupling protein 2 (UCP2)* transcripts (the protein of which functions to exchange anions and protons between the inner and outer mitochondrial membrane) in epididymal white adipose tissue of mice and in 3T3-L1 adipocytes (Anedda *et al.* 2008). However, inhibition of ROS was observed in macrophages in response to metformin treatment (Algire *et al.* 2012; Kelly *et al.* 2015). Combined, the increase in anti-oxidant genes and inhibition of ROS in some tissue contradicting the increased levels of ROS in others indicates that perhaps the induction/inhibition of ROS in response to metformin may be cell-type specific, and may further be linked to the number of mitochondria in the tissue type. This could also be explained by the treatment concentration of metformin, with higher doses inducing greater stress upon the cell/tissue. Furthermore, together, these data indicate that metformin may inhibit multiple pro-inflammatory pathways via activation of SIRT1 and the repression of NF-κB in addition to the up-regulation of *CISH*, as part of the mechanism influencing health and longevity in response to metformin.

At the genome-wide level, transcript profiles from LoVo colon cancer cells were assessed by microarray (He *et al.* 2015). These analyses revealed that at 8 h, 10 mM metformin induced 134 differentially expressed genes, whilst at 24 h 3061 genes altered expression. It is likely that a cascade-effect occurs as a result of metformin treatment, with core genes changing expression and further impacting downstream transcription. Concentration of metformin has also been documented to have alternative impacts on health and lifespan, with 0.1% (w/w) metformin in the diets of C57BL/6 mice increasing lifespan whilst 1% (w/w) shortened lifespan

(Martin-Montalvo *et al.* 2013). It has previously been suggested that metformin may accumulate in skeletal muscle and other tissues over longer periods of times, resulting in potentially different effects (Musi *et al.* 2002). Furthermore, the concentration of metformin required to activate AMPK in either cultured muscle cells (Turban *et al.* 2012; Rena *et al.* 2013) or isolated rodent muscle tissue *ex vivo* (Zhou *et al.* 2001) was between 1-2 mM/L for 3-16 h, greater than the 4.5 μM/L in plasma following administration of therapeutic doses (Bailey and Turner 1996; Hardie 2007). Rena, *et al.*, (Rena *et al.* 2013) suggest that this evidence indicates no therapeutic effects are observed in muscle cells; however, work by Martin-Montalvo, *et al.*, (Martin-Montalvo *et al.* 2013) have established an extension in lifespan of mice, with significant changes in gene expression following metformin administration. Interestingly, higher concentrations of metformin are noted in the liver when compared to other organs/tissues as a result of oral administration (Wilcock and Bailey 1993) (reviewed in (Rena *et al.* 2013)). This further provides evidence for the tissue-specific action of metformin. Furthermore, B6C3F1 mice also demonstrated lifespan extension; however, results were less significant than their C57BL/6 counterparts (Martin-Montalvo *et al.* 2013). Although *CISH* was consistently one of the most up-regulated genes between the mouse and liver tissues following metformin treatment of C57BL/6 mice, other genes were up-regulated in one but not the other (e.g. *SOCS2* in the liver, *DDIT4* in the muscle) (Martin-Montalvo *et al.* 2013). Therefore, the effects of metformin on genome function may not only be time and dose-dependent, but also strain/tissue-specific.

The interplay between genome function and genome organization is complex, and although an active area of research, many questions remain, including the extent to which disrupted nutrient sensing can impact gene expression (genome function) and how this is linked to genome organization. Furthermore, it is unclear whether or not rapamycin and metformin are mimetics of one another and of dietary restriction, although it is clear that there are key proteins modulating response to these conditions (AMPK/SIRT1). This thesis will attempt to address some of these questions, determining in the same normal human cell line whether or not metformin and rapamycin induce the same effects on genome function and organization and further potentially proposing mechanisms for these effects.

1.6 Summary

Dietary restriction has been linked to increased health and lifespan in numerous model organisms. It is proposed that the inhibition of the mammalian target of rapamycin (mTOR) pathway as a result of decreased nutrient intake is the reason for these beneficial impacts. The

mTOR pathway is well established; however, the impact of this inhibition at the level of genome function (gene expression) and genome organization (folding in three dimensional space) is poorly understood. Both genome function and organization are essential in maintaining healthy cells and are often disrupted in disease. There are several compounds, including rapamycin and metformin, which have been proposed to mimic the beneficial effects of DR. Both compounds have recently been at the forefront of research, with human trials initiated into the impact of metformin on ageing and extensive work on both of these compounds in treating cancer. This thesis will examine the impact of inhibiting nutrient sensing, via rapamycin and metformin treatment, in normal human foreskin fibroblasts (designated 2DD) in order to determine the impact on genome function and organization. This work not only has applications in understanding fundamental biology, but in further understanding how to promote living healthier for longer.

1.7 Hypothesis

Human genome organization (folding in three-dimensional space) and function (gene expression) will be altered in response to rapamycin and metformin-mediated disruption of nutrient sensing.

1.8 Objectives

The objective of my project is to determine how genome function and organization respond to altered nutrient sensing as a function of treatment with either rapamycin or metformin. In order to address the main objective of this thesis, the following questions will be answered:

1) Does disruption of nutrient sensing (via treatment with either rapamycin or metformin) in normal human foreskin fibroblasts induce changes in genome organization?

   a. Does disrupted nutrient sensing as a function of either rapamycin or metformin treatment impact cell growth and proliferation?
   b. Do significant areas of the genome (chromosomes) re-organize in response to disrupted nutrient sensing (via either rapamycin or metformin), therefore indicating changes in gene expression?

2) Are transcript profiles changing in response to rapamycin or metformin mediated disruption of nutrient sensing?

   a. Which genes change expression significantly in response to disrupted nutrient sensing?
   b. Which biological pathways are responding to disrupted nutrient sensing?

2.0 Materials and Methods

2.1 Cell Culture, Cell Counts, Cell Viability and Treatments

Healthy human foreskin fibroblasts, designated 2DD (previously described in (Bridger *et al.* 1993), were grown in 1 X Dulbecco's Modified Eagle Medium (pH 7.7; Corning, USA, Cat #: ca45000-304), containing high glucose (4.5 mg/mL), sodium pyruvate and glutamine. Media was supplemented with 10% fetal bovine serum (FBS) (Gibco, Thermo Fisher Scientific, USA, Cat #: 12483-020) and 1.0% penicillin streptomycin (GE Healthcare Life Sciences, USA, cat #: SV30010). All cells were maintained in a humidified incubator at 37^{o}C, 5.0% carbon dioxide (CO_2) (Fischer Scientific, USA, Model #: 3532). In order to prevent contact inhibition, cultures proceeded no further than 70% confluency (covering an area no greater than 70% of the culture flask). Upon reaching 70% confluency cells were passaged; briefly, cells were incubated in 3 mL TrypLE Express (Life Technologies, USA, Cat #: 12604013) before undergoing centrifugation (174 g, 3 min), aspirating supernatant and re-suspending in 10 mL of culture media. Cell counts were conducted using 20 μL of cell suspension on a 0.0025 mm^2 neubauer improved haemocytometer. Cells were seeded at a density of 3000 cells/cm^2. For cell viability counts, cell suspensions were mixed 1:1 with 0.4% (v:v) trypan blue dye (VWR international, USA, Cat #: CA97063-702), and using a haemocytometer, total stained and unstained cells counted. Fibroblasts were left 24 hours (h) after passaging to re-adhere before commencing treatments. All experiments were conducted in fibroblasts less than passage 20.

Quiescence was induced via decreased levels of FBS to 0.5% for 120 h. Media used for rapamycin and metformin treatments was identical to that used for proliferative cultures but included either 500 nM rapamycin (LC Laboratories, USA, Cat #: R-500) dissolved in dimethyl sulfoxide (DMSO), or 0.5 mM/1 mM metformin dissolved in distilled (d)H_2O (Santa Cruz Biotechnology, USA, Cat #: sc-202000a) and filtered through a (polyvinylidene fluoride) PVDF 0.22 μM pore-size syringe filter (Santa Cruz Biotechnologies, USA). Final DMSO concentrations in media were 0.046%, with parallel proliferative cultures treated with DMSO. Media was changed every 2-3 days to ensure drug presence over time. Cell counts following treatments were conducted in the same manner as described above. NB1 hTERT (immortalized NB1 fibroblasts) were grown under the same conditions and treatments carried out consistently.

2.2 Immuno-labelling

Proliferative, quiescent, rapamycin and metformin-treated cells were grown on sterilized 22 mm^2 glass coverslips under the previously described conditions (2.1). Three

biological replicates were conducted. Cells were fixed with 4.0% formaldehyde (FA) in 1 X phosphate buffered saline (PBS, pH 7.0; Sigma Aldrich, USA, Cat #: P5493-1L) for 8 min at room temperature (RT). Cells were washed a further 3 times for 3 min in 1 X PBS and permeabilized with 0.5% Triton X-100/1 X PBS for 15 min before blocking in 1.0% bovine serum albumin (BSA)/1 X PBS for 30 min. Following this, cells grown on coverslips were labelled with 25 μL primary antibody in 1.0% BSA for 1 h in a humidity chamber. Primary antibodies were; rabbit anti-LC3 (Abcam, UK, Cat #: ab48394) (1:2000 dilution) (for detection of autophagosomes associated with autophagy), rabbit anti-STAT5A/B (Abcam, UK, Cat #: ab7969) (1:200) and rabbit anti-STAT5 phospho-tyrosine 694 (Thermo Fisher Scientific, USA, Cat #: J.536.2) (1:100) (for the localization of the STAT5A/B protein). Coverslips were then washed for 2 min in 0.05% TritonX-100/1XPBS at RT. Each coverslip was incubated in 25 μL of secondary antibody, goat anti-rabbit A488 (1:200) (Stratech/Jackson Scientific, UK, cat #: 111-545-003-JIR) in a humidity chamber. All antibodies were diluted in in 1.0% BSA/1 X PBS. Nuclei were counterstained using either 20 μL Hoechst 33342 dye (H33342; Invitrogen, USA, Cat #: h3570) (1:10,000 dilution in mounting media) or 20 μL DAPI (Vector, USA, Cat #: H-1200), mounted onto glass slides and sealed with nail varnish.

For detection of the proliferative marker Ki67, cells were grown and treated as described above (2.1). Three biological replicates were conducted. Cells were fixed with 4.0% FA in 1 X PBS for 10 min at RT. Cells were dehydrated using an ethanol series (70%, 90%, 100%) at 5 min per concentration. Cells on coverslips underwent further extraction with methanol:acetone (1:1 v:v, 5 min RT). Cells were rehydrated in ethanol series (100%, 90%, 70%) at 5 min per concentration before permeabilization with 0.5% Triton X-100/1 X PBS for 15 min and blocked in 1.0% BSA/1 X PBS for 30 min. Incubation with primary antibody rabbit anti-Ki67 (Novacastra, USA, Cat #: NCL-Ki67p_CE) (1:5,000 dilution in 1.0% BSA/PBS) and secondary antibody incubation with goat anti-rabbit A488 (Stratech/Jackson Scientific, UK, Cat #: 111-545-003-JIR) (1:200 dilution in 1.0% BSA/PBS) was conducted for 1 h each in a humidity chamber, washing for 3 min in 0.05% TritonX-100/1 X PBS between antibody incubations. Nuclei were counterstained using either Hoechst 33342 (H33342) dye (1:10,000 dilution in mounting media) or DAPI (Vector, Cat #: H-1200). Images were taken at 40 X magnification with constant exposure times. Grey-scale images were imported into ImageJ (https://imagej.nih.gov/ij/), an image processing software, and an arbitrary threshold selected for all images. Any images containing above threshold were considered positive.

2.3 5-ethynyl-2-deoxyuridine Incorporation

Proliferative, quiescent, rapamycin and metformin-treated 2DD fibroblasts or NB1 hTERTs were grown on glass coverslips under the previously described conditions (2.1). Three biological replicates were conducted. Live cells were incubated for 2 h with 5 μM of 5-ethynyl-2-deoxyuridine (EdU), fixed and permeabilized using the methods previously described for immuno-fluorescence (2.2). Following permeabilization, cells were blocked in 1.0% BSA for 20 min before labelling using the Click-iT reaction cocktail (430 μL 1 X Click-iT reaction buffer, 20 μL copper sulphate ($CuSO_4$), 1.2 μL AlexaFluor555 azide and 50 μL reaction buffer additive) (Life Technologies, USA, Cat #: C10338) and incubated in a humidity chamber for 1 h. Nuclei were counterstained using either H33342 dye (1:10,000 dilution in mounting media) or DAPI.

2.4 Cell Cycle Analysis by Flow Cytometry

For flow cytometry, proliferative, quiescence-induced, rapamycin-treated and metformin-treated cells were grown for 120 h before fixing in a 70% ethanol:1 X PBS solution for 30 min, 4^{o}C. Fixed cells were pelleted at 100 g, 10 min, RT, and washed 2 times in 1 X PBS for 3 min. Fibroblasts were then re-suspended in 1ml dH_2O and 20 μL of propidium iodide solution (VWR International, USA, Cat #: CA421301-BL). 100 μg of RNase was added and samples were incubated at 37^{o}C for 20 min. Analysis was performed using the BD Accuri C6 flow cytometer, flow rate was set to slow and 10,000 events recorded. Events were plotted using forward scatter (FSC, X-axis) and side scatter (SSC, Y-axis) parameters in order to identify single cells, and gates were used to remove cellular debris and doublets from the analysis. A histogram with linear axes plotting fluorescence intensity units (X-axis) against events counted (Y-axis), and gates were set to determine the percentage of cells in G1/G0, S and G2 phase based on DNA content.

2.5 Western Blotting

Western blot analyses were conducted on protein extracts generated from proliferative, quiescent, 500 nM rapamycin-treated, and 0.5 mM/1 mM metformin-treated 2DD fibroblasts at 120 h. Following dissociation of cells from 150 cm culture dishes using 5 mL TrypLE EXpress for 3 min (Life Technologies, USA, Cat #: 12604013) cells were pelleted at 174 g, RT, supernatant removed and disrupted in 300 μL RIPA buffer (25 nM Tris-HCl pH 7.6, 150 mM NaCl, 1.0% NP-40, 1.0% sodium deoxycholate, 0.1% SDS). Protein extracts were quantified using Bradford assay (Biorad, cat #: 500-0006) and loaded with protein equivalents (amount loaded indicated in each figure). Briefly, Bradford solution was diluted 1:5 with dH_2O

and 1 mL added to cuvettes containing a BSA concentration range of 0 μg to 1000 μg in 20 μL volume. Absorbance was measured using the Protein Bradford setting (595 nm absorbance; NanoDrop 2000, Theremo Scientific, USA) and a standard curve plotted. Protein extracts were diluted 1:4, 1:10 and 1:20 in dH2O and 20 mL combined with 1 mL 1:5 Bradford assay. Extracts were then measured against the standard curve to determine protein concentration and extracts were loaded equally in each western blot assay (volume loaded indicated in respective figures). Protein extracts were loaded in 1 X lamelli buffer (2 X: 1.25 mL 1 M Tris-HCl (pH 6.8), 4.0 mL 10% (w/v) SDS, 2.0 mL glycerol, 0.5 mL 0.5M EDTA, 4 mg EDTA, 0.2 mL β-mercaptoethanol (14.3 M), to 10 mL with dH_2O) and run on a polyacrylamide gel with a 5.0% polyacrylamide top-gel in 1 X running buffer (25 mM Tris, 190 mM glycine, 0.1% SDS (pH 8.3) at 100 V for 1h 30 min. Protein was transferred to nitrocellulose membrane in transfer buffer (25 mM Tris, 190 mM glycine, 20% methanol (pH 8.3)) using semi-dry transfer equipment at 30 V for 1 h. The membrane was then blocked in 5.0% skim milk powder in Tris-buffered saline containing 0.5% Triton X-100 (SMP/TBST) for 1 h. The membrane was then incubated overnight in primary antibody diluted in 2.5% SMP/TBST at 4^oC. Primary antibodies used were rabbit anti-LIF (1:500 dilution, Abcam, UK, Cat #: ab113262), rabbit anti-p70-S6 kinase-phospho421/424 (1:500 dilution, Cell Signaling, USA, Cat #: 9204S), rabbit anti-Actin B (1:2000 dilution, Abcam, UK, Cat #: ab8227), rabbit anti-ActC1 (1:500 dilution, Abcam, UK Cat #: ab151787), rabbit anti-STAT5A/B (Abcam, UK, Cat #: ab7969) (1:2000), rabbit anti-phosphor-mTOR (ser2448) (1:500 dilution, Cell Signaling, USA, Cat #: 5536), rabbit anti-LC3b (1:7500, Abcam, UK, Cat #: ab48394), rabbit anti-AMPKα1 (1:500, Millipore EDM, cat #: 15-115), rabbit anti-AMPKα2 (1:500 Millipore EDM, Germany, cat #: 15-115), rabbit anti-AMPKα (Thr172) (1:500, Millipore EDM, Germany, cat #: 15-115)). The membrane was washed 3 X in SMP/TBST for 5 min each before incubating in secondary diluted in 2.5% SMP/TBST for 1 h. Following secondary, the membrane was washed 3 X in SMP/TBST for 5 min each, 1 X in 0.5% TBST and then developed using enhanced chemiluminescence (Fisher Scientific, USA, cat #: 45100100). Secondary antibodies used were goat anti-rabbit horse radish peroxidase (HRP) (1:5000 dilution) or donkey anti-mouse HRP (1:5000 dilution, Jackson Scientific/Cedarlane, UK, Cat #: 715-035-150).

2.6 2D FISH/Chromosome Painting and Erosion Analysis

2DD fibroblasts were grown under proliferative, quiescence-induced, 500 nM rapamycin-treated and 0.5 mM/1 mM metformin treated conditions for 120 h. Probe generation and cell preparation were conducted following the protocol detailed by Mehta and colleagues

(Mehta *et al.* 2010). Briefly, cells were dissociated from the culture flasks using 5 ml Tryple Xpress incubated for 3 min and pelleted at 174 g, RT, before incubating in 75 mM potassium chloride (KCl) for 15 min. Fibroblasts underwent drop-wise fixation with cold 3:1 (v:v) methanol:acetic acid and were washed three times in the same solution. Coverslips were prepared by "huffing" to create moisture to assist the cells in adhering and then cells were added dropwise ~1 foot to the coverslip and incubated at RT for 2 days. Coverslips were warmed and cells denatured for 2 min at 70^{o}C in 70% formamide, 2 X saline sodium citrate (SSC) followed by immediate dehydration in ice cold 70% ethanol. Coverslips then underwent a further dehydration series (90%, 100% EtOH) and left to dry at RT. Probe (15 μL of chromosome X, 10 or 18) was added and the coverslip sealed to a glass slide using rubber cement and incubated overnight in a humidity chamber at 37^{o}C. Probes were generated by Degenerative Oligo Primers (DOP)-PCR of chromosomes containing biotinylated uridine residues (biotin-16-UTP, Roche). The rubber cement was removed, coverslips lifted and washed in wash buffer A (45^{o}C; 50% formamide, 2 x SSC) for 15 min and then wash buffer B (60^{o}C; 0.5 X SCC) for 15 min. Coverslips were transferred to 1 X PBS and underwent immuno-labelling for goat anti-streptavidin-Cy3 (1:200; Vector laboratories, USA, cat #: Ba-0500) for 1 h, goat anti-streptavidin conjugated to biotin (1:200; Cedarlane, UK, cat #: 111-065-003) 1 h and then a second streptavidin-Cy3 for 1 h. A 2 min 0.05% TritonX-100/1 X PBS wash was conducted between each antibody incubation. Samples were mounted in either DAPI of H33342. Photometrics cooled charged-coupled device (CCD; Photometrics) was used to capture digital grey-scale images of random nuclei. Images were false-coloured in Adobe Photoshop (CS6). Smart Capture VP V1.4, a Leica fluorescence microscope (Leitz DMRB) with Plan Fluor 100 × oil-immersion lens was used to collect images. Newly-developed software (using Python coding language) called the Cell Nucleus Analyzer for nuclear segmentation and analysis was used and was based on the analysis software used previously (Croft *et al.* 1999). This software divides the H33342 image into five concentric shells of equal area, the first being the most peripheral and innermost denoting the interior of the nucleus. The script measures pixel intensity of H33342 and the chromosome probe in these five shells. Normalization of the probe signal was conducted by dividing the percentage of the probe by the percentage of H33342 signal in each shell. For each treatment condition (proliferating, quiescence-inducted, rapamycin or metformin-treated) ≥ 35 nuclei were measured for each chromosome. Ratios from each shell were averaged and the standard error of the mean calculated. Data were plotted as bar graphs with the X-axis representing the shell and the Y-axis the % signal chromosome/% signal H33342. Overlapping cells in the images were segmented using a semi-automatic method

based on the watershed algorithm (Vincent and Soille 1991) and user-specified markers. Both 2-tailed Student's T-tests for unequal variance and correlation calculations were performed in Microsoft Excel to demonstrate significant alterations in positioning.

2.7 RNA Extraction

RNA was extracted from proliferative, quiescent and rapamycin treated cells using either Trizol (Invitrogen) or the FastRNA Pro Green Kit with FastPrep-24 instrument (MP Biomedicals) according to the manufacturer's instructions. Briefly, cell samples were added to RNApro^{TM} solution and Lysing Matrix D. Samples were processed in the FastPrep-24 instrument for 40 seconds at setting 6.0 before centrifugation at 12,000 g for 5 min at 4^{o}C. The resulting upper phase was incubated at RTP for 5 min before addition of 300 μl of chloroform and vortexing. Samples were incubated again for 5 min at RTP and centrifuged (12,000 g, 5 min, 4^{o}C). Samples were precipitated using 500 μL of cold 100% EtOH, 20^{o}C, for 30 min. Samples were again centrifuged under the same conditions and resulting pellet washed with cold 75% EtOH, pellet dried and RNA re-suspended in nuclease-free dH_2O. For proliferative, 0.5 mM and 1 mM metformin-treated cells, RNA was extracted using RiboZol (Amresco, cat #: N580-100ML). Specifically, samples were disassociated from the surface of culture dishes using Tryple Xpress and pelleted. Cells were re-suspended in 1 mL RiboZol and incubated at RTP for 5 min. 200 μL of chloroform was added and samples vigorously mixed and incubated at room temperature for 3 min. Samples underwent centrifugation (12,000 g, 5 min, 4^{o}C) and the clear upper-phase separated from the sample. RNA was precipitated via addition of 2.5 X volume 100% EtOH and 1/10th sample volume 1.5 M sodium acetate overnight at -80^{o}C. Samples were pelleted (12,000 g, 15 min, 4^{o}C) and washed in 75% cold EtOH. The pellet was air-dried at RTP and re-suspended in nuclease-free dH_2O. RNA extraction for proliferative, quiescent and rapamycin treated fibroblasts were conducted at the same time for each replicate, as were RNA extractions for proliferative, 0.5 mM and 1 mM metformin treated samples. Three biological replicates were conducted. RNA concentration was determined using the NanoDrop2000 (Theremo Scientific) and aliquots stored at -80^{o}C to avoid RNA degradation from freeze-thaw cycles. Cultures for treatment were expanded from a single flask of fibroblasts to prevent any variation in passage or chronological age of the culture. The integrity of all RNA was determined using a Bioanalyzer (Agilent Technologies) with RNA only with an RNA integrity number (RIN) above 8.40 used for further analysis.

2.8 cDNA Synthesis

For the sample set comprising proliferative, quiescence-induced and rapamycin-treated fibroblasts, 5 μg RNA was used in each reaction with 50 ng of random hexamer used as primers in SuperScriptIII reactions. Specifically, 5 μg total RNA, 1 μL of 50 ng/μL random hexamers, 1 μL 10 mM dNTP mix made up to 10 μL with nuclease free dH_2O were incubated for 5 min at 65ºC. A master mix of 2 μL 10 X RT buffer, 4 μL of 25 mM $MgCl_2$, 2 μL 0.1 M DTT, 1 μL RNasein™ (40 U/μL) (Ambion, Cat #: AM2694) and 1 μL of SuperScriptTM III RT (200 U/μL) (Thermo Fisher; Cat #: 18080051) was added to a total reaction volume of 20 μL. Samples were incubated at 25ºC for 10 min, 50ºC for 50 min and 85ºC for 5 min. Synthesized cDNA was diluted to a total volume of 100 μL dH_2O. For all other samples, 2 μg RNA was used in an initial reaction with 1 μL of 10 μM random primers and 1 μL of 10 mM dNTP mix. Reactions were made to 14.5 μL with nuclease free dH_2O and incubated at 65ºC for 5 min before a further 1 min incubation on ice (ABM, cat #: G177). For the final reaction volume, 5.5 μL of master mix containing 4μL 5X RT buffer, 0.5 μL RNaseOFF Ribonuclease Inhibitor (40 U/μL) and 1 μL EasyScript Plus™ RTase (200 U/μL) was added to the reaction, incubated at 25ºC for 10 min, 50ºC for 50 min and 85ºC for 5 min. Synthesised cDNA was diluted to 200 μL with nuclease free dH_2O.

2.9 Reverse Transcriptase-qPCR

Following cDNA synthesis and dilution, cDNA for proliferative, quiescent and rapamycin-treated samples was further diluted 1:10. For proliferative, 0.5 mM and 1 mM metformin-treated samples, cDNA was further diluted 1:16. 1 μL of sample was used in each 10 μL reverse transcriptase (RT)-qPCR reaction with 300 nM forward and reverse primer, 1.5 μL nuclease free H_2O and 5 μL of qPCR mastermix (either BioRad, cat #: 1725272 or Life Technologies, cat #: 4472908). Each reaction was run in triplicate with no-template controls to ensure there was no contamination. Melt curve analyses were conducted to confirm the presence of single products in each reaction. RT-qPCR results were quantified using five normalizing genes (*PRDX5, EFEMP2, FAU, SPARC* and *FKBP10*) identified from RNA sequencing data. The fold change for each gene of interest was compared to each of the normalizers and the average fold change between the five genes calculated. S.E.M. were calculated for all genes of interest. A complete list of primers used for validation is given (Table 2-1).

Table 2-1: qPCR Primer Sequences

Primer sequences used in the validation of both rapamycin and metformin RNAseq datasets. F represents forward primer; R represents reverse primer sequences. All primers are given in the 5'-3' direction.

Gene/Direction	Sequence (5'-3')	Gene/Direction	Sequence (5'-3')
SPARC F	TACATCGGGCCTTGCAAATAC	**LIF F**	AGATGTCTCCGGGCCCTTAT
SPARC R	GGTGACCAGGACGTTCTTGAG	**LIF R**	ACGATGGGGAGGAGAGACAA
THY1 R	CAGGGATGAGCAAGAGGAATG	**PTGS2 F**	GCCTACTGGAAGCCAAGCAC
THY1 F	CCTGTCTTGGCTGGTAAGTGG	**PTGS2 R**	TAAAGGGACAGCCCTTCACG
PRDX5 R	GCATAGTGAAGGCCCTGAATG	**NR4A1 F**	CCCTGACCCCTGAGTTCATC
PRDX5 F	GGGGTGGAGGAAGTAATCTGG	**NR4A1 R**	TGTAGCCGTCCATGAAGGTG
EFEMP2 R	GCCCAAACCTGTGTCAACTTC	**FAM180A F**	ACCCTGGCCTACACAGCCTA
EFEMP2 F	CGGTTCTCAGAGACCTGGATG	**FAM180A R**	AGGGCCTGGAAGAGGCTAAC
FAU F	CGCATGCTTGGAGGTAAAGTC	**EREG F**	CAAGCTAACCCTGGGGAGTCT
FAU R	TTCTCCTGTTTGGCCACCTTA	**EREG R**	GCATAGGGAACTGTCCACTGC
FKBP10 F	GCCGTGCTAATCTTCAACGTC	**GEM F**	TGCTACCCCTGAGGACCACT
FKBP10 R	GGTGGTCTCATTGCAGGTCTC	**GEM R**	GCTCCCCTATGAGCACCACT
ADH1B F	TCTCCCAGTACACGGTGGTG	**EDNRB F**	CGATGGAGAGATGCCAGTGA
ADH1B R	TGCAGACCCATAACCAGTCG	**EDNRB R**	GTGCTACCTGCCCCTTTGTC
TNXB F	CCCGGAGTGCTATGGATGAT	**SOX 4 F**	GAAGAGGCCTGTTTCGCTGT
TNXB R	GAGTTCTGGGTCACGGTGGT	**SOX 4 R**	GGAGCTGGTAATGGCAGGAG
CYP21A2 F	CTGATCGGTGGCACTGAGAC	**CXCL1 F**	ATTTCTGAGGAGCCTGCAACA
CYP21A2 R	CTGCAGTCGCTGCTGAATCT	**CXCL1 R**	CCCTGCCTTCACAATGATCTC
APOD F	GCATCCAGGCCAACTACTCAC	**TGFA F**	CACATGGGTCACCAGTTGCT
APOD R	GAGGTTAACTGGGGTGGCTTC	**TGFA R**	ACTAGAGGGCAGGGGTCTCC
WISP2 F	ACAGCTGCCGGAACATAAAGA	**CXCL2 F**	GCTTATTGGTGGCTGTTCCTG
WISP2 R	TTCGGTGTGCCTCTCATGTC	**CXCL2 R**	AACACATTAGGCGCAATCCAG
PTGDS F	CGTTGTCCATGTGCAAGTCTG	**HOTAIRM1 F**	TGGGGGTTTCTGTAGGCACT
PTGDS R	TTCGGGTCTCACACTGGTTTT	**HOTAIRM1 R**	TGCACAGGTTCAAGCCATAGA
SFRP4 F	AAAAGCTGTGCAGAGGAGTGG	**LAMA F**	CATCCCTGTCCCTGTCACTG
SFRP4 R	AGGGATGGGTGATGAGGACTT	**LAMA R**	GGCTTGGGTTACTGGTCAGG
CTSK F	GGGACATGACCAGTGAAGAGG	**FOXO3 F**	TCCTCTGGGGGTGATATTGG
CTSK R	GGGCTCTACCTTCCCATTCTG	**FOXO3 R**	AGGCAGGAGACGTGTGACAA
PPL F	AAAGGCAAATACAGCCCCACT	**SATB1 F**	GACGAAGAGGCCATCCAGAC
PPL R	TGTCCACGATGTTCTTCTCCA	**SATB1 R**	TGCCGTGGTGCTTGAGATAG
APOE F	ACGAGGTGAAGGAGCAGGTG	**HIVEP1 F**	TGGATCCCAAGCCTGAACTT
APOE R	GCTCGAACCAGCTCTTGAGG	**HIVEP1 R**	TGGGACATGTTGGCTGAAAG
FABP3 F	ACTTGTGCGGGAGCTAATTGA	**PSG8 F**	GCCCGTGTGTTTGCAGATAA
FABP3 R	GTCAGCAACAGTGCAGTCAGG	**PSG8 R**	CGAGAGCCATCCACAGAATG
LTBP4 F	GGCTGGTCCTGGTTACCACT	**LACC1 F**	TCACATGGGCTCGAAAGATG
LTBP4 R	GTACGAGGCTGGCTGAGTGAC	**LACC1 R**	CAGTTTCATGCCCTGGTTCA
COL14A1 F	ACGACGTGACTGAGAACAGCA	**Neat1 F**	TCAGAGGGTTGTTTTGTTTGG
COL14A1 R	GGCCCTCTGTTAGAGGAGCAT	**Neat1 R**	ATCTGCTGCGTATGCAAGTCT
C3 F	GTCAACCACAAGCTGCTACCC	**SCN5A F**	CTCTTTGGGGCAAGATCCAG
C3 R	GCCAAGCTGGTTCTGAGAAGA	**SCN5A R**	AAGAGGTCCTGGGGGTGATT

RARRES2 F	GCCCCATAGAGACCCAAGTTC	**JAK2 F**	TGATGCTAGCCAGCAAAGATG
RARRES2 R	GTAGAAGCTGTGGGGGTCCTC	**JAK2 R**	CTGGTGGCCTCATGAAGAAAA
IL34 F	CTGAGACTTCAAGGGGTGGTG	**Cables1 F**	AGCCAAAATTGGAAGTGACCT
IL34 R	ACAGAATCCCCCTCAAAGGAA	**Cables1 R**	CACTAACACCGGGAATTCAAA
EGR2 F	TAAGTGTGGAGGGCAAAAGGA	**MTMR8 F**	GGAGAATGGCACCCTATCCA
EGR2 R	CACAACCTGGAGACCCAACTC	**MTMR8 R**	TAAGGCTGCCCACAATCTCA
IDI1 F	CTGTTGACATTTGGGCTGGAT	**LAMB4 F**	GGGCTCTGTTGAACCTGTGA
IDI1 R	CTGTGGGTGTCACATGAGAGG	**LAMB4 R**	CATTTCAACCTCCAGCCACA
IGF2 F	AAGTCGATGCTGGTGCTTCTC	**RARB F**	AGGCTGGTCTACCACCTGGA
IGF2 R	ACAGACGAACTGGAGGGTGTC	**RARB R**	AATTAGCCCCTTGGCATCAA
C1R F	AGCTCGTCTTCCAGCAGTTTG	**GNG4 F**	CATCATTCCAGTGCCTGCAT
C1R R	CCCCAGGCTTTTCTTATCAGC	**GNG4 R**	GGAGGCGTTTTCATCACACA
CFH F	TATAGACGTTGCCTGCCATCC	**Hbb R2 F**	AAGCTCGCTTTCTTGCTGTC
CFH R	GGGAGTAGGAGACCAGCCATT	**Hbb R2 R**	GATGCTCAAGGCCCTTCATA
C1S F	TCTGTGCTGGAGGAGAGAAGG	**RIT2 F**	TGCCTGTAGGTAAAAGCAAGC
C1S R	CCAGCTGCGTAGAATTTGGTC	**RIT2 R**	TCCAGCTGATTGACAAAATCC
FOSB F	CCTTCCAGACCAGCCAAGAC	**PTPRB F**	CCCGATGGACCTGCTATGAT
FOSB R	AAGTTCAAGTCCTCGGCGAC	**PTPRB R**	TCCTGGCCTTCTTGACCACT
FOS F	CCCTCACCCTTTCGGAGTC	**LBX2 F**	CGGAAGTCCTGTGCAGCTTA
FOS R	GGCCTCCTGTCATGGTCTTC	**LBX2 R**	GCGGCTTTGTCTTCAATCGT
NR4A2 F	AGCACAGGCTACGACGTCAA	**RGS4 F**	AGCAGGAAGACGCTCAGAGG
NR4A2 R	AGGTGGCTGTGTTGCTGGTA	**RGS4 R**	GGAATTCGCAAGCAGGAAAG
CRIM1 F	TTCGGGATTTACGGAACCTG	**AGT F**	CCCAGTCTGAGATGGCTCCT
CRIM1 R	CGCTTCGTACTCGGTGAGG	**AGT R**	TGTGGATGACGAGGTGGAAG
ATF3 F	TGTATTGTCCGGGCTCAGAA	**NEFM F**	GGTGGAGCGCAAAGACTACC
ATF3 R	CCCCATACCACGACTGCTTAG	**NEFM R**	AGCGGCATTTGAACCACTCT
HIST1H3A F	TCCGCCGTTATCAGAAGTCC	**ANKRD1 F**	CCGATGGATCTGGTGCTACA
HIST1H3A R	GAGCTCTGGAAACGCAGGTC	**ANKRD1 R**	TGCCTTCAAAATGCCAGTGA
PTPRN F	CTATCTGGCCCAGGAGTTGC	**CTSK F**	GCACTTTGGAAGGGAGTTGG
PTPRN R	CAGGCTTCTCTCCACGATCC	**CTSK R**	GGTCATGGGTGGAGAGAAGC
CNKSR1 F	AACCCCAGCTTCTGACGTGT	**MAPKAPK5 F**	AACCAAGTGGCCTTGGAAGA
CNKSR1 R	CTCGGGGTGAGACCATGACT	**MAPKAPK5 R**	TGCTTGGCACAAAAATCACC
MMP13 F	AGAGGCTCCGAGAAATGCAG	**HES6 F**	CAGAGGTGGCAGAAATGGTG
MMP13 R	CCGCATCTTGGCTTTTTCAT	**HES6 R**	CAGTGCACCTGCCTCTCATC
KRT16 F	CCAACTGCTCACTCGCTCAC	**LCE1F F**	TCCCAAGTGCACTCCCAAG
KRT16 R	TTCATGGAGCTGGAGGAGGT	**LCE1F R**	TGCAGCAGGAAGAGACAGGA

2.10 RNA Sequencing and Mapping

Extracted RNA from proliferative, quiescence-induced and rapamycin-treated 2DD fibroblasts were submitted to the Centre for the Analysis of Genome Evolution and Function, University of Toronto (Toronto, Canada) and poly-adenylated RNAs purified. cDNA libraries were constructed from 1 μg of RNA using random hexamers to prime the reaction with average fragment lengths of ~300bp. These libraries underwent paired-end sequencing using the Illumina GIIx to generate 75 bp reads from two biological replicates of each sample. Reads were mapped back to a human reference genome (GRCh37/hg19 assembly from Ensembl) using the TUXEDO software package including TopHat2 with the following parameters: --bowtie1 -p 8 -r 20 --solexa-quals --coverage-search--microexon-search--library-type fr-unstranded. No clipping of reads was conducted. For proliferative, 0.5 mM and 1 mM metformin treated fibroblasts, cDNA libraries were constructed as previously described and underwent 150 bp paired-end sequencing using the Illumina HiSeq 2000 machine. Sequencing was conducted on two biological replicates of each sample. Reads were trimmed using Trim Galore: --phred33 --fastqc_args "--outdir=./fastqc_analysis/" --paired --illumina --clip_R1 12 --clip_R2 12 --length 80 --stringency 2 and mapped back to a human reference genome (GRCh38/hg19 assembly from Ensembl) using the TUXEDO software package, including TopHat2 with the following parameters: --library-type fr-unstranded --coverage-search --microexon-search -p 8 -o. For both rapamycin and metformin sample sets, BAM files were imported into the quantification and visualization tool SeqMonk (http://www.bioinformatics.babraham.ac.uk/projects/seqmonk). Using the feature probe generator function, 149, 135 probes were produced for the rapamycin sample set and 169, 714 probes for the metformin sample set. Probes were produced and reads quantified within these probes using the reads per kilobase of gene per million reads (RPKM) normalization method as previously defined (Mitchell *et al.* 2012). A read value of 0.05 was added to each probe to avoid infinite values during quantification. Examination of several transcripts demonstrated that genes from treated samples had sufficient read depth that the ≥5-fold change (quiescence-induced and rapamycin-treated samples) and ≥2-fold change (metformin-treated samples) in these genes is not an artefact of low data volume. Probes were converted to genes in SeqMonk and genes that had significant fold changes in the treated fibroblasts calculated against proliferative reads as a baseline. Genes were analysed at multiple fold-change cut-offs, including either increased or decreased ≥2-fold, ≥3-fold and ≥5-fold.

2.11 Enzyme-Linked Immunosorbent Assays

Cells were cultured as described in 2.1; however, cells were grown and maintained in 3 mL of media for proliferative and rapamycin-treated fibroblasts for the duration of the experiment. Cells were grown for five days, media removed and stored at -80ºC. Sandwich Enzyme-Linked Immunosorbent (ELISA) assays for IL-6 and IL-8 were conducted according to manufacturer's instructions (R&D Systems) and quantified. Briefly, an antibody specific to the protein of interest (i.e. Il-6 or Il-8) was adsorbed to the bottom of a plate. The wells were then incubated with aliquots (500 μL) of media from each treatment, allowing the proteins of interest to bind the primary antibody. Any protein of interest present attached to this antibody and excess sample was removed by washing. A secondary antibody specific to the protein of interest and conjugated to horse radish peroxidase (HRP) was added. If binding was successful, light was given off and measured. Results were compared against a standard curve. The amount of signal obtained was directly related to the amount of target protein in the sample. Significance was calculated using one tailed Student's t-tests.

2.12 Network Analyses

Cytoscape (Shannon *et al.* 2003) and ReactomeFI (Wu *et al.* 2010) were utilized to identify enrichment of network annotation terms (Kyoto Encyclopaedia of Genes and Genomes (KEGG)) to categorize specific pathways either up-regulated or down-regulated in response to 500 nM rapamycin, quiescence-induction, or 0.5 mM/1 mM metformin treatment. Lists of Ensembl gene IDs were input to the Gene Set/Mutation Analysis function (2014 network, gene set file format) and built-in functions of ReactomeFI Analyze Network Functions used to identify KEGG and Gene Ontology (GO) term enrichment within the constructed networks (including Pathway Enrichment). Each module included a minimum of two genes to be included in KEGG analyses and GO term enrichment. GeneCodis was used to identify GO terms associated with biological processes for lists of genes that were up-regulated and down-regulated in response to the various treatment conditions. For visualization of the networks, the most significantly enriched KEGG annotation terms were uploaded to Cytoscape using CytoKEGG. The nodes were coloured based on fold change with up-regulated represented in green and down-regulated in red, with more intensely coloured nodes representing those that had the greatest fold change.

2.13 Promoter analysis

Cis-Element Overrepresentation (CLOVER) (Frith *et al.* 2004), with the TRANSFAC database, was used to identify over-represented transcription factor binding sites in the

promoters of genes that exhibited a ≥5-fold change in transcript abundance during quiescence induction or rapamycin treatment. The complete set of human promoter sequences was used as a background baseline. Transcription factor binding sites were ranked based on raw score and only contained those with p-values <0.05.

2.14 Chromatin Immuno-Precipitation

2DD cells were grown to 70% confluence in 150 mm diameter dishes and treated as previously described (2:1). The cells were fixed with 1% FA in 10 mL media for 10 min at 37ºC and washed 2 X with 10 mL PBS containing 1X protease and phosphatase inhibitors (Sigma). Cell pellets were lysed for 10 min on ice in 600 µl SDS Lysis buffer (1% SDS, 10 mM EDTA, 50 mM Tris pH 8.0) with added inhibitors. The cells were sonicated on ice, for three cycles of 60 seconds at 30% duty cycle, into chromatin fragments ~500 bp in length. For the primary antibody, 5 µg of anti-STAT5A/B (Abcam, Cat #: ab7969) was added to 10^7 cells and incubated overnight at 4ºC, followed by binding of complexes of protein A Dynabeads (Invitrogen) overnight at 4ºC. For NFATC2 (Abcam, Cat #: ab2722) or RNAPII-S5 (Abcam, Cat #: ab5131) ChIP assays, 5 µg of antibody was bound to protein G (EDM Millipore Cat #: 16-201) or protein A agarose beads (EDM Millipore Cat #: 16-157), respectively, for 2h at 4ºC. For non-specific binding controls, goat anti rabbit antibodies were bound to both protein A agarose and Dynabeads. The samples were washed with Low Salt buffer (0.1% SDS, 1% Triton X, 2 mM EDTA, 20 mM Tris pH 8.0, 150 mM NaCl), High Salt buffer (0.1% SDS, 1% Triton X, 2 mM EDTA, 20 mM Tris pH 8.0, 500 mM NaCl) and TE buffer, and eluted with 500 µL Elution buffer (1% SDS, 0.1 M $NaHCO_3$). Crosslinks were reversed with 20 µL 5M NaCl incubated at 65ºC for 5 h, followed by phenol chloroform extraction and DNA precipitation. DNA was re-suspended in 30 µL ddH2O and 0.67 µl used in 10 uL RT-qPCR reactions carried out with gene-specific (300 nM) primers. ChIP-qPCR data was normalized by the percent input method and enrichment calculated. Standard error was calculated as a function of the standard deviations between triplicates. ChIP primers used are presented in (Table 2-2).

Table 2-2: ChIP Primers

Primers designed for use in Chromatin Immuno-Precipitation (ChIP) assays. F represents forward primers whilst R represents reverse primers. All primers are given in the 5'-3' direction.

Gene/Direction	Sequence 5'-3'
CXCL1 F	GGCTGAGGCAGAGAGGATAATA
CXCL1 R	GAAGAGCGTTGTGTCTCGGAT
CXCL8 F	GCCCCCTAAGAGCAGTAACA
CXCL8 R	TGGTGAAGATAAGCCAGCCA
IDI1 F	CTTTCGGATTGGGAGGGCTT
IDI1 R	GCCAATCACGCTTTCGATCC
IFNA1 F	ACCAAAGTCTTCAGAGACCCA
IFNA1 R	TGAGCTGGTTCAGATGGATGAC
IL1B F	TGACTCGGGAAATATTCTGGGAA
IL1B R	GGAGCAGAGGCTTTGACACTA
AMIGO2 F	TGCCCCAAAGCAAAGCTCTA
AMIGO2 R	CACCCTTGGAGACCCACTTC
CXCL2F	ACTGCACTGGGTTCACGAAG
CXCL2 R	TCTCTTTCTGCCCCGAATCC
CATSPERG F	GGAAGCACAAGTAGGGACCG
CATSPERG R	AGAGGGTGCTGGAGACTACG
ATR F	AAAGAGGGACAAGAGCGGTG
ATR R	CCAGCGAGTAAAGGCCAAGA
BAZ1A F	TGGGAAAGTTGCTTTAGGGGAA
BAZ1A R	GGACCCCAGCATTCTTGAAAC
BEND7 F	CTCTTTCCACAATCCGCCCA
BEND7 R	ACTTACCCATTTGCGCTCTCT
MDM2F	TCCGCATTTGTCGCAGTTTC
MDM2 R	TAGCCGTTGCGCTATGTTTG
BMP2 F	GATTTCGCCTCCAGAGTCCC
BMP2 R	CTCCACTCCCTGCTCTCAAA
IVL F	CCCTGTGCCTAGGTCAGAAAA
IVL R	AAACCCTTTAGGGCCCCATT
JAK2 F	CATTGCCACGAAACAGCGT
JAK2 R	TTCTCCGCTTTCGGCTTTTC
LIF F	CCCAAACCCAGGTGAGTCAG
LIF R	GTTTTCCTGCCTGGCTTGTC
IL6ST F	CTCCAGTTCATGACCCCGTT
IL6ST R	TCGCCTCTCCCAGACTAGAT
JARID F	TCGCTCGGGTGTCTGGTTG
JARID R	ACAAGTTAGGGCTCCTCGGATA

3.0 Results: The Impact of Rapamycin on Genome Function and Organization

3.1 Rapamycin Reduces Cell Proliferative Rates in the NB1 hTERT Cell Line

Rapamycin treatment of immortalized or cancer-based cell lines has been extensively conducted, inducing apoptosis and autophagy whilst decreasing cell proliferation (Vignot *et al.* 2005; Petroulakis *et al.* 2006; Jimenez *et al.* 2009; Suzuki *et al.* 2011). In order to determine if this was the case and to establish experimental conditions in fibroblasts, we tested a new immortalized cell line, NB1 hTERT, under normal growth conditions (proliferative) and in the presence of 500 nM rapamycin for 48 h, 120 h, 168 h and 220 h, whilst recording cell counts in order to calculate doubling times and total population doublings within culture (Figure 3-1A & 3-1B). Population doubling times of rapamycin treated NB1 hTERTs at 220 h of treatment was 54.6 h compared to 21.3 h in proliferative samples. Some fluctuations in population doubling times of rapamycin-treated fibroblasts were noted, with a decrease at 168 h to lower than proliferative fibroblasts (Figure 3-1A). In concordance with the overall increasing doubling times, total population doublings decreased from 12.4 in the control to 7.5 in the 500 nM rapamycin-treated NB1 hTERT. To further establish that rapamycin was impacting NB1 hTERT as expected, immunofluorescence detection of the proliferative marker Ki67, a marker that is no longer present 48 h after cells stop proliferating (Kill 1996), was conducted at 48h, 120h and 217h (Figure 3-1C). Percent Ki67 reported was lower in rapamycin-treated than untreated 2DD fibroblasts at 48 h (71.7% treated vs 93.5% control), 120 h (57.7% vs. 90.1%) and 217 h (65.67% vs. 76.8%). Therefore, it was confirmed that 500 nM rapamycin treatment decreased cell population doubling times and cell proliferation in NB1 hTERT.

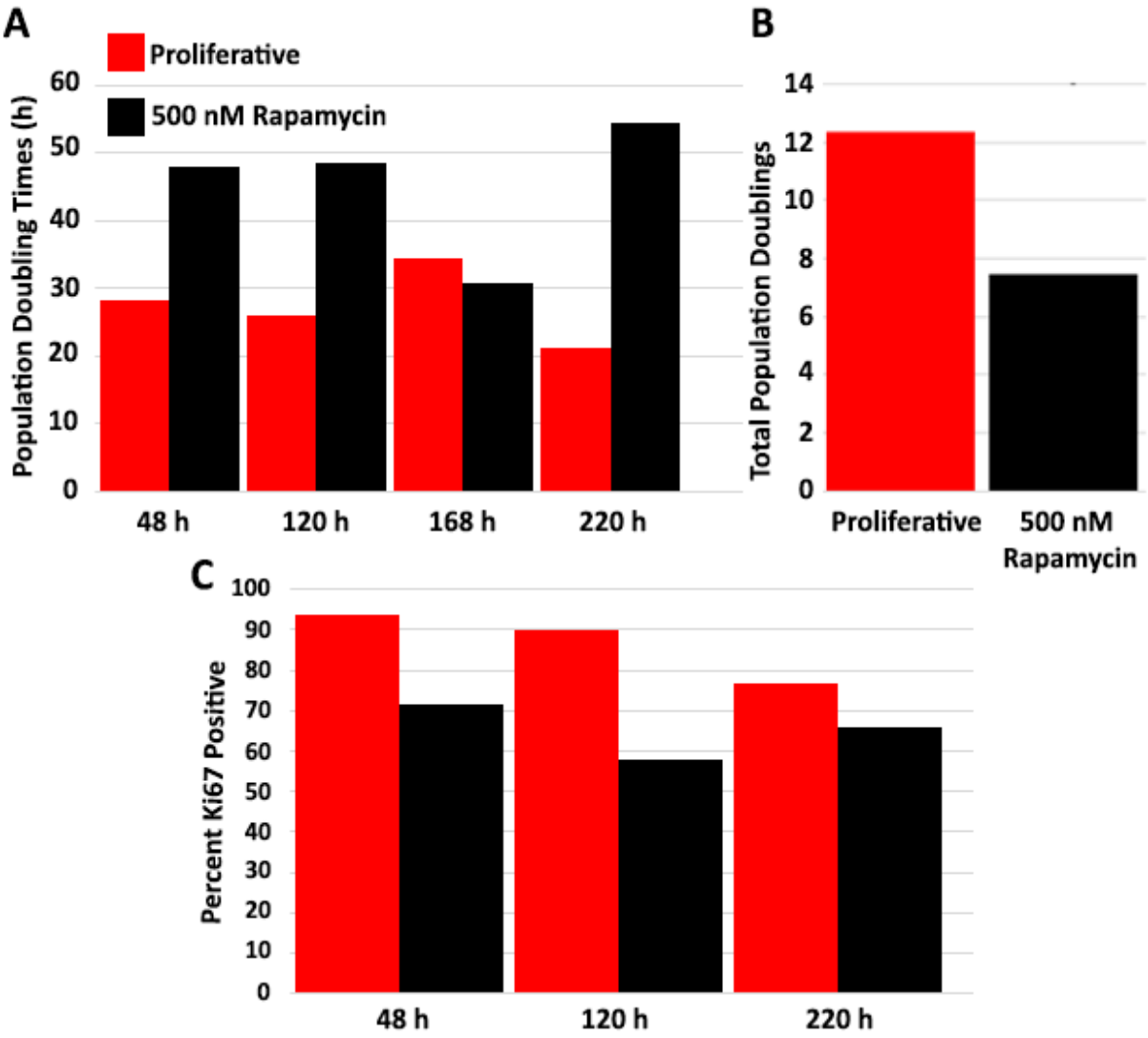

Figure 3-1: Rapamycin Decreased the Rate of NB1 hTERT Proliferation. (A) NB1 hTERT cells were grown under normal culture conditions or in the presence of 500 nM rapamycin for 48 h, 120 h, 168 h, 220 h (X-axis) (red bars represent proliferative NB1 hTERT and black bars represent 500 nM rapamycin-treated NB1 hTERT for all panels). (B) The total number of population doublings were plotted for proliferative and 500 nM rapamycin-treated cultures at 220 h. (C) Ki67 immuno-labelling of both proliferative and rapamycin-treated NB1 hTERT is shown for 48 h, 120 h, and 220 h (X-axis) with percent positive Ki67 shown on the Y-axis). Data are representative and two additional biological replicates were conducted.

3.2 Rapamycin Reduced Cell Proliferative Rates Without Inducing Cell Death in Normal Human Fibroblasts

The impact of rapamycin treatment on normal proliferating human foreskin fibroblasts (designated 2DD) was previously unknown. Given that 500 nM rapamycin treatment was demonstrated to impact proliferation of the immortalized fibroblasts cell line NB1 hTERT, the normal fibroblast cell line, 2DD, were grown in the presence of 500 nM rapamycin to determine the impact of rapamycin on genome function and organization in normal human fibroblasts. Primary 2DD were grown with 500 nM rapamycin for 72 h, 120 h, 168 h and 216 h to determine impact at various time points. Following each time point, cell counts were conducted and doubling times and total population doublings calculated (Figure 3-2A & 3-2B). Increases in doubling times (from 31 h under proliferative conditions to 224 h following rapamycin treatment) were recorded concomitant with a decrease in the total number of population doublings; at 216 h total population doublings decreased from 7.0 under proliferative conditions to 2.1 total population doublings following rapamycin treatment. Furthermore, morphological changes of the fibroblasts treated with 500 nM rapamycin at 120 h were reminiscent of quiescence (Figure 3-2C). Previously, it was demonstrated that decreased levels of serum in culture media (from 10% to 0.5%) induce quiescence, causing the population doubling times of 2DD fibroblasts to increase (Mehta *et al.* 2010). In addition to the noted changes in cellular morphology and population doubling times in response to rapamycin-treated and quiescence-induction by decreasing serum, there was no evidence of cell death (Figure 3-2D). Neither rapamycin treatment nor quiescence induction resulted in deleterious effects on the fibroblasts, with cultures exhibiting 97.3% and 96.4% viability respectively via Trypan blue staining in comparison to 97.3% in proliferative cultures (Figure 3-2D).

Given the impact of rapamycin on cell growth, proliferation and morphology, it is possible that a quiescent-like state was induced. Therefore, to establish the impact of rapamycin on cell proliferation, immunofluorescence using the proliferative marker Ki67 was performed. Following 168 h of rapamycin treatment, only 31% of fibroblasts exhibited Ki67 compared to 70% in proliferating cultures (Figure 3-3A), indicating that fewer cells were actively in the cell cycle following rapamycin treatment. 500 nM rapamycin treatment increased population doubling times whilst decreasing percent positive Ki67 2DD fibroblasts. Decreased levels of serum in culture media (from 10% to 0.5%) induce quiescence, causing the population doubling times of 2DD fibroblasts to increase and the number of Ki67 positive cells to decrease (Mehta *et al.* 2010). 2DD fibroblasts were induced into quiescence by reducing serum in culture media

to 0.5% for 120 h, with 4.3% of quiescence-induced fibroblasts Ki67 positive and doubling times >500 h across three replicates. Therefore, both rapamycin treatment and quiescence induction result in fewer cells actively proliferating (Figure 3-3A). To determine the number of cells in S-phase, or actively replicating DNA, and further validate findings from immunofluorescence, fibroblasts were incubated with the thymidine analogue, 5'-ethynyl-2'deoxyuridine (EdU) under each treatment condition. In agreement with Ki67, fewer fibroblasts incorporated EdU following rapamycin treatment and quiescence induction (Figure 3-3B). Cell cycle analysis using propidium iodide staining of proliferating, quiescent and rapamycin-treated 2DD revealed 64.4%, 91% and 72.0% of cells in G1/0 respectively (Figure 3-3C). Although it is evident that serum-induced quiescence induction has a greater impact in decreasing the number of actively proliferating 2DD fibroblasts (as measured by doubling times, Ki67 levels, EdU incorporation and flow cytometry), both decreased serum levels and rapamycin treatment exhibit similar patterns in decreasing proliferation and phenotypic changes.

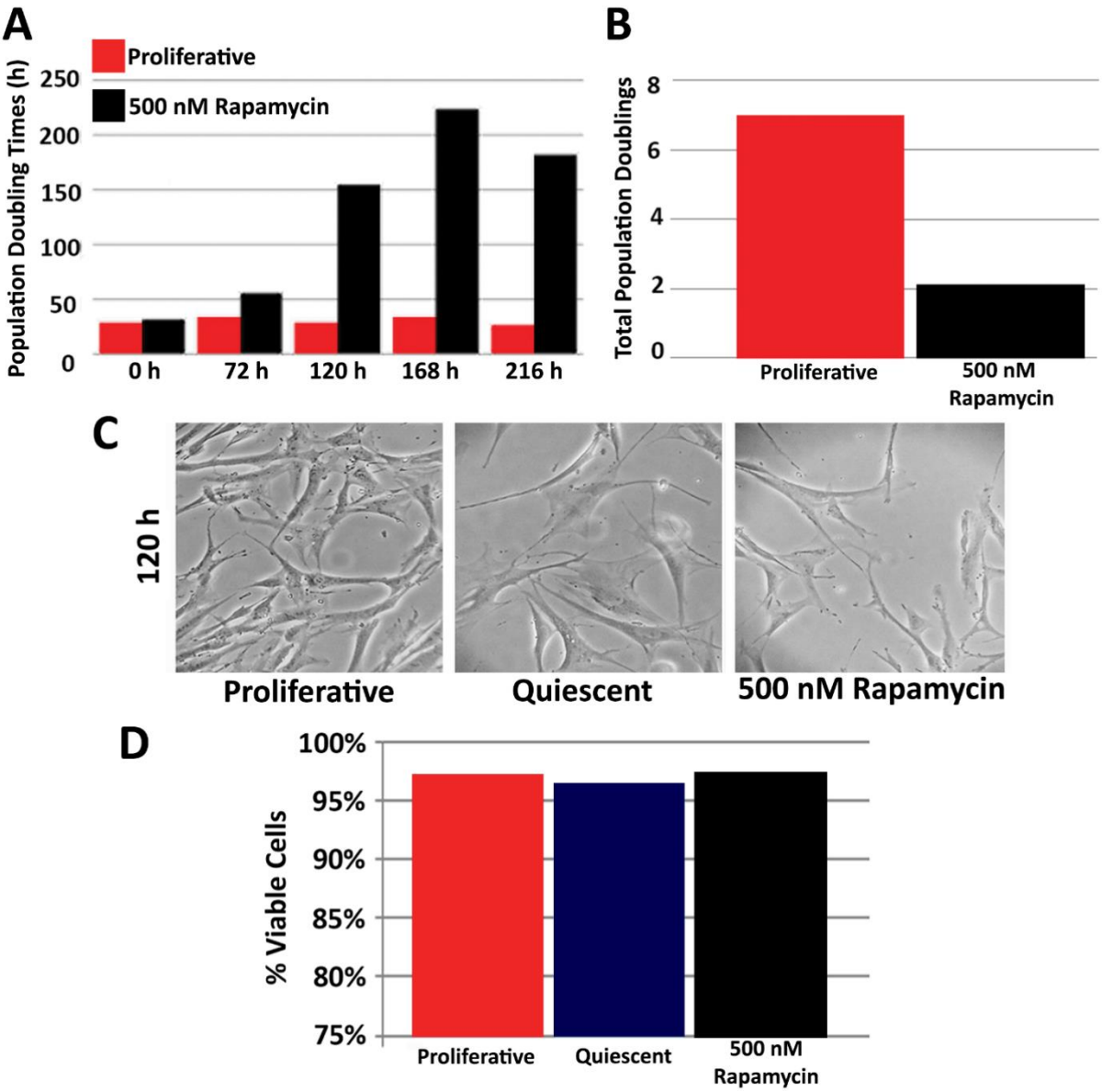

Figure 3-2: Rapamycin Decreases Doubling Times and Total Population Doublings Without Decreasing Cell Viability in 2DD Fibroblasts. (A) 2DD fibroblasts were grown under proliferative (red) and 500 nM rapamycin-treated (black) conditions, population doubling times (Y-axis) calculated over 0 h, 72 h, 120 h, 168 h and 216 h (X-axis) are shown. Red bars represent proliferative 2DD and black bars represent 500 nM rapamycin-treated 2DD, counts are representative and were replicated two additional times for A and B. (B) Total population doublings were plotted for proliferative and 500 nM rapamycin-treated cultures at 216 h. (C) Micrographs of proliferative, quiescent and 500 nM rapamycin-treated 2DD fibroblasts at 120 h of treatment. (D) Trypan blue assays were conducted at 120 h to detect percent (%) viable cells (Y-axis) for proliferative (red), quiescent (blue) and 500 nM rapamycin-treated 2DD (black) (X-axis). Data are representative and two additional biological replicates were conducted.

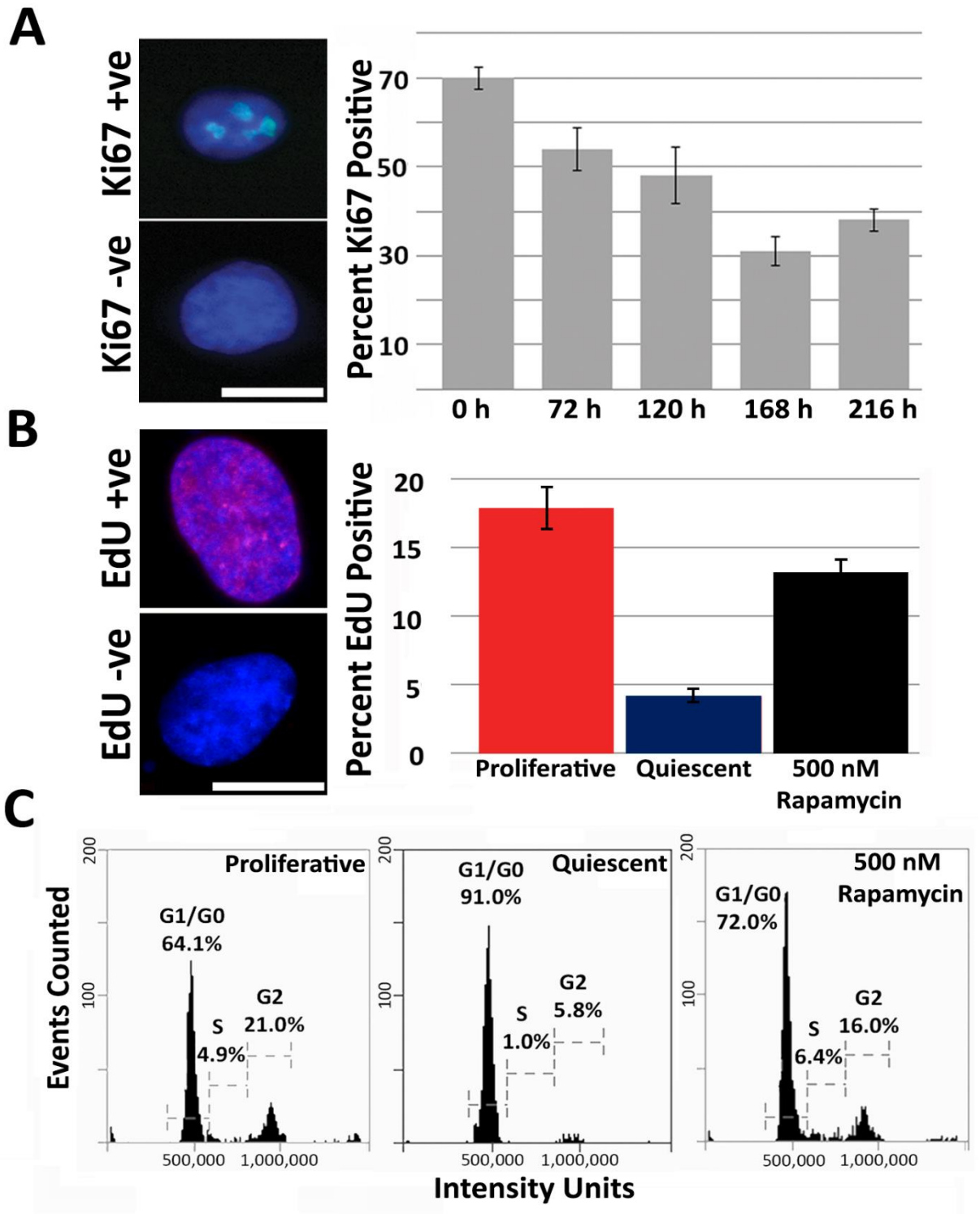

Figure 3-3: Rapamycin Decreases 2DD Fibroblast Proliferation. (A) 2DD fibroblasts were grown under either proliferative or 500 nM rapamycin treated conditions from 0 h to 216 h. Percent positive Ki67 (Y-axis) immuno-labelled 2DD following treatment with 500 nM rapamycin for 0 h, 72 h, 120 h, 168 h, 216 h (X-axis) is shown. The upper left panel is an example of a Ki67 (green) positive (+ve) fibroblast with a nucleus counterstained with Hoechst dye (H33342, blue). The upper left panel is representative of a ***(Figure 3-3 Legend Continued)***

Ki67 negative (-ve) fibroblast. (B) At 120 h, proliferative (Pro, red)), quiescence-induced (Qui, blue) and 500 nM rapamycin-treated (Rap, black) 2DD were incubated with the thymidine analogue EdU. and percentage positive for EdU reported (Y-axis). The left top panel is representative of an EdU negative (non-S-phase) fibroblast and the bottom left panel is an EdU (S-phase) positive fibroblast, with EdU in red and the nucleus counterstained with H33342 (blue). Error bars for (A) and (B) are the S.E.M., scale bar = 10 μm. (C) Pro, Qui, and Rap-treated fibroblasts were fixed and stained with propidium iodide and DNA content measured by flow cytometry at 120 h. Histograms demonstrate evens counted (Y-axis), fluorescence signal (Intensity Units, X-axis) measured and the percentage cells in G0/G1, S and G2 phase of the cell cycle for each treatment condition.

3.3 Rapamycin Inhibits mTORC1 and Induces Autophagy in 2DD Fibroblasts

In order to confirm that 500 nM rapamycin treatment was inducing the expected inhibition of the protein kinase mTOR, whole cell protein lysates were extracted and western blot analyses performed. These analyses revealed a decrease in activated phosphorylated mTOR alongside diminished levels of the downstream target of TORC1, phosphorylated p70-S6 kinase (p70-S6K) (Figure 3-4A). Inhibition of TORC1 function is well documented to induce autophagy, increasing the number autophagosomes – marked by the presence of light change 3 (LC3) foci (Ladoire *et al.* 2012). Immuno-fluorescence for LC3 revealed an increase from 18% LC3 positive cells in proliferative to 72% in 500 nM rapamycin-treated culture at 120 h (Figure 3-4B & 3-4C). Combined, these data confirm that rapamycin is inhibiting TOR function, decreasing levels of downstream phosphorylated p70-S6K and increasing autophagy in healthy human fibroblasts.

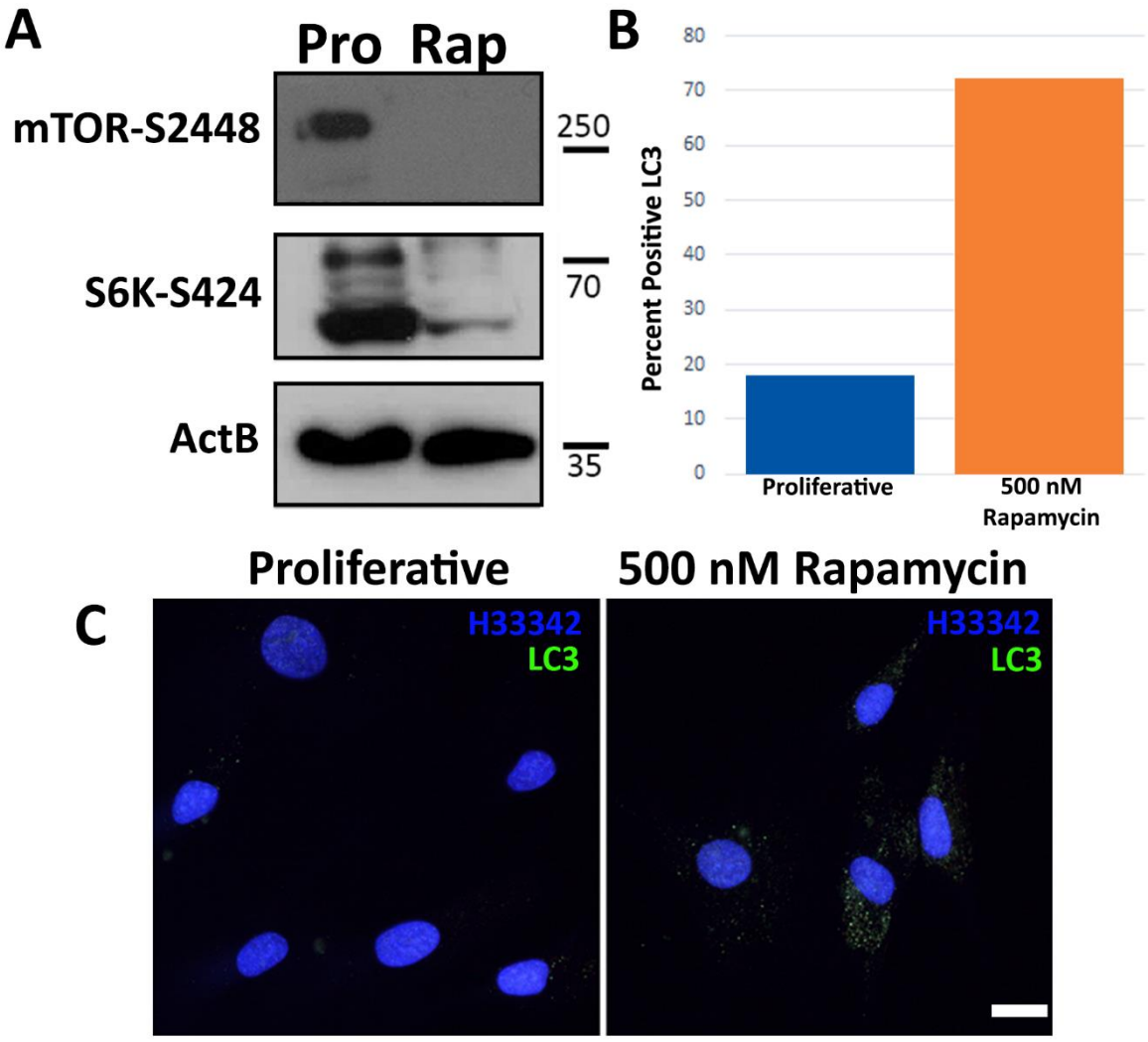

Figure 3-4: Rapamycin Inhibits mTOR Activity and Increases the Presence of Autophagy Markers in 2DD Fibroblasts. (A) Western blot analysis of protein extracts from proliferative (Pro) and rapamycin (Rap)-treated 2DD fibroblasts at 120 h. Levels of phosphorylated mTOR (serine 2448; 1st row), phosphorylated p70-S6K-S424 (serine 424, 2nd row) and ActB (loading control) (3rd row) were analyzed. Approximate molecular weights are listed to the right of the western blots. (B) Immuno-fluorescence was used to detect the precent positive of fibroblasts exhibiting LC3 foci (Y-axis) in proliferative (blue bar) and 500 nM rapamycin-treated (orange bar) 2DD fibroblasts at 120 h. (C) Representative micrographs of the LC3 protein in untreated (proliferative) and rapamycin-treated (500 nM rapamycin) fibroblasts are shown. Chromatin was counterstained with H33342 (blue). Scale bar = 10μm.

3.4 Rapamycin Treatment and Serum Restriction Induce Genome Reorganization

Previously, chromosome territories have been documented to reposition within the nuclear volume in response to decreased serum levels. Specifically, quiescence induction resulted in repositioning of chromosome 10 towards the periphery and 18 towards the interior of the nuclear volume in fibroblasts (Mehta *et al.* 2010), a finding we reproduced by conducting 2D-DNA fluorescence *in-situ* hybridization (FISH) (Figure 3-5). FISH "paints" specific chromosome territories within the nuclear volume and position is determined through erosion analysis. This analysis breaks the nucleus into five concentric rings, with the outer most shell at the periphery considered 1 and the inner most shell considered 5. The percent of each chromosome that falls into each shell is measured and divided by the counter stain signal for chromatin, therefore normalizing for DNA content of each shell. rapamycin treatment of 2DD fibroblasts induced similar re-location of chromosome 18 as quiescence, towards a more interior nuclear location. Chromosome 10 was also reported to re-locate significantly to the nuclear periphery following rapamycin treatment and quiescence induction (Figure 3-5). These findings indicate a shift in genome organization following both treatment conditions. The X chromosome remained at the nuclear periphery for all treatment conditions (Mehta *et al.* 2010). Statistical analyses (t-test) revealed confirmed significant repositioning of chromosome 18 and 10 under treatment conditions when compared to proliferative samples (p values ≤ 0.01). Furthermore, negative correlation trends were reported between chromosome 18 in proliferative vs. quiescent (R^2 value = -0.83) and proliferative vs rapamycin-treated samples (R^2 value = -0.99). Correlation calculations also revealed similarities in chromosome 10 positioning between quiescent and rapamycin treated fibroblasts (R^2 value = 0.87) than proliferative and quiescent (R^2 value = 0.43); however, T-test's did not demonstrate this as significance when comparing the ratios of signal intensity (Table 3-1).

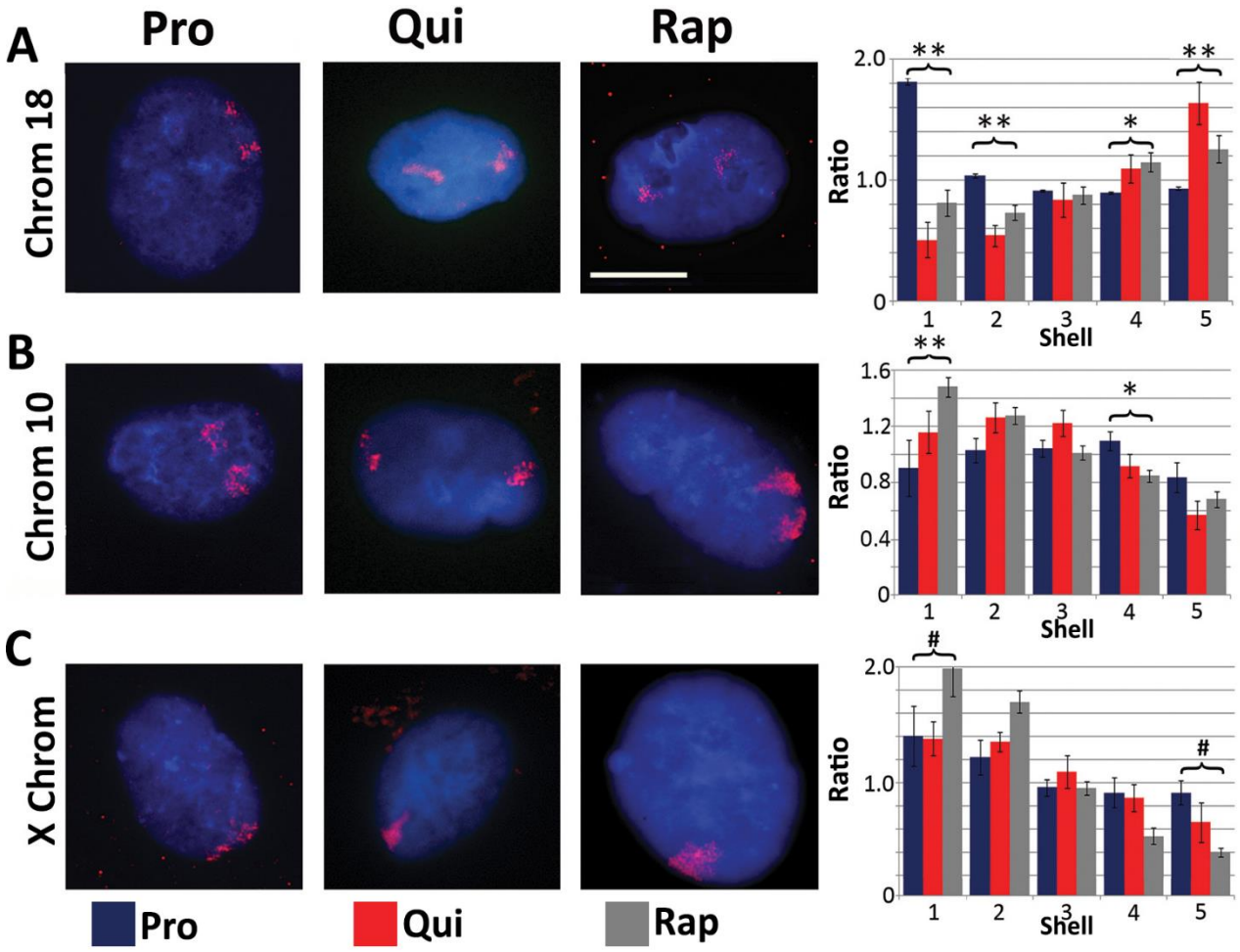

Figure 3-5: Rapamycin Treatment and Quiescence Induction Result in Chromosome Territory Repositioning in 2DD Fibroblasts. (A) Chromosomes 18, (B) 10 and (C) the X chromosome were identified in proliferating (Pro, first column), quiescent (Qui, second column) and rapamycin-treated (Rap, third column) 2DD fibroblasts by chromosome painting. Cells were fixed following 120 h of treatment. Red signal represents the identified chromosomes; chromatin was counter stained with H33342 (blue). Scale bar = 5 μm for all images. Following painting, erosion analysis was performed to designate the location of the chromosomes within the nuclear volume. Nuclei were broken into five concentric shells of area, shell 1 being most exterior and shell 5 being most interior. Graphs for each specific chromosome represents the measured ratio of % chromosome signal divided by the % H33342 signal in each shell (Y axis) to normalize for DNA content in each shell (X axis). Proliferative positioning is represented by blue bars, quiescent by red and rapamycin-treated in grey. Error bars = S.E.M. Two-tailed Student's test for unequal variance were used to demonstrate significant difference in chromosome positioning. ** indicates that both proliferative and quiescent measurements had p values ≤0.01. * indicates that ***(Figure 3-5 Legend Continued)***

only rapamycin had significant changes in chromosome positioning. # indicates a significant difference (p values ≤0.01) between quiescent and rapamycin-treated samples. Correlation calculations were also performed to demonstrate if the trend in chromosome positioning was similar or divergent between the samples. Chromosome 18 Pro vs. Qui R^2 = -0.83, Pro vs. Rap R^2 = -0.99 and Qui vs. Rap R^2 = 0.87. Chromosome 10 Pro vs. Qui R^2 = 0.43, Pro vs. Rap R^2 = 0.64 and Qui vs. Rap R^2 = 0.95. X chromosome: Pro vs. Qui R^2 = 0.84, Pro vs. Rap R^2 = 0.98 and Qui vs. Rap R^2 = 0.91.

Table 3-1: Correlation Values (R^2) for Chromosome Territory Re-Positioning in 2DD Fibroblasts in Response to 500 nM Rapamycin Treatment and Quiescence-Induction. Correlation values for chromosome territory re-positioning in 2DD fibroblasts threated for 120 h with 500 nM rapamycin or induced into quiescence by 120 h of serum starvation. Correlations are given for chromosome 18, 10 and X between Proliferative (Pro) and Quiescence (Qui), Pro against Rap and Qui against Rap.

R^2 Values	**Chromosome 18**		**Chromosome 10**		**Chromosome X**	
	Qui	Rap	Qui	Rap	Qui	Rap
Pro	-0.83	-0.99	0.43	0.64	0.84	0.98
Qui		0.87		0.95		0.91

3.5 Rapamycin Treatment and Serum Restriction Induced Divergent Transcript Profiles

Rapamycin and quiescence induction both reduced proliferative rates, decreased the number of cells exhibiting Ki67/actively replicating DNA, and induced repositioning of chromosomes 18 and 10. Given these similarities, it may be that both treatments have overlapping impacts on cellular function. To determine if similarities exist between these conditions, mRNAs were isolated from proliferative, and 5-day quiescence-induced and rapamycin-treated fibroblasts and RNA sequencing (RNAseq) with subsequent comparative transcriptome analyses conducted. Raw sequence reads from Illumina-based sequencing were mapped to a reference genome (GRh37/hg19), normalized using the reads per kilobase of gene per million reads (RPKM) method, and analyzed using the tool SeqMonk (http://www.bioinformatics.babraham.ac.uk/projects/seqmonk/). RNAseq data were validated by reverse transcriptase-quantitative PCR (RT-qPCR) by selection of a sample of genes that changed/did not change expression for both quiescence-induced and rapamycin-treated fibroblasts (Fig. 3-6). Of the 22 genes determined to have increased ≥5-fold by RNAseq in

response to quiescence when compared to proliferative 2DD fibroblasts, 19 (86%) were also increased ≥5-fold by qRT-PCR. Similarly, of the 11 genes from RNAseq data up-regulated by rapamycin treatment, 7 (64%) were ≥5-fold up-regulated by qRT-PCR (Figure 3-6). Additionally, all genes tested (17) from the rapamycin RNAseq dataset that were below the ≥5-fold cut-off, were also below the ≥5-fold cut off by RT-qPCR (Figure 3-6B).

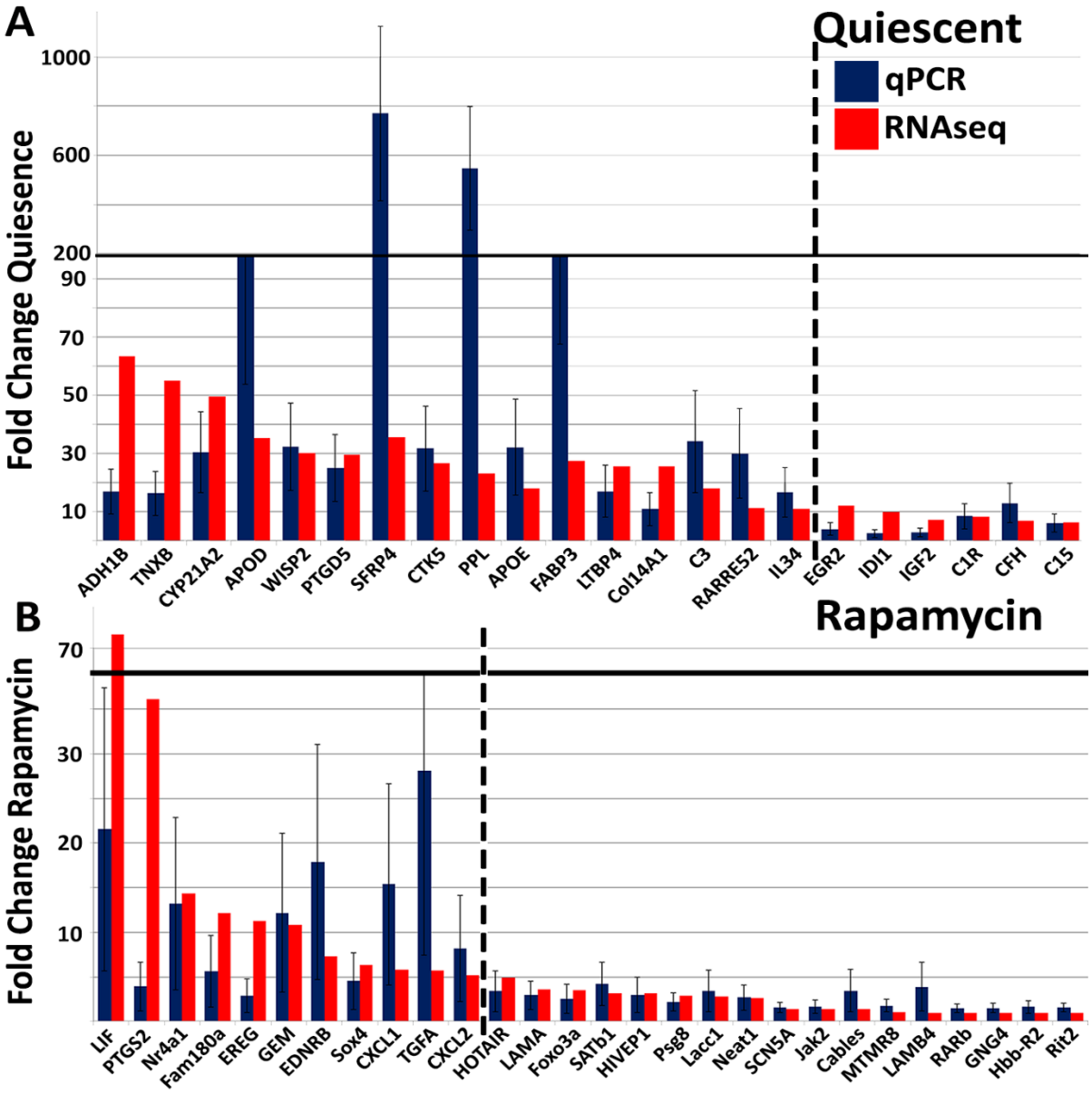

Figure 3-6: RNA-sequencing Validation of Gene Fold Changes by RT-qPCR in Response to Rapamycin Treatment and Quiescence Induction in 2DD Fibroblasts. RT-qPCR was conducted on a subset of genes identified to have changed transcript profiles by RNAseq. This was conducted for (A) 120 h quiescence-induced 2DD fibroblasts and (B) 120 h 500 nM rapamycin-treated 2DD fibroblasts. The relative fold change (using five individual normalizing genes) in these transcript profiles from proliferative cells is shown (blue bars) as well as the fold change predicted by RNAseq (red bars). The change in ***(Figure 3-6 Legend Continued)***

scale of the vertical axis is denoted by a solid black line. Values on the left of the dashed line represent genes with RNAseq values ≥5-fold with RT-qPCR comparisons; to the right of the dashed line are selected genes that were ≤5-fold by RNAseq in rapamycin-treated fibroblasts with the corresponding RT-qPCR fold changes. Error bars were generated for the RT-qPCR fold change values and represent the S.E.M.

Comparisons between RNAseq data sets were made using significant log-base (2) scatter plots. These comparisons included the log number of reads from quiescent fibroblasts or rapamycin fibroblasts against the log number of proliferative fibroblasts, with scatter plots presented for subsets of genes changing transcript profiles ≥2-fold (Figure 3-7A), ≥3-fold (Figure 3-7B) and ≥5-fold (Figure 3-7C). Further subsets of genes in these scatter plots have been highlighted. In log-transformed quiescent fibroblasts, 1176 genes changed ≥2-fold (704 up-regulated; 472 down-regulated). At ≥3-fold, 933 genes changed expression (574 up-regulated; 359 down-regulated) whilst at ≥5-fold 615 genes changed (386 up-regulated; 229 down-regulated). In significant log-base (2) transformed rapamycin-treated compared to proliferative fibroblasts 1060 genes changed transcript profile ≥2-fold (862 up-regulated; 198 down-regulated). At ≥3-fold, 832 genes changed expression, (683 up-regulated; 149 down-regulated) and at ≥5-fold 494 genes changed transcript profile (407 up-regulated; 87 down-regulated). Despite the majority of genes from both quiescence-induced and rapamycin-treated fibroblasts having similar read count values to those of proliferating cells (correlations of 0.933 and 0.946, respectively), scatter plots based on log transformed data and Venn diagrams based on fold-change data revealed little overlap between the genes changing expression under each treatment condition (Figure 3-7D). For example, analysis of gene lists at ≥5-fold revealed that only 68 genes (61 up-regulated and 7 down-regulated; 6.5%) were common between quiescent and rapamycin-treated fibroblasts (Fig. 3-7D). Further analysis of quiescence-induced and rapamycin-treated fibroblasts based on a non-log transformed fold change were in agreement with these findings, although gene numbers varied slightly due to the nature of the bioinformatics analyses (Figure 3-8). Specifically, in rapamycin-treated fibroblasts, 4404 transcripts were up-regulated ≥2-fold (3216 up-regulated; 1188 down-regulated). At ≥3-fold, 1634 transcripts changed expression (1311 up-regulated; 323 down-regulated) and at ≥5-fold, 483 genes changed transcript profile (421 up-regulated and 62 down-regulated). In response to quiescence-induction, 4840 transcripts changed expression ≥2-fold (2851 up-regulated; 1989 down-regulated), 2044 transcripts changed expression ≥3-fold (1277 up-regulated; 767 down-regulated) and just 728 transcripts changed expression ≥5-fold (469 up-regulated; 259 down-regulated). In concordance with log-base (2) transformed data, just 88 (7.8%) of transcripts

were identified as changing ≥5-fold in rapamycin-treated and quiescence-induced fibroblasts, (70 up-regulated; 18 down-regulated). Therefore, response to quiescence-induction and rapamycin-treatment in 2DD fibroblasts is predominantly divergent and unique for each condition.

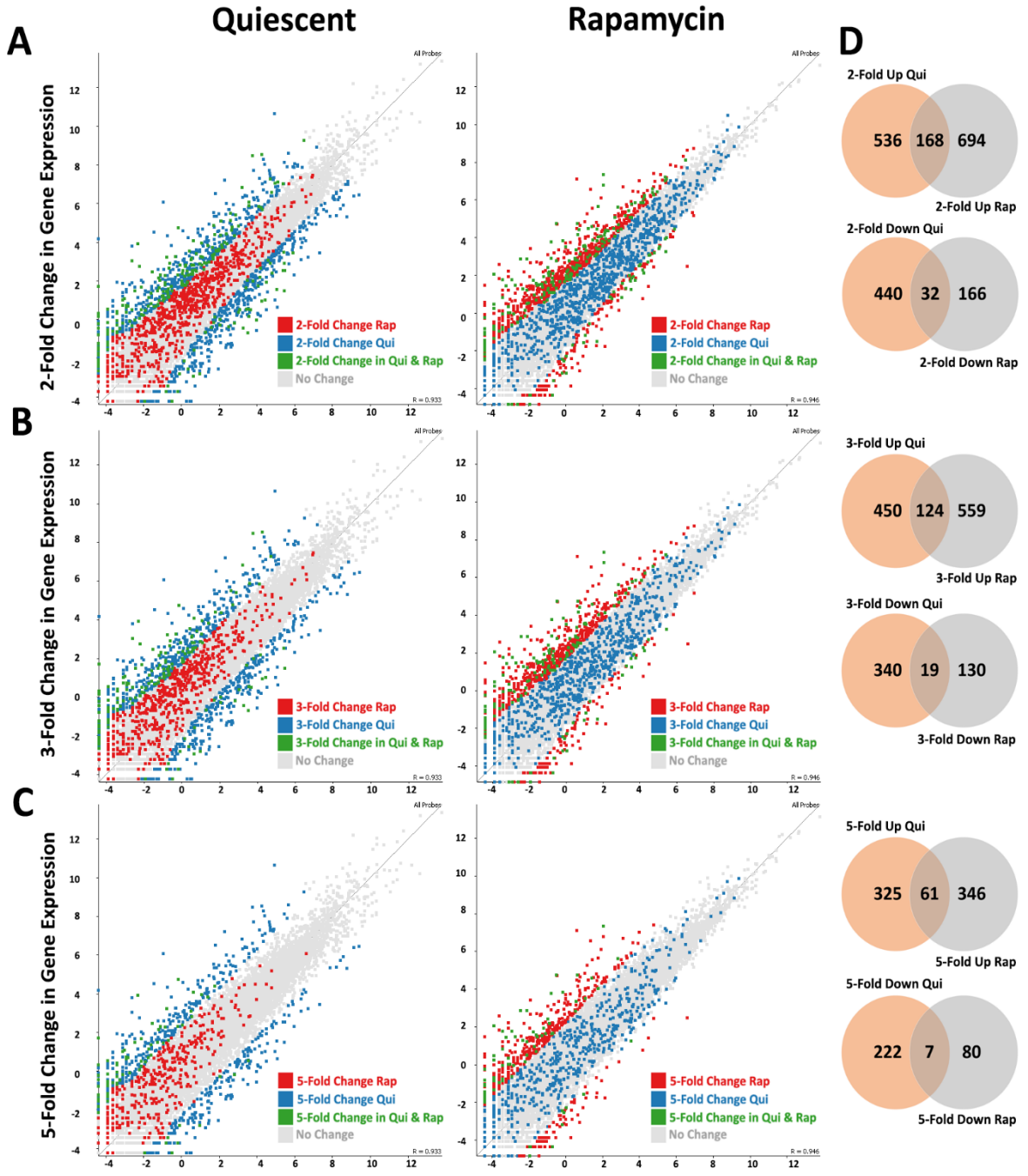

Figure 3-7: Scatter Plots and Venn Diagrams Demonstrate Divergent Transcript Profiles Between 500 nM Rapamycin-Treated and Quiescence-Induced 2DD Fibroblasts Based on Log Base (2) Transformed Data and Significance Analyses. (A) Scatter plots comparing changes in gene expression between proliferative fibroblasts and serum-induced quiescent 2DD (left panel) and between proliferative and 500 nM rapamycin- ***(Figure 3-7 Legend Continued)***

treated fibroblasts (right panel) for transcript abundance changes of ≥2 fold. (B) Scatter plots comparing changes in gene expression between proliferative 2DD fibroblasts and serum-induced quiescent 2DD (left panel) and between proliferative 2DD fibroblasts and 500 nM rapamycin-treated 2DD (right panel) for transcript abundance changes of ≥3 fold. (C) Scatter ***(Figure 3-7 Legend Continued)*** plots comparing changes between proliferative 2DD fibroblasts and serum-induced quiescent 2DD (left panel) and between proliferative 2DD fibroblasts and 500 nM rapamycin-treated 2DD (right panel) for transcript abundance changes of ≥5 fold. For all plots, the number of counts for each transcript identified by RNAseq for proliferative (X-axes) and metformin treated (Y-axes) fibroblasts was log-base2 transformed. Each square represents an individual transcript. Transcripts exhibiting a significant fold change in response to quiescence-induction when compared to proliferative samples are coloured blue, in response to 500 nM rapamycin coloured red, and overlapping between the two treatment conditions coloured green. Grey squares represent transcripts that did not change abundance at the listed cut-off values. (D) Venn diagrams demonstrating the number of genes up-regulated or down-regulated between quiescent (red) and 500 nM rapamycin (blue) treated fibroblasts in comparison to proliferative fibroblasts. Numbers in the overlapped areas indicate the number of genes changing expression in both treatment groups.

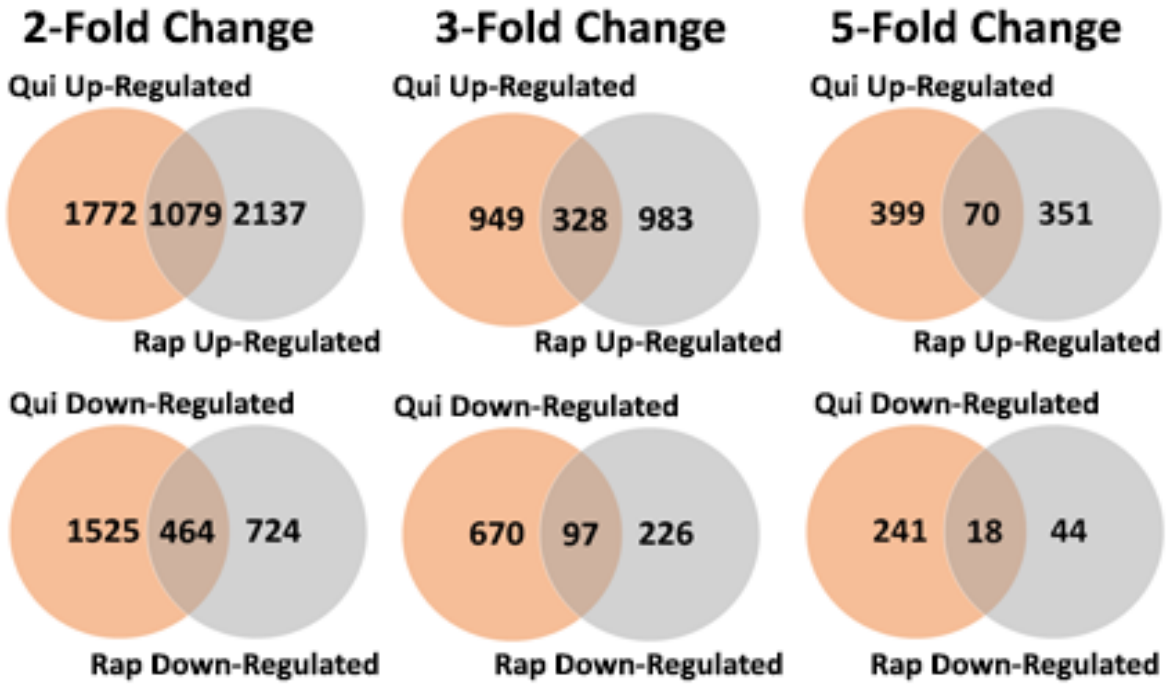

Figure 3-8: Venn Diagrams for Transcripts Changing ≥2-Fold, ≥3-Fold and ≥5-Fold in Quiescence-Induced and Rapamycin-Treated Fibroblasts by Fold Change Analysis. Venn diagrams demonstrating the number of genes up-regulated or ***(Figure 3-8 Legend Continued)***

down-regulated between quiescent (red) and 500 nM rapamycin (blue) treated fibroblasts in comparison to proliferative fibroblasts. Numbers in the overlapped areas indicate the number of genes changing expression in both treatment groups.

3.6 Network Analyses Reveal Enrichment in Cytokine-Related Pathways Following Rapamycin Treatment

To determine if there was overlap or divergence in the biological pathways enriched for by either quiescence-induction or rapamycin treatment, network analyses using genes identified as significantly changing expression (≥5-fold) were conducted. Cytoscape (Shannon *et al.* 2003) with ReactomeFI (Wu *et al.* 2010) was used to classify highly interacting groups of genes (modules) from the RNAseq datasets and to identify the associated pathway annotation terms (Kyoto Encylopedia of Genes and Genome; KEGG terms). Genes up-regulated ≥5-fold in response to quiescence-induction, and based on log-base (2) transformed and fold change analyses, 21 and 29 modules respectively were identified as over-expressed (p-vale <0.05, FDR <0.05) (Figure 3-9 & 3-10). KEGG terms associated with these modules in both analyses revealed significant enrichment in the complement and coagulation cascade, as well as for infection response, and for cadherin signalling and extracellular matrix organization (Table 3-2 & 3-5). Examination of the module associated with this term showed several genes both increasing (*Serping1, C2 and CFD)* and decreasing *(Serpine1, F2* and *F12)* transcript abundance. The enrichment of the KEGG-associated terms in up-regulated genes for the complement and coagulation pathways in response to reduced serum levels in normal human fibroblasts has only once been previously reported (Coller *et al.* 2006). Genes ≥5-fold up-regulated in response to quiescence induction in both analyses also demonstrated enrichment for Gene Ontology (GO) for Biological Processes and Molecular Function terms. In both analyses, GO Biological Processes were enriched in collagen binding, calcium dependent cell-cell adhesion and extracellular matrix organization (Figure 3-11 & Figure 3-12) (p-value <0.05, FDR <0.05). For GO Molecular Function, collagen binding and calcium ion binding were enriched (p-value <0.05, FDR <0.05) (Figure 3-11B & Figure 3-12B).

In response to quiescence-induced genes ≥5-fold down-regulated, in log-transformed and fold change analyses, 12 and 9 modules respectively, were identified. Pathway analyses revealed that Mitotic Prometaphase, Aurora B signalling and Cell cycle were down-regulated. Furthermore, for both analyses, genes down-regulated by quiescence induction were enriched for GO Biological Processes such as mitosis, cell division and mitotic cell cycle. In GO

Molecular Function, Protein Binding and ATP-binding were enriched, indicating that gene expression patterns for cellular replication are inhibited in the absence of growth factors.

Contrary to quiescence-induction, analysis of rapamycin-treated fibroblasts revealed the presence of networks of 16 distinct modules (14 up-regulated; 2 down-regulated) by log-base (2) analyses and 19 (18 up-regulated, 1 down-regulated) by fold-change analyses (Figure 3-9 & Figure 3-10). In rapamycin up-regulated genes, KEGG pathway annotation terms associated with PIP3 activates AKT signalling (in log-transformed data) and NF-κB signalling pathway and Signalling by Type 1 Insulin-like Growth Factor 1 Receptor (IGF1R) (in fold-change based analyses) were observed and linked these findings to known mTOR-associated pathways. The most significantly enriched pathway annotation terms identified for log-base (2) and fold-change analyses were Pathways in Cancer and Cytokine-Cytokine Receptor Interactions respectively (Table 3-4 & 3-7). Further examination of the network associated with the cytokine-cytokine receptor interaction pathway demonstrated up-regulation of several cytokines and provides functional relationship between *IL-6ST*, *IL-11*, *IL-1B*, *INHBA*, *CXCL-1*, *CXCL-3*, *CXCL2*, *PF4V1*, *LIF*, *IFNA1*, *BMP2*, *IL-6*, *IL-8*, *TGFBR1* genes. Four of these identified genes (*LIF*, *IL-8*, *IL-11* and *INHBA*) were ranked within the top 20 of all genes up-regulated ≥5-fold in expression. Furthermore, many of these genes belong to the IL-6 signalling pathway. GO Biological Processes term enrichment for genes up-regulated in rapamycin-treated fibroblasts further supports negative regulation of cell proliferation (p-value <0.05; FDR <0.05), whist GO molecular function demonstrates enrichment of terms for cytokine and growth factor activity (Figure 3-11 & 3-12).

Network pathway analyses for genes ≥5-fold down-regulated in response to rapamycin treatment revealed no significantly enriched KEGG annotation terms (p-value <0.05, FDR <0.05) by both analyses; however, by GO molecular function in fold-change analyses, various receptor binding activities were down-regulated. Findings based on both up-regulated and down-regulated transcripts from the rapamycin-treated dataset are divergent from quiescence-induced changes in transcript profiles, documented by few genes overlapping between treatments under both fold-change and log-base (2) analyses, alongside differential pathway enrichment.

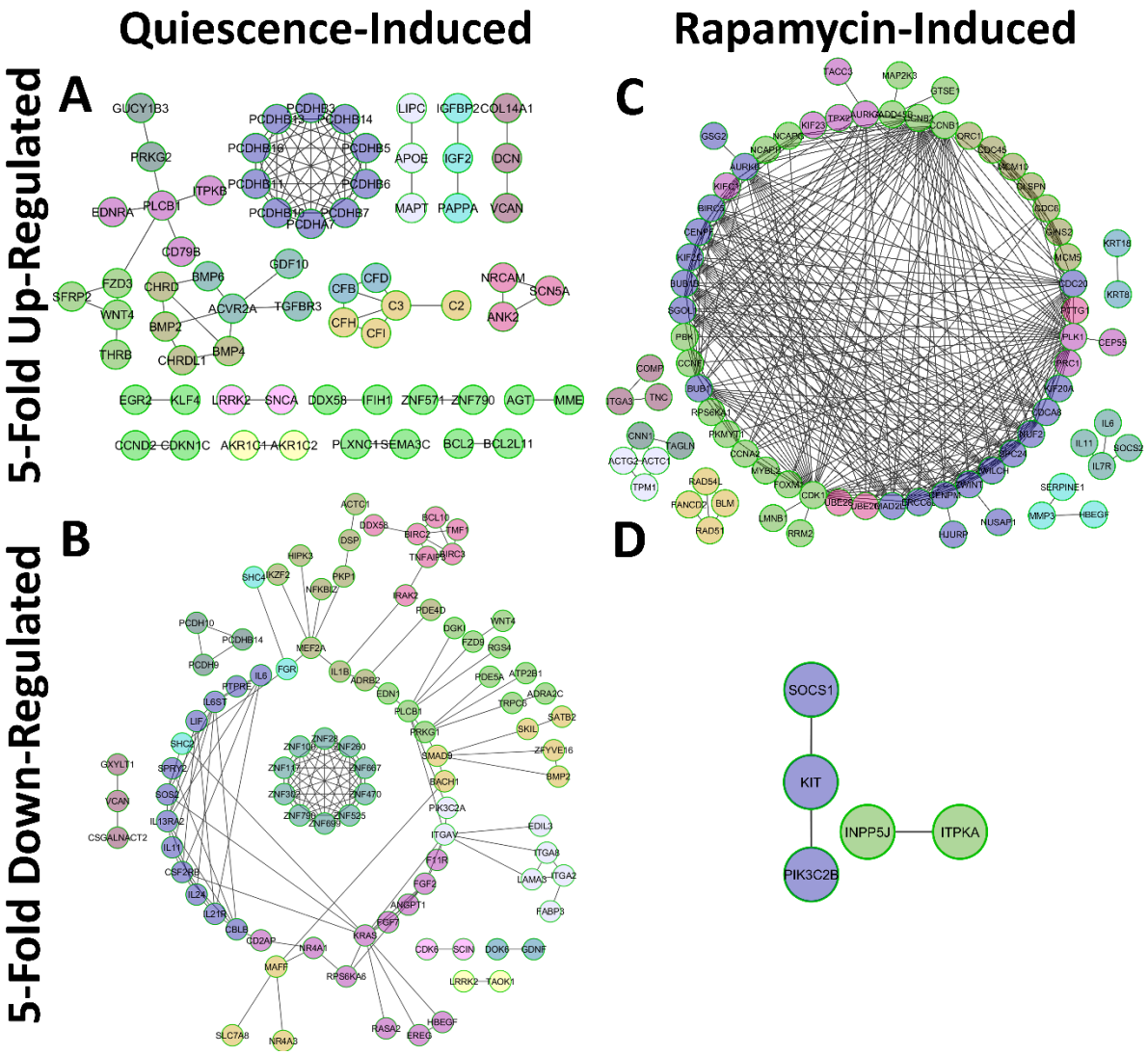

Figure 3-9: Modules Identified in Genes Changing ≥5-Fold in Response to Rapamycin Treatment and Quiescence Induction in 2DD Fibroblasts Based on Log-base (2) Analyses. Network analyses identified groups of functionally related genes (modules) in (A) ≥5-fold up-regulated quiescence-induced genes, (B) ≥5-fold down-regulated quiescence-induced genes, (C) ≥5-fold up-regulated rapamycin-induced genes, (D) ≥5-fold down regulated rapamycin-induced genes. Each node (circle) is representative of a gene whilst every colour is representative of a module. Solid lines represent genes linked within the same module and between modules based on the ReactomeFI database.

Table 3-2: Network Pathway Annotation Terms Enriched in Quiescence Up-Regulated Genes in 2DD Fibroblasts by Log-Base (2) Analyses. Genes ≥5-fold up-regulated in response to quiescence induction were analyzed for enrichment of KEGG terms. The identified enriched pathway KEGG annotation terms (GeneSet) from network analyses are listed. The total number of genes from the network identified to be up-regulated in response to quiescence and belonging to a specific pathway was identified. P-value (with 0 values equating to <0.0001) and false discovery rates (FDR) are presented. All P-Value and FDR are <0.05. Nodes identify specific genes/proteins from our datasets present in the networks. Gene lists identified by log-base (2) transforming data.

	Protein From Network	P-Value	FDR	Nodes
Cadherin signaling pathway(P)	12	0	1.60E-04	PCDHB14,PCDHB13,PCDHB11,PCDHB10, PCDHB16,PCDHA7,PCDHB7,PCDHB5,PCDHB6, PCDHB3,FZD3,WNT4
Complement and coagulation cascades(K)	10	0	1.60E-04	SERPING1,TFPI,C3,C2,CFH,CFI,CFD, BDKRB2,CFB,PROS1
Extracellular matrix organization(R)	15	0.0001	0.008629	LTBP4,MADCAM1,ADAMTS5,COL14A1, VCAN,FMOD,PCOLCE2,MFAP4,DCN, BMP4,BMP2,LAMA2,COL21A1,CTSK,LUM

Table 3-3: Network Pathway Annotation Terms Enriched in Quiescence Down-Regulated Genes in 2DD Fibroblasts by Log-Base (2) Analyses. Genes ≥5-fold down-regulated in response to quiescence induction were analysed for enrichment of KEGG terms. The identified enriched pathway KEGG annotation terms (GeneSet) from network analyses are listed. The total number of genes from the network identified to be up-regulated in response to quiescence and belonging to a specific pathway was identified. P-value (with 0 values equating to <0.0001) and false discovery rates (FDR) are presented. All P-Value and FDR are <0.05. Nodes identify specific genes/proteins from our datasets present in the networks. Gene lists identified by log-base (2) transforming data.

	Protein From Network	P-Value	FDR	Nodes
Mitotic Prometaphase(R)	22	0	3.54E-14	AURKB,CDCA8,MAD2L1,ZWINT,NUF2,CDC20,NCAPH,NCAPG,BUB1,ZWILCH, BIRC5,CCNB1,CCNB2,SGOL1,SPC24,ERCC6L,PLK1,KIF2C,CDK1,BUB1B, CENPM,CENPF
PLK1 signaling events(N)	14	0	2.12E-13	AURKA,CDC20,CLSPN,TPX2,BUB1,CCNB1,KIF20A,PRC1,SGOL1,SPC24, ERCC6L,PLK1,CDK1,BUB1B
Mitotic Metaphase and Anaphase(R)	19	0	4.91E-11	AURKB,PTTG1,CDCA8,MAD2L1,ZWINT,NUF2,CDC20,BUB1,ZWILCH,BIRC5, SGOL1,SPC24,ERCC6L,PLK1,KIF2C,UBE2C,BUB1B,CENPM,CENPF
Aurora B signaling(N)	11	0	6.25E-10	AURKA,AURKB,CDCA8,NCAPH,NCAPG,BUB1,BIRC5,KIF20A, SGOL1,KIF23,KIF2C
Cell cycle(K)	16	0	6.30E-10	PTTG1,CCNA2,MAD2L1,CDC20,CDC6,GADD45B,BUB1,CCNB1,CCNB2, PKMYT1,ORC1,PLK1,CDC45,CDK1,MCM5,BUB1B
Cell Cycle Checkpoints(R)	14	0	2.64E-08	MAD2L1,CDC20,CLSPN,CDC6,CCNB1,CCNB2,PKMYT1,MCM10,ORC1, CDC45,CDK1,UBE2C,MCM5,BUB1B
FOXM1 transcription factor network(N)	9	0	2.09E-07	AURKB,CCNA2,BIRC5,CCNB1,CCNB2,PLK1,CDK1,FOXM1,CENPF
Oocyte meiosis(K)	12	0	1.43E-06	AURKA,PTTG1,MAD2L1,CDC20,BUB1,CCNB1,CCNB2,RPS6KA1,PKMYT1, SGOL1,PLK1,CDK1
APC/C-mediated degradation of cell cycle proteins(R)	10	0	4.21E-06	AURKA,AURKB,PTTG1,MAD2L1,CDC20,CCNB1,PLK1,CDK1,UBE2C,BUB1B

Mitotic G2-G2/M phases(R)	10	0	7.03E-05	AURKA,CCNA2,MYBL2,CCNB1,CCNB2,PKMYT1,PLK1,CDK1,FOXM1,CENPF
Progesterone-mediated oocyte maturation(K)	9	0	8.54E-05	CCNA2,MAD2L1,BUB1,CCNB1,CCNB2,RPS6KA1,PKMYT1,PLK1,CDK1
E2F transcription factor network(N)	8	0	9.30E-05	SERPINE1,CCNA2,MYBL2,TK1,CDC6,RRM2,ORC1,CDK1
Mitotic G1-G1/S phases(R)	10	0	1.64E-04	MYBL2,CDC6,RRM2,CCNB1,PKMYT1,MCM10,ORC1,CDC45,CDK1,MCM5
ATR signaling pathway(N)	6	0	2.29E-04	CCNA2,CLSPN,CDC6,RAD51,FANCD2,PLK1
p53 signaling pathway(K)	7	0	7.23E-04	SERPINE1,GTSE1,RRM2,GADD45B,CCNB1,CCNB2,CDK1
p73 transcription factor network(N)	7	0.0001	0.001074	SERPINE1,CCNA2,RAD51,BUB1,CCNB1,PLK1,CDK1
Aurora A signaling(N)	5	0.0001	0.001074	AURKA,AURKB,TPX2,BIRC5,TACC3
Mitotic Telophase/Cytokinesis(R)	3	0.0009	0.014663	KIF20A,PLK1,KIF23
cdk regulation of dna replication(B)	3	0.0018	0.028243	CDC6,ORC1,MCM5

Table 3-4: Network Pathway Annotation Terms Enriched in Rapamycin Up-Regulated Genes in 2DD Fibroblasts by Log-Base (2) Analyses. Genes ≥5-fold up-regulated in response to rapamycin treatment were analysed for enrichment of KEGG terms. The identified enriched pathway KEGG annotation terms (GeneSet) from network analyses are listed. The total number of genes from the network identified to be up-regulated in response to quiescence and belonging to a specific pathway was identified. P-value (with 0 values equating to <0.0001) and false discovery rates (FDR) are presented. All P-Value and FDR are <0.05. Nodes identify specific genes/proteins from our datasets present in the networks. Gene lists identified by log-base (2) transforming data.

	Protein From Network	P-Value	FDR	Nodes
Pathways in cancer(K)	22	0	0.002177	PTGS2,FGF7,FGF2,SOS2,IL6,PTGER2,CDK6,KRAS,BMP2,CBLB,LAMA3, TGFA,HHIP,FZD9,BIRC3,BIRC2,FGF13,WNT4,ITGAV,NKX3-1,ITGA2,PLCB1
Signaling pathways regulating pluripotency of stem cells(K)	12	0	0.003616	FGF2,INHBA,RIF1,IL6ST,LIF,KRAS,BMP2,SMAD9,FZD9,JARID2,WNT4,SKIL
TGF-beta signaling pathway(P)	8	0.0001	0.018955	INHBA,ZFYVE16,GDF6,BMP2,SMAD9,BMP6, GDNF,SKIL
Jak-STAT signaling pathway(K)	11	0.0002	0.018955	IL13RA2,SOS2,IL6,IL11,IL24,SPRY2,CSF2RB, IL6ST,LIF,CBLB,IL21R
TNF signaling pathway(K)	9	0.0002	0.018955	PTGS2,IL6,IL1B,TNFAIP3,EDN1,LIF,CXCL1, BIRC3,BIRC2
ErbB signaling pathway(K)	8	0.0002	0.018955	EREG,SOS2,HBEGF,KRAS,CBLB,TGFA,SHC2,SHC4
Signaling by EGFR(R)	11	0.0004	0.026294	FGF7,FGF2,EREG,IL6,RICTOR,HBEGF,NR4A1,SPRY2,IL6ST,KRAS,PAG1
Platelet homeostasis(R)	6	0.0004	0.027269	PDE5A,FGR,PRKG1,ATP2B1,TRPC6,PLA2G4A
Validated transcriptional targets of AP1 family members Fra1 and Fra2(N)	5	0.0006	0.031558	IL6,MGP,THBD,LIF,LAMA3
Signaling by FGFR(R)	10	0.0006	0.031558	FGF7,FGF2,EREG,IL6,RICTOR,HBEGF,NR4A1,SPRY2,IL6ST,KRAS
NOD-like receptor signaling pathway(K)	6	0.0007	0.031558	IL6,IL1B,TNFAIP3,CXCL1,BIRC3,BIRC2

Hypertrophic cardiomyopathy (HCM)(K)	7	0.0009	0.034605	CACNB2,ACTC1,IL6,PRKAA2,ITGAV,ITGA2,ITGA8
MAPK signaling pathway(K)	13	0.001	0.034605	CACNB2,TAOK1,FGF7,FGF2,SOS2,RASA2,RPS6KA6,IL1B,NR4A1,KRAS, PLA2G4A,FGF13,MAP3K2
Gastrin-CREB signalling pathway via PKC and MAPK(R)	11	0.001	0.034605	GPR68,IL6,DGKI,HBEGF,IL6ST,EDN1,KRAS,TRPC6,AGT,F2RL1,PLCB1
Signaling by SCF-KIT(R)	9	0.001	0.034764	FGF7,FGF2,EREG,IL6,RICTOR,HBEGF,NR4A1,IL6ST,KRAS
Small cell lung cancer(K)	7	0.0011	0.035635	PTGS2,CDK6,LAMA3,BIRC3,BIRC2,ITGAV,ITGA2
Glioma(K)	6	0.0013	0.036366	SOS2,CDK6,KRAS,TGFA,SHC2,SHC4
Cell adhesion molecules (CAMs)(K)	9	0.0014	0.036366	VCAN,NRCAM,CLDN4,F11R,NLGN1, ITGAV,ITGA8,CD274,ICOSLG
NF-kappa B signaling pathway(K)	7	0.0015	0.036366	PTGS2,IL1B,BCL10,TNFAIP3,DDX58,BIRC3,BIRC2
Signaling by Type 1 Insulin-like Growth Factor 1 Receptor (IGF1R)(R)	7	0.0015	0.036366	FGF7,FGF2,IL6,IL6ST,KRAS,PRKAA2,SHC2
FGF signaling pathway(P)	7	0.0016	0.036366	FGF7,FGF2,SOS2,SPRY2,KRAS,FGF13,MAP3K2
Signalling by NGF(R)	13	0.0016	0.036366	MEF2A,FGF7,FGF2,EREG,SOS2,IL6,RICTOR,HBEGF,FGD4,NR4A1, IL6ST,KRAS,SHC2
Signaling by ERBB4(R)	9	0.0017	0.036366	FGF7,FGF2,EREG,IL6,RICTOR,HBEGF,NR4A1,IL6ST,KRAS
Integrins in angiogenesis(N)	5	0.0018	0.038509	FGF2,PIK3C2A,EDIL3,F11R,ITGAV
CD40/CD40L signaling(N)	4	0.0021	0.041874	TNFAIP3,CBLB,BIRC3,BIRC2
Cell surface interactions at the vascular wall(R)	7	0.0023	0.042963	ANGPT1,SLC7A8,THBD,F11R,KRAS,ITGAV,PROS1
Signaling by ERBB2(R)	9	0.0024	0.042963	FGF7,FGF2,EREG,IL6,RICTOR,HBEGF,NR4A1,IL6ST,KRAS
Chronic myeloid leukemia(K)	6	0.0024	0.042963	SOS2,CDK6,KRAS,CBLB,SHC2,SHC4
SHP2 signaling(N)	5	0.0026	0.044254	ANGPT1,IL6,IL6ST,KRAS,PAG1
ErbB receptor signaling network(N)	3	0.0027	0.046727	EREG,HBEGF,TGFA

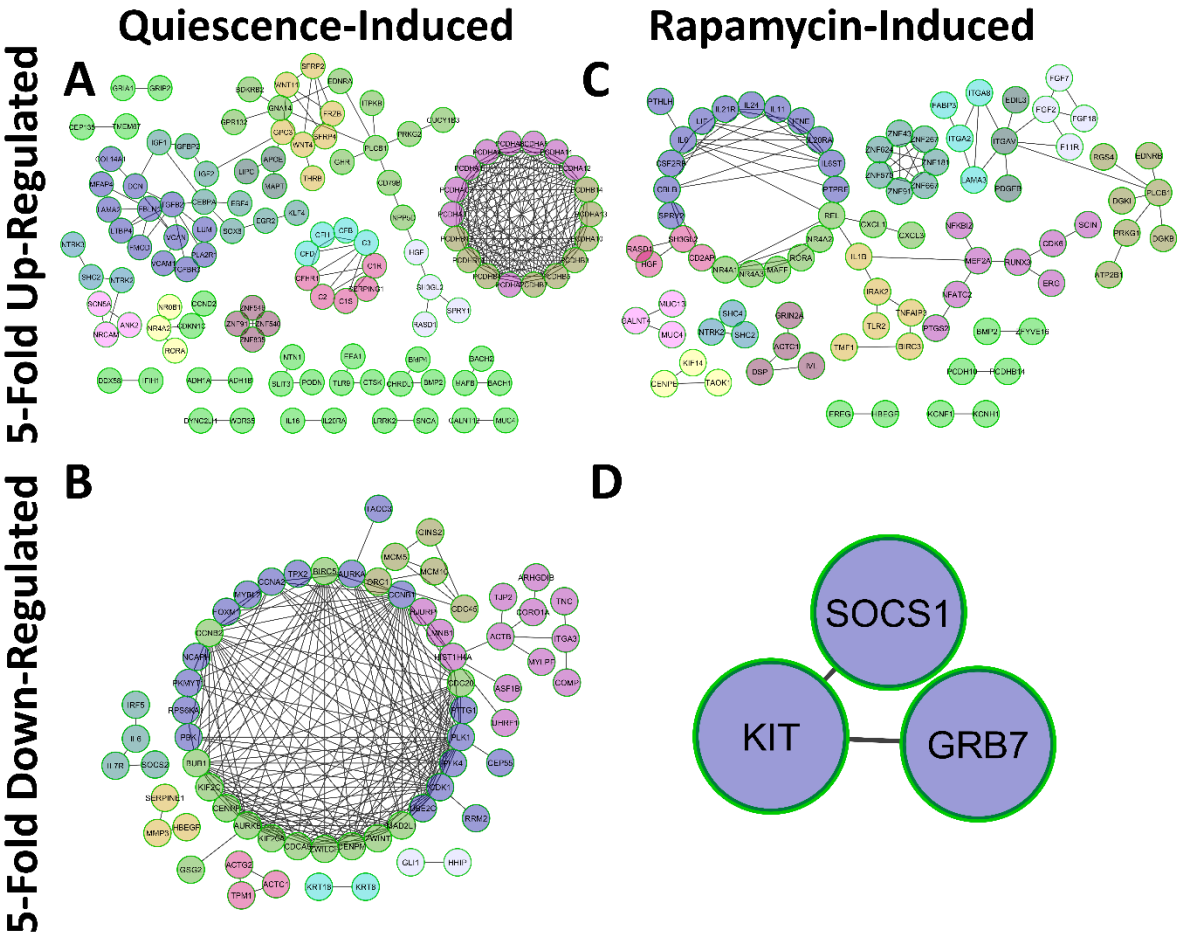

Figure 3-10: Modules Identified in Genes Changing Expression ≥5-Fold in Response to Rapamycin Treatment and Quiescence Induction Based On Comparative Fold Change Analyses in 2DD Fibroblasts. Network analyses identified groups of functionally related genes (modules) in (A) ≥5-fold up-regulated quiescence-induced genes, (B) ≥5-fold down-regulated quiescence-induced genes, (C) ≥5-fold up-regulated rapamycin-induced genes, (D) ≥5-fold down regulated rapamycin-induced genes. Each node (circle) is representative of a gene whilst every colour is representative of a module. Solid lines represent genes linked within the same module and between modules based on the ReactomeFI database.

Table 3-5: Network Pathway Annotation Terms Enriched in Quiescence Up-Regulated Genes in 2DD Fibroblasts by Fold Change Analyses. Genes ≥5-fold up-regulated in response to quiescence induction were analysed for enrichment of KEGG terms. The identified enriched pathway KEGG annotation terms (GeneSet) from network analyses are listed. The total number of genes from the network identified to be up-regulated in response to quiescence and belonging to a specific pathway was identified. P-value (with 0 values equating to <0.0001) and false discovery rates (FDR) are presented. All P-Value and FDR are <0.05. Nodes identify specific genes/proteins from our datasets present in the networks. Gene lists identified by comparative fold change analyses.

	Protein From Network	P-Value	FDR	Nodes
Cadherin signaling pathway(P)	18	0	1.33E-08	PCDHB14,PCDHB12,PCDHB11,PCDHA11,PCDHA12,PCDHA8, PCDHA2,PCDHA3,PCDHA4,PCDHA5,PCDHA1,PCDHB7,PCDHB5, PCDHB3,PCDHB4,WNT4,PCDHAC2,WNT11
Wnt signaling pathway(P)	23	0	2.12E-05	PCDHB14,PCDHB12,PCDHB11,GNA14,PCDHA11,PCDHA12,FRZB, SFRP2,SFRP4,PCDHA8,PCDHA2,PCDHA3,PCDHA4,PCDHA5, PCDHA1,PCDHB7,PCDHB5,PCDHB3,PCDHB4,WNT4, PCDHAC2,PLCB1,WNT11
Complement and coagulation cascades(K)	11	0	1.12E-04	SERPING1,TFPI,C3,C2,CFH,CFD,BDKRB2,CFB,PROS1,C1R,C1S
Extracellular matrix organization(R)	18	0	0.002188	LTBP4,ADAMTS5,COL14A1,VCAN,FMOD,TGFB2,PCOLCE2, MFAP4,DCN,VCAM1,MATN1,BMP4,BMP2,LAMA2,COL21A1, FBLN1,CTSK,LUM
Response to elevated platelet cytosolic Ca2+(R)	9	0.0001	0.013269	SERPING1,HGF,IGF1,IGF2,TGFB2,CFD,CD36,CLU,PROS1
Staphylococcus aureus infection(K)	7	0.0003	0.026255	C3,C2,CFH,CFD,CFB,C1R,C1S

Table 3-6: Network Pathway Annotation Terms Enriched in Quiescence Down-Regulated Genes in 2DD Fibroblasts by Fold Change Analyses. Genes ≥5-fold down-regulated in response to quiescence induction were analyzed for enrichment of KEGG terms. The identified enriched pathway KEGG annotation terms (GeneSet) from network analyses are listed. The total number of genes from the network identified to be up-regulated in response to quiescence and belonging to a specific pathway was identified. P-value (with 0 values equating to <0.0001) and false discovery rates (FDR) are presented. All P-Value and FDR are <0.05. Nodes identify specific genes/proteins from our datasets present in the networks. Gene lists identified by comparative fold change analyses.

	Protein From Network	P-Value	FDR	Nodes
Mitotic Prometaphase(R)	16	0	5.92E-11	AURKB,CDCA8,MAD2L1,ZWINT,CDC20,NCAPH,BUB1,ZWILCH,BIRC5,CCNB1, CCNB2,PLK1,KIF2C,CDK1,CENPM,CENPF
FOXM1 transcription factor network(N)	10	0	2.55E-08	AURKB,CCNA2,TGFA,BIRC5,CCNB1,CCNB2,PLK1,CDK1,FOXM1,CENPF
Cell cycle(K)	13	0	7.35E-07	PTTG1,CCNA2,MAD2L1,CDC20,BUB1,CCNB1,CCNB2,PKMYT1,ORC1, PLK1,CDC45,CDK1,MCM5
Mitotic Metaphase and Anaphase(R)	14	0	1.43E-06	AURKB,PTTG1,CDCA8,MAD2L1,ZWINT,CDC20,BUB1, ZWILCH,BIRC5,PLK1,KIF2C,UBE2C,CENPM,CENPF
Aurora B signaling(N)	8	0	3.38E-06	AURKA,AURKB,CDCA8,NCAPH,BUB1,BIRC5,KIF20A,KIF2C
PLK1 signaling events(N)	8	0	5.78E-06	AURKA,CDC20,TPX2,BUB1,CCNB1,KIF20A,PLK1,CDK1
Mitotic G2-G2/M phases(R)	11	0	8.54E-06	AURKA,CCNA2,MYBL2,CCNB1,CCNB2,PKMYT1,PLK4,PLK1,CDK1,FOXM1,CENPF
Oocyte meiosis(K)	11	0	8.78E-06	AURKA,PTTG1,MAD2L1,CDC20,BUB1,CCNB1,CCNB2,RPS6KA1,PKMYT1,PLK1,CDK1
Cell Cycle Checkpoints(R)	11	0	1.01E-05	MAD2L1,CDC20,CCNB1,CCNB2,PKMYT1,MCM10,ORC1,CDC45,CDK1,UBE2C,MCM5

APC/C-mediated degradation of cell cycle proteins(R)	9	0	2.90E-05	AURKA,AURKB,PTTG1,MAD2L1,CDC20,CCNB1,PLK1,CDK1,UBE2C
Progesterone-mediated oocyte maturation(K)	9	0	6.31E-05	CCNA2,MAD2L1,BUB1,CCNB1,CCNB2,RPS6KA1,PKMYT1,PLK1,CDK1
E2F transcription factor network(N)	7	0	7.32E-04	SERPINE1,CCNA2,MYBL2,TK1,RRM2,ORC1,CDK1
Mitotic G1-G1/S phases(R)	9	0	8.24E-04	MYBL2,RRM2,CCNB1,PKMYT1,MCM10,ORC1,CDC45,CDK1,MCM5
Gastrin-CREB signalling pathway via PKC and MAPK(R)	11	0	8.24E-04	EDN1,MCHR1,KISS1,IL6,RPS6KA1,HBEGF,MMP3,P2RY6,ADRA1D,CDK1,OXTR
Aurora A signaling(N)	5	0	0.00109	AURKA,AURKB,TPX2,BIRC5,TACC3
p53 signaling pathway(K)	6	0.0002	0.004892	SERPINE1,GTSE1,RRM2,CCNB1,CCNB2,CDK1
p73 transcription factor network(N)	6	0.0003	0.007304	SERPINE1,CCNA2,BUB1,CCNB1,PLK1,CDK1
Mitotic Prophase(R)	5	0.0013	0.024442	CCNB1,CCNB2,HIST1H4A,PLK1,CDK1
Nicotinic acetylcholine receptor signaling pathway(P)	3	0.0027	0.048744	ACTG2,ACTC1,ACTB

Table 3-7: Network Pathway Annotation Terms Enriched in Rapamycin Up-Regulated Genes in 2DD Fibroblasts by Fold Change Analyses. Genes ≥5-fold up-regulated in response to rapamycin treatment were analysed for enrichment of KEGG terms. The identified enriched pathway KEGG annotation terms (GeneSet) from network analyses are listed. The total number of genes from the network identified to be up-regulated in response to quiescence and belonging to a specific pathway was identified. P-value (with 0 values equating to <0.0001) and false discovery rates (FDR) are presented. All P-Value and FDR are <0.05. Nodes identify specific genes/proteins from our datasets present in the networks. Gene lists identified by comparative fold change analyses.

	Protein From Network	P-Value	FDR	Nodes
Cytokine-cytokine receptor interaction(K)	18	0	0.001921	HGF,INHBA,CCL20,IL6,TNFSF15,IL11,IL1B,IL24,CSF2RB, IL6ST,IFNE,LIF,BMP2,IL20RA,CXCL1,CXCL3,PDGFB,IL21R
Validated transcriptional targets of AP1 family members Fra1 and Fra2(N)	7	0	0.001921	IL6,MGP,THBD,NFATC2,LIF,LAMA3,IVL
Pathways in cancer(K)	20	0.0001	0.016348	PTGS2,HGF,FGF7,FGF2,IL6,CDK6,LPAR5,BMP2,CBLB,LAMA3,EDNRB,TGFA, BIRC3,FGF18,PDGFB,ITGAV,NKX3-1,ITGA2,PLCB1,RASGRP3
Signaling by EGFR(R)	12	0.0001	0.017694	SH3GL2,FGF7,FGF2,EREG,IL6,RICTOR,HBEGF,NR4A1, SPRY2,IL6ST,FGF18,PDGFB
ErbB receptor signaling network(N)	4	0.0002	0.017694	AREG,EREG,HBEGF,TGFA
Signaling by FGFR(R)	11	0.0002	0.017694	FGF7,FGF2,EREG,IL6,RICTOR,HBEGF,NR4A1,SPRY2,IL6ST, FGF18,PDGFB
Jak-STAT signaling pathway(K)	11	0.0003	0.017694	IL6,IL11,IL24,SPRY2,CSF2RB,IL6ST,IFNE,LIF, CBLB,IL20RA,IL21R
Signalling by NGF(R)	15	0.0003	0.017694	MEF2A,SH3GL2,FGF7,FGF2,EREG,IL6,RICTOR, HBEGF,FGD4,NR4A1,IL6ST,NTRK2,FGF18,PDGFB,SHC2
TNF signaling pathway(K)	9	0.0003	0.017694	PTGS2,CCL20,IL6,IL1B,TNFAIP3,LIF,CXCL1,CXCL3,BIRC3

Signaling by SCF-KIT(R)	10	0.0004	0.01849	FGF7,FGF2,EREG,IL6,RICTOR,HBEGF,NR4A1, IL6ST,FGF18,PDGFB
PIP3 activates AKT signaling(R)	8	0.0005	0.02404	FGF7,FGF2,EREG,RICTOR,HBEGF,NR4A1,FGF18,PDGFB
Signaling by ERBB4(R)	10	0.0006	0.026028	FGF7,FGF2,EREG,IL6,RICTOR,HBEGF,NR4A1, IL6ST,FGF18,PDGFB
Signaling by ERBB2(R)	10	0.0009	0.035945	FGF7,FGF2,EREG,IL6,RICTOR,HBEGF,NR4A1,IL6ST,FGF18,PDGFB

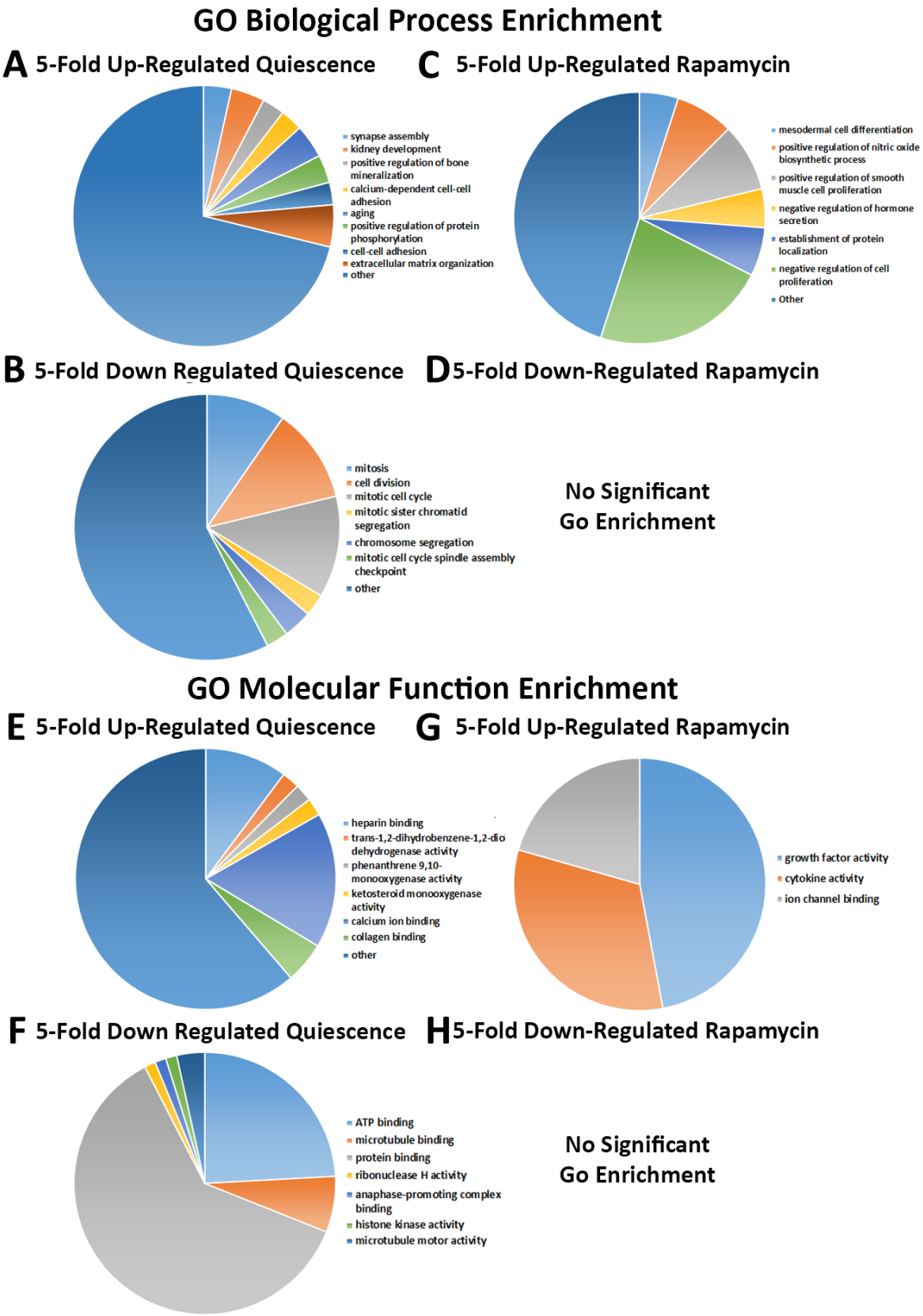

Figure 3-11: GO Term Enrichment in Quiescent-Induced and Rapamycin-Treated Gene Sets Based on Log-Base (2) Analyses in 2DD Fibroblasts. GO Biological Process terms significantly enriched for in quiescence (A) up-regulated and (B) down-regulated genes (≥5-fold), as well as rapamycin-induced (C) up-regulated and (D) ***(Figure 3-11 Legend Continued)***

down-regulated genes (≥5-fold). GO Molecular Process terms significantly enriched for in quiescence (E) up-regulated and (F) down-regulated genes (≥5-fold), as well as rapamycin-induced (G) up-regulated and (H) down-regulated genes (≥5-fold). P-value < 0.05, FDR < 0.05.

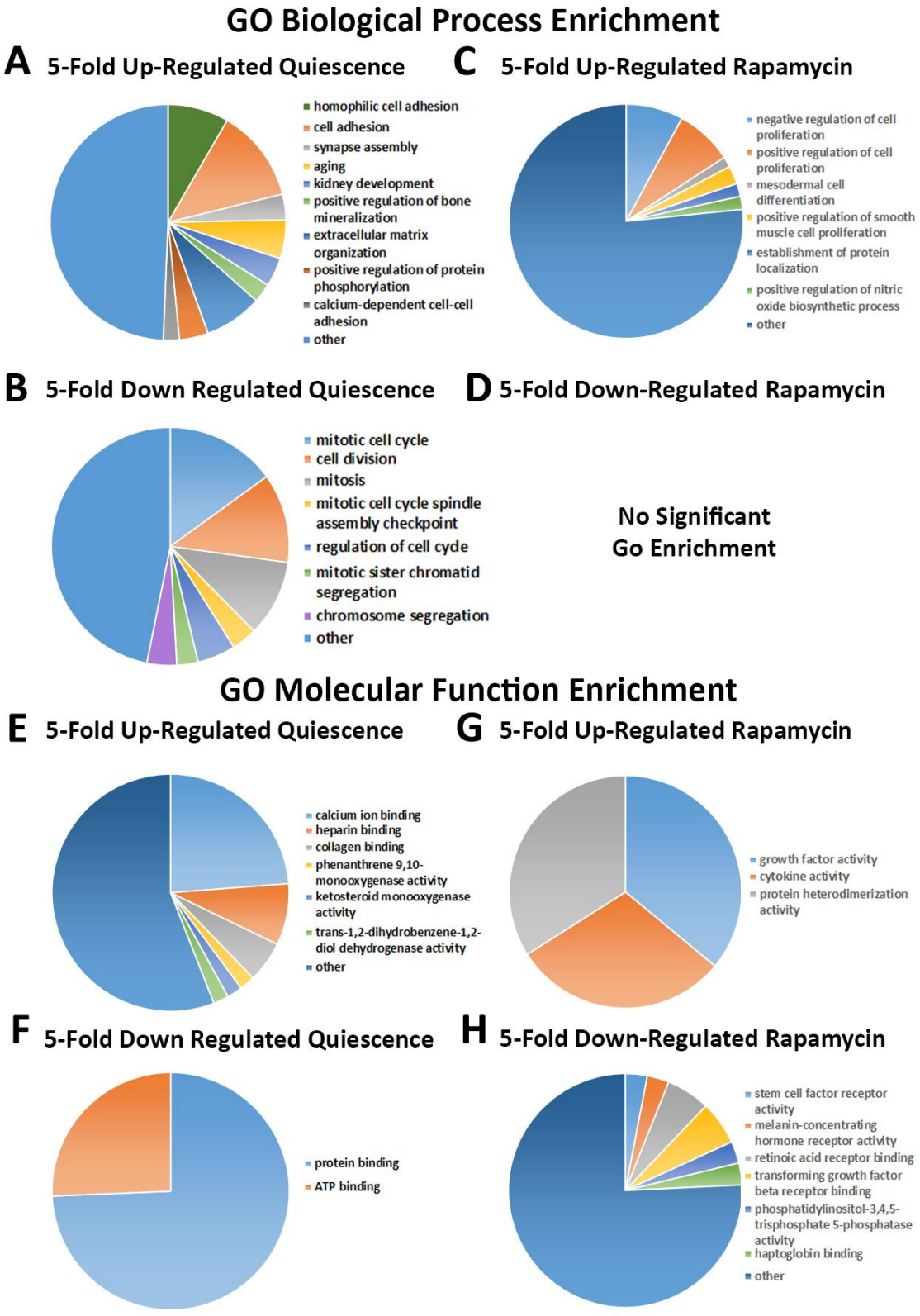

Figure 3-12: GO Term Enrichment in Quiescence-Induced and Rapamycin-Treated Gene Sets Based on Fold Change Analyses in 2DD Fibroblasts. GO Biological Process terms significantly enriched for in quiescence (A) up-regulated and (B) down-regulated genes (≥5-fold), as well as rapamycin-induced (C) up-regulated and (D) down-regulated genes (≥5-fold). GO Molecular Process terms significantly enriched for in quiescence (E) up-regulated and (F) down-regulated genes (≥5-fold), as well as rapamycin-induced (G) up-regulated and (H) down-regulated genes (≥5-fold). P-value < 0.05, FDR < 0.05.

3.7 Changes Induced by Rapamycin at the Transcript Level Alter Protein Expression

In order to determine that changes induced by rapamycin treatment of 2DD fibroblasts were influential at the protein level, western blots and enzyme linked immuno-sorbent assays (ELISA) were performed on the protein equivalents of genes changing significantly in response to treatment conditions. The actin, alpha cardiac muscle 1 (*ActC1*) gene had the highest fold increase as a function of rapamycin treatment, as demonstrated by BEDgraphs of the raw sequence reads (Figure 3-13A). Western blot analyses confirmed that this increase in transcript abundance equated to an increase in the ACTC1 protein (Figure 3-13B). Western blot analysis further confirmed an increase in the presence of LIF in response to rapamycin treatment when compared to proliferative samples (Figure 3-13B). Cytokine-cytokine receptor interaction was one of the most enriched for pathways in genes ≥5 fold up-regulated in response to rapamycin treatment, with the genes encoding for the cytokines IL-6, IL-8 and the protein Leukaemia Inhibitory Factor (LIF) present within the pathway. ELISA analyses of IL-6 and IL-8 confirmed that these cytokines were produced in response to rapamycin treatment and secreted into the cell media (Figure 3-13C). Therefore, rapamycin induces changes in gene expression that are enriched for in the cytokine-cytokine receptor interaction pathway which are conserved at the protein level, with overall rapamycin eliciting a response in fibroblasts that is broadly enriched for in cytokines.

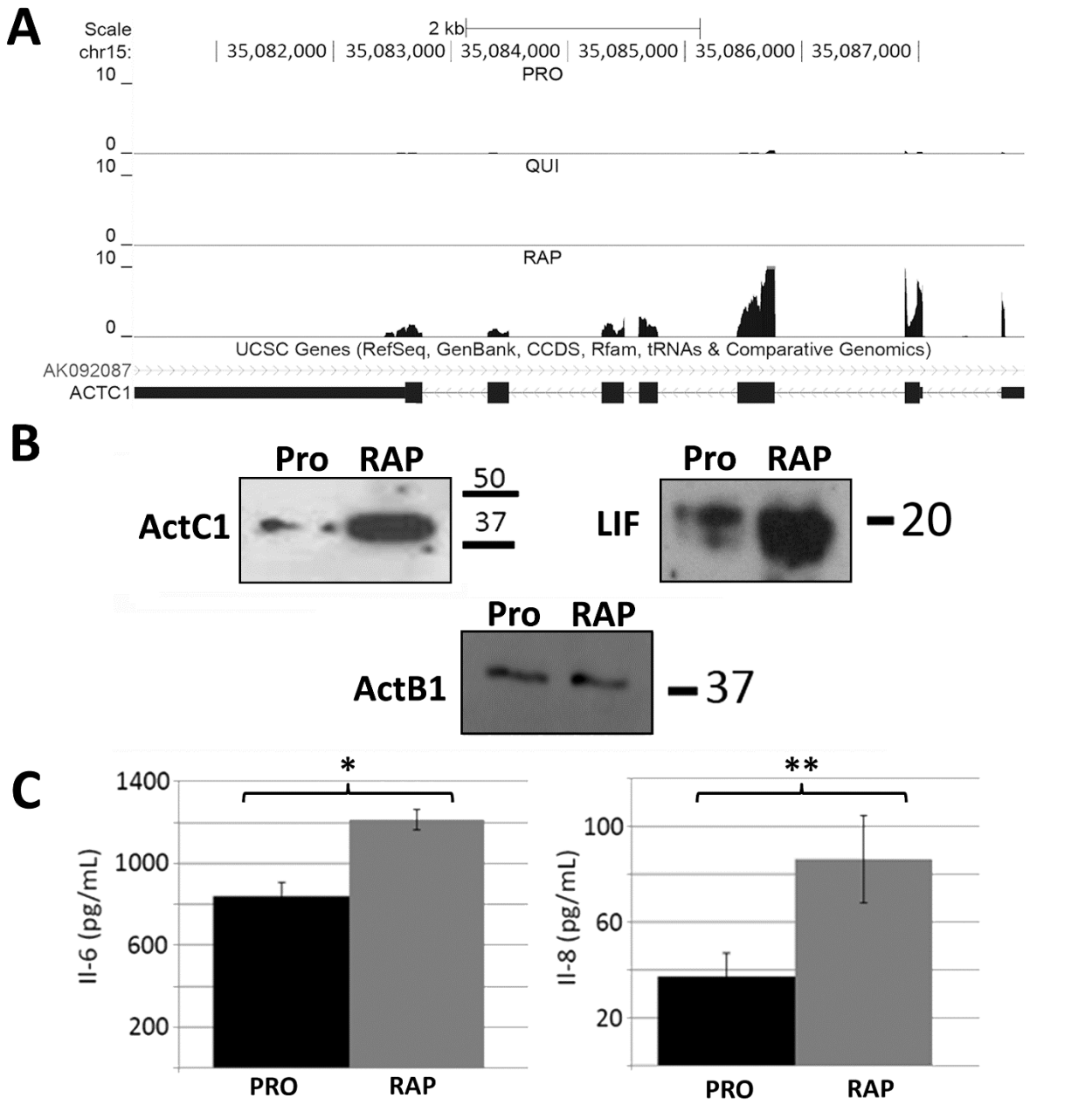

Figure 3-13: Proteins Levels of LIF, Il-6 and Il-8 Increase in Response to Rapamycin Treatment in 2DD Fibroblasts. (A) BEDgraph for *ActC1* demonstrating the total number of RNAseq reads from the *ActC1* gene from proliferative (PRO), quiescent (QUI) and rapamycin (RAP) treated fibroblasts. Low numbers of reads were observed in PRO samples with very few reads observed in QUI samples. Scale at the top of the panel represents the genomic location with the scale on the left of the graphs representing the number of reads. The light grey cap represents where the reads mapped exceed the scale. Bottom row demonstrates the coding regions with genomic locations, with arrow heads indicating the direction of the gene and the blue bars the coding regions. (B) Western blot of whole cell-protein extracts from (PRO) and rapamycin-treated (RAP) fibroblasts for ActC1, LIF (~20 kDa) and the load control ActB1 (~37 kDa). Molecular weights (in kDa) are shown to the right of ***(Figure Legend 3-13 Continued)***

the blots. (C) Sandwich ELISA assays confirmed that rapamycin-induced increases in transcript profiles from IL-6 and IL-8 genes also caused increased levels of secreted cytokines. Three biological replicates of culture media from proliferative (PRO) and 5-day rapamycin-treated (RAP) fibroblasts. P-values for one tailed student's t-tests are shown for IL-6 (*p=0.006) and IL-8 (**p=0.038). Error bars = S.E.M.

3.8 STAT5A/B Binding Sites Are Enriched in Rapamycin-Induced Gene Expression

It is possible that rapamycin-induced changes in gene expression are being mediated by specific transcription factors. Therefore, transcription factor motif searches using the *cis*-element over-representation (CLOVER) algorithm were conducted (Frith *et al.* 2004). Analyses were focused on promoter regions from 1000 bp upstream to 50 bp downstream of the transcription start site of genes that exhibited ≥5- fold change in expression. Several binding motifs for the Signal Transducer and Activator of Transcription (STAT) family were enriched in the promoters of genes up-regulated by rapamycin (Figure 3-14A). Up-regulated genes from rapamycin-treated datasets, such as *IL-6ST* and *LIF*, are known to be regulated by the STAT5A/B transcription factor (Salas *et al.* 2011). Furthermore, unlike other members of the STAT family, STAT5A/B had a significant number of reads in the rapamycin compared too proliferative RNA-seq datasets, indicating that it was expressed. Therefore, analysis was focused on the STAT5A/B transcription factor in order to determine whether or not STAT5A/B is involved in mediated changes in gene expression in response to rapamycin. CLOVER analyses revealed that of the 421 identified up-regulated genes by fold change in response to rapamycin treatment, 144 (34.2%) contained a STAT5A/B consensus binding element. These findings were significant compared to genomic background (p-value <0.05). To confirm increased presence of active (phosphorylated) STAT5A/B in the cell nucleus, immuno-fluorescence microscopy and subsequent line scans demonstrated that cells treated with rapamycin have larger, brighter foci of STAT5A/B within the nucleus (Figure 3-14B & 3-14C). However, this was only apparent in a sub-population (40%) of labelled cells. Although transcript levels of STAT5A/B did not significantly increase by RNAseq, western blot analysis of rapamycin-treated 2DD whole protein lysates at 120 h revealed an increase in the amount of STAT5A/B, indicating that rapamycin may stabilize STAT5A/B protein levels and drive transcription of STAT5A/B-mediated genes (Figure 3-14D).

In order to confirm the increase of STAT5A/B transcription factor binding in genes up-regulated by rapamycin treatment at 120 h, chromatin immuno-precipitation (ChIP) assays were performed. These assays revealed occupancy of STAT5A/B in the promoters of every

rapamycin up-regulated gene tested (15) (Figure3-14E). *MMP2*, *XPO7*, and *ActinB*, which do not contain STAT5A/B elements, alongside intergenic region of chromosome 18, did not exhibit significant STAT5A/B above input, acting as negative controls. Furthermore, ChIP for RNA polymerase II was used as a positive control to validate enrichment of these assays. These findings demonstrate that STAT5A/B promoter occupancy increased in rapamycin-treated fibroblasts and that STAT5A/B may be a factor key in mediating the reported cytokine response.

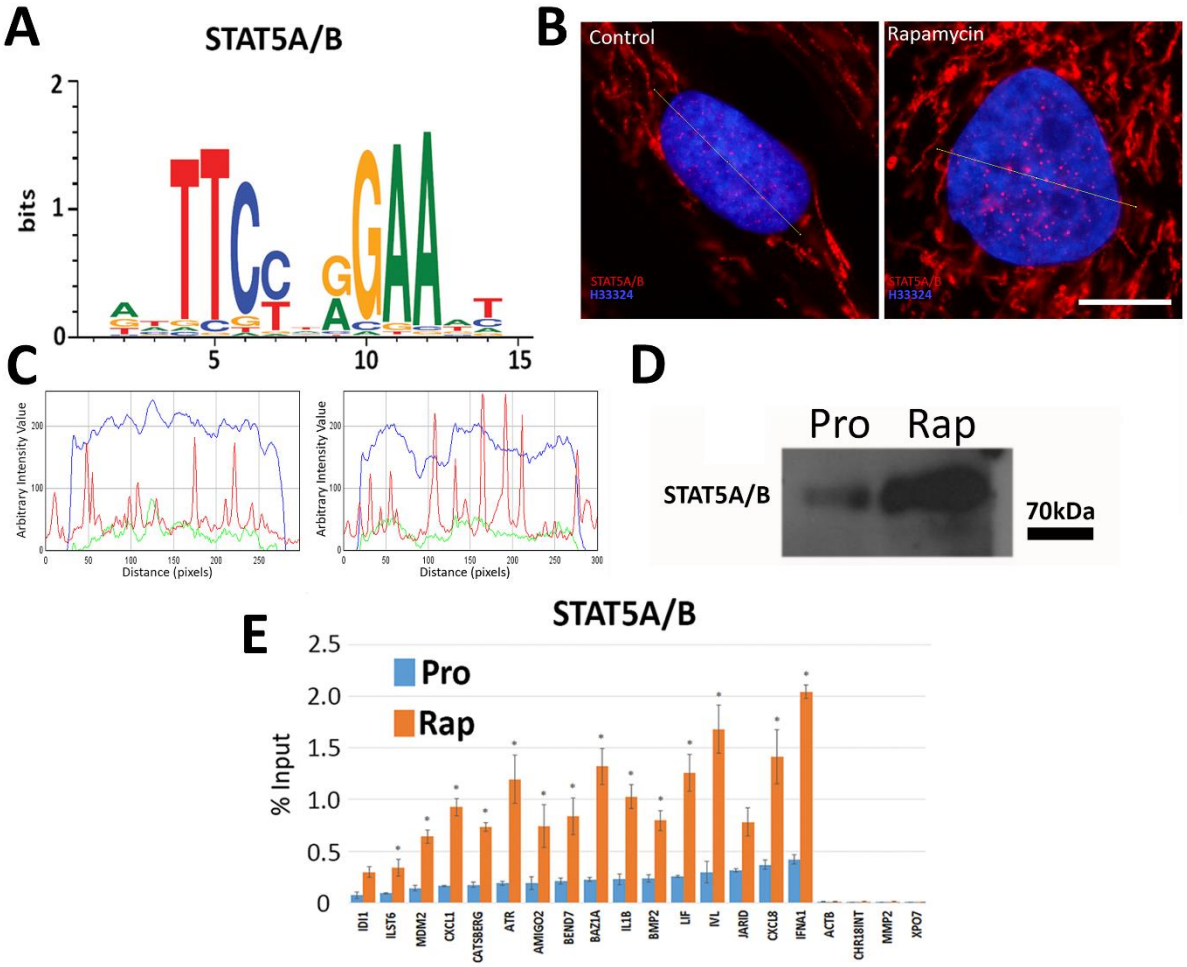

Figure 3-14: Increased STAT5A/B Promoter Occupancy in Genes Up-Regulated in Response to Rapamycin in 2DD Fibroblasts. Using CLOVER, promoters of genes that increased expression following rapamycin treatment were identified as enriched in STAT5A/B transcription factor binding sites. (A) Position weight matrix/sequence logo of this binding site is shown. Scale to the left represents the log-base (2) of the information content of each nucleotide and the bottom scale represents the position of those nucleotides within the binding site. (B) Immuno-fluorescence for phosphorylated Y694-STAT5A/B (Y694P; red) in proliferating (Control) and rapamycin-treated (rapamycin) ***(Figure 3-14 Legend Continued)***

fibroblasts. Chromatin is counterstained with H33342 (blue). Scale bar = 10 μm. (C) Representative line scans (measured in arbitrary intensity units, yellow lines) of immunofluorescence for phosphorylated Y694-STAT5A/B (Y694P; red) in proliferating (Control) and rapamycin-treated (rapamycin) fibroblasts showing larger brighter foci of STAT5A/B (red) in a subpopulation of fibroblasts. Chromatin is counterstained with H33342 (blue). Intensity values for STAT5A/B (red lines) and chromatin (blue lines) are represented graphically. Pixel dimensions = 49.6 nm. (D) Western blot analysis of STAT5A/B (70kDa) of proliferative (PRO) and rapamycin treated (RAP) fibroblasts. (E) ChIP assays were used to compare promoter occupancy of STAT5A/B in proliferative (Pro/blue) and rapamycin treated (Rap/orange) samples. Promoters analysed (X-axis) and the percent enrichment over input reported (Y-axis). Error bars = S.E.M. and * = significant enrichment, p-values ≤0.05.

3.9 CLOVER Analyses Revealed Further Transcription Factor Binding Sites in Rapamycin Up-Regulated Genes

In addition to the examined STAT5A/B consensus sites and binding reported in response to rapamycin treatment, CLOVER screens of genes up-regulated ≥5-fold in response to rapamycin treatment revealed the presence of binding elements for Nuclear Factor of Activated T Cells (NFAT) transcription factor family in 346 of the 422 genes up-regulated by rapamycin treatment (82.0%) (Figure 3-15A). A significant increase in the level of NFATC2 transcript was also noted as a result of rapamycin treatment. NFAT family members are putatively involved in cell proliferation, apoptosis and tumorigenesis, and interestingly have been proposed to drive expression of several cytokines (Domhan *et al.* 2014). It has further been reported that NFATC2 may act to repress STAT5A/B function (Kojima *et al.* 2013). 30.9% of promoters contained both STAT5A/B and NFAT binding elements, with 90.9% of promoters that had STAT5A/B sites also having NFAT sites (Figure 3-15A). ChIP analyses of *CXCL-1*, *CXCL-2* and *JARID*, which had increased STAT5A/B occupancy, exhibited decreased NFATC2 binding in rapamycin-treated 2DD fibroblasts; however, *JAK2*, *ATR*, *IDI-1*, *IVL* and *LIF* showed little or no binding of NFATC2 under both conditions (proliferative and rapamycin-treated) (Figure 3-15B).

A family of proteins, known as Suppressor of Cytokine Synthesis (SOCS), are negative regulators of cytokine signalling and are documented to control STAT5 localization; binding and sequestering STAT5 molecules in the cytoplasm, controlling transcriptional activation and function of STAT5 (Zhao *et al.* 2010; Lee *et al.* 2013). RNAseq datasets for rapamycin-treated fibroblasts revealed a decrease of 5.05 fold in *SOCS1* transcript, qRT-PCR with biological

replicates demonstrating a 2.7+/-0.06-fold decrease in *SOCS1*. In addition to these findings, ChIP for STAT5A/B revealed increased promoter occupancy of *SOCS1* (Figure 3-15C).

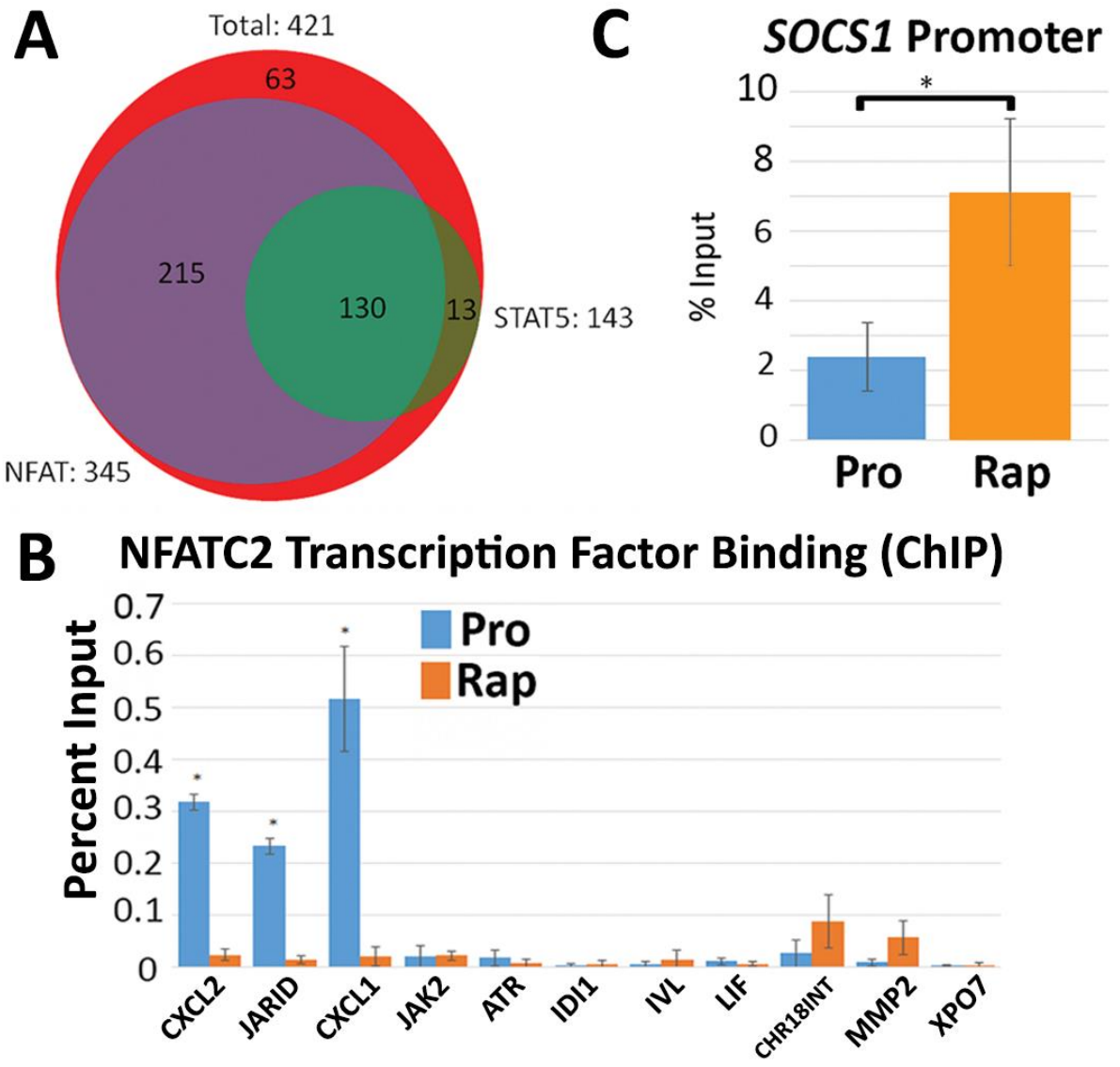

Figure 3-15: Overlap Between STAT5A/B and NFATC2 Promoters in Genes Up-Regulated by Rapamycin Treatment, But No Increase in NFACT2 Promoter Occupancy. (A) Venn diagram indicating the number of genes up-regulated by rapamycin (red; 421 genes) that shared STAT5A/B (green; 143 genes) and NFAT (purple; 345 genes) binding sites. (B) ChIP of SOCS1 promoter in proliferative (Pro; blue) and rapamycin (Rap; orange) samples. Error bars = S.E.M. and * = $p \leq 0.05$. (C) ChIP assays were also performed for NFATC2 promoter occupancy. Proliferative (Pro/blue) and rapamycin treated (Rap/orange) samples were compared. Promoters analysed are given at the bottom and the percent enrichment over input reported.

3.10 Removal of Rapamycin from Culture Following Treatments Shifts Growth Profiles of Fibroblasts Towards Proliferation

In order to determine if removal of 500 nM rapamycin would result in 2DD fibroblasts returning to a normal, proliferative, phenotype, a number of assays were repeated 120 h after rapamycin removal. These assays included; population doubling times, flow cytometry, Ki67 Immunofluorescence and EdU incorporation. Cell counts were recorded following 120 h of treatment and then 120 h post-treatment for a total of 240 h. Both population doubling times and total population doublings were calculated at both time points (Fig. 3-16A). Following 120 h of 500 nM rapamycin treatment in 2DD fibroblasts, population doubling times were increased, in keeping with previously reported findings (Figure 3-2A & 3-14A). 120 h post-removal of rapamycin treatment, population doubling times were still higher than that of the untreated control, but lower than that following the initial rapamycin treatment (Figure 3-14A). In keeping with these findings, total population doublings were lower than the control following rapamycin removal; however, were higher than at 120 h of rapamycin treatment. Furthermore, after 120 h treatment removal, no significant difference (student's t-test: $p \geq 0.05$) was detected between 120 h post-treatment and proliferative 2DD fibroblasts. Immuno-labelling with the proliferative marker Ki67 revealed little difference between post-rapamycin treatment and proliferative samples (69.0% and 69.5% respectively) (Fig. 3-16B & 3-16D). Following removal of 500 nM rapamycin treatment for 120 h, the percent of cells actively incorporating EdU increased in post-rapamycin treated 2DD fibroblasts when compared to proliferative fibroblasts (Figure 3-16C & 3-16D). In order to determine the number of cells in each stage of the cell cycle, a cell cycle assay incorporating propidium iodide and utilizing flow cytometry was conducted. In samples supplemented with proliferative growth media following 120 h of rapamycin treatment, there was an increase in cells in both S-phase (in agreement with data from EdU incorporation (Figure 3-15C)) and in cells in G2/M phase when compared to control samples, concordant with a decrease in cells in G1/0.

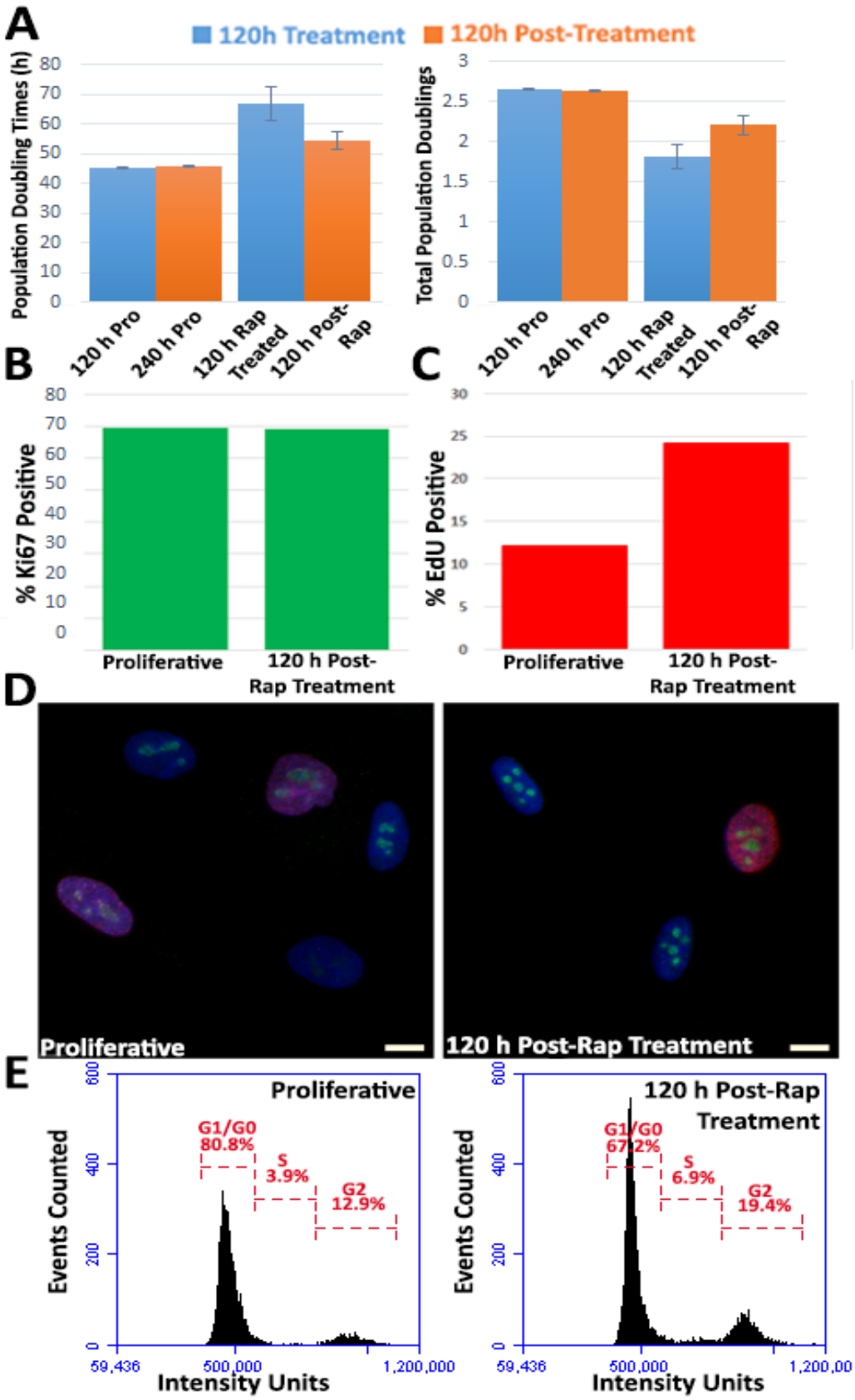

Figure 3-16: Removal of Rapamycin After 120 h of Treatment in 2DD Fibroblasts Induces Potentially Synchronized and Accelerated Rates of Proliferation. (A) Population doubling times (h) (Y-axis) and total population doublings (Y-axis) ***(Figure 3-16 Legend Continued)***

for proliferative and 500 nM rapamycin-treated fibroblasts at 120 h of treatment (blue) and 120 h post-treatment (orange). Error bars = S.E.M. (B) Representative graph for percent positive Ki67 (Y-axis) for proliferative (120 h Pro) and rapamycin-treated fibroblasts at 120 h post-treatment (120 h Post-Rap). (C) Representative graph for percent positive EdU (Y-axis) in proliferative (120 h Pro) and 500 nM rapamycin-treated fibroblasts 120 h post-treatment (120 h Post-Rap). (D) Representative images of immunofluorescence for proliferative (Left) and 120 h post-500 nM rapamycin treatment (120 h Post-Rap Treatment, Right) of Ki67 labelling (green) and EdU incorporation (red). Chromatin is counterstained with H33342. (E) Propidium iodine cell cycle analysis for proliferative and 500 nM rapamycin-treated fibroblasts 120 h post-treatment (120 h Post-Rap Treatment). Cells counted (Events Counted; Y-axis) and FL2-A (X-axis).

3.11 Discussion

Primary human foreskin fibroblasts (2DD) were treated in culture with 500 nM rapamycin for 120 h. Experiments conducted following this incubation revealed rapamycin-induced phenotypic changes in 2DD resembling quiescence. Rapamycin treatment and serum-reduction caused re-localization of chromosomes 18 and 10 within the nuclear volume. RNA sequencing analyses demonstrated significantly divergent transcriptional profiles between rapamycin-treated and quiescence-induced fibroblasts. In particular, rapamycin up-regulated cytokine/chemokine related genes whilst quiescence up-regulated genes from the complement and coagulation cascade by fold-change analysis. Although log-base (2) analyses revealed enrichment in pathways in cancer in response to rapamycin treatment, many of these genes were cytokines, linking this finding back to the cytokine/chemokine enrichment observed in fold change analyses. This slight variability reveals the importance of the type of bioinformatics analyses and in identified networks being based only on the current state of knowledge – it is likely there are as of yet unidentified networks in the transcripts enriched for pathways in cancer that will further link this finding back to the cytokine-cytokine receptor pathway. Furthermore, these observations confirmed that although rapamycin decreased cell proliferation without causing cell death, it did not result in a cellular state similar to quiescence induced by serum reduction. In addition, increased occupancy of STAT5A/B in the promoters of rapamycin up-regulated genes implicating this factor as part of the mechanism mediating rapamycin-induced changes in gene expression. Finally, removal of 500 nM rapamycin treatment for 120 h resulted in increased numbers of cells in S-phase, likely the result of cells re-entering the same stage of the cell-cycle at the same time after becoming synchronised in the slower, rapamycin-induced state.

Network analyses of both quiescence-induced and rapamycin-treated fibroblasts revealed enrichment of several distinct biological pathways. Cellular quiescence is defined as a state of reversible growth/proliferation arrest. In transcripts up-regulated by quiescence-induction, the complement and coagulation cascade was enriched (Table 3-1 & 3-4). This is the first report of this finding in normal human fibroblasts. As protein products of these genes are linked with serine-type peptidase/endopeptidase activity and are secreted into the extracellular space, they may have roles in mediating the extracellular matrix. A condition that may be monitored by neighbouring cells in order to determine environmental conditions. Furthermore, genes such as *SERPING1* and *CFHL1* were up-regulated by serum/mitogen removal in normal fetal lung fibroblasts (Coller *et al.* 2006); however, this work did not identify enrichment in GO

terms associated with the complement and coagulation pathway. It is possible that common genes are involved in regulating quiescence across cell types inducing similar serine-type peptidase/endopeptidase activity. In both fold change and log-base (2) RNAseq analyses, down-regulated genes in response to quiescence were enriched for pathways such as mitotic prometaphase, aurora B signalling and cell cycle. Genes such as *FOXM1* and *CCNB1* were present in these enriched pathways as well as the study in fetal lung fibroblasts (Coller *et al.* 2006). These observations demonstrate commonalities between these different, although similar, cell types in response to quiescence induced by serum reduction. Furthermore, serum reduction in culture could be considered a type of dietary restriction, although it has not been documented to have the health and lifespan benefits of other DR-based systems. Despite this, the divergent findings between rapamycin treatment and quiescence-induction provide initial evidence that rapamycin may not directly mimic dietary restriction; however, further work is needed in other dietary restriction based conditions that promote health and lifespan.

Rapamycin treatment induced the up-regulation of genes enriched for in the cytokine-cytokine receptor pathway, in particular genes related to IL-6 (*IL-6*, *IL-8*, *IL-11* and *LIF*). These findings confirmed previous computation-based predictions (Zhao *et al.* 2010; Lee *et al.* 2013; Domhan *et al.* 2014). Contrary to the enrichment of cytokines in normal human fibroblasts in response to rapamycin, findings in human oral keratinocytes revealed inhibition of interleukin-1 beta (*IL-1*β), *TNF*α and *IFN-*β and enhancement of *IL-12p70* expression. Laberge and colleagues further indicated that mTOR inhibition via rapamycin, or via the knockdown of mTOR components decreases IL-6/cytokine production in senescence fibroblasts (Laberge *et al.* 2015). In human macrophages, rapamycin increased TNF, and IL-6 levels (Su *et al.* 2015) whilst in orbital fibroblasts, rapamycin increased TNFa induced IL-6 and IL-8 secretion by inhibiting PDCD4 degradation (Lee *et al.* 2013). IL-6 production has previously been linked to stress-induced premature senescence (SIPS)/replicative senescence and the senescence-associated secretory phenotype (SASP), with the accumulation of SASP cells associated with disease and ageing (Garbers *et al.* 2013; Kojima *et al.* 2013); however, it is unlikely that fibroblasts have entered SIPS/SASP as cells retained the ability to proliferate, albeit at a slower rate. In support of this, no pathway enrichment was identified for these terms and upon removal of rapamycin treatment, fibroblasts re-entered the cell cycle. It is possible that rapamycin is creating a balance between two states, inducing cytokine production whilst repressing SASP. Furthermore, an indirect interaction between STAT5A/B and mTOR has been proposed in T-cells and in response to cytokine signaling (Saleiro and Platanias 2015); however, the

mechanism involved with this is unclear. This finding is important in relation to our data given the link between mTOR inhibition and promoting improved health and lifespan, meaning that inhibition of mTOR via rapamycin treatment could be promoting improved health and lifespan via cytokine induction mediated by STAT5A/B. Our findings, combined with the literature, suggest that response to rapamycin is potentially cell-type specific and dose-dependent. Given that it has previously been documented that cytokines are enriched in old, senescent fibroblasts, this novel finding of cytokine enrichment in young proliferating fibroblasts in response to rapamycin, alongside previous work documenting links between cytokines, mTOR and STAT5A/B, hints at an important role for cytokines in regulating aging and the balance between young and old.

ELISAs provided further evidence of IL-6 and IL-8 production, displaying an increase in the amount of both proteins secreted from fibroblasts treated with rapamycin. Increased levels of these cytokines were detected within the culture media after 120 h, but the fold change values were not as dramatic as those observed at the transcript level. This finding raises the possibility that IL-6 and IL-8 could affect adjacent cells within the environment. Western blotting confirmed increased levels of LIF, which is also an IL-6-related secreted protein. Future investigations of these proteins should reveal if these signals are part of the program caused by disrupted nutrient sensing which promotes increased cellular health and longevity.

Transcription factor motif screens and subsequent ChIP analysis revealed the novel identification of STAT5A/B as one of the factors binding up-regulated gene promoters in response to rapamycin in 2DD fibroblasts. One of the genes identified to have a STAT5A/B binding site in the promoter encodes the Suppressor of Cytokine Signaling (SOCS) family member, *SOCS1*. The SOCS1 protein, which is a negative regulator of Janus kinases (JAK) and STAT proteins, has previously been reported to sequester STAT5A/B in the cytoplasm (Galic *et al.* 2014). In rapamycin-treated fibroblasts, *SOCS1* transcript abundance was decreased 5.05 fold in our RNAseq dataset. The increase in STAT5A/B-mediated transcription of several cytokine genes agrees with the model in which SOCS1 forms part of the negative feedback loop; decreased expression of the *SOCS1* gene possibly leads to decreased protein levels in the cytoplasm (Dimitriou *et al.* 2008). This loss of SOCS1 protein would, therefore, allow STAT5A/B to translocate into the nucleus, where it binds and drives the expression of a large number of genes (Peltola *et al.* 2004) . In addition, several of the cytokines we observed to be up-regulated, such as *IL-6* and *LIF*, are reported to up-regulate the expression of SOCS1 (Krebs and Hilton 2000). We did not observe an up-regulation of *SOCS1* expression; however, this

could be due to the ongoing treatment with rapamycin. Future studies will need to examine how STAT5A/B and decreased expression of the *SOCS1* gene are linked to inhibition of mTOR by rapamycin. Although rapamycin has been partially linked with cytokine production in other cell types (Zhao *et al.* 2010; Lee *et al.* 2013; Domhan *et al.* 2014), this work further proposes the potential mechanisms involved with this stimulation, identifying STAT5A/B and decreased levels of *SOCS1* transcription as being involved with this rapamycin-mediated response. Other *SOCS* family members have a range of functions in different cell types, often acting to form a negative feedback loop for cytokine signaling (Dimitriou *et al.* 2008). Immune responses implicated in signaling from *SOCS* family members have been linked to obesity and type II diabetes (Galic *et al.* 2014) . While decreased expression of other *SOCS* family members was observed, these genes did not reach our criteria for significance. However, these observations may implicate *SOCS* family members as potential global regulators controlling rapamycin-mediated transcription programs in other cell types. In addition to STAT5A/B involvement with rapamycin-mediated gene induction, we also identified NFATC2 binding sites to be significantly enriched in these promoters. Previous studies have identified a physical interaction between STAT5A/B and NFATC2, with NFATC2 acting as a negative regulator (Zheng *et al.* 2011). The increased transcription of the *NFATC2* gene may be a response to increased activity of STAT5A/B; the resulting NFATC2 protein functioning to sequester and inhibit continued STAT5A/B-mediated transcription. ChIP analyses demonstrated, at least in a subset of promoters analyzed, that NFATC2 is not interfering with STAT5A/B promoter occupancy.

In conclusion, it has been demonstrated that rapamycin induced a significant change in the transcript profiles of normal 2DD human foreskin fibroblasts, distinguishing rapamycin treatment from quiescence induction by serum reduction. Furthermore, an increase in cytokine/chemokine expression and production, including *IL-6*, *IL-8* and *LIF*, was observed, coinciding with increased STAT5A/B promoter occupancy at many of these genes. This STAT5A/B-mediated regulation of gene expression provides novel insight into the mechanisms through which rapamycin treatment impacts cell proliferation, gene expression and cytokine production. These observations link TOR inhibition with changes in genome function and organization independent of quiescence; changes which have the potential to regulate cellular health and longevity which, in turn may influence the ageing process at the tissue/organ/organismal level. Future work should include an expansion into other foreskin fibroblast lines to see if this is maintained regardless of genomic background/individual genome types.

4.0 The Impact of Metformin on Genome Function and Organization

4.1 Metformin Reduces Cell Proliferative Rates in NB1 hTERT Fibroblasts

Metformin has been documented to impact autophagy (both increasing and decreasing dependent on the cell line) and reduce cancer cell proliferation across numerous cell lines (Anisimov *et al.* 2011; Ashinuma *et al.* 2012; Alimova *et al.* 2014; Brodowska *et al.* 2014; He *et al.* 2015). Further, metformin has been linked to a decreased incidence of cancer in type II diabetic patients (Evans *et al.* 2005). In order to confirm these findings and investigate the impact of metformin in a novel cell line, the NB1 hTERT cell line was treated with concentrations of 0.5-25 mM metformin. Following treatment, cell counts were taken at 72 and population doubling times and total population doublings calculated (Fig. 4-1A & 4-1B). Metformin treatments in the literature are generally very high and not physiologically relevant. Here, concentrations were chosen to be both more physiologically relevant but to also overlap with concentrations that have previously resulted in an impact in culture. At 72 h, cell population doubling times in response to 5 mM (23.4 h), 10 mM (45.4 h) and 25 mM (106.9 h) metformin were longer than the control (20.7 h) (Figure 6A). A decrease in total population doublings at 5 mM (3.6 compared to a control of 4.3 after 120 h of treatment), with significant decreases observed at 10 mM and 25 mM metformin (2.6 and 1.2 respectively in comparison to the proliferative sample at 4.3) was also documented (Fig. 4-1B). No obvious morphological changes were noted (Fig. 4-1D). Trypan blue staining revealed no deleterious effects in response to metformin treatment, although a slight change between proliferative (97.3% viable) and treated with 0.5 mM (92.1% viable), 1 mM Met (93.9% viable), 5 mM (98.3%), 10 mM (95.3%), and 25 mM (91.8%) metformin treatment cells (Fig. 4-1C) was noted.

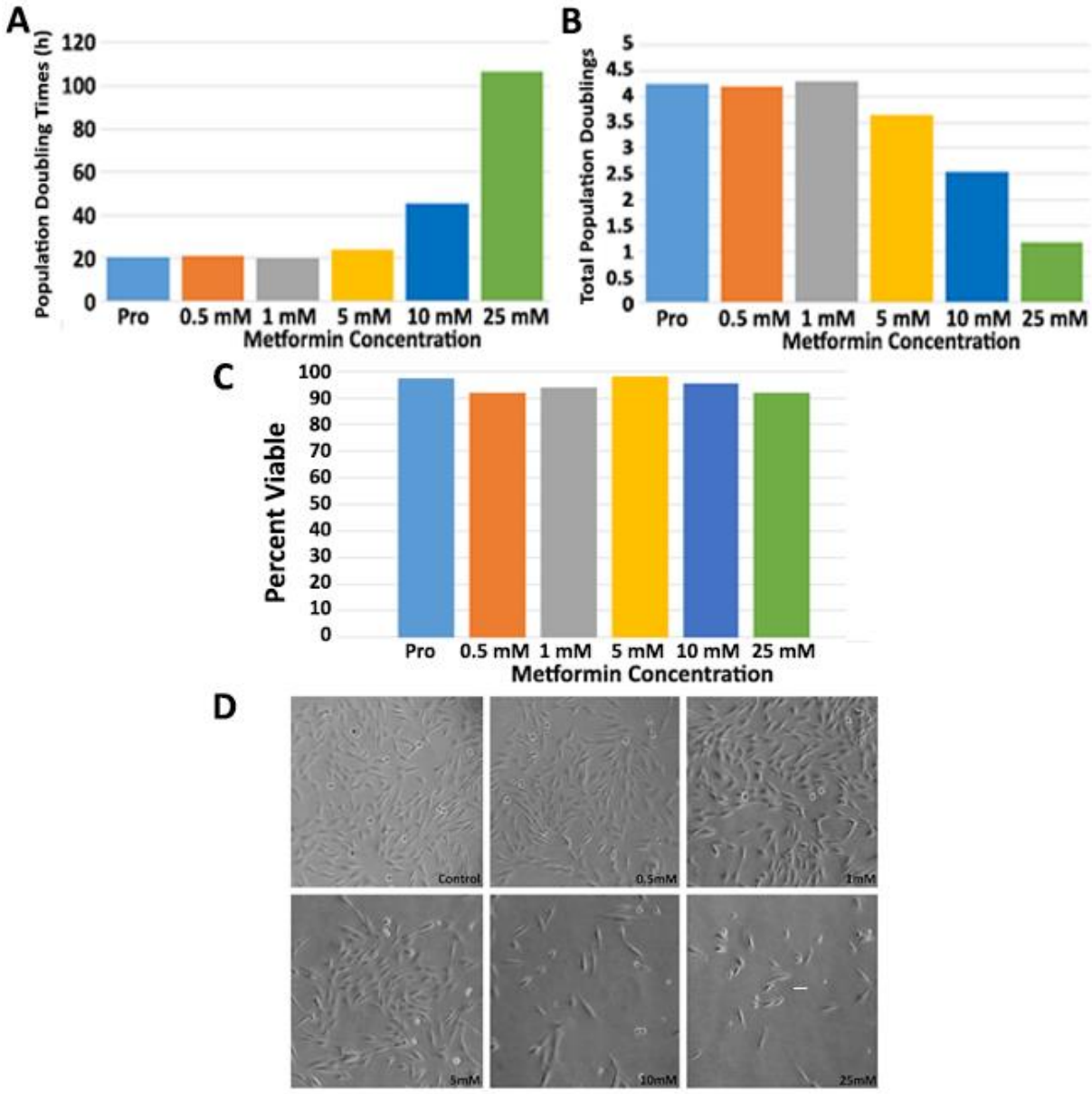

Figure 4-1: Metformin Decreased the Rate of NB1 hTERT Proliferation. (A) NB1 hTERT cells were grown under normal culture conditions or in the presence of 0.5 mM, 1 mM, 5 mM, 10 mM or 25mM metformin for 120h (X-axis). Population doubling times were calculated for each treatment, including control (Y-axis). (B) The total number of population doublings were plotted for control and metformin-treated cultures at 120 h. (C) Trypan blue assays of both control and metformin-treated NB1 hTERT are shown with both viable and non-viable values given (X-axis) with percent (%) cells on the Y-axis). Data is representative of single biological replicates, with additional replicates (data not shown) demonstrating parallel trends. (D) Representative, greyscale, light microscopy images for each metformin treatment (control, 0.5 mM and 1 mM (top)) and (5 mM, 10 mM, 25 mM (bottom)) at 120 h.

4.2 Metformin Reduces Cell Proliferative Rates in Normal Human Fibroblasts

To establish the impact of metformin on healthy human proliferative cells, fibroblasts were treated with 0.5 mM or 1 mM metformin in filtered dH_2O for either 72 h or 120 h. Due to a lack of literature on metformin in normal human cell lines, these concentrations were chosen to determine whether or not lower metformin concentrations would impact cell growth and proliferation at a more physiologically relevant level. Population doubling times were measured and total population doublings calculated, representative replicates are given (Figure 4-2A and 4-2B). An increase in population doubling times was observed under both conditions at both time points, with the average population doubling time following 72 h in culture increasing from 40.1 h in proliferating fibroblasts to 49 h and 54 h in 0.5 mM and 1 mM metformin treated cultures respectively. Similarly, following 120 h of treatment, population doubling times increased from 46 h in the proliferating culture to 52 h under both 0.5 mM and 1 mM metformin treatments. In agreement with the increase in population doubling times, a decrease in total cell population doublings was observed, with proliferative samples at 72 h doubling a total of 1.8 times, and treated samples (0.5 mM metformin and 1 mM metformin) decreasing to 1.5 and 1.3 total population doublings respectively (Figure 4-2B). At 120 h a similar trend was observed, with the proliferative samples having undergone total population doubling of 2.6, and treated samples both having a total population doubling of 2.3. There was no evidence of an increase in cell death in response to metformin treatments, confirmed via staining with trypan blue (Figure 4-2C). It was previously demonstrated that rapamycin, a potential mimetic of caloric restriction, caused cells to flatten in a similar manner to quiescent fibroblasts [76]. This feature was not induced by treatment with metformin at either 72 h or 120 h (Figure 4-2D). In order to further determine the impact of metformin on proliferation, 2DD fibroblasts were fixed and labelled for the proliferative marker Ki67. Fibroblasts were treated for 120 h at either 0.5 mM, 1 mM, 5 mM, 10 mM or 25 mM metformin, with a decrease in the percent positive Ki67 fibroblasts from the control (67.8%) at 0.5 mM (56.8%), 1 mM (57.7%), 5 mM (56.2%) and 25 mM (43.4%) (Figure 4-3A & 4-3C). No significant change was observed at 10 mM metformin treatment (65.9%) (student t-tests, $p>0.05$). This data was further confirmed through the use of 5'-ethynyl-2'deoxyuridine (EdU), a thymidine analogue which is actively incorporated into cells replicating DNA. Cells were treated with metformin concentrations ranging from 0.5 mM to 25 mM for 120 h. EdU incorporation demonstrated a decrease in S-phase between proliferative (16.9%) and 0.5mM metformin treated (12.6%, $P<0.05$) fibroblasts. Similar, but less significant, decreases were observed at 1 mM (14.1%) and 10 mM (15.7%) metformin treatment; however, at the high-dose of 25 mM metformin, EdU incorporation was at 6.7%. An

increase in EdU incorporation was observed at 5 mM (17.5%) (Figure 4-3A & C). Cell cycle analysis using propidium iodide and flow cytometry data further confirms that the number of cells in G1/0 in response to metformin is increasing following 120 h of treatment, from 74.0% in proliferative samples, to 79.0% in 0.5 mM metformin and 78.8% in 1 mM metformin (Figure 4-3D).

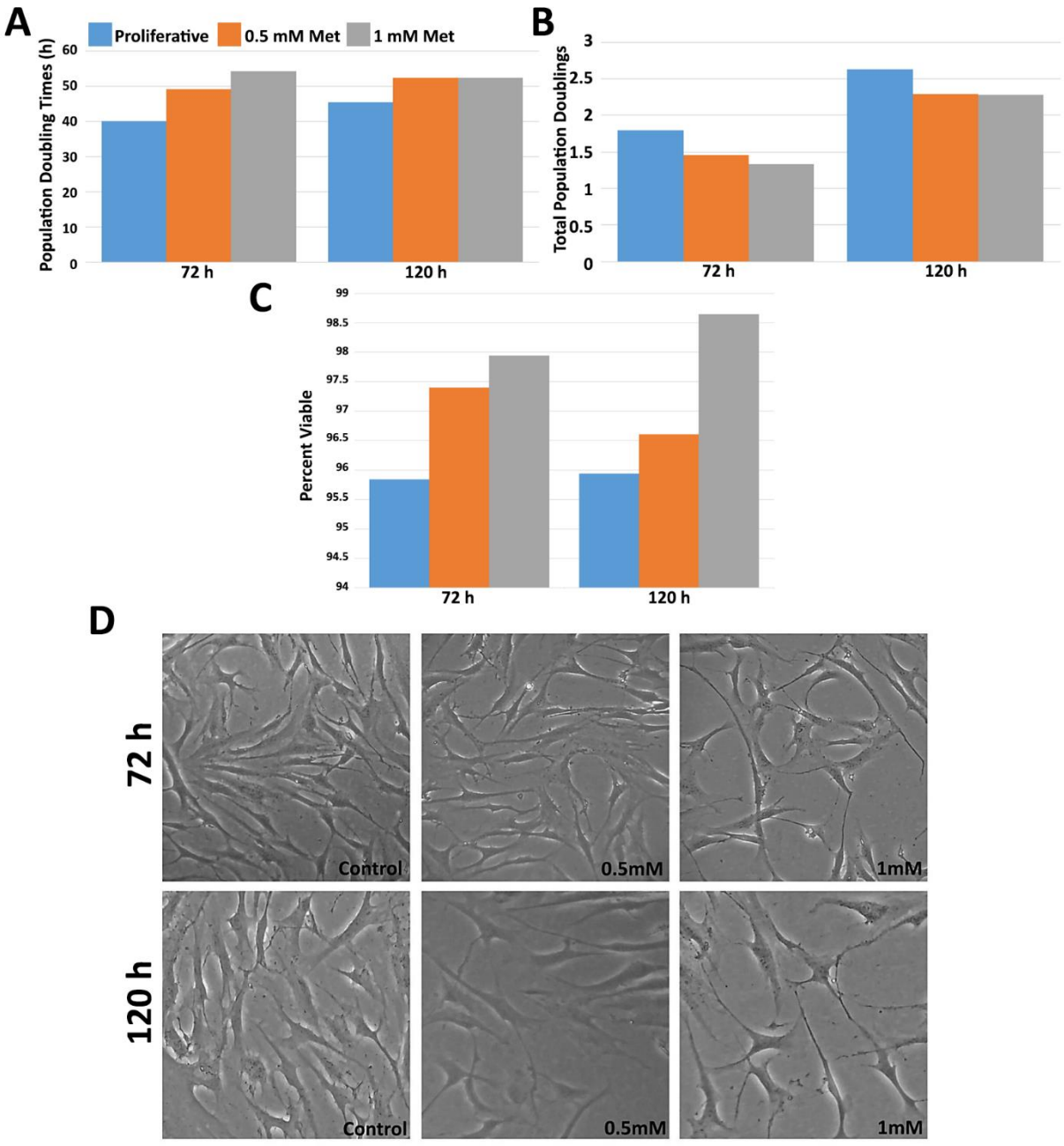

Figure 4-2: Metformin Increased the Rate of 2DD Foreskin Fibroblast Population Doubling Times, Decreasing the Rate of 2DD Proliferation. (A) 2DD cells were grown under normal culture conditions or in the presence of 0.5 mM or 1 mM metformin for 72 h or 120 h (X-axis). Population doubling times were calculated for each treatment, including control (Y-axis). (B) The total number of population doublings were ***(Figure 4-2 Legend Continued)***

plotted for control and metformin-treated cultures at 72 h and 120 h. (C) Trypan blue assays of both control and metformin-treated 2DD at 120 h are shown with both viable and non-viable values given (X-axis) with percent (%) cells on the Y-axis). Data is representative of single biological replicates, with additional replicates (data not shown) demonstrating parallel trends. (D) Representative, greyscale, light microscopy images for each metformin treatment (control, 0.5 mM and 1 mM met at 72 h (top) and 120 h (bottom).

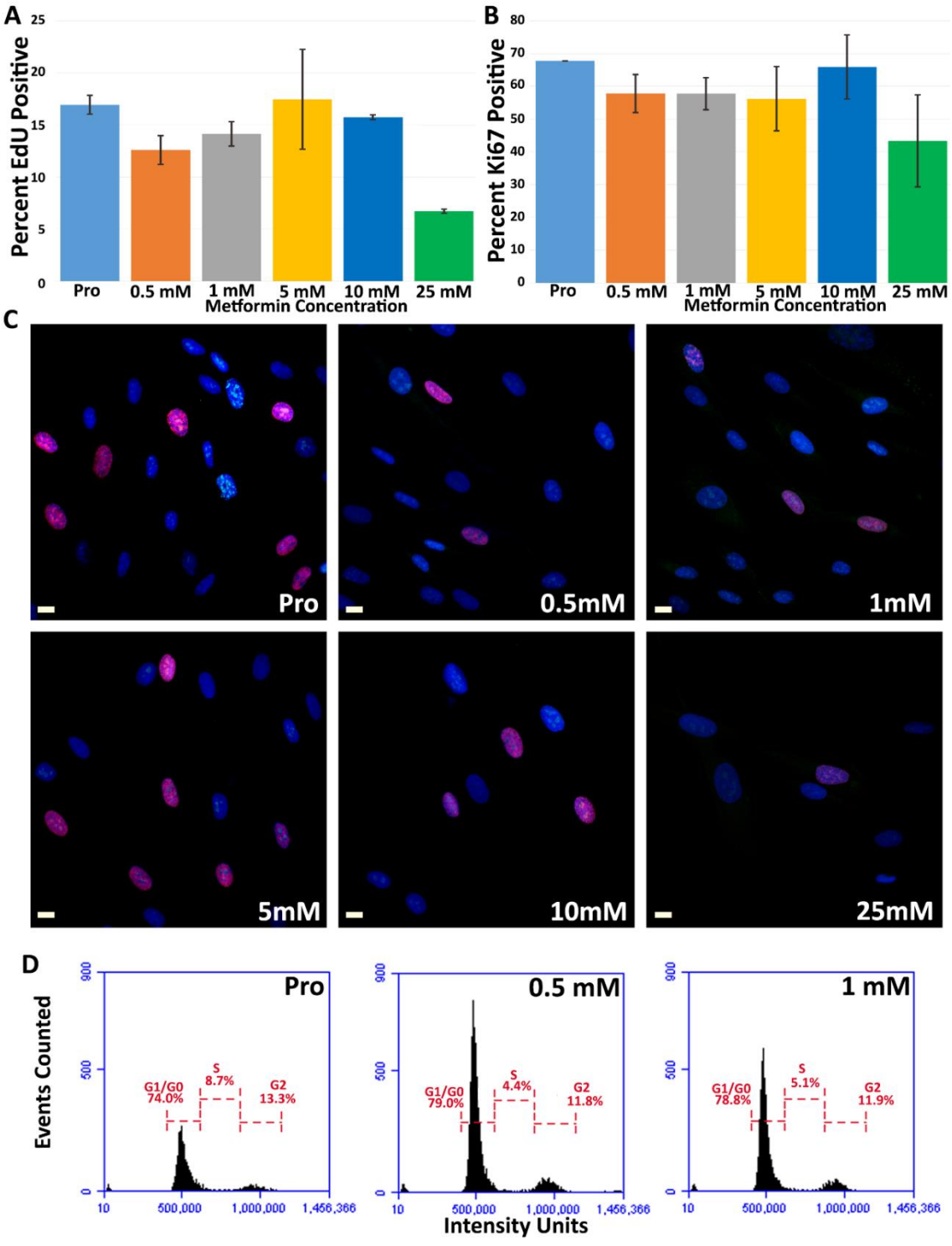

Figure 4-3: 0.5 mM and 1 mM Metformin Decreased 2DD Fibroblast Proliferation. (A) 2DD fibroblasts were grown under either proliferative conditions or treated with 0.5 mM, 1 mM, 5 mM, 10 mM or 25 mM metformin treatment for 120 h. Percent positive Ki67 (Y-axis) Immuno-labelled 2DD following treatment with metformin (X-axis) is shown. (B) Proliferative and metformin treated (0.5 mM, 1 mM, 5 mM, 10 mM or 25 mM) (X-axis) 2DD were incubated with the thymidine analogue EdU. and percentage positive for EdU reported (Y-axis) at 120 h. Error bars for (A) and (B) are the S.E.M., scale bar = 10 μm. (C) Representative merged microscopy images of proliferation and metformin treated (0.5 mM, 1 mM, 5 mM, 10 mM and 25 mM metformin) immuno-labelled for Ki67 (green) or EdU stained (red). Chromatin is counterstained with H33342. Scale bar = 10 μm (D) Pro, 0.5 mM and 1mM metformin-treated fibroblasts were fixed and stained with propidium iodide and DNA content measured by flow cytometry. Histograms demonstrate events counted (Y-axis), fluorescence signal (Intensity Units, X-axis) measured and the percentage cells in G0/G1, S and G2 phase of the cell cycle for each treatment condition.

4.3 Metformin Increases phosphorylated-AMPK (Thr172) and Decreases LC3 (a marker of autophagy) in Normal Human Fibroblasts

Metformin has previously been proposed to inhibit mTOR through activation of AMPK. Activation of AMPK is dependent on phosphorylation of AMPK at Thr172. In order to confirm that metformin is acting in a manner physiologically relevant and as indicated by literature, western blots using whole cell lysates for phosphorylated AMPK (Thr172) were conducted (Figure 4-4), with an increase in phosphorylated AMPK observed. A decrease in the α1 subunit of AMPK and no change in α2 were also documented. These findings were in agreement with metformin inducing phosphorylation of AMPK potentially resulting in inhibition of mTOR. Inhibition of mTOR often results in an increase in autophagy, the process by cellular components are recycled. Autophagy is often increased in response to decreases in a cells nutrient availability (Blagosklonny 2010). In the normal human 2DD fibroblast, a decrease in autophagy concordant with an increase in treatment concentration was noted (Figure 4-4). Although the literature frequently lists metformin as inducing an increase in autophagy, this decrease is not without precedent, with GO enrichment analyses of the liver and muscle of mice fed metformin revealing enrichment for downregulation of autophagy (Martin-Montalvo *et al.* 2013). Furthermore, Yang, *et al.*, report no increase in HepG2 cells as a result of metformin treatment (10 mM, 24h) whilst Song, *et al.*, report autophagy to increase in the presence of 0.5 mM metformin. To further validate these findings, higher concentrations of metformin were

used to treat both 2DD and NB1 hTERT fibroblasts. Western blot analyses of 2DD and NB1 hTERTs exposed to 0.5 mM, 5 mM and 10 mM of metformin for 120 h were conducted (Figure 4-4). This analysis revealed no change in LC3II expression using two different antibodies from separate sources, providing further confidence in these findings. These findings were confirmed by immunofluorescence, with a decrease from 7.9% LC3 positive fibroblasts in proliferative samples to 3.3% in response to 0.5 mM metformin treatment and 4.4% in response to 1 mM metformin treatment. (Figure 4-5).

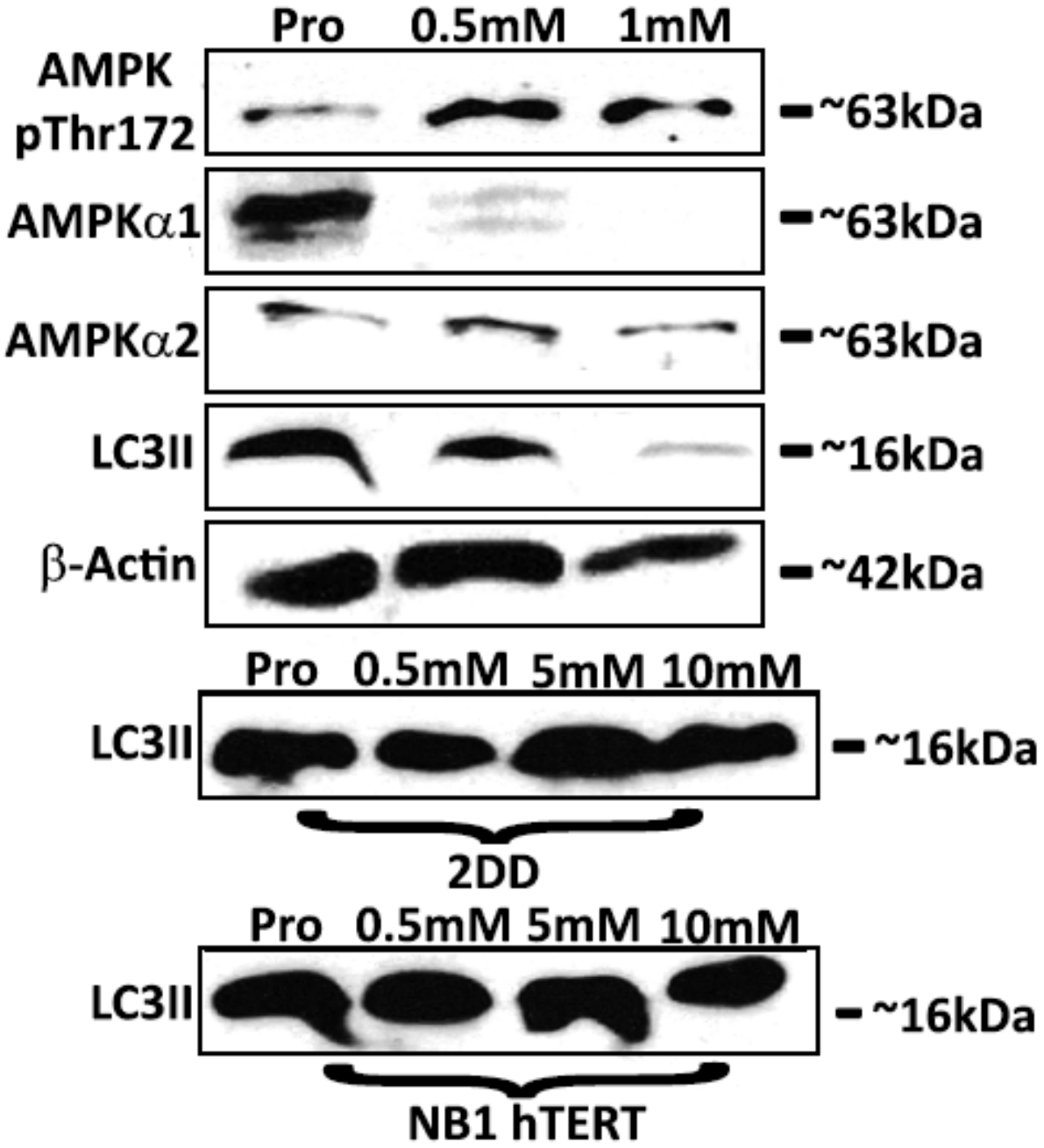

Figure 4-4: Western Blot Analyses of AMPK and LC3 in 2DD and NB1 hTERT Fibroblasts. Western blot analyses from whole cell lysates of ***(Figure 4-4 Legend Continued)***

2DD treated under proliferative, 0.5 mM metformin and 1 mM metformin treatment for 120 h. Protein analysed is listed on the left with protein size (kDa) on the right. The bottom two panels represent an analyses of 2DD (top) and NB1 hTERT (bottom) cell-lines treated under control conditions and with 0.5 mM, 5.0 mM and 10 mM metformin for 120 h. LC3II is detected at 16 ~kDa. For LC3II and β-Actin antibodies, 15 μg of protein was loaded. For all other antibodies 40 μg was loaded.

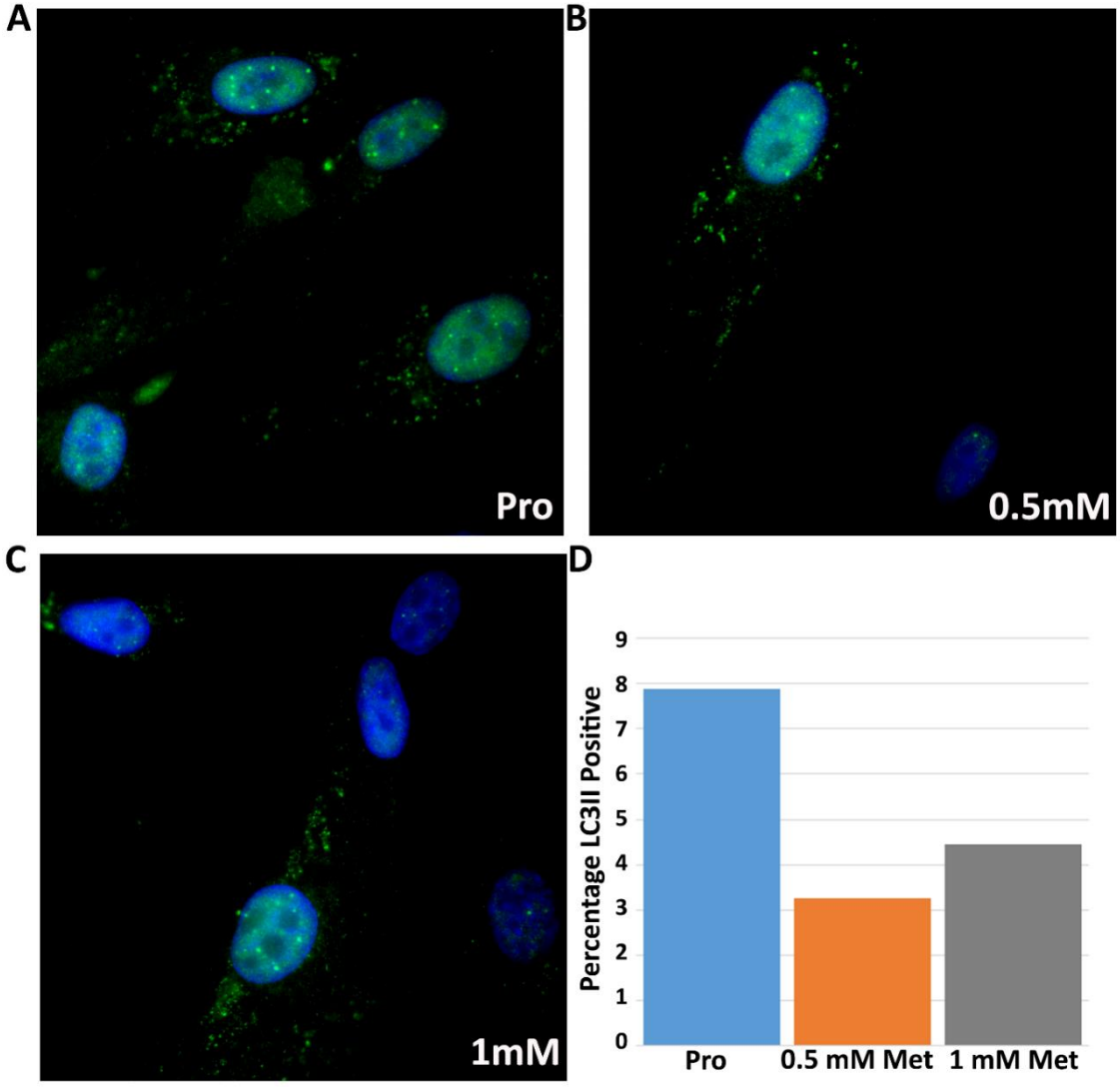

Figure 4-5: Detection of LC3I/II Indicates a Decrease in Autophagy as a Result of 0.5 mM and 1 mM Metformin Treatment in 2DD Fibroblasts. Representative immunofluorescence to detect LC3I/II (green) in proliferative (A), 0.5 mM metformin-treated (B) and 1 mM metformin treated (C) fibroblasts. Chromatin is counterstained with H33342 (blue). Scale bar = 10 μm. (D) Bars for control (pro), 0.5 mM metformin (orange) and 1 mM metformin (grey) -treated fibroblasts demonstrating the percent of nuclei identified as positive (Y-axis) for LC3I/II.

4.4 Metformin Treatment Induces Genome Re-organization in 2DD Fibroblasts

Based on previous work that chromosome territories rapidly re-position in response to serum reduction in culture (Mehta *et al.* 2010) and that in this work, rapamycin treatment, a proposed mimetic of metformin similarly demonstrated re-positioning of chromosomes 10 and 18 in 2DD fibroblasts, FISH was conducted for chromosomes X, 10 and 18 under proliferative conditions, 0.5 mM metformin and 1 mM metformin treatment at 120 h (Figure 4-6). Treatment of 2DD fibroblasts with 0.5 mM metformin induced statistically significant (student t-test, $p \leq 0.05$) re-positioning of chromosomes 10 and 18, 10 towards the nuclear periphery and 18 towards the nuclear interior when compared to untreated counterparts. At 1 mM metformin treatment, repositioning of chromosome 10 was not significant; however, chromosome 18 also re-positioned to the nuclear interior. Chromosome X was used as a control with no significant change in positioning documented, remaining at the nuclear periphery. These findings are similar to that of quiescence-induction and rapamycin treatment. Furthermore, significant difference was reported between 0.5 mM metformin and 1 mM metformin treatments, with chromosome 10 at 1 mM metformin occupying a more interior location when compared to 0.5 mM metformin treatment, and chromosome 18 in response to both 0.5 mM and 1 mM metformin located to the nuclear interior, but 1 mM metformin treated samples more so. In addition to these findings, correlation trends reported supported these findings.

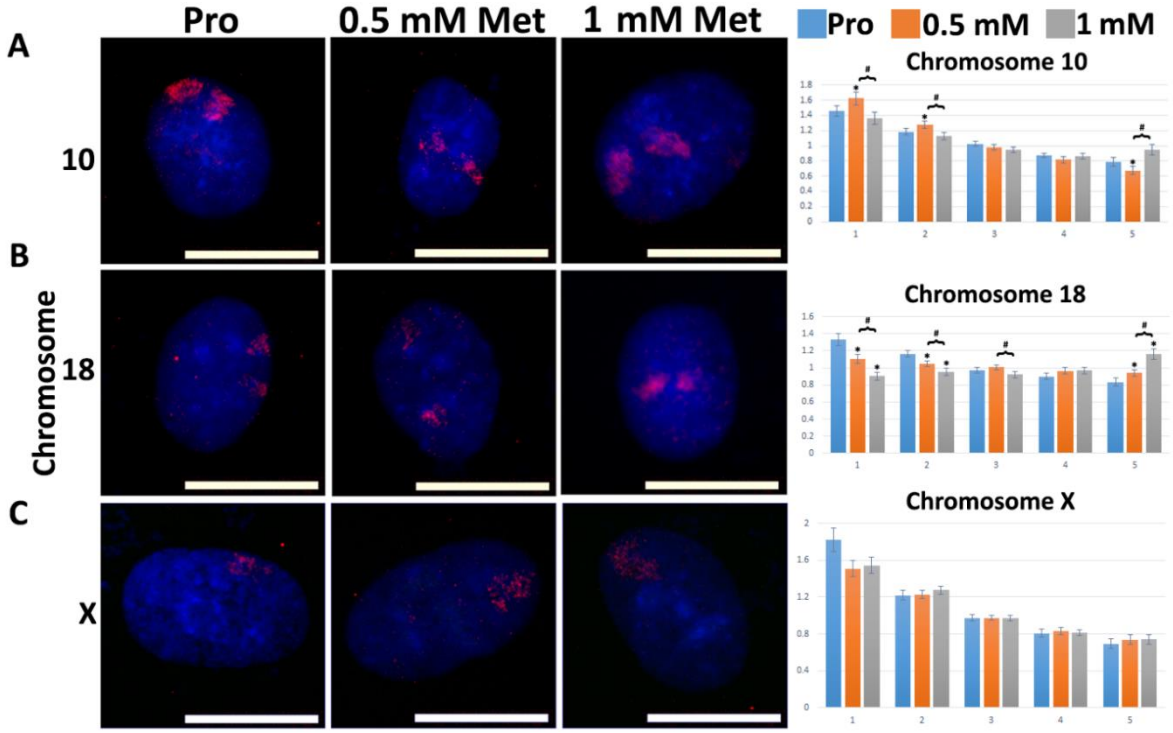

Figure 4-6: 0.5 mM and 1 mM Metformin Treatments Induce Chromosome Territory Repositioning in 2DD Fibroblasts. Chromosomes 10 (top row), 18 (middle row) and the X chromosome (bottom row) were identified in control (Pro, first column), 0.5 mM metformin treated (0.5 mM Met, second column) and 1 mM metformin treated (1 mM Met, third column) 2DD fibroblasts by chromosome painting. Red signal represents the identified chromosomes; chromatin was counter stained with H33342 (blue). Scale bar = 10 μm for all images. Following painting, erosion analysis was performed to designate the location of the chromosomes within the nuclear volume. Nuclei were broken into five concentric shells of area, shell 1 being most exterior and shell 5 being most interior. Graphs for each specific chromosome represents the measured ratio of % chromosome signal divided by the % H33342 signal in each shell (Y axis) to normalize for DNA content in each shell (X axis). Control positioning is represented by blue bars, 0.5 mM metformin-treated by orange and 1 mM metformin-treated in grey. Error bars = S.E.M. Two tailed Student's test for unequal variance were used to demonstrate significant difference in chromosome positioning. * Indicates p-value ≤0.05 between control and treatment group. # Indicates significant difference (p-value ≤0.05) between 0.5 mM and 1 mM metformin treatment. Correlation calculations were also performed to demonstrate if the trend in chromosome positioning was similar or divergent between the samples. Chromosome 10 proliferative R^2 =0.96, 0.5 mM metformin R^2=0.96 and 1 mM metformin R^2=0.75. Chromosome 18 proliferative R^2=0.95, 0.5 mM metformin ***(Figure 4-6 Legend Continued)***

R^2=0.98 and 1 mM metformin R^2=0.66. Chromosome X proliferative R^2=0.89, 0.5 mM metformin R^2=0.96 and 1 mM metformin R^2=0.95.

Table 4-1: Correlation Values (R^2) for Chromosome Territory Re-Positioning in 2DD Fibroblasts in response to 0.5 or 1 mM metformin treatment. Correlation values for chromosome territory re-positioning in 2DD fibroblasts threated for 120 h with either 0.5 mM or 1 mM metformin treatment at 120 h. Correlations are given for chromosome 18, 10 and X for proliferative (Pro), 0.5 mM metformin (0.5 mM Met) and 1 mM metformin (1 mM Met).

R^2 Values	**Chromosome 10**	**Chromosome 18**	**Chromosome X**
Pro	0.96	0.95	0.89
0.5 mM Met	0.96	0.96	0.96
1 mM Met	0.75	0.75	0.95

To further investigate the impact of cell proliferative state on chromosome territory positioning, and to control for cell cycle stage in these analyses, nuclei were also labelled with the proliferative marker Ki67 (Figure 4-6). Whilst findings remained consistent in chromosome 18 regardless of cell proliferative state (re-localizing towards the nuclear interior), chromosome 10 was analysed to have re-positioned to the nuclear exterior in Ki67 negative fibroblasts, whilst towards the interior in Ki67 positive fibroblasts. As with combined samples, there was some significant variance between 0.5 mM and 1 mM metformin treatments, indicated a potential dose-dependent response.

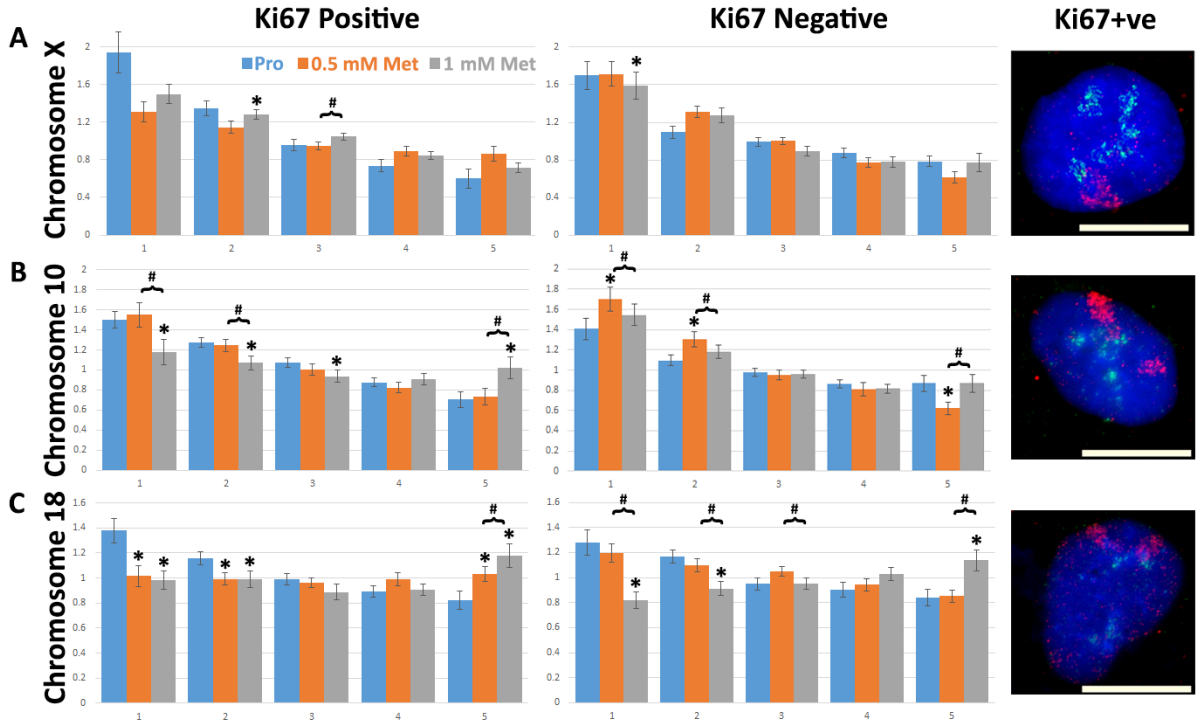

Figure 4-7: Chromosome Territory Positioning in Response to Metformin in Both Ki67 Positive and Negative 2DD Fibroblasts. Chromosome X (top row), 10 (middle row) and 18 (bottom row) were identified in Chromosomes 10 (top row), 18 (middle row) and the X chromosome (bottom row) were identified in control, 0.5 mM and 1 mM metformin treated 2DD fibroblasts by chromosome painting. The first column of graphs is for Ki67 positive (+ve) nuclei, the second column for Ki67 negative (-ve) nuclei, the third column is representative images of control in X, 10 and 18 for proliferative nuclei. Red signals represents the identified chromosomes; green signal represents Ki67 positive fibroblasts;*)* chromatin was counter stained with H33342 (blue). Scale bar = 5 μm for all images. Following painting, nuclei were separated based on positive and negative signal for Ki67 and erosion analysis was performed to designate the location of the chromosomes within the nuclear volume. Nuclei were broken into five concentric shells of area, shell 1 being most exterior and shell 5 being most interior. Graphs for each specific chromosome represents the measured ratio of % chromosome signal divided by the % H33342 signal in each shell (Y axis) to normalize for DNA content in each shell (X axis). Control positioning is represented by blue bars, 0.5 mM metformin by orange and 1 mM metformin in grey. Error bars = S.E.M. Two tailed Student's test for unequal variance were used to demonstrate significant difference in chromosome positioning. * Indicates p-value ≤0.05 between control and treatment group. # Indicates significant difference (p-value ≤0.05) between 0.5mM and 1mM metformin treatment.

4.5 Metformin Treatment induces a Transcript Profile Divergent to rapamycin Treatment by reverse transcriptase qPCR

A number of genes were selected for investigation based on rapamycin treatments of 2DD fibroblasts and on the metformin literature. As rapamycin and metformin are both proposed to be mimetics of caloric restriction, it was expected that genes changing in response to rapamycin treatment would also change in response to metformin treatment. Very little work has been conducted in understanding the specific genes changing expression in response to metformin treatment. Martin-Montalvo *et al.* (Martin-Montalvo *et al.* 2013), however, have identified a number of genes significantly changing expression in response to long term treatment with 0.1% (w/w) and 1% (w/w) metformin in the liver and muscle tissue of male C57BL/6 mice. Although the lower treatment extended mean lifespan by 5.83%, 1% (w/w) was toxic to mice, shortening lifespan by 14.4%. Microarray profiling of the mice tissues determined a global gene expression shift towards caloric restriction. From this, the *cytokine-inducible SH2-containing protein* (*CISH*) gene was determined as one of the most highly changing genes in both metformin-treated (11.6 fold) and caloric restriction (11.58 fold) treated mice.

To determine if *CISH*, and other selected genes, were responding to metformin treatment in accordance with the literature, 2DD fibroblasts were treated with 0.5 mM and 1 mM metformin for 120 h, RNA extracted, cDNA libraries made and expression tested by qPCR. It was determined that CISH increased expression by 6.8 fold and 5.3 fold respectively. Work by Takiyama *et al.*, documented an increase in *Hypoxia Inducible Factor (HIF-1a)* expression in Zucker diabetic fatty rats, whilst *DNA-Damage Inducible Transcript 4 (DDIT4)* and *Peroxisome Proliferator-Activated Receptor Alpha (PPARa)* have been demonstrated to increase expression in cancer models and mice in response to metformin treatment, with both further being implicated in alternative pathways for the compound [79]. Despite the literature, no significant change in the expression of these genes in normal foreskin fibroblasts following metformin treatment was observed at 0.5mM metformin, although 1mM metformin fold change was greater than (>)2 for *DDIT4*, with *HIF-1a* expression documented at 1.9 and -1.4 respectively for each treatment, *DDIT4* expression changed 1.7 and 2.2 fold respectively, and *PPARa* changed 1.8 and 2.7 fold respective to each treatment (Figure 4-8A).

It has been proposed that both metformin and rapamycin mimic dietary restriction and therefore mimic one another. As such, a number of genes of interest identified as changing significantly following 500 nM rapamycin treatment in the same 2DD fibroblast cell line were investigated. These included; *ACTC1* (266.8 fold up-regulated following rapamycin treatment),

IL-8 (24.0 fold up-regulated), *IL-11* (37.2 fold up-regulated), *LIF* (73.0 fold up-regulated) and *NFATC2* (6.85 fold up-regulated) [76]. Following 120 h of treatment with either 0.5mM metformin or 1mM metformin, these genes did show an increase in expression; and although changes for *IL*-8, *IL-11*, *LIF* and *NFATC2* were greater than two fold in at least one treatment concentration, changes were much lower than those observed following rapamycin treatment. *IL-11* had the greatest response at 0.5mM metformin, with an increase of 5 fold; however, at 1 mM, this value decreased to 2.3 fold. *IL-8* also decreased from a fold change of 2.2 at 0.5 mM metformin to 1.9 at 1mM metformin treatment. *ACTC1* and *NFATC2* demonstrated similar trends, whilst *LIF* increased from 3.0 fold at 0.5 mM metformin to 3.4 fold at 1 mM metformin (Figure 3-8B).

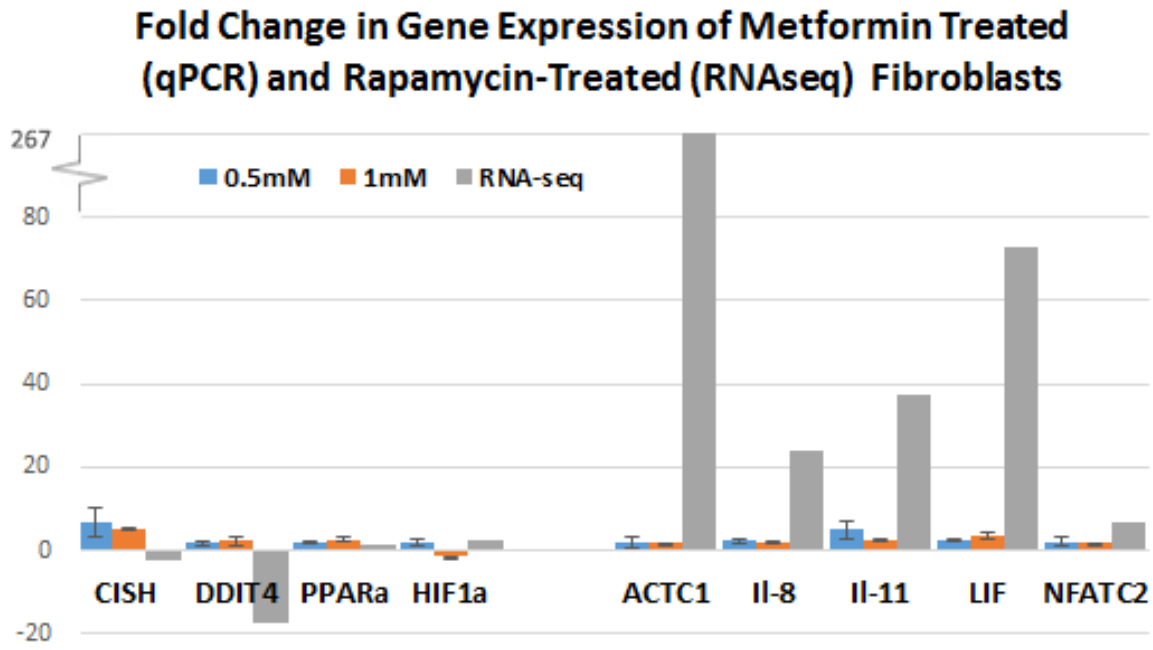

Figure 4-8: Gene Expression Data for Genes of Interest in Metformin Treated Fibroblasts Compared to Rapamycin Treated 2DD Fibroblasts Demonstrated Divergence. To determine the impact of metformin on genes previously reported to be altered in response to treatment, qPCR was performed on *CISH*, *DDIT4*, *PPARa*, and *HIF1a*. To provide initial indications on whether or not the same genes responding to rapamycin treatment also respond to metformin in 2DD fibroblasts, qPCR was performed on *ACTC1*, *IL-8*, *IL-11*, and *LIF*. *NFATC2* was tested based on its proposed involvement in the previously noted response to rapamycin. Fold change (Y-axis) is noted to the left hand side of the figure, whilst 0.5 mM treatment (blue bars), 1 mM treatment (orange bars) and RNAseq-based changed in response to 500 nM rapamycin (grey bars) are plotted along the X-axis. Error bars = S.E.M.

4.6 Metformin Treatment induces a Transcript Profile Enriched in AP-1 Transcription Factor Network (Fold Change Analyses) and Cytokine-Cytokine receptor pathways (Log-Base (2) Transformed)

Metformin has previously been proposed to mimic caloric restriction and has documented similar effects across numerous model organisms to rapamycin-treatment. Although repositioning of chromosome territories was observed in response to metformin treatment, changes in chromosome location were not identical to that of rapamycin-treatment in the same cell line. To further investigate whether metformin and rapamycin treatments were having divergent impacts on genome function, mRNA were isolated from proliferative, 0.5 mM and 1 mM 120 h metformin treated fibroblasts. RNAseq with subsequent comparative transcriptome analyses were conducted. Raw sequence reads from Illumina-based sequencing were mapped to the GRCh38/hg19 reference genome, normalized using RPM and analysed using the bioinformatics tool SeqMonk (http://www.bioinformatics.bbsrc.ac.uk/projects/seqmonk/).

Comparisons between RNAseq datasets of 0.5 mM metformin to 1 mM metformin were made comparing the log-base (2) number of reads from 0.5 mM metformin-treated fibroblasts or 1 mM metformin-treated fibroblasts (Figure 4-9) against the log number of reads from proliferative fibroblasts. A subset of genes of interest that changed transcript profiles in either 0.5 mM or 1 mM metformin treated fibroblasts have been highlighted and genes changing expression in both treatment conditions represented in green. In 2DD fibroblasts treated with 0.5 mM metformin, 443 genes changed expression ≥2-fold (264 up-regulated; 179 down-regulated), 263 ≥3-fold (154 up-regulated; 109 down-regulated), and 78 ≥5-fold (44 up-regulated; 34 down-regulated). In 1 mM metformin-treated 2DD fibroblasts, 413 genes changed expression ≥2-fold (208 up-regulated; 205 down-regulated), 265 ≥3-fold (132 up-regulated; 133 down-regulated), and 76 ≥5-fold (34 up-regulated; 42 down-regulated)**.** The majority of genes from both 0.5 mM and 1 mM metformin treatments had similar read count values to those of proliferating cells (correlations of 0.996 for both), with the scatter plots demonstrating some overlap between genes changing expression; however, further analysis revealed that 180 genes (106 up-regulated; 74 down-regulated) changing ≥2-fold expression overlapped between treatments. Similarly, 109 genes ≥3-fold expression (63 up-regulated; 46 down-regulated) and 31 genes ≥5-fold expression (20 up-regulated; 11 down-regulated) overlapped between 0.5 mM and 1 mM metformin treatments. Therefore, based on log-base (2) analyses the two treatment concentrations induce varied transcript expression. The second analysis, based on fold-change

in gene expression comparing 0.5mM metformin and 1mM metformin to proliferative fibroblast RNAseq datasets revealed similar findings with greater overlap between genes changing expression in 0.5 mM and 1 mM metformin treatment (Figure 4-10). RNAseq data were validated by RT-qPCR by a selection of sample genes that changed/did not change expression in 0.5mM and 1mM metformin-treated fibroblasts (Figure 4-11).

To determine if there was overlap or divergence in the modules and biological pathways enriched for by either 0.5 mM or 1 mM metformin treatment, network analyses using genes identified as significantly changing (≥3-fold) were conducted. Cytoscape [248] with ReactomeFI [249] was used to classify highly-interacting groups of genes (modules) from the RNAseq datasets and to identify the associated pathway annotation terms (Kyoto Encylopedia of Genes and Genome; KEGG terms). Two analyses were conducted, one for log-base (2) transformed data and one for fold-change based data. In log-base (2) transformed data, transcripts up-regulated in response to 0.5 mM metformin treatment, 7 modules were identified (Figure 4-12), whilst in transcripts up-regulated in response to 1 mM metformin treatment, 4 modules were identified (Figure 4-12). In fold-change analysed transcripts, 2 modules were identified in 0.5 mM metformin up-regulated transcripts, and 1 module in 1 mM metformin up-regulated transcripts (p-vale <0.05, FDR <0.05) (Figure 4-12). No modules or networks were detected in either analysis of 0.5 mM and 1 mM metformin up-regulated transcripts.

To further confirm that biological pathways were divergent between 0.5 mM and 1 mM metformin treatment, network analyses were conducted. In log-base (2) transformed data for both 0.5 mM and 1 mM metformin treatments, the cytokine-cytokine receptor pathway was enriched for in genes changing expression ≥3-fold (p-vale <0.05, FDR <0.05) (Table 4-2 & 4-3). These transcripts further revealed enrichment for influenza and interferon alpha/beta signalling. In fold change based analysis, the AP-1 transcription factor pathway was most enriched for both 0.5 mM and 1 mM metformin treated fibroblasts (p-vale <0.05, FDR <0.05) (Table 4-4 & 4-5). GO terms for biological processes and molecular function continued these findings, with similar enrichment in terms between 0.5 mM and 1 mM metformin treatments for each analysis. Specifically, log-transformed transcripts in response to 0.5 mM and 1 mM metformin were enriched for GO biological processes in ageing, and GO molecular function in double-stranded DNA binding and sequence specific binding (p-vale <0.05, FDR <0.05) (Figure 4-13). Similarly, in fold-change based data, transcripts changing in response to 0.5 mM and 1 mM metformin treatment were enriched for in GO biological processes such as cytokine-

mediated signalling pathways, whilst cytokine and chemokine activity was enriched for in GO molecular function (p-vale <0.05, FDR <0.05) (Figure 4-13).

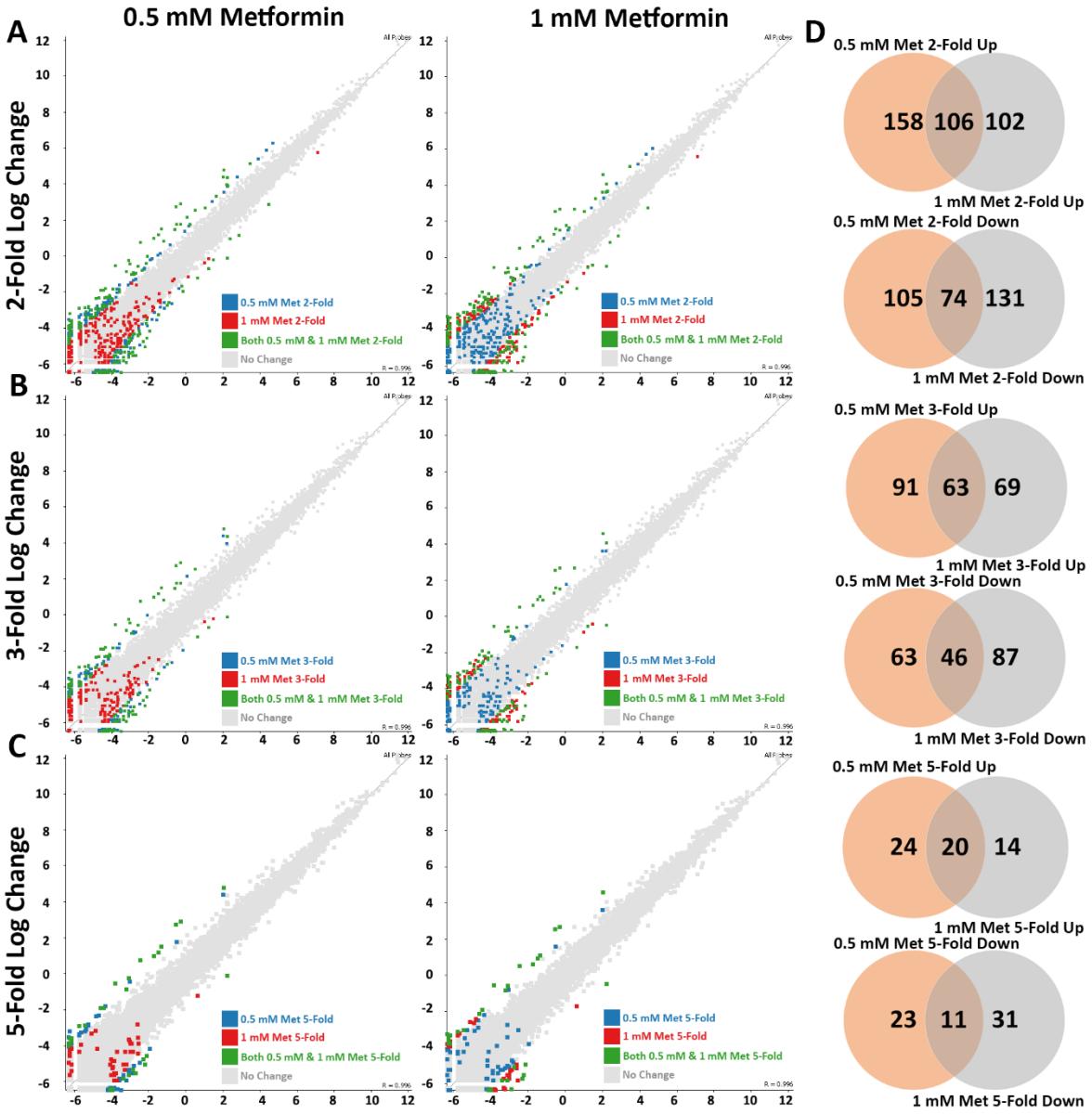

Figure 4-9: Scatter Plots and Venn Diagrams Demonstrate Different Transcript Profiles Following 0.5 mM and 1 mM Metformin Treatment in 2DD Fibroblasts. (A) Scatter plots comparing changes in gene expression between proliferative 2DD fibroblasts and 2DD treated with 0.5 mM metformin (left panel) and between proliferative 2DD fibroblasts and 2DD treated with 1 mM metformin (right panel) for transcript abundance changes of 2-fold. (B) Scatter plots comparing changes in gene expression between proliferative 2DD fibroblasts and 2DD treated with 0.5 mM metformin (left panel) and between proliferative ***(Figure 4-9 Legend Continued)*** 2DD fibroblasts and 2DD treated with 1 mM metformin (right panel) for transcript abundance

changes of 3 fold. (C) Scatter plots comparing changes between proliferative 2DD fibroblasts and 2DD treated with 0.5 mM metformin (left panel) and between proliferative 2DD fibroblasts and 2DD treated with 1 mM metformin (right panel) for transcript abundance changes of 5-fold. For all plots, the number of counts for each transcript identified by RNAseq for proliferative (X-axes) and metformin treated (Y-axes) fibroblasts was log-base (2) transformed. Each square represents an individual transcript. Transcripts exhibiting a significant fold change in response to 0.5 mM metformin when compared to proliferative samples are coloured blue, in response to 1 mM metformin coloured red, and overlapping between the two treatment conditions coloured green. Grey squares represent transcripts that did not change abundance at the listed cut-off values. (D) Venn diagrams demonstrating the number of genes up-regulated or down-regulated between 0.5 mM (blue) and 1 mM metformin (red) treated fibroblasts in comparison to proliferative fibroblasts. Numbers in the overlapped areas indicate the number of genes changing expression in both treatment groups.

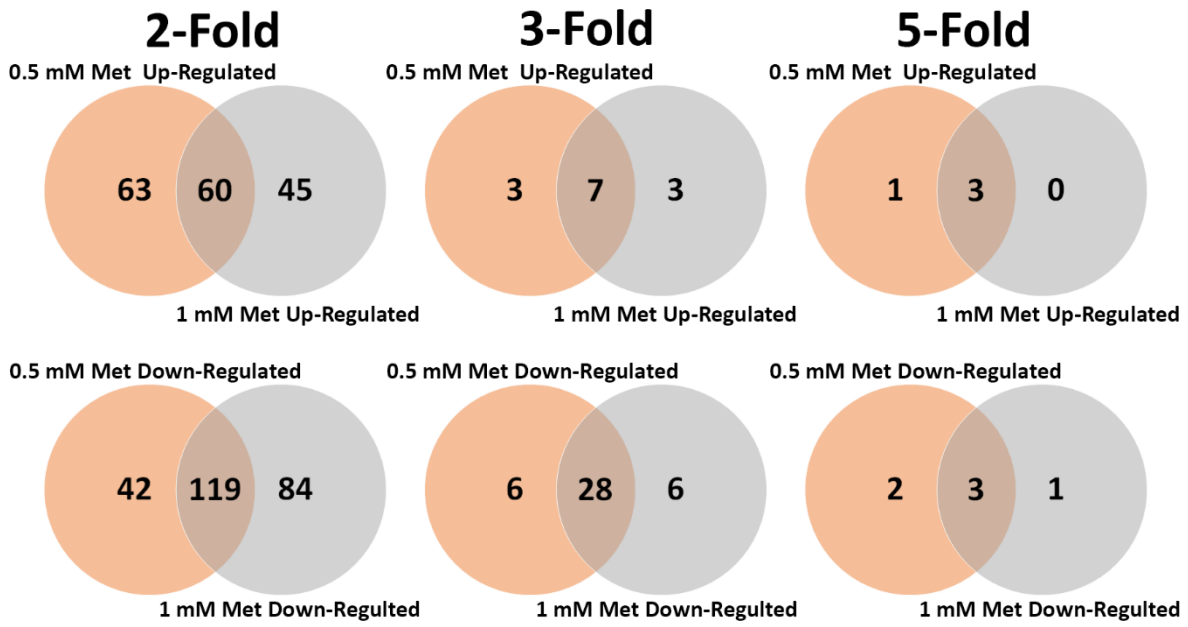

Figure 4-10: Venn Diagrams for Transcripts Changing ≥2-Fold, ≥3-Fold and ≥5-Fold in 0.5 mM and 1 mM Metformin-Treated Fibroblasts Based on Fold Change Analysis in 2DD Fibroblasts. Venn diagrams demonstrating the number of genes up-regulated or down-regulated in 0.5 mM (red) and 1 mM (blue) metformin-treated fibroblasts compared to proliferative fibroblasts. Numbers in the overlapping regions indicate the number of transcripts changing expression in response to both 0.5 mM and 1 mM metformin treatment.

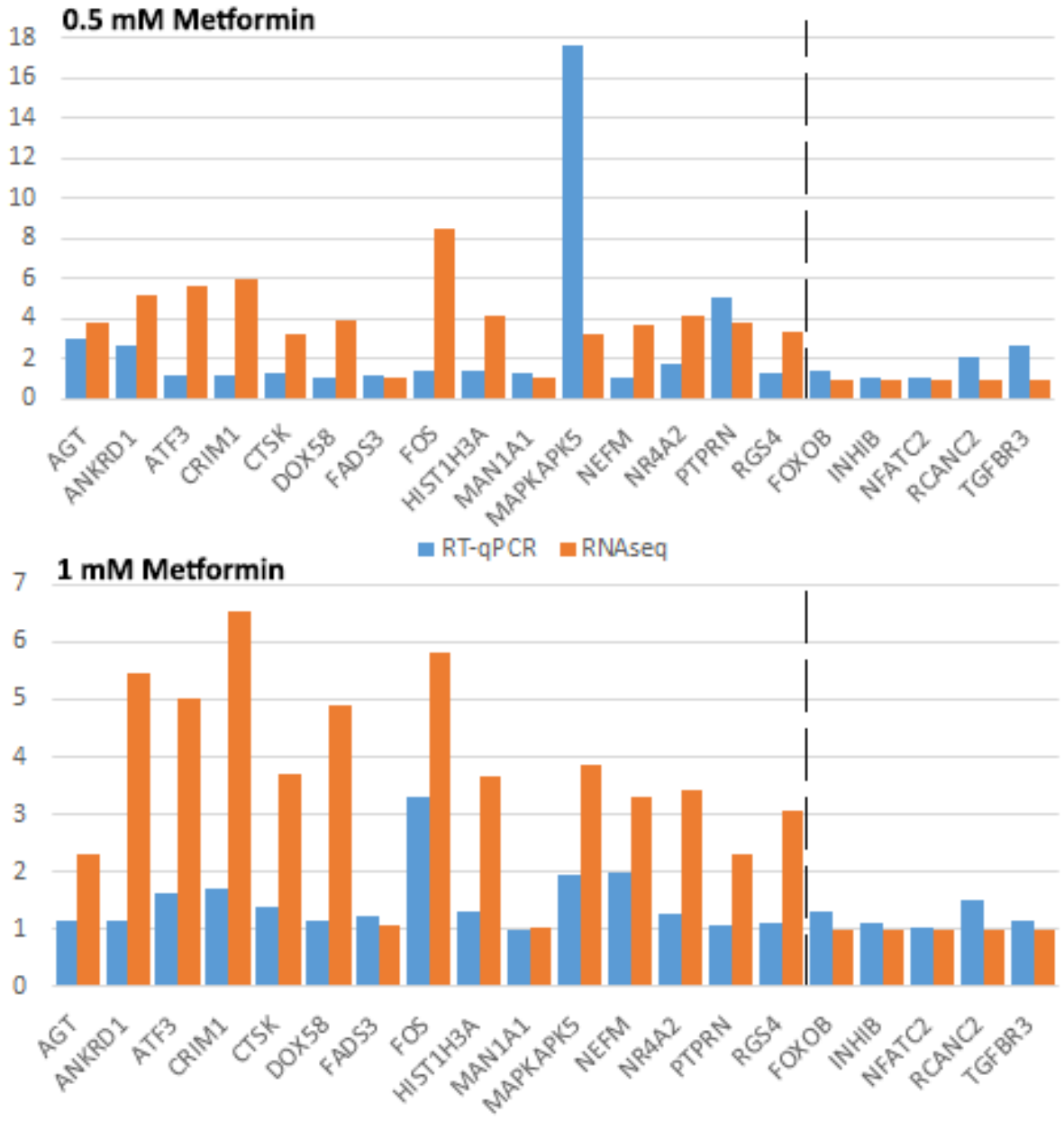

Figure 4-11: RNA-Sequencing Validation of Gene Fold Changes by RT-qPCR in Response to 0.5 mM and 1 mM Metformin Treatment in 2DD Fibroblasts. RT-qPCR was conducted on a subset of genes identified to have changed transcript profiles by RNAseq. This was conducted for 0.5 mM and 1 mM metformin-treated fibroblasts. The relative fold change (using five individual normalizing genes) in these transcript profiles from proliferative cells is shown (blue bars) as well as the fold change predicted by RNAseq (orange bars. Values on the right of the dashed line represent control genes with RNAseq values and RT-qPCR comparisons; to the left of the dashed line are selected genes that were ≥2-fold by RNAseq in 0.5 mM metformin-treated fibroblasts with the corresponding RT-qPCR fold changes.

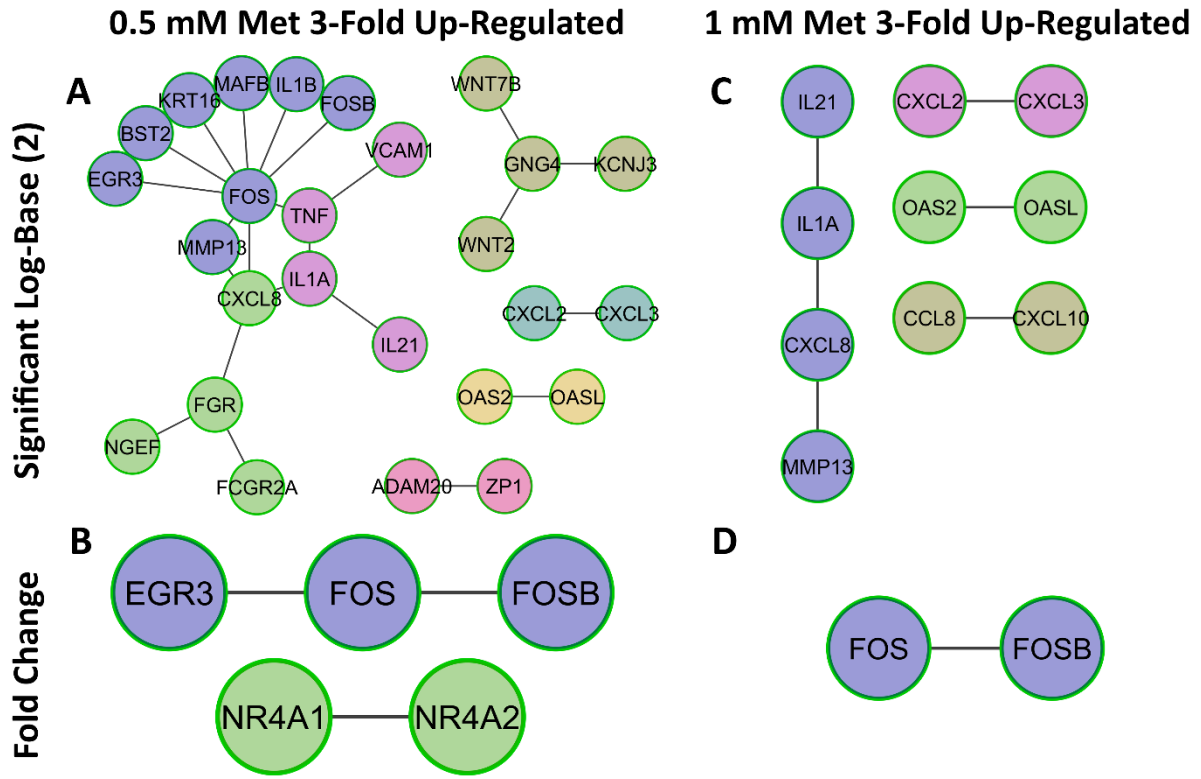

Figure 4-12: Modules Identified in Genes Up-Regulated ≥3-fold in Response to 0.5 mM and 1mM Metformin Treatment in 2DD Fibroblasts. Network analyses identified groups of functionally related genes (modules in ≥3-fold up-regulated (A) 0.5 mM and (B) 1 mM metformin-induced genes based on log-base (2) transformed data. Modules are also presented for (C) 0.5 mM and (D) 1 mM metformin-induced genes based on fold-change data. Each node (circle) is representative of a gene whilst every colour is representative of a module. Solid lines represent genes linked within the same module and between modules based on the ReactomeFI database.

Table 4-2: Network Pathway Annotation Terms Enriched in 0.5mM Metformin Up-Regulated Genes in 2DD Fibroblasts by Log-Base (2) Analyses. Genes ≥5-fold up-regulated in response to 0.5 mM metformin treatment were analyzed for enrichment of KEGG terms. The identified enriched pathway KEGG annotation terms (GeneSet) from network analyses are listed. The total number of genes from the network identified to be up-regulated in response to 0.05 mM metformin and belonging to a specific pathway was identified. P-value (with 0 values equating to <0.0001) and false discovery rates (FDR) are presented. All P-Value and FDR are <0.05. Nodes identify specific genes/proteins from our datasets present in the networks. Gene lists identified by log-base (2) transforming data.

	Protein From Network	p-Value	FDR	Nodes
Influenza A(K)	10	0	1.30E-05	IL1B,MX1,IL1A,OAS1,OAS2,TNFSF10,HLA-DMB,TNF,RSAD2,CXCL8
Interferon alpha/beta signaling(R)	7	0	1.47E-05	MX1,MX2,BST2,OAS1,OAS2,OASL,RSAD2
Cytokine-cytokine receptor interaction(K)	10	0	1.79E-04	IL1B,IL1A,IL21,CCL8,TNFSF10,TNF,CXCL3,CXCL2,CXCL8,TNFRSF18
Leishmaniasis(K)	6	0	2.53E-04	IL1B,IL1A,HLA-DMB,FOS,TNF,FCGR2A
Salmonella infection(K)	6	0	4.68E-04	IL1B,IL1A,FOS,CXCL3,CXCL2,CXCL8
Measles(K)	7	0	4.68E-04	IL1B,MX1,IL1A,OAS1,OAS2,TNFSF10, CCND2
Rheumatoid arthritis(K)	6	0	4.68E-04	IL1B,IL1A,HLA-DMB,FOS,TNF,CXCL8
Legionellosis(K)	5	0	5.44E-04	IL1B,TNF,CXCL3,CXCL2,CXCL8
TNF signaling pathway(K)	6	0	0.00102	IL1B,FOS,TNF,CXCL3,CXCL2,VCAM1
Inflammatory bowel disease (IBD)(K)	5	0	0.00102	IL1B,IL1A,IL21,HLA-DMB,TNF
signal transduction through il1r(B)	4	0	0.001226	IL1B,IL1A,FOS,TNF
Pertussis(K)	5	0.0001	0.001552	IL1B,IL1A,FOS,TNF,CXCL8
Osteoclast differentiation(K)	6	0.0001	0.001829	IL1B,IL1A,FOS,FOSB,TNF,FCGR2A
HTLV-I infection(K)	8	0.0001	0.001829	WNT2,ATF3,HLA-DMB,FOS, CCND2,TNF,VCAM1,WNT7B
Graft-versus-host disease(K)	4	0.0001	0.001829	IL1B,IL1A,HLA-DMB,TNF

Type I diabetes mellitus(K)	4	0.0001	0.002076	IL1B,IL1A,HLA-DMB,TNF
Calcineurin-regulated NFAT-dependent transcription in lymphocytes(N)	4	0.0001	0.00253	FOS,EGR3,TNF,CXCL8
NF-kappa B signaling pathway(K)	5	0.0002	0.002551	IL1B,TNF,CXCL2,CXCL8,VCAM1
Malaria(K)	4	0.0002	0.002551	IL1B,TNF,CXCL8,VCAM1
Cellular roles of Anthrax toxin(N)	3	0.0002	0.002551	IL1B,TNF,VCAM1
Interleukin signaling pathway(P)	4	0.0003	0.003571	IL1A,IL21,FOS,CXCL8
NOD-like receptor signaling pathway(K)	4	0.0003	0.003794	IL1B,TNF,CXCL2,CXCL8
nfkb activation by nontypeable hemophilus influenzae(B)	3	0.0003	0.00437	IL1B,TNF,CXCL8
IL27-mediated signaling events(N)	3	0.0004	0.005089	IL1B,EBI3,TNF
Herpes simplex infection(K)	6	0.0006	0.006606	IL1B,OAS1,OAS2,HLA-DMB,FOS,TNF
Chemokine signaling pathway(K)	6	0.0006	0.00677	GNG4,FGR,CCL8,CXCL3,CXCL2,CXCL8
AP-1 transcription factor network(N)	4	0.0006	0.006926	ATF3,FOS,FOSB,CXCL8
Interferon gamma signaling(R)	4	0.0007	0.00699	OAS1,OAS2,OASL,VCAM1
African trypanosomiasis(K)	3	0.0009	0.009192	IL1B,TNF,VCAM1
Apoptosis(K)	4	0.0013	0.01344	IL1B,IL1A,TNFSF10,TNF
Death Receptor Signalling(R)	2	0.0021	0.018673	TNFSF10,TNF
il-10 anti-inflammatory signaling pathway(B)	2	0.0021	0.018673	IL1A,TNF
Chagas disease (American trypanosomiasis)(K)	4	0.0027	0.022433	IL1B,FOS,TNF,CXCL8
Senescence-Associated Secretory Phenotype (SASP)(R)	3	0.0027	0.022433	IL1A,FOS,CXCL8
stress induction of hsp regulation(B)	2	0.0028	0.022433	IL1A,TNF
Toll-like receptor signaling pathway(K)	4	0.0029	0.022879	IL1B,FOS,TNF,CXCL8

Tuberculosis(K)	5	0.003	0.024349	IL1B,IL1A,HLA-DMB,TNF,FCGR2A
cadmium induces dna synthesis and proliferation in macrophages(B)	2	0.0032	0.025662	FOS,TNF
ATF-2 transcription factor network(N)	3	0.0042	0.029098	ATF3,FOS,CXCL8
Downstream signaling in naïve CD8+ T cells(N)	3	0.0052	0.036575	FOS,TNF,TNFRSF18
Fertilization(R)	2	0.0062	0.043088	ADAM20,ZP1
nf-kb signaling pathway(B)	2	0.0062	0.043088	IL1A,TNF
Hepatitis C(K)	4	0.0064	0.044476	OAS1,OAS2,TNF,CXCL8

Table 4-3: Network Pathway Annotation Terms Enriched in 1mM Metformin Up-Regulated Genes in 2DD Fibroblasts by Log-Base (2) Analyses. Genes ≥5-fold up-regulated in response to 1 mM metformin treatment were analyzed for enrichment of KEGG terms. The identified enriched pathway KEGG annotation terms (GeneSet) from network analyses are listed. The total number of genes from the network identified to be up-regulated in response to 1 mM metformin and belonging to a specific pathway was identified. P-value (with 0 values equating to <0.0001) and false discovery rates (FDR) are presented. All P-Value and FDR are <0.05. Nodes identify specific genes/proteins from our datasets present in the networks. Gene lists identified by log-base (2) transforming data.

	Proteins From Network	p-Value	FDR	Nodes
Interferon alpha/beta signaling(R)	7	0	8.46E-06	MX1,MX2,BST2,OAS1,OAS2,OASL,RSAD2
Influenza A(K)	9	0	1.83E-05	CXCL10,IL1B,MX1,IL1A,OAS1,OAS2,HLA-DMB,RSAD2,CXCL8
Cytokine-cytokine receptor interaction(K)	8	0	0.002562	CXCL10,IL1B,IL1A,IL21,CCL8,CXCL3,CXCL2,CXCL8
Measles(K)	6	0.0001	0.002562	IL1B,MX1,IL1A,OAS1,OAS2,CCND2
Salmonella infection(K)	5	0.0001	0.002659	IL1B,IL1A,CXCL3,CXCL2,CXCL8
GPCR ligand binding(R)	9	0.0001	0.00333	CXCL10,WNT2,PTH1R,MCHR1, TAS1R1,CXCL3,CXCL2,CXCL8, HTR2A
Legionellosis(K)	4	0.0002	0.004676	IL1B,CXCL3,CXCL2,CXCL8
TNF signaling pathway(K)	5	0.0002	0.00521	CXCL10,IL1B,CXCL3,CXCL2,VCAM1
Inflammatory bowel disease (IBD)(K)	4	0.0003	0.00707	IL1B,IL1A,IL21,HLA-DMB
Interferon gamma signaling(R)	4	0.0004	0.008443	OAS1,OAS2,OASL,VCAM1
Leishmaniasis(K)	4	0.0005	0.008443	IL1B,IL1A,HLA-DMB,FCGR2A
Prion diseases(K)	3	0.0008	0.013048	IL1B,IL1A,C8G
Rheumatoid arthritis(K)	4	0.001	0.014865	IL1B,IL1A,HLA-DMB,CXCL8
NF-kappa B signaling pathway(K)	4	0.0011	0.014865	IL1B,CXCL2,CXCL8,VCAM1
Graft-versus-host disease(K)	3	0.0012	0.015521	IL1B,IL1A,HLA-DMB

Type I diabetes mellitus(K)	3	0.0014	0.01636	IL1B,IL1A,HLA-DMB
Malaria(K)	3	0.0019	0.02221	IL1B,CXCL8,VCAM1
Chemokine signaling pathway(K)	5	0.0023	0.025641	CXCL10,CCL8,CXCL3, CXCL2,CXCL8
Interleukin signaling pathway(P)	3	0.0026	0.025641	IL1A,IL21,CXCL8
NOD-like receptor signaling pathway(K)	3	0.0028	0.028346	IL1B,CXCL2,CXCL8
Osteoclast differentiation(K)	4	0.004	0.035567	IL1B,IL1A,FOSB,FCGR2A
Cellular roles of Anthrax toxin(N)	2	0.004	0.036279	IL1B,VCAM1
AP-1 transcription factor network(N)	3	0.005	0.040171	ATF3,FOSB,CXCL8
Pertussis(K)	3	0.0061	0.048571	IL1B,IL1A,CXCL8

Table 4-4: Network Pathway Annotation Terms Enriched in 0.5mM Metformin Up-Regulated Genes in 2DD Fibroblasts by Fold Change Analyses. Genes ≥5-fold up-regulated in response to 0.5 mM metformin treatment were analyzed for enrichment of KEGG terms. The identified enriched pathway KEGG annotation terms (GeneSet) from network analyses are listed. The total number of genes from the network identified to be down-regulated in response to 1 mM metformin and belonging to a specific pathway was identified. P-value (with 0 values equating to <0.0001) and false discovery rates (FDR) are presented. All P-Value and FDR are <0.05. Nodes identify specific genes/proteins from our datasets present in the networks. Gene lists identified by log-base (2) transforming data.

	Proteins From Network	p-Value	FDR	Nodes
AP-1 transcription factor network(N)	3	0	0.004281	FOS,ATF3,FOSB
HTLV-I infection(K)	4	0.0001	0.004281	VCAM1,FOS,ATF3,CCND2
Calcineurin-regulated NFAT-dependent transcription in lymphocytes(N)	2	0.0008	0.040847	FOS,EGR3
ATF-2 transcription factor network(N)	2	0.0012	0.045389	FOS,ATF3
Amphetamine addiction(K)	2	0.0017	0.045389	FOS,FOSB
Prolactin signaling pathway(K)	2	0.0019	0.045389	FOS,CCND2
Glucocorticoid receptor regulatory network(N)	2	0.0022	0.045389	FOS,NR4A1
Circadian entrainment(K)	2	0.0034	0.04696	FOS,KCNJ3
Estrogen signaling pathway(K)	2	0.0036	0.04696	FOS,KCNJ3
TNF signaling pathway(K)	2	0.0043	0.04696	VCAM1,FOS
Cholinergic synapse(K)	2	0.0046	0.04696	FOS,KCNJ3
Dopaminergic synapse(K)	2	0.0061	0.04696	FOS,KCNJ3
Osteoclast differentiation(K)	2	0.0061	0.04696	FOS,FOSB
Hepatitis B(K)	2	0.0075	0.04696	FOS,EGR3
Generic Transcription Pathway(R)	2	0.0076	0.04696	NR4A2,NR4A1
Oxytocin signaling pathway(K)	2	0.0089	0.04696	FOS,KCNJ3
Viral carcinogenesis(K)	2	0.0145	0.04696	EGR3,CCND2
MAPK signaling pathway(K)	2	0.0221	0.04696	FOS,NR4A1

Fc epsilon receptor (FCERI) signaling(R)	2	0.0334	0.04696	FOS,NR4A1
PI3K-Akt signaling pathway(K)	2	0.0386	0.04696	CCND2,NR4A1

Table 4-5: Network Pathway Annotation Terms Enriched in 1mM Metformin Up-Regulated Genes in 2DD Fibroblasts by Fold Change Analyses. Genes ≥5-fold up-regulated in response to 0.5 mM metformin treatment were analyzed for enrichment of KEGG terms. The identified enriched pathway KEGG annotation terms (GeneSet) from network analyses are listed. The total number of genes from the network identified to be down-regulated in response to 1 mM metformin and belonging to a specific pathway was identified. P-value (with 0 values equating to <0.0001) and false discovery rates (FDR) are presented. All P-Value and FDR are <0.05. Nodes identify specific genes/proteins from our datasets present in the networks. Gene lists identified by log-base (2) transforming data.

	Proteins From Network	**p-Value**	**FDR**	**Nodes**
HTLV-I infection(K)	4	0	5.16E-04	VCAM1,FOS,ATF3,CCND2
AP-1 transcription factor network(N)	3	0	5.16E-04	FOS,ATF3,FOSB
ATF-2 transcription factor network(N)	2	0.0005	0.021043	FOS,ATF3
Amphetamine addiction(K)	2	0.0007	0.021043	FOS,FOSB
Prolactin signaling pathway(K)	2	0.0008	0.021043	FOS,CCND2
Glucocorticoid receptor regulatory network(N)	2	0.0009	0.021043	FOS,NR4A1
TNF signaling pathway(K)	2	0.0019	0.033352	VCAM1,FOS
Osteoclast differentiation(K)	2	0.0026	0.033352	FOS,FOSB
MAPK signaling pathway(K)	2	0.0097	0.033352	FOS,NR4A1
Fc epsilon receptor (FCERI) signaling(R)	2	0.0149	0.033352	FOS,NR4A1
PI3K-Akt signaling pathway(K)	2	0.0172	0.033352	CCND2,NR4A1

GO Biological Process Enrichment

A 3-Fold Up-Regulated 0.5 mM Met

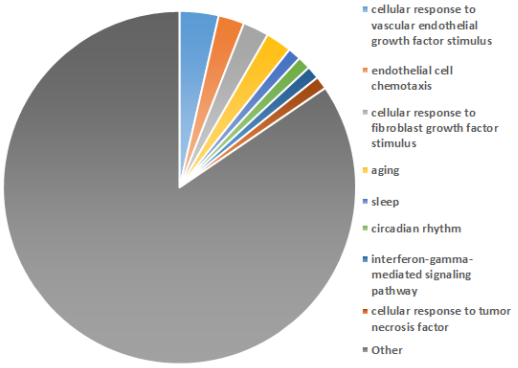

C 3-Fold Up-Regulated 1 mM Met

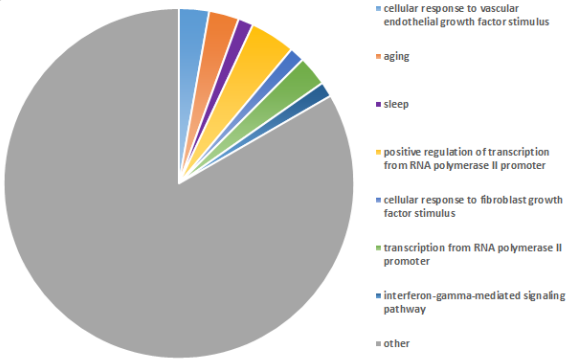

B 3-Fold log-base (2) Up-Regulated 0.5 mM Met

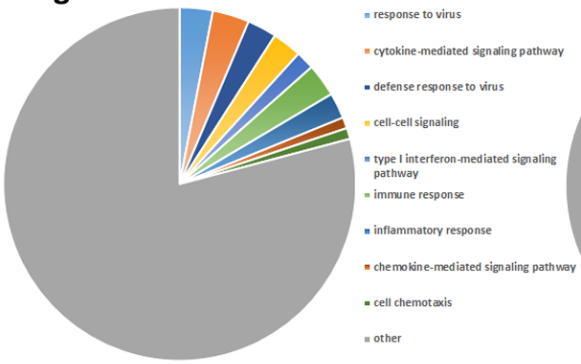

D 3-Fold log-base (2) Up-Regulated 1 mM Met

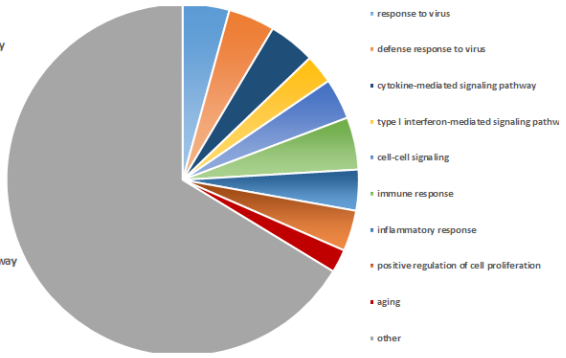

GO Molecular Function Enrichment

E 3-Fold Up-Regulated 0.5 mM Met

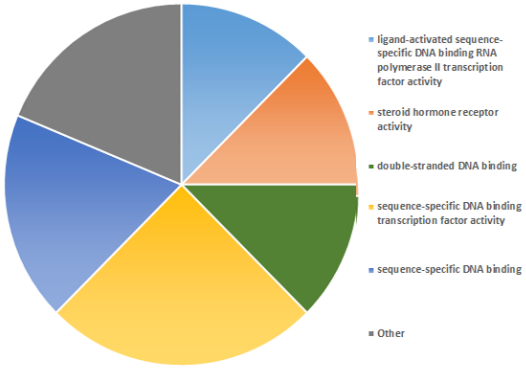

G 3-Fold Up-Regulated 1 mM Met

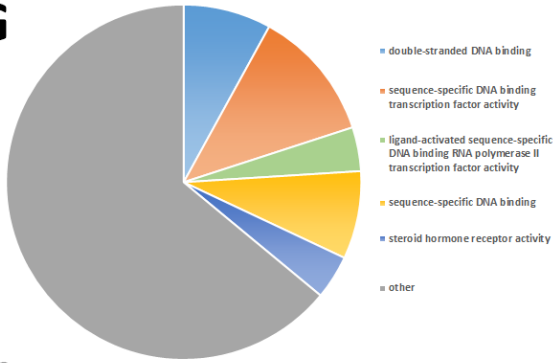

F 3-Fold log-base (2) Up-Regulated 0.5 mM Met

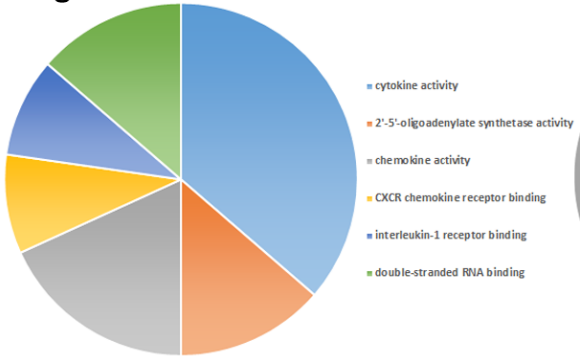

H 3-Fold log-base (2) Up-Regulated 1 mM Met

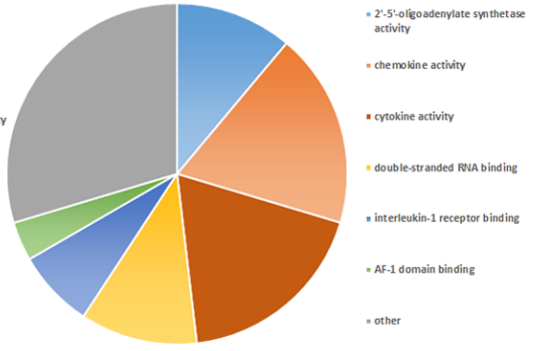

Figure 4-13: GO Term Enrichment in 0.5 mM and 1 mM Metformin Up-Regulated Gene Sets Based on Fold Change Analyses and Log-Base (2) Transformed 2DD Fibroblast Data. GO Biological Process terms significantly enriched for in genes ≥3-fold up-regulated in response to 0.5 mM metformin for both (A) log-base (2) transformed data and (B) fold change based data. Pie chart demonstrating GO term enrichment for Biological Process in genes ≥3-fold up-regulated in response to 1 mM metformin for both (C) log base (2) transformed data and (D) fold change based data. GO Molecular function terms significantly enriched for in genes ≥3-fold up-regulated in response to 0.5 mM metformin for both (E) log base (2) transformed data and (F) fold change based data. Pie chart demonstrating GO term enrichment for Molecular Process in genes ≥3-fold up-regulated in response to 1 mM metformin for both (G) log base (2) transformed data and (H) fold-change based data.

Removing Metformin Treatment for 120 h Results in Return to Untreated Phenotype and Transcript Profiles

In order to determine whether or not removal of 0.5 mM metformin or 1 mM metformin treatments would result in 2DD fibroblasts returning to a normal, proliferative, phenotype, a number of assays were repeated, including; population doubling times, flow cytometry, Ki67 Immunofluorescence and EdU incorporation. Cell counts were recorded following 120 h of treatment and then 120 h post-treatment for a total of 240 h. Both population doubling times and total population doublings were calculated at both time points (Figure 4-14A). At 120 h of either 0.5 mM or 1 mM metformin treatment, population doubling times and total population doublings were consistent with previous findings (Figure 4-2). 120 h following removal of treatment, population doubling times and total population doublings shifted towards a proliferative profile, with no significant difference ($p \geq 0.05$) detected between proliferative and 0.5 mM or 1 mM metformin treated samples (Figure 4-12A). Immuno-labelling with the proliferative marker Ki67 was conducted and revealed that in 2DD post- 0.5 mM and 1 mM metformin treatments, levels of the marker were much higher (81.0% and 73.1% respectively) than in proliferative 2DD (69.5%) (Figure 4-14B & 4-14D). EdU incorporation in 0.5 mM and 1 mM 120 h post-metformin treatment 2DD fibroblasts revealed a slight increase in cells in S-phase from 12.2% in proliferative samples to 17.0 and 15.8 in 0.5 mM and 1 mM post-treatment fibroblasts respectively (Figure 4-14C & Figure 4-14D) In order to determine the number of cells in each stage of the cell cycle, a cell cycle assay incorporating propidium iodide and utilizing flow cytometry was conducted. In samples supplemented with proliferative growth media following 120 h of metformin treatment, both 0.5 mM and 1 mM metformin treatment

revealed a slight increase in fibroblasts in G2/M and a slight decrease in S-phase (conversely to the slight increase in S-phase by EdU); however, these samples show no significant however, these samples show no significant difference to proliferative samples with the numbers of cells in G1/0 at 81.4% and 80.3% respectively compared to proliferative of 80.8% (Figure 4-14B).

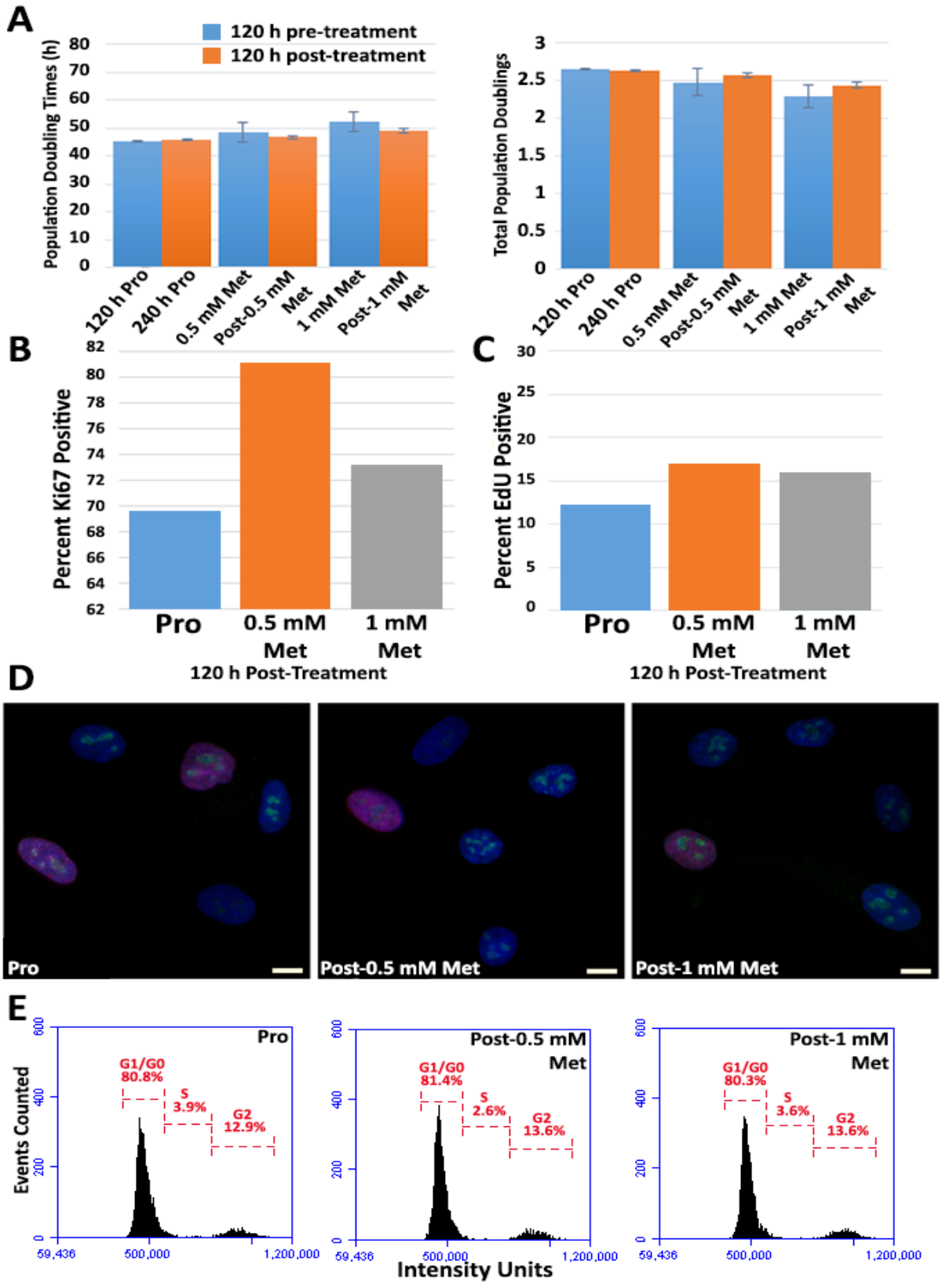

Figure 4-14: Removal of 0.5 mM and 1 mM Metformin after 120 h of Treatment Induces a Shift Towards Proliferative Characteristics in Normal 2DD Fibroblasts. (A) Population doubling times (h) (Y-axis) and total population doublings (Y-axis) for proliferative (120 h Pro; 240 h Pro), 120 h 0.5 mM (0.5 mM Met) and 1 mM metformin (1 mM Met)-treated and 120 h 0.5 mM (Post-0.5 mM Met) and 1 mM (Post-1 mM Met) metformin post-treatment fibroblasts (X-axis) at 120 h of treatment (blue) and 120 h post-treatment (orange). Error bars = S.E.M. (B) Representative graph for percent positive Ki67 (Y-axis) in proliferative and metformin-treated fibroblasts 120 h post-treatment. (C) Representative graph for percent positive EdU (Y-axis) for proliferative and metformin-treated fibroblasts at 120h post-treatment. (D) Representative images of immunofluorescence for proliferative (Pro, Left), 0.5 mM metformin (0.5mM Met, Centre) and 1 mM metformin (1mM Met, Right) -treated fibroblasts. Ki67 labelling (green) and EdU incorporation (red). Chromatin is counterstained with H33342. Scale bar = 10 μm. (E) Propidium iodine cell cycle analysis for proliferative, 0.5 mM metformin and 1 mM metformin-treated fibroblasts 120 h post-treatment. Cell counts (Y-axis) and FL2-A (X-axis).

4.7 Rapamycin Treatment and Metformin Treatment Induce Different Biological Impacts at 120 h of Treatment

For the first time it is possible to determine whether or not metformin and rapamycin are mimicking one another at the transcriptomic level in the same normal cell line, as proposed by the literature. In log transformed analyses, genes changing ≥3-fold up-regulated between 0.5 mM metformin and 500 nM rapamycin-treated fibroblasts revealed just three genes (*FGR, FOSB, IL1B*) overlapping between treatments (0.4%), whilst no overlap was noted in down-regulated data. In fold change analyses, 3 genes (*NR4A2, NR4A1, FOSB*) overlapped (30% of 0.5 mM metformin up-regulated genes, but 0.23% of total genes). Again, there was no overlap between 0.5 mM metformin and 500 nM rapamycin down-regulated genes. These findings were similar in genes ≥3-fold up-regulated in response to 1 mM metformin when compared to 500 nM rapamycin treatment for both log-base (2) transformed data and fold change analyses with 2 (*FOSB, IL1B*) of 813 (0.25%) genes overlapping in log-base (2) up-regulated samples and 1 of 281 genes changing expression in down-regulated genes. In fold change analyses, 2 of 1319 (0.15%) genes were common between 1 mM metformin and rapamycin in up-regulated data and no genes overlapped in down-regulated data (Figure 4-15).

In log-base (2) transformed analyses comparing 0.5 mM metformin treatment and quiescence-induction, 9 of 719 (1.25%) genes (*FGF9, CYP21A2, GDF10, AP001610.5,*

SIPA1L2 AC106786.1, *CCND2*, *H19*, *GAP43*) overlapped in ≥3-fold up-regulated groups, whilst there was no overlap in down-regulated groups. In fold change analyses, 4 of 1283 (0.31%) up-regulated genes (*NR4A2*, *KCNJ3*, *VCAM1*, *CCND2*) were common between 0.5 mM metformin and quiescence. Conversely to log-base (2) transformed data, 3 of 798 (0.38%) genes (overlapped between 0.5 mM metformin and quiescence-induced down-regulated groups. Finally, when comparing genes changing ≥3-fold between 1 mM metformin-treatment and quiescence-induction, 8 (*AATK*, *FGF9*, *AP001610.5*, *SIPA1L2*, *TMEM229B*, *CCND2*, *H19*, *GAP43*) of 689 (1.15%) genes were common in log-base (2) up-regulated genes, whilst there was no overlap in down-regulated groups. In fold change analyses findings were similar, with 3 (*H19*, *VCA1*, *CCND2*) of 1284 (2.34%) genes overlapping in up-regulated groups and 3 (*LRRC38*, *PRPRB*, *ANKRD1*) of 798 (0.38%) genes overlapping in groups down regulated by 1 mM metformin treatment or quiescence-induction (Figure 4-15).

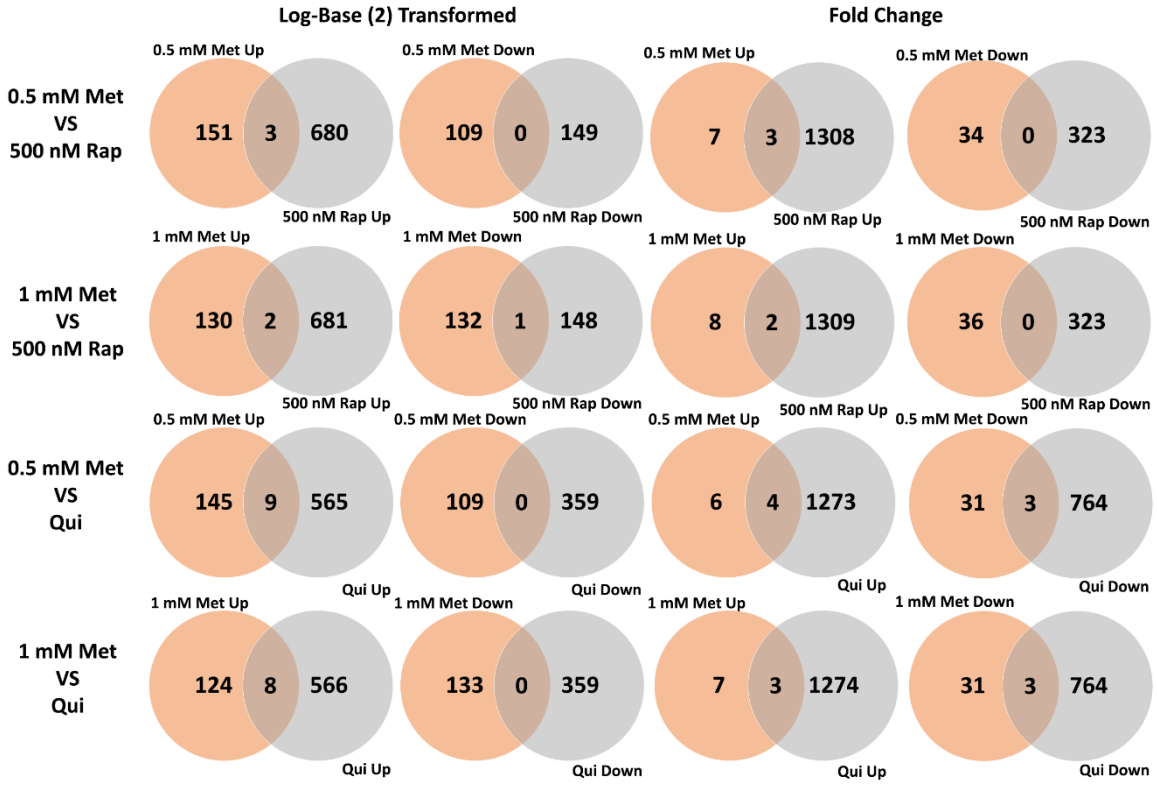

Figure 4-15: Venn diagrams for both log-base (2) transformed and fold change based data demonstrating divergence between 0.5 mM and 1 mM metformin treatments with 500 nM rapamycin treatment and quiescence-induction in 2DD Fibroblasts. Log-base (2) Venn diagrams (left) for (A) 0. 5 mM metformin (Met) vs 500 nM rapamycin (Rap), (B) 1 mM Met vs 500 nM Rap, (C) 0.5 mM Met vs quiescence induction and ***(Figure 4-15 Legend Continued)***

(D) 1 mM Met vs quiescence induction in 2DD fibroblasts. Overlapping regions represent overlap in transcripts between treatments. Fold change based (right) Venn diagrams for (A) 0.5 mM Met vs 500 nM Rap, (B) 1 mM Met vs 500 nM Rap, (C) 0.5 mM Met vs quiescence induction and (D) 1 mM Met vs quiescence induction in 2DD fibroblasts. Overlapping regions represent overlap in transcripts between treatments. In all diagrams, metformin treatment (either 0.5 mM or 1 mM) is in red and rapamycin-treatment or quiescence induction in blue.

4.8 Discussion

We observed that 0.5 mM and 1 mM metformin treatment decreased cell proliferative rates, including levels of Ki67 and EdU positive fibroblasts, and induced the re-localization of chromosomes 18 and 10 within the nuclear volume. These re-localizations were similar, but not identical to that of rapamycin-treatment and quiescence induction. A decrease in autophagy was detected with an increase in phosphorylated AMPK (Thr172). Furthermore, whilst transcript profiles between 0.5 mM and 1 mM metformin somewhat divergent, pathway analysis and GO term analysis revealed very similar enrichment. When considering type of analysis, it is clear that log transforming the data generated slightly divergent datasets to analyses based on fold change, and although the resultant pathway enrichment for both 0.5 mM and 1 mM metformin treatments were divergent between analyses, there were still strong similarities and links between the datasets that support both analyses as important in determining the impact of metformin treatment in primary normal human fibroblasts.

Although similar findings were reported in both 0.5 mM metformin and 1 mM metformin in terms of both growth assays (Ki67), detection of AMPK phosphorylation and autophagy (western blots), pathway enrichment and GO biological and molecular processes, with the majority of genes changing expression at all fold-cut offs overlapping substantially, there were still a number of genes that were not shared between the two treatments. Pathway analysis of the overlapping genes in both ≥3-fold up and down-regulated genes in log-base (2) transformed data revealed enrichment for cytokine-cytokine receptor interaction and AP-1 transcription factor network enrichment. Pathway analyses of overlapping genes in the fold change analyses for metformin treatments revealed similar findings, with the AP-1 transcription factor network as most enriched. Analysis of non-shared transcripts for 0.5 mM metformin log based analyses showed little pathway enrichment but included processes such as death receptor signalling, fertilization, WNT signalling pathway and IL-27 mediated signalling events whilst genes responding to 1 mM metformin but not overlapping demonstrated no pathway enrichment. These findings indicate that whilst 0.5 mM metformin induces more genes to change expression, the impact of metformin in fibroblasts is dose dependent and perhaps a higher concentration here has resulted in a more specific cellular response, with transcripts not common between treatments being non-specific responses. It is important to note; however, that interactions between these genes may not yet have been identified and that databases such as Cytoscape with ReactomeFI are only as useful as the information available to-date. In fold change analyses, genes not overlapping between the treatments demonstrated no networks.

Despite the difference in analyses, the AP-1 transcription factor was among the most enriched pathways in response to fold-change, and still ranked significantly in pathway enrichment for log-base (2) transformed data. Furthermore, the AP-1 transcription factor network was enriched for both 0.5 mM and 1 mM metformin treatments.

The transcription factor activator protein-1 (AP-1) represents hetero- and homo-dimers of the FOS and JUN proteins. c-FOS and c-JUN are mostly expressed in mammalian cells in response to growth factors, cytokines, oxidative stress and pharmacological stimuli. This can lead to regulation of cell proliferation, differentiation and inflammation (Chiu *et al.* 1988; Curran and Franza 1988). Furthermore, the AP-1 transcription factor network is extensively involved in both NF-κB and TNF-α signalling (Fujioka *et al.* 2004), pathways which were also enriched in these analyses.

The enrichment of AP-1 transcription factor network has been linked to ageing – increasing in rat kidneys with age. Metformin is a proposed mimetic of caloric restriction; however, in the case of caloric restriction AP-1 transcription factors were decreased in rat kidney (Kim *et al.* 2002), whereas in human fibroblasts in response to metformin AP-1 transcription factor network was enriched in up-regulated genes. Therefore, it is possible that caloric restriction and metformin induce divergent effects in order to increase health and lifespan. Although this increase in AP-1 transcription factor activity was observed in rats, it has previously been reported that DNA binding activity of the AP-1 transcription factor decreases with age in human lung fibroblast (MRC-5) culture (Sheerin *et al.* 2001) and that AP-1 transcription factor activity is required for initiation of DNA synthesis and is lost during cellular ageing (Riabowol *et al.* 1992), therefore the enrichment of the AP-1 transcription factor network pathway in genes up-regulated in response to metformin is promising in using metformin as a drug to improve health and lifespan.

AP-1 transcription factor has extensively been linked to the modulation of reactive oxygen species (ROS), specifically ROS induction via NF-κB and AP-1 transcription factors (Zhou *et al.* 2001). AP-1 and NF-kB pathways may be interacting with one another, modulating the activity of each other. NF-kB regulates *elk-1*, which is activated by ERK to induce expression of c-FOS and FOS-b in response to certain stimuli in human pancreatic tumor cell line (Fujioka *et al.* 2004). Blocking NF-kB activation inhibits AP-1 activity and NF-kB activity is involved in ROS and serum induced AP-1 activation (Fujioka *et al.* 2004). Metformin has previously been documented to decrease ROS levels in both cancer and healthy cell cultures

(Algire *et al.* 2012; Queiroz *et al.* 2014). It could be that metformin is inducing expression of genes associated with the AP-1 transcription network pathway, priming cells for ROS assault. Alternatively, it could be that metformin is reducing ROS via the AP-1 transcription factor pathway.

Cytokine-Cytokine receptor interactions were enriched in the log transformed analysis of 0.5 mM and 1 mM metformin treated fibroblasts. AP-1 transcription factor network was also enriched in this analysis, although less so than in the fold change analyses. Furthermore, relationships between AMPK, AP-1 and IL-6 expression have been identified. Specifically, it is thought that IL-6 inhibition of adrenal androgen release is mediated via the activation of AMPK, specifically that IL-6 activates AMPK (Ruderman *et al.* 2006), increasing expression of AP-1 family members (Xiao *et al.* 2004). Given this link it could be possible that this pathway is involved in numerous other cell regulatory processes, including growth and repair.

A key assumption has been made within the literature, that metformin is a mimetic of dietary restriction. Based on these findings, this is unlikely completely the case, and may depend on the definition of "mimetic". DR has been clearly documented to decrease energy and induce changes in the cellular ratio of AMP:ATP and NAD:NADH. The key players involved in the mediation of this process, and the ultimate extension of health and lifespan associated with DR are AMPK and SIRT1(Bordone and Guarente 2005; Greer *et al.* 2007; Onken and Driscoll 2010; Mercken *et al.* 2014; Gillespie *et al.* 2016), often affecting common down-stream targets such as NF-κB. SIRT1 has been documented to suppress AP-1 transcriptional activity, directly interacting with c-FOS and c-JUN (Zhang *et al.* 2009), although there is some controversy, with some groups suggesting that SIRT1 interacts with c-Jun and JunD but not c-FOS. This could be a cell and organism dependent factor in which members of the AP-1 transcription network pathway SIRT1 interacts with. These findings provide a link between the enrichment of the AP-1 transcription factor network and the AMPK/SIRT1 interaction that has been extensively linked to DR and other DR mimetics, possible benefiting health and lifespan. Therefore, although there is extensive divergence in the literature over transcriptome profiles and genes changing expression in response to both metformin and DR, these changes may be mediated by the same key modulators.

As a mimetic of DR, metformin has often also been proposed as mimicking rapamycin (another DR mimetic). Comparative analyses of genes changing expression ≥3-fold between 500 nM rapamycin-treated, serum-reduction induced quiescence and 0.5 mM or 1 mM

metformin-treated 2DD fibroblasts demonstrated little overlap between genes changing expression in response to metformin and rapamycin treatments, and between genes changing expression in response to both rapamycin and metformin treatments and quiescence-induction. Although there is clear divergence between treatments, it is important to consider that there are far lower numbers of genes are changing expression in metformin treatments and therefore a higher percentage of these genes are shared. Despite this, combined with pathway analysis, it is evident that metformin-treatment and rapamycin-treatment induce divergent transcript profiles in 2DD fibroblasts.

In summary, it has been demonstrated for the first time in normal human fibroblasts that the impact of metformin on foreskin cells in culture extends to changes in genome organization, repositioning chromosomes within the nuclear volume. Furthermore, it has been demonstrated that two different methods of bioinformatics analyses (log-base (2) transformed and fold change) may reveal different outcomes, highlighting a need to determine which method may be more appropriate for differential gene expression analyses. This work has also strengthened the argument for metformin inducing dose and cell/tissue/organism-dependent responses. Finally, novel enrichment of the AP-1 transcription factor network has been documented as enriched in response to both 0.5 mM and 1 mM metformin, proposing a potential downstream effector pathway for metformin treatment mediated by the well-established SIRT1/AMPK interaction.

5.0 Conclusions

It was observed that both rapamycin and metformin treatment of normal human foreskin fibroblasts (2DD) for 120 h impacted genome function (gene expression) and genome organization (positioning of chromosomes within the nucleus). Specifically, in response to 500 nM rapamycin, 2DD exhibited decreased cell proliferation with no evidence of cell death. In addition, cellular morphology appeared more flattened, reminiscent of quiescence-induction. In order to determine whether or not rapamycin was inducing a quiescent-like state, chromosome territory positioning was monitored, with chromosome 10 moving to the periphery and 18 to the interior under both rapamycin-treatment and quiescence-induction. However, analysis of transcript profiles by RNAseq and subsequent pathway analyses revealed that rapamycin-treated and quiescence-induction induced divergent responses. Specifically, in response to quiescence-induction in 2DD fibroblasts, genes up-regulated ≥5-fold were demonstrated enrichment in the complement and coagulation. Divergent from quiescence-induction, genes up-regulated ≥5-fold in response to rapamycin-treatment demonstrated enrichment of the cytokine-cytokine receptor pathway. Changes at the transcript level were confirmed as biologically having an impact through western blot assays to measure protein expression and ELISA assays to monitor cytokine secretion. Analysis of the promoter regions of genes changing ≥5-fold in response to rapamycin was conducted using cis-element over-representation analysis (CLOVER). These analyses identified transcription factor binding sites that were enriched in genes significantly changing expression in response to rapamycin. CLOVER, combined with biological analysis via chromatin immuno-precipitation (ChIP) assays, identified and confirmed signal transduction and activator of transcription 5A/B (STAT5A/B) as a potential mediator of genes changing expression in response to rapamycin treatment. This STAT5A/B-mediation of gene expression provides novel insight into how rapamycin functions to impact cell proliferation, chromosome territory positioning, gene expression and cytokine production. These findings further linked TOR inhibition with changes in genome function and organization independent of quiescence.

Treatment with either 0.5 mM or 1 mM metformin, as with rapamycin treatment, resulted in decreased cell proliferation in healthy human fibroblasts with no evidence of cell death; however, decreases in cell proliferation and increases in population doubling times were less drastic than those observed in rapamycin treatment. Chromosome territory positioning of chromosomes 10 and 18 at 120 h of treatment were assayed, with chromosome 10 moving towards the periphery and 18 to the interior under 0.5 mM metformin treatment whilst at 1 mM

only chromosome 10 exhibited significant re-positioning to the nuclear periphery. RNA sequencing and subsequent pathway analyses revealed that despite the differences in chromosome territory positioning, both 0.5 mM and 1 mM metformin up-regulated genes demonstrated enrichment for the AP-1 transcription factor pathway whilst no pathways were enriched for in the significantly down-regulated transcripts. Future aims could examine a potential link between the AP-1 transcription factor pathway and its potential mediation by the SIRT1/AMPK interaction previously highlighted as key in modulating health and lifespan.

Finally, although it has frequently been suggested that rapamycin and metformin are mimetics of dietary restriction, and therefore of one another, these observations indicate a clear divergence in transcript profiles in both log-base (2) transformed or fold-change based analyses; however, it is possible that although inducing divergent transcript profiles, rapamycin and metformin induce changes in gene expression that eventually result in the same downstream effects resulting in previously reported health and lifespan extension.

These findings highlight that the proposed mimetics of dietary restriction, rapamycin and metformin, induced divergent transcript profiles. Therefore, it is important to be cognisant of rapamycin and metformin functioning differentially to mimic dietary restriction and the potential of various targets in improving health and lifespan as part of the human aging process.

6.0 Future Directions

These observations and conclusions raise many more questions and avenues of investigation. It has been established that normal human foreskin fibroblasts induced into quiescence, or treated with either rapamycin or metformin, exhibit numerous changes in both genome organization and genome function. In order to further understand these changes in genome organization, and to establish whether or not re-organization of the genome is involved in the mechanism mediating changes in gene expression, various analysis could be conducted. Firstly, a sliding-window algorithm could be used to identify potential regions of the genome that contain clusters of genes that are like regulated in response to rapamycin and metformin. Further analyses of genome folding within these regions using chromosome conformation capture (3C) could be used to determine if these particular regions containing activated/repressed gene clusters change in response to these conditions. 3C is only able to examine a single genomic interaction either between two genes or a gene-enhancer. Therefore, since changes in chromosome territory positioning is indicative of changes in organization genome wide, Hi-C, a derivative of 3C, could be employed to examine changes in folding across the entire genome, enabling the identification of other regions that are linked to the differential expression of rapamycin and metformin responsive genes.

In order to identify the mechanism mediating the identified changes in genome function in response to metformin treatment, the *cis*-element overrepresentation (CLOVER) algorithm could be employed to identify over- and under-represented transcription factor binding sites in genes significantly changing expression. As with the rapamycin-base findings, chromatin immuno-precipitation (ChIP) assays could then be used to confirm if the identified transcription factors are physically binding to the promoter region of the genes of interest. ChIP-sequencing (ChIP-seq) could then be conducted on both rapamycin and metformin-treated samples to identify genome-wide protein-DNA interactions (transcription factors binding to the promoter regions of genes across the genome). Within the literature a diverse range of cell-types have been treated with either rapamycin or metformin; therefore, it is likely that these findings may be cell-type dependent. In order to establish whether or not a common mechanism is mediating response to either rapamycin or metformin, experiments should be repeated across cell-types. If the data sets are available, it may also be possible to conduct meta-analyses to determine if any common pathways exist. Finally, to identify the significance of the proposed mechanisms mediating the response to treatments, knock-down and knock-out studies should be conducted in cell culture to determine if these mechanisms are responsible for the changes in genome organization and function in cells. If successful, these studies should be repeated in model

organisms. Findings from these experiments could further provide evidence as to the importance of these mechanisms in extending both health and lifespan.

Metformin and rapamycin have both been proposed as mimetics of dietary restriction, inducing similar health and lifespan extending benefits across species; however, little work has been conducted in the same cell line treated under conditions of dietary restriction, metformin or rapamycin treatment. In order to provide new insight into the impact of these conditions on genome function and organization, conducting further cell growth assays, chromosome territory positioning, RNAseq and ChIP in foreskin fibroblasts treated under conditions of dietary restriction will provide novel insight into the extent to which metformin and rapamycin mimic caloric restriction, further providing new perspectives on the impact of these treatment conditions on improving health and lifespan.

Finally, in order to understand the importance of genome organization and function in disease, experiments could be conducted in fibroblast cells suffering from Hutchinson-Gilford Progeria Syndrome (HGPS). These patients exhibit an accelerated ageing phenotype, succumbing to cardiovascular disease or stroke at approximately 15 years of age. In HGPS fibroblasts, chromosome mis-localization and genome-wide changes in gene expression have been reported. Having established the impact of metformin, rapamycin and dietary restriction in normal human fibroblasts, with extensive literature documenting the health and lifespan extending-benefits of these compounds, expanding these treatment conditions to HGPS cells could result in re-positioning of mis-localized chromosomes to that or normal human fibroblasts. Genome function (changes in gene expression) could be examined by RNAseq to determine if function is also restored to that of normal human fibroblasts. Further analyses, such as ChIPseq and knock out analyses on transcription factors identified as potentially mediating changes in gene expression induced by rapamycin or metformin, could further elucidate mechanisms involved in HGPS and those promoting a shift towards increasing health and lifespan, particularly as rapamycin and metformin have previously been documented to alter health and lifespan across numerous model organisms.

In summary, the future directions of this work are numerous and could range from understanding the fundamental impact of rapamycin and metformin on genome function and organization. These findings could further improve understanding of the fundamental biology of ageing. This work could then be extended to investigations in disease phenotypes, specifically those involving premature or accelerated ageing such as HGPS.

7.0 References

Abraham, R.T. and Widerrecht, G.J. (1996). "Immunopharmacology of rapamycin." *Annual Review of Immunology* **14**(1): 483-510.

Algire, C., Moiseeva, O., Deschenes-Simard, X., Amrein, L., Petruccelli, L., Birman, E., Viollet, B., Ferbeyre, G. and Pollak, M.N. (2012). "Metformin reduces endogenous reactive oxygen species and associated DNA damage." *Cancer Prevention Research* **5**(4): 536-543.

Alimova, I.N., Liu, B., Fan, Z., Edgerton, S.M., Dillon, T., Lind, S.E. and Thor, A.D. (2014). "Metformin inhibits breast cancer cell growth, colony formation and induces cell cycle arrest *in vitro*." *Cell Cycle* **8**(6): 909-915.

Alvers, A.L., Fishwick, L.K., Wood, M.S., Hu, D., Chung, H.S., Dunn, W.A., Jr., and Aris, J.P. (2009). "Autophagy and amino acid homeostasis are required for chronological longevity in *Saccharomyces cerevisiae*." *Aging Cell* **8**(4): 353-369.

Anedda, A., Rial, E. and Gonzalez-Barroso, M.M. (2008). "Metformin induces oxidative stress in white adipocytes and raises uncoupling protein 2 levels." *Journal of Endocrinology* **199**(1): 33-40.

Anisimov, V.N., Berstein, L.M., Popovich, I.G., Zabezhinski, M.A., Egormin, P.A., Piskunova, T.S., Semenchenko, A.V., Tyndyk, M.L., Yurova, M.N., Kovalenko, I.G. and Poroshina, T.E. (2011). "If started early in life, metformin treatment increases life span and postpones tumors in female SHR mice." *Aging* **3**(2): 148-157.

Arican-Goktas, H.D., Ittiprasert, W., Bridger, J.M. and Knight, M. (2014). "Differential spatial repositioning of activated genes in *Biomphalaria glabrata* snails infected with *Schistosoma mansoni*." *PLOS Neglected Tropical Diseases* **8**(9): 1-10.

Arunachalam, G., Samuel, S.M., Marei, I., Ding, H. and Triggle, C.R. (2014). "Metformin modulates hyperglycaemia-induced endothelial senescence and apoptosis through SIRT1." *British Journal of Pharmacology* **171**(2): 523-535.

Ashinuma, H., Takiguchi, Y., Kitazono, S., Kitazono-Saitoh, M., Kitamura, A., Chiba, T., Tada, Y., Kurosu, K., Sakaida, E., Sekine, I., Tanabe, N., Iwama, A., Yokosuka, O. and

Tatsumi, K. (2012). "Antiproliferative action of metformin in human lung cancer cell lines." *Oncology Reports* **28**(1): 8-14.

Bailey, C.J. and Turner, R.C. (1996). "Metformin." *The New England Journal of Medicine* **334**(1): 574-579.

Baker, D.J., Wijshake, T., Tchkonia, T., LeBrasseur, N.K., Childs, B.G., van de Sluis, B., Kirkland, J.L. and van Deursen, J.M. (2011). "Clearance of $p16^{Ink4a}$-positive senescent cells delays ageing-associated disorders." *Nature* **479**(7372): 232-236.

Bar-Peled, L. and Sabatini, D.M. (2014). "Regulation of mTORC1 by amino acids." *Trends in Cell Biology* **24**(7): 400-406.

Bauer, A. and Bronstrup, M. (2014). "Industrial natural product chemistry for drug discovery and development." *Natural Product Reports* **31**(1): 35-60.

Belmont, A.S. (2014). "Large-scale chromatin organization: the good, the surprising, and the still perplexing." *Current Opinion in Cell Biology* **26**(1): 69-78.

Ben Sahra, I., Laurent, K., Loubat, A., Giorgetti-Peraldi, S., Colosetti, P., Auberger, P., Tanti, J.F., Le Marchand-Brustel, Y. and Bost, F. (2008). "The antidiabetic drug metformin exerts an antitumoral effect *in vitro* and *in vivo* through a decrease of cyclin D1 level." *Oncogene* **27**(25): 3576-3586.

Ben Sahra, I., Regazzetti, C., Robert, G., Laurent, K., Le Marchand-Brustel, Y., Auberger, P., Tanti, J.F., Giorgetti-Peraldi, S. and Bost, F. (2011). "Metformin, independent of AMPK, induces mTOR inhibition and cell-cycle arrest through REDD1." *Cancer Research* **71**(13): 4366-4372.

Bickmore, W.A. (2013). "The spatial organization of the human genome." *Annual Review of Genomics and Human Genetics* **14**(1): 67-84.

Bjedov, I. and Partridge, L. (2011). "A longer and healthier life with TOR down-regulation: genetics and drugs." *Biochemical Society Transactions* **39**(2): 460-465.

Bjedov, I., Toivonen, J.M., Kerr, F., Slack, C., Jacobson, J., Foley, A. and Partridge, L. (2010). "Mechanisms of life span extension by rapamycin in the fruit fly *Drosophila melanogaster*." *Cell Metabolism* **11**(1): 35-46.

Blagosklonny, M.V. (2010). "Calorie restriction: decelerating mTOR-driven aging from cells to organisms (including humans)." *Cell Cycle* **9**(4): 683-688.

Blommaart, E.F.C., Luiken, J.J.F.P., Blommaart, P.J.E., Woerkom, G.M. and Meijer, A.J. (1995). "Phosphorylation of ribosomal protein S6 is inhibitory for autophagy in isolated rat hepatocytes." *Journal of Biological Chemistry* **270**(5): 2320-2326.

Bodkin, N.L., Alexander, T.M., Ortmeyer, H.K., Johnson, E. and Hansen, B.C. (2003). "Mortality and morbidity in laboratory-maintained rhesus monkeys and effects of long-term dietary restriction." *Journals of Gerontology Series A: Biological Sciences and Medical Sciences* **58**(3): 212-219.

Bolzer, A., Kreth, G., Solovei, I., Koehler, D., Saracoglu, K., Fauth, C., Muller, S., Eils, R., Cremer, C., Speicher, M.R. and Cremer, T. (2005). "Three-dimensional maps of all chromsomes in human male fibroblast nuclei and prometaphase rosettes " *PLOS Biology* **3**(5): 826-842.

Bordone, L. and Guarente, L. (2005). "Calorie restriction, SIRT1 and metabolism: understanding longevity." *Nature Reviews Molecular Cell Biology* **6**(4): 298-305.

Boyle, S., Gilchrist, S., Bridger, J.M., Mahy, N.L., Ellis, J.A. and Bickmore, W. (2001). "The spatial organization of human chromosomes within the nuclei of normal and emerin-mutant cells." *Human Molecular Genetics* **10**(3): 211-219.

Branco, M.R. and Pombo, A. (2006). "Intermingling of chromosome territories in interphase suggests role in translocations and transcription-dependent associations." *PLOS Biology* **4**(5): 780-788.

Bray, S.J. (2006). "Notch signalling: a simple pathway becomes complex." *Nature Reviews: Molecular Cell Biology* **7**(9): 678-689.

Bridger, J.M., Boyle, S., Kill, I.R. and Bickmore, W.A. (2000). "Re-modelling of nuclear architecture in quiescent and senescent human fibroblasts " *Current Biology* **10**(1): 149-152.

Bridger, J.M., Kill, I.R., O'Farrell, M. and Hutchison, C.J. (1993). "Internal lamin structures within G1 nuclei of human dermal fibroblast." *Journal of Cell Science* **104**(1): 297-306.

Brodowska, K., Theodoropoulou, S., Meyer Zu Horste, M., Paschalis, E.I., Takeuchi, K., Scott, G., Ramsey, D.J., Kiernan, E., Hoang, M., Cichy, J., Miller, J.W., Gragoudas, E.S. and Vavvas, D.G. (2014). "Effects of metformin on retinoblastoma growth *in vitro* and *in vivo*." *International Journal of Oncology* **45**(6): 2311-2324.

Brugarolas, J., Lei, K., Hurley, R.L., Manning, B.D., Reiling, J.H., Hafen, E., Witters, L.A., Ellisen, L.W. and Kaelin, W.G., Jr. (2004). "Regulation of mTOR function in response to hypoxia by REDD1 and the TSC1/TSC2 tumor suppressor complex." *Genes & Development* **18**(23): 2893-2904.

Buschbeck, M. and Di Croce, L. (2010). "Approaching the molecular and physiological function of macroH2A variants." *Epigenetics* **5**(2): 118-123.

Buschbeck, M., Uribesalgo, I., Wibowo, I., Rue, P., Martin, D., Gutierrez, A., Morey, L., Guigo, R., Lopez-Schier, H. and Di Croce, L. (2009). "The histone variant macroH2A is an epigenetic regulator of key developmental genes." *Nature Structural & Molecular Biology* **16**(10): 1074-1079.

Cabelof, D.C., Yanamadalaa, S., Raffoul, J.J., Guo, Z., Soofi, A. and Heydari, A.R. (2002). "Caloric restriction promotes genomic stability by induction of base excision repair and reversal of its age-related decline." *DNA Repair (Amst)* **2**(3): 295-307.

Cabreiro, F., Au, C., Leung, K.Y., Vergara-Irigaray, N., Cocheme, H.M., Noori, T., Weinkove, D., Schuster, E., Greene, N.D. and Gems, D. (2013). "Metformin retards aging in *C. elegans* by altering microbial folate and methionine metabolism." *Cell* **153**(1): 228-239.

Calabrese, V., Cornelius, C., Cuzzocrea, S., Iavicoli, I., Rizzarelli, E. and Calabrese, E.J. (2011). "Hormesis, cellular stress response and vitagenes as critical determinants in aging and longevity." *Molecular Aspects of Medicine* **32**(4): 279-304.

Camardo, J. (2003). "The rapamune era of immunosuppression 2003: the journey from the laboratory to clinical transplantation." *Transplantation Proceedings* **35**(3): 18-24.

Cao, K., Blair, C.D., Faddah, D.A., Kieckhaefer, J.E., Olive, M., Erdos, M.R., Nabel, E.G. and Collins, F.S. (2011). "Progerin and telomere dysfunction collaborate to trigger cellular senescence in normal human fibroblasts." *The Journal of Clinical Investigation* **121**(7): 2833-2844.

Cao, K., Capell, B.C., Erdos, M.R., Djabali, K. and Collins, F.S. (2007). "A lamin A protein isoform overexpressed in Hutchinson-Gilford progeria syndrome interferes with mitosis in progeria and normal cells." *Proceedings of the National Academy of Sciences* **104**(12): 4949-4954.

Cao, K., Graziotto, J.J., Blair, C.D., Mazzulli, J.R., Erdos, M.R., Krainc, D. and Collins, F.S. (2011). "Rapamycin reverses cellular phenotypes and enhances mutant protein clearance in Hutchinson-Gilford progeria syndrome cells." *Science Translational Medicine* **3**(89): 1-11.

Caron, H., Schaik, B., van der Mee, M., Baas, F., Riggins, G., van Sluis, P., Hermus, M.C., van Asperen, R., Boon, K., Voute, P.A., Heisterkamp, S., van Kampen, A. and Versteeg, R. (2001). "The human transcriptome map: clustering of highly expressed genes in chromosmal domains." *Science* **291**(1): 1289-1292.

Carter, D., Chakalova, L., Osborne, C.S., Dai, Y.F. and Fraser, P. (2002). "Long-range chromatin regulatory interactions *in vivo*." *Nature Genetics* **32**(4): 623-626.

Cavalli, G. and Misteli, T. (2013). "Functional implications of genome topology." *Nature Structural & Molecular Biology* **20**(3): 290-299.

Chambeyron, S., Da Silva, N.R., Lawson, K.A. and Bickmore, W.A. (2005). "Nuclear re-organisation of the *Hoxb* complex during mouse embryonic development." *Development* **132**(9): 2215-2223.

Champ, C.E., Baserga, R., Mishra, M.V., Jin, L., Sotgia, F., Lisanti, M.P., Pestell, R.G., Dicker, A.P. and Simone, N.L. (2013). "Nutrient restriction and radiation therapy for cancer treatment: when less is more." *Oncologist* **18**(1): 97-103.

Chen, C., Liu, Y., Liu, Y. and Zheng, P. (2009). "mTOR regulation and therapeutic rejuvenation of aging hematopoietic stem cells." *Science Signaling* **2**(98): 1-16.

Chen, H.Y. and Maklakov, A.A. (2014). "Condition dependence of male mortality drives the evolution of sex differences in longevity." *Current Biology* **24**(20): 2423-2427.

Chiu, R., Boyle, W.J., Meek, J., Smeal, T., Hunter, T. and Karin, M. (1988). "The c-Fos protein interacts with c-Jun/AP-1 to stimulate transcription of AP-1 responsive genes." *Cell* **54**(1): 541-552.

Cho, R.J., Campbell, M.J., Winzeler, E.A., Steinmemtz, L., Conway, A., Wodicka, L., Wolfsberg, T.G., Gabrielian, A.E., Landsman, D., Lockhart, D.J. and Davis, R.W. (1998). "A genome-wide transcriptional analysis of the mitotic cell cycle." *Molecular Cell* **2**(1): 65-73.

Ciabrelli, F. and Cavalli, G. (2015). "Chromatin-driven behavior of topologically associating domains." *Journal of Molecular Biology* **427**(3): 608-625.

Codogno, P., Mehrpour, M. and Proikas-Cezanne, T. (2012). "Canonical and non-canonical autophagy: variations on a common theme of self-eating?" *Nature Reviews: Molecular Cell Biology* **13**(1): 7-12.

Cohen, B.A., Mitra, R.D., Hughes, J.D. and Church, G.M. (2000). "A computational analysis of whole-genome expression data reveals chromosomal domains of gene expression." *Nature Genetics* **26**(1): 65-73.

Coller, H.A., Sang, L. and Roberts, J.M. (2006). "A new description of cellular quiescence." *PLOS Biology* **4**(3): 329-349.

Colman, R.J., Anderson, R.M., Johnson, S.C., Kastman, E.K., Kosmatka, K.J., Beasley, T.M., Allison, D.B., Cruzen, C., Simmons, H.A., Kemnitz, J.W. and Weindruch, R. (2009). "Caloric restriction delays disease onset and mortality in rhesus monkeys." *Science* **325**(201): 201-204.

Colman, R.J., Beasley, T.M., Kemnitz, J.W., Johnson, S.C., Weindruch, R. and Anderson, R.M. (2014). "Caloric restriction reduces age-related and all-cause mortality in rhesus monkeys." *Nature Communications* **5**(3557): 1-5.

Conway, J.F. and Steven, A.C. (1999). "Methods for reconstructing density maps of "single" particles from cryoelectron micrographs to subnanometer resolution." *Journal of Structural Biology* **128**(1): 106-118.

Cope, N.F., Fraser, P. and Eskiw, C.H. (2010). "The yin and yang of chromatin spatial organization." *Genome Biology* **11**(204): 1-8.

Coppe, J.P., Desprez, P.Y., Krtolica, A. and Campisi, J. (2010). "The senescence-associated secretory phenotype: the dark side of tumor suppression." *Annual Review of Pathology* **5**(1): 99-118.

Cremer, T. and Cremer, C. (2001). "Chromosome territories, nuclear architecture and gene regulation in mammalian cells." *Nature Reviews Genetics* **2**(1): 292-301.

Cremer, T., Cremer, M., Dietzel, S., Muller, S., Solovei, I. and Fakan, S. (2006). "Chromosome territories-a functional nuclear landscape." *Current Opinion in Cell Biology* **18**(3): 307-316.

Croft, J.A., Bridger, J.M., Boyle, S., Perry, P., Teague, P. and Bickmore, W. (1999). "Differences in the localization and morphology of chromosomes in the human nucleus." *The Journal of Cell Biology* **145**(6): 1119-1131.

Cruzen, C. and Colman, R.J. (2009). "Effects of caloric restriction on cardiovascular aging in non-human primates and humans." *Clinics in Geriatric Medicine* **25**(4): 733-743.

Cuervo, A.M. (2008). "Autophagy and aging: keeping that old broom working." *Trends in Genetics* **24**(12): 604-612.

Curran, T. and Franza, B. (1988). "Fos and Jun: the AP-1 connection." *Cell* **55**(3): 395-397.

Das, A., Durrant, D., Koka, S., Salloum, F.N., Xi, L. and Kukreja, R.C. (2014). "Mammalian target of rapamycin (mTOR) inhibition with rapamycin improves cardiac function in type 2 diabetic mice: potential role of attenuated oxidative stress and altered contractile protein expression." *The Journal of Biological Chemistry* **289**(7): 4145-4160.

Dechat, T., Shimi, T., Adam, S.A., Rusinol, A.E., Andres, D.A., Spielmann, H.P., Sinensky, M.S. and Goldman, R.D. (2007). "Alterations in mitosis and cell cycle progression caused by a mutant lamin A known to accelerate human aging." *Proceedings of the National Academy of Sciences* **104**(12): 4955-4960.

Dimitriou, I.D., Clemenza, L., Scotter, A.J., Chen, G., Guerra, F.M. and Rottapel, R. (2008). "Putting out the fire: coordinated suppression of the innate and adaptive immune systems by SOCS1 and SOCS3 proteins." *Immunological Reviews* **224**(1): 265-283.

Domhan, S., Schwager, C., Wei, Q., Muschal, S., Sommerer, C., Morath, C., Wick, W., Maercker, C., Debus, J., Zeier, M., Huber, P.E. and Abdollahi, A. (2014). "Deciphering the systems biology of mTOR inhibition by integrative transcriptome analysis." *Current Pharmaceutical Design* **20**(1): 88-100.

Dowling, R.J., Goodwin, P.J. and Stambolic, V. (2011). "Understanding the benefit of metformin use in cancer treatment." *BMC Medicine* **9**(33): 1-6.

Dowling, R.J., Zakikhani, M., Fantus, I.G., Pollak, M. and Sonenberg, N. (2007). "Metformin inhibits mammalian target of rapamycin-dependent translation initiation in breast cancer cells." *Cancer Research* **67**(22): 10804-10812.

Drissen, R., Palstra, R.J., Gillemans, N., Splinter, E., Grosveld, F., Philipsen, S. and de Laat, W. (2004). "The active spatial organization of the β-*globin* locus requires the transcription factor EKLF." *Genes & Development* **18**(1): 2485-2490.

Dubochet, J., Adrian, M., Chang, J., Homo, J., Lepault, J., McDowall, A.W. and Schultz, P. (1988). "Cryo-electron microscopy of vitrified specimens." *Quarterly Review of Biophysics* **21**(2): 129-228.

Dumont, F.J. and Su, Q. (1996). "Mechanism of action of the immunosuppressant rapamycin." *Life Sciences* **58**(5): 373-395.

Eissenberg, J.C. and Elgin, S.C.R. (2014). "HeterocEncyclopedia of Life Scienceshromatin and euchromatin." *Encyclopedia of Life Sciences* **1**(1): 1-9.

El-Mir, M.Y., Nogueira, V., Fontaine, E., Averet, N., Rigoulet, M. and Leverve, X. (2000). "Dimethylbiguanide inhibits cell respiration via an indirect effect targeted on the respiratory chain complex I." *Journal of Biological Chemistry* **275**(1): 223-228.

Ellisen, L.W., Ramsayer, K.D., Johannessen, C.M., Yang, A., Beppu, H., Minda, K., Oliner, J.D., McKeon, C. and Haber, D.A. (2002). "*REDD1*, a developmentally regulated transcriptional target of p63 and p53, links p63 to regulation of reactive oxygen species." *Molecular Cell* **10**(1): 995-1005.

Eskiw, C.H., Rapp, A., Carter, D.R. and Cook, P.R. (2008). "RNA polymerase II activity is located on the surface of protein-rich transcription factories." *Journal of Cell Science* **121**(12): 1999-2007.

Evans, D.S., Kapahi, P., Hsueh, W.C. and Kockel, L. (2011). "TOR signaling never gets old: aging, longevity and TORC1 activity." *Ageing Research Reviews* **10**(2): 225-237.

Evans, J.M.M., Donnelly, L.A., Emslie-Smith, A.M., Alessi, D.R. and Morris, A.D. (2005). "Metformin and reduced risk of cancer in diabetic patients." *The BMJ* **330**(1): 1304-1305.

Fang, L., Wang, H., Zhou, L. and Yu, D. (2011). "FOXO3a reactivation mediates the synergistic cytotoxic effects of rapamycin and cisplatin in oral squamous cell carcinoma cells." *Toxicology and Applied Pharmacology* **251**(1): 8-15.

Felsenfeld, G. and Groudine, M. (2003). "Controlling the double helix." *Nature* **421**(6921): 448-453.

Feng, Y., Ke, C., Tang, Q., Dong, H., Zheng, X., Lin, W., Ke, J., Huang, J., Yeung, S.C. and Zhang, H. (2014). "Metformin promotes autophagy and apoptosis in esophageal squamous cell carcinoma by downregulating Stat3 signaling." *Cell Death & Disease* **5**(1088): 1-12.

Finch, J.T., Lutter, L.C., Rhodes, D., Brown, R.S., Rushton, B., Levitt, M. and Klug, A. (1977). "Structure of nucleosome core particles of chromatin." *Nature* **269**(1): 29-36.

Finlan, L.E., Sproul, D., Thomson, I., Boyle, S., Kerr, E., Perry, P., Ylstra, B., Chubb, J.R. and Bickmore, W.A. (2008). "Recruitment to the nuclear periphery can alter expression of genes in human cells." *PLOS Genetics* **4**(3): 1-13.

Fischer, K. and Austad, S.N. (2011). "The development of small primate models for aging research." *ILAR Journal* **52**(1): 78-88.

Fok, W.C., Livi, C., Bokov, A., Yu, Z., Chen, Y., Richardson, A. and Perez, V.I. (2014). "Short-term rapamycin treatment in mice has few effects on the transcriptome of white adipose tissue compared to dietary restriction." *Mechanisms of Ageing and Development* **140**(1): 23-29.

Fontana, L., Villareal, D.T., Das, S.K., Smith, S.R., Meydani, S.N., Pittas, A.G., Klein, S., Bhapkar, M., Rochon, J., Ravussin, E. and Holloszy, J.O. (2015). "Effects of 2-year calorie restriction on circulating levels of IGF-1, IGF-binding proteins and cortisol in nonobese men and women: a randomized clinical trial." *Aging Cell* **15**(1): 22–27.

Fontana, L., Weiss, E.P., Villareal, D.T., Klein, S. and Holloszy, J.O. (2008). "Long-term effects of calorie or protein restriction on serum IGF-1 and IGFBP-3 concentration in humans." *Aging Cell* **7**(5): 681-687.

Foretz, M., Hebrard, S., Leclerc, J., Zarrinpashneh, E., Soty, M., Mithieux, G., Sakamoto, K., Andreelli, F. and Viollet, B. (2010). "Metformin inhibits hepatic gluconeogenesis in mice independently of the LKB1/AMPK pathway via a decrease in hepatic energy state." *Journal of Clinical Investigation* **120**(7): 2355-2369.

Fraga, M.F., Ballestar, E., Paz, M.F., Ropero, S., Setien, F., Ballestar, M.L., Heine-Suner, D., Cigudosa, J.C., Urioste, M., Benitez, J., Boix-Chornet, M., Sanchez-Aguilera, A., Ling, C., Carlsson, E., Poulsen, P., Vaag, A., Stephan, Z., Spector, T.D., Wu, Y.Z., Plass, C. and Esteller, M. (2005). "Epigenetic differences arise during the lifetime of monozygotic twins." *Proceedings of the National Academy of Sciences* **102**(30): 10604-10609.

Fraser, P. and Bickmore, W. (2007). "Nuclear organization of the genome and the potential for gene regulation." *Nature* **447**(7143): 413-417.

Frias, M.A., Thoreen, C.C., Jaffe, J.D., Schroder, W., Sculley, T., Carr, S.A. and Sabatini, D.M. (2006). "mSin1 is necessary for Akt/PKB phosphorylation, and its isoforms define three distinct mTORC2s." *Current Biology* **16**(18): 1865-1870.

Frith, M.C., Fu, Y., Yu, L., Chen, J.F., Hansen, U. and Weng, Z. (2004). "Detection of functional DNA motifs via statistical over-representation." *Nucleic Acids Research* **32**(4): 1372-1381.

Fujioka, S., Niu, J., Schmidt, C., Sclabas, G.M., Peng, B., Uwagawa, T., Li, Z., Evans, D.B., Abbruzzese, J.L. and Chiao, P.J. (2004). "NF-κB and AP-1 connection: mechanism of NF-κB-dependent regulation of AP-1 activity." *Molecular Cell Biology* **24**(17): 7806-7819.

Fussner, E., Ching, R.W. and Bazett-Jones, D.P. (2011). "Living without 30 nm chromatin fibers." *Trends in Biochemical Sciences* **36**(1): 1-6.

Galic, S., Sachithanandan, N., Kay, T.W. and Steinberg, G.R. (2014). "Suppressor of cytokine signalling (SOCS) proteins as guardians of inflammatory responses critical for regulating insulin sensitivity." *Biochemical Journal* **461**(2): 177-188.

Ganley, I.G., Lam du, H., Wang, J., Ding, X., Chen, S. and Jiang, X. (2009). "ULK1.ATG13.FIP200 complex mediates mTOR signaling and is essential for autophagy." *Journal of Biological Chemistry* **284**(18): 12297-12305.

Garbers, C., Kuck, F., Aparicio-Siegmund, S., Konzak, K., Kessenbrock, M., Sommerfeld, A., Haussinger, D., Lang, P.A., Brenner, D., Mak, T.W., Rose-John, S., Essmann, F., Schulze-Osthoff, K., Piekorz, R.P. and Scheller, J. (2013). "Cellular senescence or EGFR signaling induces Interleukin 6 (IL-6) receptor expression controlled by mammalian target of rapamycin (mTOR)." *Cell Cycle* **12**(21): 3421-3432.

Gillespie, Z.E., Pickering, J. and Eskiw, C.H. (2016). "Better living through chemistry: caloric restriction (CR) and CR mimetics alter genome function to promote increased health and lifespan." *Frontiers in Genetics* **7**(142): 1-21.

Greer, E.L., Dowlatshahi, D., Banko, M.R., Villen, J., Hoang, K., Blanchard, D., Gygi, S.P. and Brunet, A. (2007). "An AMPK-FOXO pathway mediates longevity induced by a novel method of dietary restriction in *C. elegans*." *Current Biology* **17**(19): 1646-1656.

Gribble, K.E., Jarvis, G., Bock, M. and Mark Welch, D.B. (2014). "Maternal caloric restriction partially rescues the deleterious effects of advanced maternal age on offspring." *Aging Cell* **13**(4): 623-630.

Guelen, L., Pagie, L., Brasset, E., Meuleman, W., Faza, M.B., Talhout, W., Eussen, B.H., de Klein, A., Wessels, L., de Laat, W. and van Steensel, B. (2008). "Domain organization of human chromosomes revealed by mapping of nuclear lamina interactions." *Nature* **453**(7197): 948-951.

Hands, S.L., Proud, C.G. and Wyttenbach, A. (2009). "mTOR's role in ageing: protein synthesis or autophagy?" *Aging* **1**(7): 586-597.

Hansen, M., Taubert, S., Crawford, D., Libina, N., Lee, S.J. and Kenyon, C. (2007). "Lifespan extension by conditions that inhibit translation in *Caenorhabditis elegans*." *Aging Cell* **6**(1): 95-110.

Hara, K., Yonezawa, K., Weng, Q.P., Kozlowski, M.T., Belham, C. and Avruch, J. (1998). "Amino acid sufficiency and mTOR regulate p70 S6 Kinase and eIF-4E BP1 through a common effector mechanism." *Journal of Biological Chemistry* **273**(23): 14484-14494.

Hardie, D.G. (2006). "Neither LKB1 nor AMPK are the direct targets of metformin." *Gastroenterology* **131**(1): 973-983.

Hardie, D.G. (2007). "AMP-activated protein kinase as a drug target." *Annual Review of Pharmacology and Toxicology* **47**(1): 185-210.

Hardie, D.G. (2011). "AMP-activated protein kinase: an energy sensor that regulates all aspects of cell function." *Genes & Development* **25**(18): 1895-1908.

Hardie, D.G., Ross, F.A. and Hawley, S.A. (2012). "AMPK: a nutrient and energy sensor that maintains energy homeostasis." *Nature Reviews: Molecular Cell Biology* **13**(1): 251-262.

Harrison, D.E., Strong, R., Sharp, Z.D., Nelson, J.F., Astle, C.M., Flurkey, K., Nadon, N.L., Wilkinson, J.E., Frenkel, K., Carter, C.S., Pahor, M., Javors, M.A., Fernandez, E. and Miller, R.A. (2009). "Rapamycin fed late in life extends lifespan in genetically heterogeneous mice." *Nature* **460**(7253): 392-395.

Hawley, S.A., Boudeau, J., Reid, J.L., Mustard, K.J., Udd, L., Makela, T.P., Alessi, D.R. and Hardie, D.G. (2003). "Complexes between the LKB1 tumor suppressor, STRADα/β and MO25α/β are upstream kinases in the AMP-activated protein kinase cascade." *The Journal of Biology* **2**(28): 1-16.

He, J., Wang, K., Zheng, N., Qiu, Y., Xie, G., Su, M., Jia, W. and Li, H. (2015). "Metformin suppressed the proliferation of LoVo cells and induced a time-dependent metabolic and transcriptional alteration." *Scientific Reports* **5**(17423): 1-16.

Holde, K. (1995). "Chromatin higher order structure: chasing a mirage?" *Journal of Biological Chemistry* **270**(1): 8373-8376.

Holley, W.R., Mian, I.S., Park, S.J., Rydberg, B. and Chatterjee, N. (2002). "A model for interphase chromosomes and evaluation of radiation-induced aberrations." *Radiation Research* **158**(1): 568-580.

Hosokawa, N., Hara, T., Kaizuka, T., Kishi, C., Takamura, A., Miura, Y., Iemura, S., Natsume, T., Takehana, K., Yamada, N., Guan, J.L., Oshiro, N. and Mizushima, N. (2009). "Nutrient-dependent mTORC1 association with the ULK1-Atg13-FIP200 complex required for autophagy." *Molecular Biology of the Cell* **20**(7): 1981-1991.

Hsu, P.P., Kang, S.A., Rameseder, J., Zhang, Y., Ottina, K.A., Lim, D., Peterson, T.R., Choi, Y., Gray, N.S., Yaffe, M.B., Marto, J.A. and Sabatini, D.M. (2011). "The mTOR-regulated

phosphoproteome reveals a mechanism of mTORC1-mediated inhibition of growth factor signaling." *Science* **332**(1): 1317-1322.

Hughes, A.L. and Yeager, M. (1997). "Molecular evolution of the vertebrate immune system." *BioEssays* **19**(9): 777-786.

Hundal, R.S., Krssak, M., Dufour, S., Laurent, D., Lebon, V., Chandramouli, V., Inzucchi, S.E., Schumann, W.C., Petersen, K.F., Landau, B.R. and Shulman, G.I. (2000). "Mechanism by which metformin reduces glucose production in type 2 diabetes." *Diabetes* **49**(12): 2063-2069.

Hurst, L.D., Pal, C. and Lercher, M.J. (2004). "The evolutionary dynamics of eukaryotic gene order." *Nature Reviews Genetics* **5**(4): 299-310.

Iborra, F.J., Pombo, A., Jackson, D.A. and Cook, P.R. (1996). "Active RNA polymerases are localized within discrete transcription 'factories' in human nuclei." *Journal of Cell Science* **109**(1): 1427-1436.

Inness, C.L. and Metcalfe, N.B. (2008). "The impact of dietary restriction, intermittent feeding and compensatory growth on reproductive investment and lifespan in a short-lived fish." *Proceedings of the Royal Society B: Biological Sciences* **275**(1644): 1703-1708.

Inoki, K., Li, Y., Xu, T. and Guan, K.L. (2003). "Rheb GTPase is a direct target of TSC2 GAP activity and regulates mTOR signaling." *Genes & Development* **17**(15): 1829-1834.

Inoki, K., Li, Y., Zhu, T., Wu, J. and Guan, K.L. (2002). "TSC2 is phosphorylated and inhibited by Akt and suppresses mTOR signalling." *Nature Cell Biology* **4**(9): 648-657.

Jacinto, E., Loewith, R., Schmidt, A., Lin, S., Ruegg, M.A., Hall, A. and Hall, M.N. (2004). "Mammalian TOR complex 2 controls the actin cytoskeleton and is rapamycin insensitive." *Nature Cell Biology* **6**(11): 1122-1128.

Jimenez, R.H., Boylan, J.M., Lee, J.S., Francesconi, M., Castellani, G., Sanders, J.A. and Gruppuso, P.A. (2009). "Rapamycin response in tumorigenic and non-tumorigenic hepatic cell lines." *PLOS One* **4**(10): 1-11.

Johnson, S.C., Rabinovitch, P.S. and Kaeberlein, M. (2013). "mTOR is a key modulator of ageing and age-related disease." *Nature* **493**(7432): 338-345.

Joos, S., Falk, M.H., Lichter, P., Haluska, F.G., Henglein, B., Lenoir, G.M. and Bornkamm, G.W. (1992). "Variable breakpoints in Burkitt lymphoma cells with chromosomal t(8;14) translocation separate c-*myc* and the IgH locus up to several hundred kb." *Human Molecular Genetics* **1**(8): 625-632.

Jung, C.H., Jun, C.B., Ro, S.H., Kim, Y.M., Otto, N.M., Cao, J., Kundu, M. and Kim, D.H. (2009). "ULK-Atg13-FIP200 complexes mediate mTOR signaling to the autophagy machinery." *Molecular Biology of the Cell* **20**(7): 1992-2003.

Jung, C.H., Ro, S.H., Cao, J., Otto, N.M. and Kim, D.H. (2010). "mTOR regulation of autophagy." *FEBS Letters* **584**(7): 1287-1295.

Kabil, H., Partridge, L. and Harshman, L.G. (2007). "Superoxide dismutase activities in long-lived Drosophila melanogaster females: chico1 genotypes and dietary dilution." *Biogerontology* **8**(2): 201-208.

Kaeberlein, M. and Kennedy, B.K. (2007). "Protein translation, 2007." *Aging Cell* **6**(1): 731-734.

Kaeberlein, M. and Kennedy, B.K. (2011). "Hot topics in aging research: protein translation and TOR signaling." *Aging Cell* **10**(1): 185-190.

Kaizuka, T., Hara, T., Oshiro, N., Kikkawa, U., Yonezawa, K., Takehana, K., Iemura, S., Natsume, T. and Mizushima, N. (2010). "Tti1 and Tel2 are critical factors in mammalian target of rapamycin complex assembly." *Journal of Biological Chemistry* **285**(26): 20109-20116.

Kamakaka, R.T. and Biggins, S. (2005). "Histone variants: deviants?" *Genes & Development* **19**(1): 295-316.

Kannan, K. and Fridell, Y.W. (2013). "Functional implications of *Drosophila* insulin-like peptides in metabolism, aging, and dietary restriction." *Frontiers in Physiology* **4**(288): 1-8.

Kantidakis, T., Ramsbottom, B.A., Birch, J.L., Dowding, S.N. and White, R.J. (2010). "mTOR associates with TFIIIC, is found at tRNA and 5S rRNA genes, and targets their repressor Maf1." *Proceedings of the National Academy of Sciences* **107**(26): 11823-11828.

Kato, K., Gong, J., Iwama, H., Kitanaka, A., Tani, J., Miyoshi, H., Nomura, K., Mimura, S., Kobayashi, M., Aritomo, Y., Kobara, H., Mori, H., Himoto, T., Okano, K., Suzuki, Y., Murao, K. and Masaki, T. (2012). "The antidiabetic drug metformin inhibits gastric cancer cell proliferation *in vitro* and *in vivo*." *Molecular Cancer Therapeutics* **11**(3): 549-560.

Kealy, R.D., Lawler, D.F., Ballam, J.M., Mantz, S.L., Biery, D.N., Greeley, E.H., Lust, G., Segre, M., Smith, G.K. and Stowe, H.D. (2002). "Effects of diet restriction on life span and age-related changes in dogs." *Journal of the American Veterinary Medical Association* **220**(9): 1315-1320.

Kelly, B., Tannahill, G.M., Murphy, M.P. and O'Neil, L.A.J. (2015). "Metformin inhibits the production of reactive oxygen species from NADH:ubiquinone oxidoreductase to limit induction of Interleukin-1β (IL-1β) and boosts Interleukin-10 (IL-10) in Lipopolysaccharide (LPS)-activated macrophages." *Journal of Biological Chemistry* **290**(1): 20348-20359.

Kill, I.R. (1996). "Localisation of the Ki-67 antigen within the nucleolus." *Journal of Cell Science* **109**(1): 1253-1263.

Kim, D.H., Sarbassov, D.D., Ali, S.M., Latek, R.R., Guntur, K.V.P., Erdjument-Bromage, H., Tempst, P. and Sabatini, D.M. (2003). "GβL, a positive regulator of the rapamycin-sensitive pathway required for the nutrient-sensitive interaction between Raptor and mTOR." *Molecular Cell* **11**(1): 895-904.

Kim, H.J., Jung, K.J., Seo, A.Y., Choi, J.S., Yu, B.P. and Chung, H.Y. (2002). "Calorie restriction modulates REDOX-sensitive AP-1 during the aging process." *Journal of the American Aging Association* **25**(1): 123-130.

Kleinjan, D.A. and van Heyningen, V. (2005). "Long-range control of gene expression: emerging mechanisms and disruption in disease." *The American Journal of Human Genetics* **76**(1): 8-32.

Kojima, H., Inoue, T., Kunimoto, H. and Nakajima, K. (2013). "IL-6-STAT3 signaling and premature senescence." *JAKSTAT* **2**(4): 1-9.

Kong, Y., Cui, H., Ramkumar, C. and Zhang, H. (2011). "Regulation of senescence in cancer and aging." *Journal of Aging Research* **2011**(1): 1-15.

Koren, I., Reem, E. and Kimchi, A. (2010). "DAP1, a novel substrate of mTOR, negatively regulates autophagy." *Current Biology* **20**(12): 1093-1098.

Kornberg, R. (1974). "Chromatin structure: a repeating unit of histones and DNA." *Science* **184**(4139): 868-871.

Kosak, S.T. and Groudine, M. (2004). "Gene order and dynamic domains." *Science* **306**(1): 644-647.

Krebs, D.L. and Hilton, D.J. (2000). "SOCS: physiological suppressors of cytokine signaling." *Journal of Cell Science* **113**(16): 2813-2819.

Kubben, N., Adriaens, M., Meuleman, W., Voncken, J.W., van Steensel, B. and Misteli, T. (2012). "Mapping of lamin A- and progerin-interacting genome regions." *Chromosoma* **121**(5): 447-464.

Kupper, K., Kolbl, A., Biener, D., Dittrich, S., von Hase, J., Thormeyer, T., Fiegler, H., Carter, N.P., Speicher, M.R., Cremer, T. and Cremer, M. (2007). "Radial chromatin positioning is shaped by local gene density, not by gene expression." *Chromosoma* **116**(3): 285-306.

Laberge, R.M., Sun, Y., Orjalo, A.V., Patil, C.K., Freund, A., Zhou, L., Curran, S.C., Davalos, A.R., Wilson-Edell, K.A., Liu, S., Limbad, C., Demaria, M., Li, P., Hubbard, G.B., Ikeno, Y., Javors, M., Desprez, P.Y., Benz, C.C., Kapahi, P., Nelson, P.S. and Campisi, J. (2015). "mTOR regulates the pro-tumorigenic senescence-associated secretory phenotype by promoting IL1A translation." *Nature Cell Biology* **17**(8): 1049-1061.

Ladoire, S., Chaba, K., Martins, I., Sukkurwala, A.Q., Adjemian, S., Michaud, M., Poirier-Colame, V., Andreiuolo, F., Galluzzi, L., White, E., Rosenfeldt, M., Ryan, K.M., Zitvogel, L. and Kroemer, G. (2012). "Immunohistochemical detection of cytoplasmic LC3 puncta in human cancer specimens." *Autophagy* **8**(8): 1175-1184.

Lan, F., Cacicedo, J.M., Ruderman, N. and Ido, Y. (2008). "SIRT1 modulation of acetylation status, cytosolic localization, and activity of LKB1." *Journal of Biological Chemistry* **283**(41): 27628-27635.

Laplante, M. and Sabatini, D.M. (2009). "mTOR signalling at a glance." *Journal of Cell Science* **122**(20): 3589-3594.

Laplante, M. and Sabatini, D.M. (2012). "mTOR signaling in growth control and disease." *Cell* **149**(2): 274-293.

Laplante, M. and Sabatini, D.M. (2013). "Regulation of mTORC1 and its impact on gene expression at a glance." *Journal of Cell Science* **126**(8): 1713-1719.

Lau, A.W., Liu, P., Inuzuka, H. and Gao, D. (2014). "SIRT1 phosphorylation by AMP-activated protein kinase regulates p53 acetylation." *American Journal of Cancer Research* **4**(3): 245-255.

Leclerc, G.M., Leclerc, G.J., Kuznetsov, J.N., DeSalvo, J. and Barredo, J.C. (2013). "Metformin induces apoptosis through AMPK-dependent inhibition of UPR signaling in ALL lymphoblasts." *PLOS One* **8**(8): 1-10.

Lee, J.M. and Sonnhammer, E.L.L. (2003). "Genomic gene clustering analysis of pathways in eukaryotes." *Genome Research* **13**(1): 875-882.

Lee, W.M., Paik, J.S., Cho, W.K., Oh, E.H., Lee, S.B. and Yang, S.W. (2013). "Rapamycin enhances TNF-α-induced secretion of IL-6 and IL-8 through suppressing PDCD4 degradation in orbital fibroblasts." *Current Eye Research* **38**(6): 699-706.

Lercher, M.J., Urrutia, A.O., Pavlicek, A. and Hurst, L.D. (2003). "A unification of mosaic structures in the human genome." *Human Molecular Genetics* **12**(19): 2411-2415.

Li, W., Ma, W., Zhong, H., Liu, W. and Sun, Q. (2014). "Metformin inhibits proliferation of human keratinocytes through a mechanism associated with activation of the MAPK signaling pathway." *Experimental and Therapeutic Medicine* **7**(2): 389-392.

Li, Y., Daniel, M. and Tollefsbol, T.O. (2011). "Epigenetic regulation of caloric restriction in aging." *BioMed Central Medicine* **9**(98): 1-12.

Liao, C.Y., Rikke, B.A., Johnson, T.E., Diaz, V. and Nelson, J.F. (2010). "Genetic variation in the murine lifespan response to dietary restriction: from life extension to life shortening." *Aging Cell* **9**(1): 92-95.

Lieberman, P.M. (2008). "Chromatin organization and virus gene expression." *Journal of Cellular Physiology* **216**(2): 295-302.

Luger, K., Mader, A.W., Richmond, R.K., Sargent, D.F. and Richmond, T.J. (1997). "Crystal structure of the nucleosome core particle at 2.8 A˚ resolution." *Nature* **389**: 251-260.

Ma, L., Chen, Z., Erdjument-Bromage, H., Tempst, P. and Pandolfi, P.P. (2005). "Phosphorylation and functional inactivation of TSC2 by Erk implications for tuberous sclerosis and cancer pathogenesis." *Cell* **121**(2): 179-193.

Ma, X.M. and Blenis, J. (2009). "Molecular mechanisms of mTOR-mediated translational control." *Nature Reviews: Molecular Cell Biology* **10**(1): 307-318.

MacDonald, B.T. and He, X. (2012). "Frizzled and LRP5/6 receptors for Wnt/β-catenin signaling." *Cold Spring Harbor Perspectives in Biology* **4**(12): 1-23.

Maeshima, K. and Eltsov, M. (2008). "Packaging the genome: the structure of mitotic chromosomes." *The Journal of Biochemistry* **143**(2): 145-153.

Maeshima, K., Imai, R., Tamura, S. and Nozaki, T. (2014). "Chromatin as dynamic 10-nm fibers." *Chromosoma* **123**(3): 225-237.

Manning, B.D., Tee, A.R., Logsdon, M.N., Blenis, J. and Cantley, L.C. (2002). "Identification of the tuberous sclerosis complex-2 tumor suppressor gene product tuberin as a target of the phosphoinositide 3-kinase/Akt pathway." *Molecular Cell* **10**(1): 151-162.

Martin-Montalvo, A., Mercken, E.M., Mitchell, S.J., Palacios, H.H., Mote, P.L., Scheibye-Knudsen, M., Gomes, A.P., Ward, T.M., Minor, R.K., Blouin, M.J., Schwab, M., Pollak, M., Zhang, Y., Yu, Y., Becker, K.G., Bohr, V.A., Ingram, D.K., Sinclair, D.A., Wolf, N.S., Spindler, S.R., Bernier, M. and de Cabo, R. (2013). "Metformin improves healthspan and lifespan in mice." *Nature Communications* **4**(2192): 1-12.

Marz, A.M., Fabian, A.K., Kozany, C., Bracher, A. and Hausch, F. (2013). "Large FK506-binding proteins shape the pharmacology of rapamycin." *Molecular and Cellular Biology* **33**(7): 1357-1367.

Matharu, N.K. and Ahanger, S.H. (2015). "Chromatin insulators and topological domains: adding new dimensions to 3D genome architecture." *Genes* **6**(3): 790-811.

Mattison, J.A., Roth, G.S., Beasley, T.M., Tilmont, E.M., Handy, A.M., Herbert, R.L., Longo, D.L., Allison, D.B., Young, J.E., Bryant, M., Barnard, D., Ward, W.F., Qi, W., Ingram, D.K. and de Cabo, R. (2012). "Impact of caloric restriction on health and survival in rhesus monkeys from the NIA study." *Nature* **489**(7415): 318-321.

Mayer, C. and Grummt, I. (2006). "Ribosome biogenesis and cell growth: mTOR coordinates transcription by all three classes of nuclear RNA polymerases." *Oncogene* **25**(48): 6384-6391.

McCay, C.M., Crowell, M.F. and Maynard, L.A. (1935). "The effect of retarded growth upon the length of life span and upon the ultimate body size." *Journal of Nutrition* **10**(1): 63-79.

Meaburn, K.J., Cabuy, E., Bonne, G., Levy, N., Morris, G.E., Navelli, G., Kill, I.R. and Bridger, J.M. (2007). "Primary laminopathy fibroblasts display altered genome organization and apoptosis." *Aging Cell* **6**(1): 139-153.

Meaburn, K.J., Gudla, P.R., Khan, S., Lockett, S.J. and Misteli, T. (2009). "Disease-specific gene repositioning in breast cancer." *Journal of Cell Biology* **187**(6): 801-812.

Mehta, I.S., Amira, M., Harvey, A.J. and Bridger, J.M. (2010). "Rapid chromosome territory relocation by nuclear motor activity in response to serum removal in primary human fibroblasts." *Genome Biology* **11**(1): 1-17.

Mehta, I.S., Eskiw, C.H., Arican, H.D., Kill, I.R. and Bridger, J.M. (2011). "Farnesyltransferase inhibitor treatment restores chromosome territory positions and active chromosome dynamics in Hutchinson-Gilford progeria syndrome cells." *Genome Biology* **12**(8): 1-14.

Mercken, E.M., Hu, J., Krzysik-Walker, S., Wei, M., Li, Y., McBurney, M.W., de Cabo, R. and Longo, V.D. (2014). "SIRT1 but not its increased expression is essential for lifespan extension in caloric-restricted mice." *Aging Cell* **13**(1): 193-196.

Metaxakis, A. and Partridge, L. (2013). "Dietary restriction extends lifespan in wild-derived populations of *Drosophila melangoster* " *PLOS One* **8**(9): 1-6.

Miller, R.A., Harrison, D.E., Astle, C.M., Fernandez, E., Flurkey, K., Han, M., Javors, M.A., Li, X., Nadon, N.L., Nelson, J.F., Pletcher, S., Salmon, A.B., Sharp, Z.D., Van Roekel, S.,

Winkleman, L. and Strong, R. (2014). "Rapamycin-mediated lifespan increase in mice is dose and sex dependent and metabolically distinct from dietary restriction." *Aging Cell* **13**(3): 468-477.

Mitchell, J.A., Clay, I., Umlauf, D., Chen, C., Moir, C.A., Eskiw, C.H., Schoenfelder, S., Chakalova, L., Nagano, T. and Fraser, P. (2012). "Nuclear RNA sequencing of the mouse erythroid cell transcriptome." *PLOS One* **7**(11): 1-14.

Mitchell, J.A. and Fraser, P. (2008). "Transcription factories are nuclear subcompartments that remain in the absence of transcription." *Genes & Development* **22**(1): 20-25.

Mizushima, N., Levine, B., Cuervo, A.M. and Klionsky, D.J. (2008). "Autophagy fights disease through cellular self-digestion." *Nature* **451**(7182): 1069-1075.

Murphy, C.T. and Hu, P.J. (2013). "Insulin/insulin-like growth factor signaling in *C. elegans*." *WormBook* **164**(1): 1-43.

Musi, N., Hirshman, M.F., Nygren, J., Svanfeldt, M., Bavenholm, P., Rooyackers, O., Zhou, G., Williamson, J.M., Ljunqvist, O., Efendic, S., Moller, D.E., Thorell, A. and Goodyear, L.J. (2002). "Metformin increases AMP-activated protein kinase activity in skeletal muscle of subjects with type 2 diabetes." *Diabetes* **51**(1): 2074-2081.

Na, H.J., Park, J.S., Pyo, J.H., Jeon, H.J., Kim, Y.S., Arking, R. and Yoo, M.A. (2015). "Metformin inhibits age-related centrosome amplification in *Drosophila* midgut stem cells through AKT/TOR pathway." *Mechanisms of Ageing and Development* **149**(1): 8-18.

Nelson, L.E., Valentine, R.J., Cacicedo, J.M., Gauthier, M.S., Ido, Y. and Ruderman, N.B. (2012). "A novel inverse relationship between metformin-triggered AMPK-SIRT1 signaling and p53 protein abundance in high glucose-exposed HepG2 cells." *American Journal of Physiology* **303**(1): 1-17.

Niehrs, C. (2012). "The complex world of WNT receptor signalling." *Nature Reviews: Molecular Cell Biology* **13**(12): 767-779.

Noll, M. (1974). "Subunit structure of chromatin." *Nature* **251**(1): 249-251.

Oakhill, J.S., Steel, R., Chen, Z.P., Scott, J.W., Ling, N., Tam, S. and Kemp, B.E. (2011). "AMPK is a direct adenylate charge-regulated protein kinase." *Science* **332**(6036): 1433-1435.

Olins, A.L. and Olins, D.E. (1974). "Spheroid chromatin units (v Bodies)." *Science* **183**(4122): 330-332.

Onken, B. and Driscoll, M. (2010). "Metformin induces a dietary restriction-like state and the oxidative stress response to extend *C. elegans* hsealthspan via AMPK, LKB1, and SKN-1." *PLOS One* **5**(1): 1-13.

Orchard, T.J., Temprosa, M., Goldberg, R., Haffner, S., Ratner, R., Marcovina, S. and Fowler, S. (2005). "The effect of metformin and intensive lifestyle intervention on the metabolic syndrome: the diabetes prevention program randomized trial." *Annals of Internal Medicine* **142**(8): 611-619.

Osborne, C.S., Chakalova, L., Brown, K.E., Carter, D., Horton, A., Debrand, E., Goyenechea, B., Mitchell, J.A., Lopes, S., Reik, W. and Fraser, P. (2004). "Active genes dynamically colocalize to shared sites of ongoing transcription." *Nature Genetics* **36**(10): 1065-1071.

Oudet, P., Gross-Bellard, M. and Chambon, P. (1975). "Electron microscopic and biochemical evidence that chromatin structure is a repeating unit." *Cell* **4**(4): 281-300.

Owen, M.R., Doran, E. and Halestrap, A.P. (2000). "Evidence that metformin exerts its anti-diabetic effects through inhibition of complex 1 of the mitochondrial respiratory chain." *Biochemical Journal* **348**: 607-614.

Pajvani, U.B., Qiang, L., Kangsamaksin, T., Kitajewski, J., Ginsberg, H.N. and Accili, D. (2013). "Inhibition of Notch uncouples Akt activation from hepatic lipid accumulation by decreasing mTORC1 stability " *Nature Medicine* **19**(8): 1054-1060.

Pehrson, J.R. and Fried, V.A. (1992). "MacroH2A, a core histone containing a large nonhistone region." *Science* **257**(5075): 1398-1400.

Peltola, K.J., Paukku, K., Aho, T.L., Ruuska, M., Silvennoinen, O. and Koskinen, P.J. (2004). "Pim-1 kinase inhibits STAT5-dependent transcription via its interactions with SOCS1 and SOCS3." *Blood* **103**(10): 3744-3750.

Peterson, T.R., Laplante, M., Thoreen, C.C., Sancak, Y., Kang, S.A., Kuehl, W.M., Gray, N.S. and Sabatini, D.M. (2009). "DEPTOR is an mTOR inhibitor frequently overexpressed in multiple myeloma cells and required for their survival." *Cell* **137**(5): 873-886.

Petroulakis, E., Mamane, Y., Le Bacquer, O., Shahbazian, D. and Sonenberg, N. (2006). "mTOR signaling: implications for cancer and anticancer therapy." *British Journal of Cancer* **94**(2): 195-199.

Phillips-Cremins, J.E. and Corces, V.G. (2013). "Chromatin insulators: linking genome organization to cellular function." *Molecular Cell* **50**(4): 461-474.

Powers, R.W., 3rd, Kaeberlein, M., Caldwell, S.D., Kennedy, B.K. and Fields, S. (2006). "Extension of chronological life span in yeast by decreased TOR pathway signaling." *Genes & Development* **20**(2): 174-184.

Queiroz, E.A., Puukila, S., Eichler, R., Sampaio, S.C., Forsyth, H.L., Lees, S.J., Barbosa, A.M., Dekker, R.F., Fortes, Z.B. and Khaper, N. (2014). "Metformin induces apoptosis and cell cycle arrest mediated by oxidative stress, AMPK and FOXO3a in MCF-7 breast cancer cells." *PLOS One* **9**(5): 1-18.

Raman, A., Colman, R.J., Cheng, Y., Kemnitz, J.W., Baum, S.T., Weindruch, R. and Schoeller, D.A. (2005). "Reference body composition in adult rhesus monkeys: glucoregulatory and anthropometric indices." *The Journals of Gerontology, Series A: Biological Sciences* **60A**(12): 1518-1524.

Ramsey, J.J., Colman, R.J., Binkley, N.C., Christensen, J.D., Gresl, T.A., Kemnitz, J.W. and Weindruch, R. (2000). "Dietary restriction and aging in rhesus monkeys: the University of Wisconsin study." *Experimental Gerontology* **35**(1): 1131-1149.

Ray, P.D., Huang, B.W. and Tsuji, Y. (2012). "Reactive oxygen species (ROS) homeostasis and redox regulation in cellular signaling." *Cell Signal* **24**(5): 981-990.

Reik, W. and Walter, J. (2001). "Genomic imprinting: parental influence on the genome." *Nature Reviews Genetics* **2**(1): 21-32.

Rena, G., Pearson, E.R. and Sakamoto, K. (2013). "Molecular mechanism of action of metformin: old or new insights?" *Diabetologia* **56**(9): 1898-1906.

Riabowol, K., Schiff, J. and M.Z., G. (1992). "Transcription factor AP-1 activity is required for initiation of DNA synthesis and is lost during cellular aging." *Proceedings of the National Academy of Sciences* **89**(1): 157-161.

Richter, J.D. and Sonenberg, N. (2005). "Regulation of cap-dependent translation by eIF4E inhibitory proteins." *Nature* **433**(1): 477-480.

Rodriguez-Paredes, M. and Esteller, M. (2011). "Cancer epigenetics reaches mainstream oncology." *Nature Medicine* **17**(3): 330-339.

Roux, P.P., Ballif, B.A., Anjum, R., Gygi, S.P. and Blenis, J. (2004). "Tumor-promoting phorbol esters and activated Ras inactivate the tuberous sclerosis tumor suppressor complex via p90 ribosomal S6 kinase." *Proceedings of the National Academy of Sciences* **101**(37): 13489-13494.

Ruderman, N.B., Keller, C., Richard, A.M., Saha, A.K., Luo, Z., Xiang, X., Giralt, M., Ritov, V.B., Menshikova, E.V., Kelley, D.E., Hidalgo, J., Pedersen, B.K. and Kelly, M. (2006). "Interleukin-6 regulation of AMP-activated protein kinase: potential role in the systemic response to exercise and prevention of the metabolic syndrome." *Diabetes* **55**(Supplement 2): 48-54.

Ruvinsky, I. and Meyuhas, O. (2006). "Ribosomal protein S6 phosphorylation: from protein synthesis to cell size." *Trends in Biochemical Sciences* **31**(6): 342-348.

Salas, E.M., Garcia-Barchino, M.J., Labiano, S., Shugay, M., Perez-Encinas, M., Quinteiro, C., Garcia-Delgado, M., Vizmanos, J.L. and Novo, F.J. (2011). "LIF, a novel STAT5-regulated gene, is aberrantly expressed in myeloproliferative neoplasms." *Genes Cancer* **2**(5): 593-596.

Saleiro, D. and Platanias, L.C. (2015). "Intersection of mTOR and STAT signaling in immunity." *Trends in Immunology* **36**(1): 21-29.

Santos, R.X., Correia, S.C., Cardoso, S., Carvalho, C., Santos, M.S. and Moreira, P.I. (2011). "Effects of rapamycin and TOR on aging and memory: implications for Alzheimer's disease." *Journal of Neurochemistry* **117**(6): 927-936.

Sarbassov, D.D., Ali, S.M., Kim, D.H., Guertin, D.A., Latek, R.R., Erdjument-Bromage, H., Tempst, P. and Sabatini, D.M. (2004). "Rictor, a novel binding partner of mTOR, defines a rapamycin-insensitive and raptor-independent pathway that regulates the cytoskeleton." *Current Biology* **14**(14): 1296-1302.

Sarbassov, D.D., Ali, S.M. and Sabatini, D.M. (2005). "Growing roles for the mTOR pathway." *Current Opinion in Cell Biology* **17**(6): 596-603.

Sarbassov, D.D., Ali, S.M., Sengupta, S., Sheen, J.H., Hsu, P.P., Bagley, A.F., Markhard, A.L. and Sabatini, D.M. (2006). "Prolonged rapamycin treatment inhibits mTORC2 assembly and Akt/PKB." *Molecular Cell* **22**(2): 159-168.

Saucedo, L.J., Gao, X., Chiarelli, D.A., Li, L., Pan, D. and Edgar, B.A. (2003). "Rheb promotes cell growth as a component of the insulin/TOR signalling network." *Nature Cell Biology* **5**(6): 566-680.

Scheuermann, M.O., Tajbakhsh, J., Kurz, A., Saracoglu, K., Eils, R. and Lichter, P. (2004). "Topology of genes and nontranscribed sequences in human interphase nuclei." *Experimental Cell Research* **301**(2): 266-279.

Schneider, R. and Grosschedl, R. (2007). "Dynamics and interplay of nuclear architecture, genome organization, and gene expression." *Genes & Development* **21**(23): 3027-3043.

Schoenfelder, S., Sexton, T., Chakalova, L., Cope, N.F., Horton, A., Andrews, S., Kurukuti, S., Mitchell, J.A., Umlauf, D., Dimitrova, D.S., Eskiw, C.H., Luo, Y., Wei, C.L., Ruan, Y., Bieker, J.J. and Fraser, P. (2010). "Preferential associations between co-regulated genes reveal a transcriptional interactome in erythroid cells." *Nature Genetics* **42**(1): 53-61.

Sehgal, S.N., Baker, H. and Vezina, C. (1975). "Rapamycin (AY-22,989), a new antifungal antibiotic. II fermentation, isolation and characterization " *The Journal of Antibiotics* **28**(10): 727-732.

Shannon, P., Markiel, A., Ozier, O., Baliga, N.S., Wang, J.T., Ramage, D., Amin, N., Schwikowski, B. and Ideker, T. (2003). "Cytoscape: a software environment for integrated models of biomolecular interaction networks." *Genome Research* **13**(1): 2498-2504.

Shapira, M., Kakiashvili, E., Rosenberg, T. and Hershko, D.D. (2006). "The mTOR inhibitor rapamycin down-regulates the expression of the ubiquitin ligase subunit Skp2 in breast cancer cells." *Breast Cancer Research* **8**(4): 1-9.

Shaw, R.J., Kosmatka, M., Bardeesy, N., Hurley, R.L., Witters, L.A., DePinho, R.A. and Cantley, L.C. (2004). "The tumor suppressor LKB1 kinase directly activates AMP-activated kinase and regulates apoptosis in response to energy stress." *Proceedings of the National Academy of Sciences* **101**(10): 3329-3335.

Sheerin, A., thomson, K.S.J. and Goyns, M.H. (2001). "Altered composition and DNA binding activity of the AP-1 transcription factor during the ageing of human fibroblast." *Mechanims of Ageing and Development* **122**: 1813-1824.

Shimobayashi, M. and Hall, M.N. (2014). "Making new contacts: the mTOR network in metabolism and signalling crosstalk." *Nature Reviews: Molecular Cell Biology* **15**(3): 155-162.

Shor, B., Wu, J., Shakey, Q., Toral-Barza, L., Shi, C., Follettie, M. and Yu, K. (2010). "Requirement of the mTOR kinase for the regulation of Maf1 phosphorylation and control of RNA polymerase III-dependent transcription in cancer cells." *Journal of Biological Chemistry* **285**(20): 15380-15392.

Shoshani, T., Faerman, A., Mett, I., Zelin, E., Tenne, T., Gorodin, S., Moshel, Y., Elbaz, S., Budanov, A., Chajut, A., Kalinski, H., Kamer, I., Rozen, A., Mor, O., Keshet, E., Leshkowitz, D., Einat, P., Skaliter, R. and Feinstein, E. (2002). "Identification of a novel hypoxia-inducible factor 1-responsive gene, RTP801, involved in apoptosis." *Molecular and Cellular Biology* **22**(7): 2283-2293.

Siggens, L. and Ekwall, K. (2014). "Epigenetics, chromatin and genome organization: recent advances from the ENCODE project." *Journal of Internal Medicine* **276**(3): 201-214.

Slack, C., Foley, A. and Partridge, L. (2012). "Activation of AMPK by the putative dietary restriction mimetic metformin is insufficient to extend lifespan in *Drosophila*." *PLOS One* **7**(10): 1-7.

Smith, D.L., Jr., Elam, C.F., Jr., Mattison, J.A., Lane, M.A., Roth, G.S., Ingram, D.K. and Allison, D.B. (2010). "Metformin supplementation and life span in Fischer-344 rats." *The Journals of Gerontology, Series A: Biological Sciences* **65**(5): 468-474.

Song, C.W., Lee, H., Dings, R.P., Williams, B., Powers, J., Santos, T.D., Choi, B.H. and Park, H.J. (2012). "Metformin kills and radiosensitizes cancer cells and preferentially kills cancer stem cells." *Scientific Reports* **2**(362): 1-9.

Spellman, P.T. and Rubin, G.M. (2002). "Evidence for large domains of similarly expressed genes in the *Drosophila* genome." *Journal of Biology* **1**(5): 1-8.

Spilianakis, C.G., Lalioti, M.D., Town, T., Lee, G.R. and Flavell, R.A. (2005). "Interchromosomal associations between alternatively expressed loci." *Nature* **435**(7042): 637-645.

Stanfel, M.N., Shamieh, L.S., Kaeberlein, M. and Kennedy, B.K. (2009). "The TOR pathway comes of age." *Biochimica et Biophysica Acta* **1790**(10): 1067-1074.

Straub, T. (2003). "Heterochromatin dynamics." *PLOS Biology* **1**(1): 23-24.

Su, X., Yu, Y., Zhong, Y., Giannopoulou, E.G., Hu, X., Liu, H., Cross, J.R., Ratsch, G., Rice, C.M. and Ivashkiv, L.B. (2015). "Interferon-gamma regulates cellular metabolism and mRNA translation to potentiate macrophage activation." *Nature Immunology* **16**(8): 838-849.

Suzuki, M., Endo, M., Shinohara, F., Echigo, S. and Rikiishi, H. (2011). "Rapamycin suppresses ROS-dependent apoptosis caused by selenomethionine in A549 lung carcinoma cells." *Cancer Chemotherapy and Pharmacology* **67**(5): 1129-1136.

Takahara, T., Hara, K., Yonezawa, K., Sorimachi, H. and Maeda, T. (2006). "Nutrient-dependent multimerization of the mammalian target of rapamycin through the N-terminal HEAT repeat region." *Journal of Biological Chemistry* **281**(39): 28605-28614.

Takeda-Watanabe, A., Kitada, M., Kanasaki, K. and Koya, D. (2012). "SIRT1 inactivation induces inflammation through the dysregulation of autophagy in human THP-1 cells." *Biochemical and Biophysical Research Communications* **427**(1): 191-196.

Tolhuis, B., Palstra, R.J., Splinter, E., Grosveld, F. and de Laat, W. (2002). "Looping and interaction between hypersensitive sites in the active β-globin locus." *Molecular Cell* **10**(1): 1453-1465.

Tumaneng, K., Schlegelmilch, K., Russell, R.C., Yimlamai, D., Basnet, H., Mahadevan, N., Fitamant, J., Bardeesy, N., Camargo, F.D. and Guan, K.L. (2012). "YAP mediates crosstalk between the Hippo and PI(3)K-TOR pathways by suppressing PTEN via miR-29." *Nature Cell Biology* **14**(12): 1322-1329.

Turban, S., Stretton, C., Drouin, O., Green, C.J., Watson, M.L., Gray, A., Ross, F., Lantier, L., Viollet, B., Hardie, G.H., Marette, A. and Hundal, H.S. (2012). "Defining the contribution of AMP-activated protein kinase (AMPK) and protein kinase C (PKC) in regulation of glucose uptake by metformin in skeletal muscle cells." *Journal of Biological Chemistry* **287**(24): 20088-20099.

Um, J.H., Kim, S.J., Kim, D.W., Ha, M.Y., Jang, J.H., Kim, D.W., Chung, B.S., Kang, C.D. and Kim, S.H. (2003). "Tissue-specific changes of DNA repair protein Ku and mtHSP70 in aging rats and their retardation by caloric restriction." *Mechanisms of Ageing and Development* **124**(8-9): 967-975.

Vakoc, C.R., Letting, D.L., Gheldof, N., Sawado, T., Bender, M.A., Groudine, M., Weiss, M.J., Dekker, J. and Blobel, G.A. (2005). "Proximity among distant regulatory elements at the beta-globin locus requires GATA-1 and FOG-1." *Molecular Cell* **17**(3): 453-462.

Valvezan, A.J., Huang, J., Lengner, C.J., Pack, M. and Klein, P.S. (2013). "Oncogenic mutations in adenomatous polyposis coli (Apc) activate mechanistic target of rapamycin complex 1 (mTORC1) in mice and zebrafish." *Disease Models & Mechanisms* **7**(1): 63-71.

Vander Haar, E., Lee, S.I., Bandhakavi, S., Griffin, T.J. and Kim, D.H. (2007). "Insulin signalling to mTOR mediated by the Akt/PKB substrate PRAS40." *Nature Cell Biology* **9**(3): 316-323.

Vignot, S., Faivre, S., Aguirre, D. and Raymond, E. (2005). "mTOR-targeted therapy of cancer with rapamycin derivatives." *Annals of Oncology* **16**(4): 525-537.

Vincent, L. and Soille, P. (1991). "Watersheds in digital spaces: an efficient algorithm based on immersion simulations." *IEEE Transactions on Pattern Analysis and Machine Intelligence* **13**(6): 583-598.

Walker, G., Houthoofd, K., Vanfleteren, J.R. and Gems, D. (2005). "Dietary restriction in *C. elegans*: from rate-of-living effects to nutrient sensing pathways." *Mechanisms of Ageing and Development* **126**(9): 929-937.

Wang, L., Harris, T.E., Roth, R.A. and Lawrence, J.C., Jr. (2007). "PRAS40 regulates mTORC1 kinase activity by functioning as a direct inhibitor of substrate binding." *Journal of Biological Chemistry* **282**(27): 20036-20044.

Weber, C.M. and Henikoff, S. (2014). "Histone variants: dynamic punctuation in transcription." *Genes & Development* **28**(7): 672-682.

Weindruch, R. and Walford, R.L. (1982). "Dietary restriction in mice beginning at 1 year of age: effect on life-span and spontaneous cancer incidence." *Science* **215**(4538): 1415-1418.

Wilcock, C. and Bailey, C.J. (1993). "Accumulation of metformin by tissues of the normal and diabetic mouse." *Xenobiotica* **24**(1): 49-57.

Wilkinson, J.E., Burmeister, L., Brooks, S.V., Chan, C.C., Friedline, S., Harrison, D.E., Hejtmancik, J.F., Nadon, N., Strong, R., Wood, L.K., Woodward, M.A. and Miller, R.A. (2012). "Rapamycin slows aging in mice." *Aging Cell* **11**(4): 675-682.

Witters, L.A. (2001). "The blooming of the French lilac." *Journal of Clinical Investigation* **108**(8): 1105-1107.

Woods, A., Johnstone, S.R., Dickerson, K., Leiper, F.C., Fryer, L.G.D., Neumann, D., Schlattner, U., Wallimann, T., Carlson, M. and Carling, D. (2003). "LKB1 is the upstream kinase in the AMP-activated protein kinase cascade." *Current Biology* **13**(22): 2004-2008.

Wu, G., Feng, X. and Stein, L. (2010). "A human functional protein interaction network and its application to cancer data analysis." *Genome Biology* **11**(5): 1-23.

Xiao, B., Sanders, M.J., Underwood, E., Heath, R., Mayer, F.V., Carmena, D., Jing, C., Walker, P.A., Eccleston, J.F., Haire, L.F., Saiu, P., Howell, S.A., Aasland, R., Martin, S.R.,

Carling, D. and Gamblin, S.J. (2011). "Structure of mammalian AMPK and its regulation by ADP." *Nature* **472**(7342): 230-233.

Xiao, W., Hodge, D.R., Wang, L., Yang, X., Zhang, X. and Farrar, W.L. (2004). "NF-κB activates IL-6 expression through cooperation with c-Jun and IL6-AP1 site, but is independent of its IL6-NFκB regulatory site in autocrine human multiple myeloma cells." *Cancer Biology & Therapy* **10**(1): 1007-1017.

Xu, W., Deng, Y.Y., Yang, L., Zhao, S., Liu, J., Zhao, Z., Wang, L., Maharjan, P., Gao, S., Tian, Y., Zhuo, X., Zhao, Y., Zhou, J., Yuan, Z. and Wu, Y. (2015). "Metformin ameliorates the proinflammatory state in patients with carotid artery atherosclerosis through sirtuin 1 induction." *Translational Research* **166**(5): 451-458.

Yamada, Y., Colman, R.J., Kemnitz, J.W., Baum, S.T., Anderson, R.M., Weindruch, R. and Schoeller, D.A. (2013). "Long-term calorie restriction decreases metabolic cost of movement and prevents decrease of physical activity during aging in rhesus monkeys." *Experimental Gerontology* **48**(11): 1226-1235.

Zhang, J. and Liu, F. (2014). "Tissue-specific insulin signaling in the regulation of metabolism and aging." *International Union of Biochemistry and Moleclar Biology Life* **66**(7): 485-495.

Zhang, R., Chen, H.Z., Liu, J.J., Jia, Y., Zhang, Z., Yang, R.F., Zhang, Y., Xu, J., Wei, Y., Liu, D. and Liang, C. (2009). "SIRT1 suppresses activator protein-1 transcriptional activity and cyclooxygenase-2 expression in macrophages." *Journal of Biological Chemistry* **285**(10): 7097-7110.

Zhang, S., Cai, G., Fu, B., Feng, Z., Ding, R., Bai, X., Liu, W., Zhuo, L., Sun, L., Liu, F. and Chen, X. (2012). "SIRT1 is required for the effects of rapamycin on high glucose-inducing mesangial cells senescence." *Mechanisms of Ageing and Development* **133**(6): 387-400.

Zhao, B., Tumaneng, K. and Guan, K.L. (2011). "The Hippo pathway in organ size control, tissue regeneration and stem cell self-renewal." *Nature Cell Biology* **13**(8): 877-883.

Zhao, J., Benakanakere, M.R., Hosur, K.B., Galicia, J.C., Martin, M. and Kinane, D.F. (2010). "Mammalian target of rapamycin (mTOR) regulates TLR3 induced cytokines in human oral keratinocytes." *Molecular Immunology* **48**(1): 294-304.

Zheng, J., Fang, F., Zeng, X., Medler, T.R., Fiorillo, A.A. and Clevenger, C.V. (2011). "Negative cross talk between NFAT1 and Stat5 signaling in breast cancer." *Molecular Endocrinology* **25**(12): 2054-2064.

Zhou, G., Myers, R., Li, Y., Chen, Y., Shen, X., Fenyk-Melody, J., Wu, M., Ventre, J., Doebber, T., Fujii, N., Musi, N., Hirshman, M.F., Goodyear, L.J. and Moller, D.E. (2001). "Role of AMP-activated protein kinase in mechanism of metformin action." *Journal of Clinical Investigation* **108**(8): 1167-1174.

Zhou, L.Z.H., Johnson, A.O. and Rando, T.A. (2001). "NFκB and AP-1 mediate transcriptional responses to oxidative stress in skeletal muscle cells." *Free Radical Biology & Medicine* **31**(11): 1405-1416.

Zhou, Y., Luoh, S., Zhang, Y., Watanabe, C., Wu, T.D., Ostland, M., Wood, W.I. and Zhang, Z. (2003). "Genome-wide identification of chromosomal regions of increased tumor expression by transcriptome analysis." *Cancer Research* **63**: 5781-5784.

Zoncu, R., Efeyan, A. and Sabatini, D.M. (2011). "mTOR: from growth signal integration to cancer, diabetes and ageing." *Nature Reviews: Molecular Cell Biology* **12**(1): 21-35.